DOCTOR OF SCIENCES

Histidine biosynthesis, cell separation and copper homeostasis in Brucella abortus

ROBA, Agnes

Award date:
2022

Awarding institution:
University of Namur

Histidine biosynthesis, cell separation and copper homeostasis in *Brucella abortus*

Agnès Roba

Dissertation in preparation of the degree of PhD in Sciences

2021

Jury Members:

Prof. R. Martin Roop II, East Carolina University, USA
Dr. Coralie Fumeaux, Université de Lausanne, Switzerland
Prof. Laurence Van Melderen, Université Libre de Bruxelles, Belgium
Prof. Géraldine Laloux, Université Catholique de Louvain, Belgium
Prof. Jean-Yves Matroule, President, Université de Namur, Belgium
Prof. Xavier De Bolle, Promoter, Université de Namur, Belgium

“Everything in excess is opposed to nature”.

Hippocrates

"Words are, in my not-so-humble opinion, our most inexhaustible source of magic. Capable of both inflicting injury, and remedying it".

'Harry Potter And The Deathly Hallows – Part 2', 2011, J.K. Rowling

“Don’t rush everything in this divine time“

Little Simz

« Même si je passe le temps
Sans intérêt pour ça
La vie c'est fait pour ça
C'est tester sa naissance

Aimer tous les moment
C'est se mentir dans le sens
C'est se mentir dans le froid
C'est noyer son essence
C'est lâcher le combat
De l'infiniment petit face à l'infiniment grand
Se perdre dans le profond
Sans voir à la surface
Dans les mots d'un prophète
Les réponses aux questions
Je les laisse aux grosses têtes

On nait, on vit, on meurt
Aussi vite qu'un cri, qu'un pleur
Aussi bête qu'un vide, qu'une fleur
On est en vie on meurt
Aussi rien qu'un fil, qu'une heure »

Odezenne

SUMMARY

Brucella spp. are collectively responsible for a worldwide zoonosis called brucellosis. Inside its bovine host, *Brucella abortus* invades and survives inside cells. In particular, *Brucella* is adapted to survive in a nutrient restricted environment. Indeed, this bacterium possesses many biosynthetic pathways, that allows *Brucella* to make up essential building blocks on its own. Some of these biosynthetic pathways become essential during macrophage infection, suggesting either that the end product of the pathway is limited, or that it is particularly crucial for intracellular survival. In this work, we investigated the requirement of *Brucella* for the histidine biosynthesis pathway.

First, we found that *hisB*, a histidine auxotroph mutant is defective for intracellular multiplication and also surprisingly displays a chaining phenotype. The intensity of this phenotype varies with the culture medium and is exacerbated inside host cells. We investigated how those chains were generated, and found out that chaining bacteria consist of contiguous peptidoglycan, and likely result from the defective cleavage of peptidoglycan during cell separation. Suppression of the chaining phenotype revealed two essential genes with a crucial role during cell division in *B. abortus, dipM* and *cdlP*. While DipM is strictly localized at the division site, CdlP is localized at the growth pole and the division site. Depletion of *dipM* and *cdlP* results in swelling at the division site. Altogether, the unexpected chaining phenotype of the *hisB* mutant allowed the discovery of new actors of cell division in *B. abortus*.

In the second part of this work, we investigated the impact of the deletion of histidine biosynthesis genes on copper homeostasis in *B. abortus*. Histidine is an amino acid that has the ability to coordinate different metal ions. Accordingly, most of the predicted proteins of *B. abortus* that are histidine-enriched are involved in metal homeostasis or use metals as cofactors. We found that four histidine auxotroph mutants (*hisA, hisB, hisC* and *hisD*) showed both lower replication inside macrophages and increased sensitivity to copper. We also found that *B. abortus* does not show this increased sensitivity to copper when actors classically described as involved in copper resistance, namely *cueO* and *copA*, are deleted. Furthermore, we were able to isolate suppressors of each histidine auxotroph mutant, in which spontaneous mutations restored copper resistance. Fifteen of the 22 mutations found in suppressors occurred inside the *opp* operon, coding for an oligopeptide transporter. Overall, our data suggest that histidine might have a much more important role than expected for copper resistance in *B. abortus*.

ACKNOWLEDGEMENTS

Tout d'abord je voudrais remercier mon promoteur, Xavier. C'est grâce à toi que j'ai voulu faire cette thèse. Avec ta bonne humeur, ton humour, ton enthousiasme légendaire et ton goût de la vie et des bonnes choses, tu auras été une bulle d'oxygène dans un monde académique trop souvent austère, critique et rabat-joie. Ton ouverture d'esprit m'impressionnera toujours, c'est un plaisir et un privilège de pouvoir discuter avec toi, et j'espère qu'on continuera encore à le faire dans le futur !

Ensuite je remercie tous les chefs de l'URBM pour leur aide scientifique, et je pense en particulier à Jean-Yves qui aura toujours été une oreille attentive, a toujours montré de l'intérêt pour mes recherches et s'est toujours montré généreux en conseils et coups de mains dans les sujets qu'il connait par cœur. Merci à Régis et Francesco pour leur esprit critique. Vous avez fait de l'URBM un environnement très stimulant pour la recherche en microbiologie.

L'âme de l'URBM ne serait rien, mais alors rien sans leurs héros du quotidien, les véritables piliers que sont Aurélie, Elodie, Françoise et Mathieu. Vous faites un boulot formidable et je ne sais comment vous remercier pour tous les efforts que vous faites au quotidien pour nous faciliter le travail et faire de l'URBM un endroit plus gai. Entre les moments papote, les échanges de recettes de cuisine, les bons plans de voyages, les memes à la machine à café, les super sorties de labo, les caféine awards, les p'tites billes (let it beee) et j'en passe, je dirai juste une chose : je ne vous oublierai jamais !

J'aurai eu le plaisir de cotoyer de nombreux chercheurs en URBM, et je commencerai donc par les plus anciens. Bruce, Carlo, Popo, vous saviez comme personne mettre une ambiance de feu lors des beer hours, et pour ça merci ! C'est aussi pour ça qu'on aime l'URBM… Gwen et Pauline, mille merci pour tous vos coups de main pour des questions liées au cuivre, mais de manière plus générale pour votre aide, votre gentillesse et votre disponibilité qui m'auront été précieuses. Girls, you rock !!! Anthony, Elie et Jérôme, je vous remercie pour votre aide au labo, et parce qu'on peut toujours compter sur vous pour rire (ou boire) un coup ! Aravind, thanks for the good time we spent here and there, I wish you all the best wherever you are. Alex, thanks for always showing interest in my research, for helping me and guiding me many times, and most of all encouraging me. It may not seem like much, but it's actually a lot. José and Tania, the lab can be happy to have people as sweet as you around. I wish you all the best in your projects to come, and I'd be very happy to meet you again outside of the lab.

I make a special paragraph for my dear Aish, who was particularily present this last year, especially during difficult times. Your tremendous energy lifted me many times, scientifically but also as a person. I may not be your colleague anymore, but you can always count on me as a friend.

Nous arrivons ensuite à la Xa team, qu'on peut élargir à la Eric team. Pour commencer, Katy et Vicky vous avez mis la barre très haut. Vous étiez toutes les deux très inspirantes, notament par votre culture scientifique et surtout Vicky pour ce qui est de l'efficacité et l'organisation (sans rancune Katy) ! Mathilde, qu'est-ce qu'on aura bien rigolé dans ce bureau à échanger des musiques honteuses et beaucoup de chocolat ! Aurore, profite bien du soleil californien et bonne chance à toi pour tes nouvelles aventures ! Pierre, on aura fait un sacré chemin ensembles, non sans embuches et obstacles. Je te remercie sincèrement pour toutes les fois où tu m'as aidée, et j'espère que l'avenir sera plus paisible pour toi comme pour moi. Angy, un immense merci pour avoir toujours été attentive à moi, scientifiquement comme humainement. Ta maturité et ton expérience m'auront été d'une grande aide à bien des reprises. Merci pour ton écoute, tes conseils et ta générosité

presque sans limite. Elo, un tout grand merci pour ton aide pour les manips et au labo en général, pour ton efficacité et ton envie de toujours apprendre des nouvelles choses. La Xa team a de la chance de t'avoir ! Caro, merci pour ta maturité et ton ouverture d'espirt. Tu feras des grandes choses, j'en suis sûre ! Eme, une vraie lionne se cache dans le petit bout de femme que tu es ! Déjà bravo pour le chemin que vous avez parcouru, courage pour la fin, ne lachez rien, et vous connaissant je suis sûre que vous allez briller ! Chantal, merci pour la lumière et la chaleur que tu dégages avec ton sourire, ça aura été un plaisir de te cotoyer, et c'est pas fini ! Adélie, merci pour ton dynamisme et ta positive attitude, bonne chance pour la suite ! Enfin, last but not least, la petite dernière : Charline ! On aura fait un sacré duo pendant ton mémoire, et t'encadrer m'aura apporté beaucoup humainement et scientifiquement, tu m'as appris plein de choses ! Un grand merci aussi pour le soutien pendant la rédaction, c'était vraiment précieux ! Je suis déjà très fière de toi, et je te souhaite tout le meilleur pour la suite !

Heureusement, pendant la thèse et toutes ses difficultés, il y avait aussi toute une vie en dehors du labo (#worklifebalance). D'abord merci à mes super copains et copines d'avoir toujours été là pour m'écouter, ou juste me changer les idées : Alice, Brunelle, Gwen, Maïté, Manon, Marie, Mimilou, Momo, Péné, Sam, Soph, Zozo et tous les autres, je vous envoie un océan d'amour ! Ensuite en parallèle à la thèse, il y a eu l'aventure savate boxe française. Cela aura été une véritabe soupape de décompression, sauf quand coach Alain en rajoutait une couche en nous pressant comme des citrons avant les compétitions ! Sans rancune, on t'aime quand même ;-) Merci aux amis (à la famille ?) du club, Emma, Eve, Gwen, Lisa, Yoran, Zélie, les frères Verpoorten et tous les autres, vous êtes exceptionnels ! Un immense merci également à Tim, que j'ai rencontré durant la dernière année de ma thèse, et qui m'a apporté un soutien sans limite pendant la période difficile de la rédaction. Quoi que tu fasses, je te souhaite tout le meilleur ! Un tout tout grand merci à Antoine de m'avoir filé un super coup de main pour la figure de conclusion ! Mec, t'es une star !

Enfin, en plus de la famille que j'ai choisi, il y a ceux qui ont toujours été là, et quelle chance j'ai de les avoir… Mes chers parents, merci pour tout ce que vous m'avez apporté, et toutes les fois où m'avez réconforté. Magali, ma grande sœur, mon rocher, mon moteur, merci pour tout. Merci encore à Magali et maman pour avoir corrigé les fautes de frappes et d'anglais. Je vous aime très fort !

Au microscope du BL3, tu auras été mon plus fidèle compagnon pendant cette aventure. Tu m'auras fait voir bien des déceptions, mais surtout beaucoup de belles choses. On se quitte en bons termes, mais il était temps que ça se termine !

Merci à NARILIS et en particulier à Virginie pour son aide, et pour m'avoir permis à de nombreuses reprises de me connecter à la communauté scientifique en organisant des séminaires, conférences et en m'ayant permis d'obtenir une bourse de voyage pour un congrès en Afrique du Sud.

Merci au FNRS de m'avoir fait confiance et d'avoir financé ce projet.

Merci également à tous les acteurs du projet SANA d'avoir généré cet élan de solidarité dans la lutte contre le Covid en mars 2020, j'ai été heureuse d'y avoir participé. Merci également à la ministre Valérie Glatigny d'avoir bataillé pour que les doctorants qui ont contribué à un effort collectif contre le Covid aient droit à une prolongation de financement.

Finally I thank all the jury members, Prof. M. Roop, Dr. C. Fumeaux, Prof. G. Laloux, Prof. L. Van Melderen and Prof. J.-Y. Matroule for their critical reading of the thesis and for their helpful suggestions to improve the manuscript.

TABLE OF CONTENTS

TABLE OF ABBREVIATIONS

αKG	α-ketoglutarate
ABC	ATP-binding cassette
aBCV	autophagic *Brucella-containing* vacuole
ACV	*Anaplasma-containing* vacuole
AICAR	5-amino-1-(5-phospho-D-ribosyl)imidazole-4-carboxamide
BAM	β-barrel assembly machinery
BCV	*Brucella-containing* vacuole
ChIP-seq	chromatin immunoprecipitation followed by deep-sequencing
EAA	Essential amino acids
ER	Endoplasmic reticulum
FCV	*Francisella-containing* vacuole
FDAAs	fluorescent D-amino acids
gDNA	genomic DNA
ICP-MS	Inductively coupled plasma-mass spectrometry
IGP	Imidazole glycerol phosphate
IGPD	Imidazole glycerol phosphate dehydratase
INF-γ	interferon-γ
KO	Knock-out
LCV	Legionella-containing vacuole
Ldt	LD-transpeptidase
LPS	lipopolysaccharide
mDAP	meso-diaminopimelic acid
Mn	Manganese
NAG	N-acetylglucosamine
NAM	N-acetylmuramic acid
NEAA	Non essential amino acids
Nramp1	natural resistance–associated macrophage protein 1
PBP	Penicillin binding protein
PCV	Pathogen-containing vacuole
PG	Peptidoglycan
R-LPS	rough lipopolysaccharide
ROS	Reactive oxygen species
S-LPS	smooth lipopolysaccharide
T4SS	Type 4 secretion system
TCA	Tricarboxylic acid
Tn-seq	Transposon sequencing
TRSE	Texas red-X succinimidyl ester
TSB	Tryptic soy broth
WT	Wild-type

INTRODUCTION

The study and characterization of histidine auxotroph mutants of *B. abortus* led us to explore many aspects of bacterial biology, including amino acid metabolism, cell morphology, envelope biogenesis and remodeling, cell division, but also metal homeostasis. We will therefore introduce all of these aspects in this Introduction, although they may seem *a priori* unrelated. Of course, we will also introduce *B. abortus* and its ability to hide inside host cells.

1. AMINO ACID METABOLISM AT THE HOST-BACTERIA INTERFACE

Animals represent a rich source of nutrients that can be exploited by bacteria, for better or worse. The access to nutrients is a driving force for symbiotic relationships between bacteria and animals which collaborate for the acquisition of food. Sometimes however the acquisition of food by some pathogenic bacteria is detrimental for the host: one of the partners exploits the other. The acquisition of amino acids, crucial building blocks for the synthesis of proteins, is at the heart of host-bacteria relationships, which can be tumultuous, passionate, tragic and fortunately sometimes harmonious.

1.1 Amino acids are key building blocks for life

Amino acids are the building blocks of proteins, and the amino acid sequence determines their structure and function. Amino acids also have specific functions once they are transformed, for example as hormones (histamine is synthesized from histidine, thyroxine from tyrosine and epinephrine from phenylalanine), melanin, porphyrin ring (heme) or the nicotinamide ring of NAD. They are also the precursors for nitrogen-containing compounds, such as the purines and pyrimidines (Nelson & Cox, 2017).

There are 20 proteinogenic amino acids. They can either be synthesized *de novo* or taken in from dietary sources. Humans cannot synthesize 8 of them: phenylalanine, valine, threonine, tryptophan, methionine, leucine, isoleucine, lysine, and histidine. Therefore, we need to acquire them from our diet, and we call them essential amino acids (EAA) (Young, 1994). The other amino acids can be synthesized *de novo*, and are thus called non-essential amino acids (NEAA). The essentiality of certain amino acids depends on the species. For example, bovines require less EAA because symbiotic bacteria in their rumen can synthesize some of them (Bergman, 1990).

In comparison with mammals, bacteria display a great metabolic plasticity. Their genomes encode many biosynthetic pathways that allow them to grow on very simple diets. Many bacteria are indeed able to synthesize all 20 AA, meaning that they can grow in the absence of any AA, provided that they have enough carbon and nitrogen sources to build them up (Nelson & Cox, 2017).

Another possible fate for the AA is degradation by oxidation to meet the energy needs of the cell. The degraded AA can be processed as fuel for the Tricarboxylic Acid (TCA) cycle. For example, glutamate is deaminated by the glutamate dehydrogenase to generate ammonia and α-ketoglutarate (αKG), an intermediate of the TCA cycle.

1.2 Amino acids at the heart of symbiotic interactions

Mammals lack many biosynthetic pathways that are present in other domains of life, and therefore they rely on a complex and varied diet to acquire all the building blocks they need. In most animals, this complex diet also comes with a complex intestinal flora, which allows them to harvest otherwise indigestible nutrients. In humans, the gut microbiota is often pictured as an organ *per se* and the gut microbiome*, i.e*. the genome of all the microorganisms living in the gut, would contain more than 100 times the number of genes in our own genome (Bäckhed et al., 2005). The importance of

microbiota for nutrition is even better illustrated in ruminants. These animals harbor a huge diversity of bacteria, protozoans but also archaea and fungi in their rumen, which is crucial for the nutrition of these organisms feeding mostly on polysaccharides. Microorganisms of the rumen provide 70 % of the daily energy requirement of its host, and synthesize essential amino acids and vitamins for them (Bergman, 1990).

In the precise case of amino acid metabolism, an interesting example of symbiosis is the close association of the aphid *Acyrthosiphon pisum* with its symbiont *Buchnera aphidicola*. These sap-feeding insects have evolved a very intimate symbiotic relationship that allows them to get all the required amino acids despite feeding on phloem, which is very poor in EAA but contains large amounts of NEAA (Figure 1) (Sandström & Pettersson, 1994). The obligate and mutualistic endosymbiont *B. aphidicola* is located within specialized insect cells named bacteriocytes, where it receives NEAA from its host (McLean & Houk, 1973). In turn, the bacteria, which are completely dependent on their host, are able to synthesize and supply EAA to their host (Figure 1 B). The partners are thus interdependent and complementary in terms of nutritional requirements (Sasaki & Ishikawa, 1995).

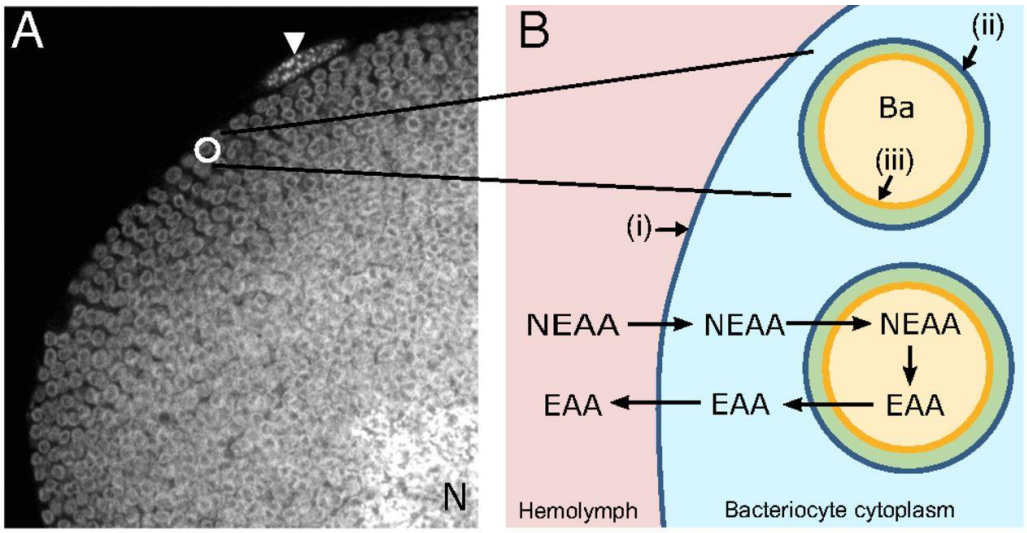

Figure 1. The aphid/*Buchnera* symbiotic boundary and the role in amino acid exchange. (A) *A. pisum* bacteriocytes each harbor thousands of bacterial endosymbionts (*Buchnera aphidicola*). A greyscale confocal (magnification: 630×) image showing DAPI-associated fluorescence (identifying nuclear and *Buchnera* DNA) through an *A. pisum* bacteriocyte packed full with *Buchnera* endosymbionts (visualized by their typical spherical shape, 3 µm in diameter). N represents the host nucleus. The arrowhead indicates a sheath cell on the bacteriocyte periphery. (B) Schematic representation of the aphid/*Buchnera* boundary highlighting the endosymbiotic paradigm, where the host supplies symbiont with NEAA and the symbiont provides host with EAAs. A series of membranes separate the hemolymph from the symbiont: (i) the aphid (host) bacteriocyte membrane (blue) separates hemolymph from bacteriocyte cytosol; (ii) the host-derived symbiosomal membrane (blue) separates each individual Buchnera from the bacteriocyte cytosol; (iii) the outer and inner membranes (yellow) of the Gram-negative *Buchnera*. Ba, *B. aphidicola* (adapted from (Feng et al., 2019)).

1.3 The fight for amino acids: when bacteria feed on their host

The relationship between animals and bacteria is regrettably not always profitable, as mentioned before. Some bacteria take advantage of their host, without giving them something in exchange, and sometimes even causing them harm. Along the evolution, some pathogenic bacteria have become highly dependent on their animal hosts. Us, humans that have lost the ability to make many metabolites by ourselves as we became dependent on our microbiomes and a complex and varied diet. Similarly, "specialist" pathogenic bacteria that are very well adapted to their host do not need to spend energy building up what is available around them. Those bacteria therefore have lost certain functions or metabolic pathways that were not useful anymore inside their host. Genomic reduction is indeed recurrent in the evolution of pathogenic bacteria, especially in obligate intracellular bacteria (Moran, 2002; Olive & Sassetti, 2016).

Legionella pneumophila is an intracellular Gram-negative bacterium that replicates within aquatic amoeba. Upon the inhalation of contaminated aerosols by a human host, *L. pneumophila* can be internalized by alveolar macrophages where it replicates in a similar fashion as in amoeba (Swanson & Hammer, 2000), inside a vacuole called *Legionella*-containing vacuole (LCV) which is derived from rough endoplasmic reticulum (ER) vesicles. The bacterium translocates around 300 effectors into the host cell via its type IV secretion system, subsequently allowing it to avoid lysosomal fusion. *L. pneumophila* is auxotrophic for seven amino acids: leucine, isoleucine, methionine, valine, threonine, cysteine and arginine (Price et al., 2014). However, it is able to efficiently manipulate the host cell to serve up amino acids directly into the LCV. First, *L. pneumophila* induces the upregulation of the host amino acid transporter SLC1A5 (Wieland et al., 2005). Moreover, *Legionella* uses the host proteasome to generate free amino acids for itself. The effector AnkB is secreted and anchored at the LCV surface and acts as a platform for proteasomal degradation of polyubiquitinated proteins by interacting with the host SCF1 ubiquitin ligase (Price et al., 2011). Host protein degradation provides the pathogen with the amino acids it needs (Figure 2).

Francisella tularensis and *Anaplasma phagocytophilum* both manage to obtain amino acids from their host cell by manipulating autophagy. *F. tularensis* has to scavenge nutrients from the host cell as it is auxotrophic for 13 amino acids (Steele et al., 2013). The bacterium is first internalized by phagocytosis and it then escapes the phagosome to reach the cytosol. Thanks to a type VI secretion system, *F. tularensis* induces ATG5-independent macroautophagy, which is required for intracellular multiplication (Figure 2). Failure to replicate due to inhibition of macroautophagy can be rescued by supplying excess pyruvate or amino acids, which supports the idea that this process is hijacked to provide nutrients to the pathogen (Steele et al., 2013). *A. phagocytophilum* is a tick-borne obligate intracellular pathogen and it proliferates in an autophagosome-like compartment. The effector protein Ats-1 is secreted in the cytosol via the type IV secretion system and binds Beclin-1, which is involved in autophagosome nucleation. Newly formed autophagosomes fuse with the *A. phagocytophilum*-containing vacuole (ACV), feeding the pathogen with amino acids (Figure 2) (de la Fuente et al., 2017; Niu

et al., 2012) For *F. tularensis* and *A. phagocytophilum,* manipulation of autophagy would be also a way to override iron starvation (Best & Abu Kwaik, 2019).

In contrast to *Legionella, Anaplasma* and *Francisella*, some intracellular pathogens maintain broad biosynthetic abilities, despite their adaptation to intracellular survival. *Salmonella typhimurium*, *Mycobacterium tuberculosis* and *Brucella abortus,* for example are able to synthesize the full set of amino acids. These intracellular bacteria evolve in a pathogen-containing vacuole (PCV) which is poor in amino acids. Therefore, the ability to synthesize amino acids is crucial for intracellular survival and persistence (Zhang & Rubin, 2013).

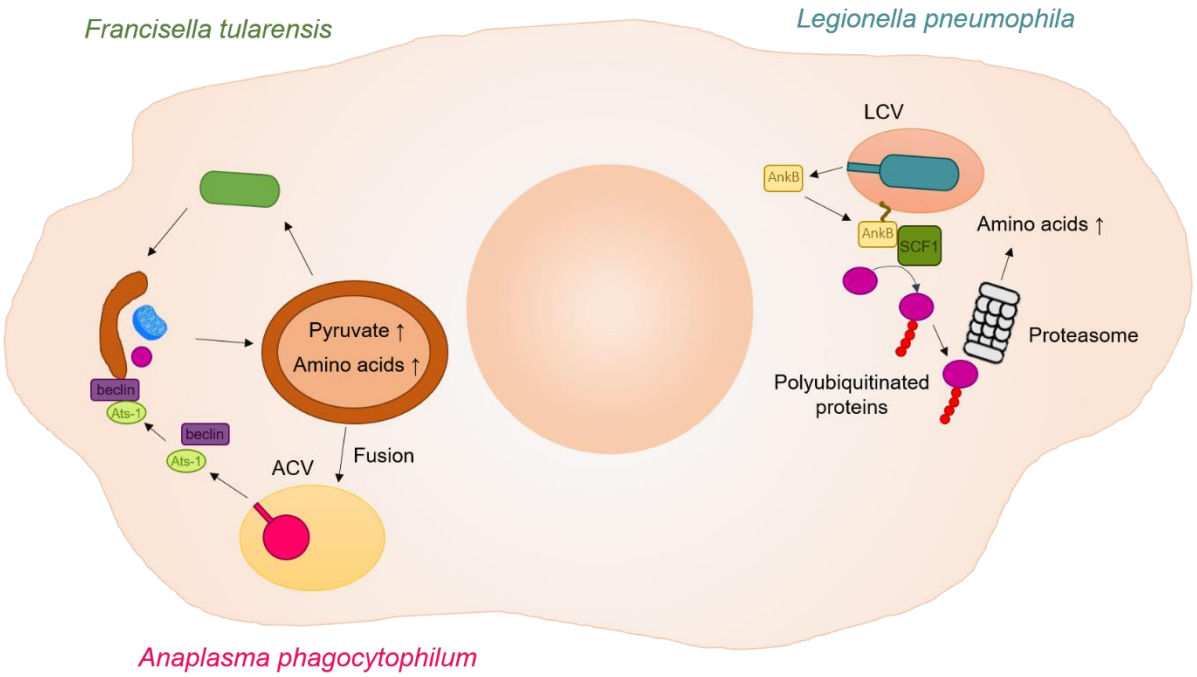

Figure 2. *Francisella tularensis*, *Legionella pneumophila* and *Anaplasma phagocytophilum* exploit host machineries to obtain amino acids. *F. tularensis* induces macroautophagy in the host cell to acquire amino acids and pyruvate. *A. phagocytophilum* injects the Ats-1 effector through its type 4 secretion system (T4SS) to recruit beclin and induce host autophagy. The fusion of autophagosomes with the *A. phagocytophilum*-containing vacuole (ACV) feeds the bacterium with amino acids. *L. pneumophila* increases the amino acid availability in the *Legionella*-containing vacuole (LCV) by recruiting the proteasome close to the LCV surface. The T4SS effector AnkB induces protein ubiquitination and proteasomal degradation by recruiting the ubiquitin ligase SCF1.

2. *BRUCELLA ABORTUS*, AN ALPHAPROTEOBACTERIUM WITH A PATHOGENIC LIFESTYLE

2.1 Alphaproteobacteria are a very diverse group of bacteria

Alphaproteobacteria have very diverse lifestyles. They comprise intracellular animal pathogens, some of which are obligate (*Rickettsia, Anaplasma*) and others facultative (*Brucella, Bartonella*). Other alphaproteobacteria are associated with vegetal hosts, as symbionts (*Rhizobium, Sinorhizobium*, …) or pathogens (*Agrobacterium*), and others are insect or nematode symbionts (*Wolbachia*). In general, alphaproteobacteria have a close relationship with eukaryotic cells, which is further exemplified by the fact that the ancestor of mitochondria was also probably from this group, or closely related (Gray et al., 1999). However, some bacteria from this group are free-living, such as for example bacteria from the genus *Caulobacter, Ochrobactrum* and *Rhodobacter* (Teyssier et al., 2004).

The group of the alphaproteobacteria is further divided into several orders, including the Rickettsiales and the Rhizobiales. Members of the order Rickettsiales display a very high genetic divergence, but apart from a few rare exceptions they have all converged towards a strict pathogenic lifestyle. Accordingly, they also have genomes of reduced size. On the contrary, bacteria from the Rhizobiales are adapted to many different lifestyles, although they show a rather low genetic divergence. Among them, bacteria of the genus *Brucella* are intracellular pathogens of animals (Muñoz-Gómez et al., 2019; Teyssier et al., 2004).

2.2 The genus *Brucella* and brucellosis

Bacteria of the genus *Brucella* are responsible for a worldwide zoonosis termed brucellosis, which affects a wide range of mammals including humans (G. Pappas et al., 2006). 12 species of the genus *Brucella* have been identified so far, and each one has a preferred host (Figure 3) (Godfroid, 2018). “Classical” species have been first isolated from infected domestic animals (cows, sheep, goats, pigs, camels, reindeer, and dogs) (Moreno, 2014). More recently, *B. abortus* which typically infects cattle, has also been found to infect wild land animals such as bisons and elks (Kamath et al., 2016). Other “Atypical” species have been identified in wild land animals such as hares, foxes, and rodents and sea mammals (dolphins, whales, seals, and walruses) (Guzmán-Verri et al., 2012; Whatmore & Foster, 2021). Animal brucellosis is characterized by epididymitis in males or placentitis and abortion in pregnant females (Carvalho Neta et al., 2010). Extensive proliferation of the bacteria in the placenta of a pregnant mammal can ultimately cause its disruption, leading to abortion or the birth of a weak and infected offspring (Roop et al., 2009). The contaminated expelled fetus contains high loads of bacteria, and bacteria can rapidly disseminate from one animal to another (Moreno & Moriyón, 2006).

The “classical” species *B. melitensis*, *B. suis, B. abortus*, and *B. canis* can also accidentally infect humans and cause a debilitating disease named “undulant fever” or Malta fever (Moreno & Moriyón, 2006). The main clinical manifestations of this disease

are undulant fever and weakness. In the absence of treatment, human brucellosis becomes chronic and can lead to musculoskeletal, cardiac and neurological complications (Dean et al., 2012). However, human brucellosis is usually not transmitted from person to person and can be treated with antibiotics. Humans are typically infected by ingestion of dairy products or by direct contact with infected animals (G. Pappas et al., 2006).

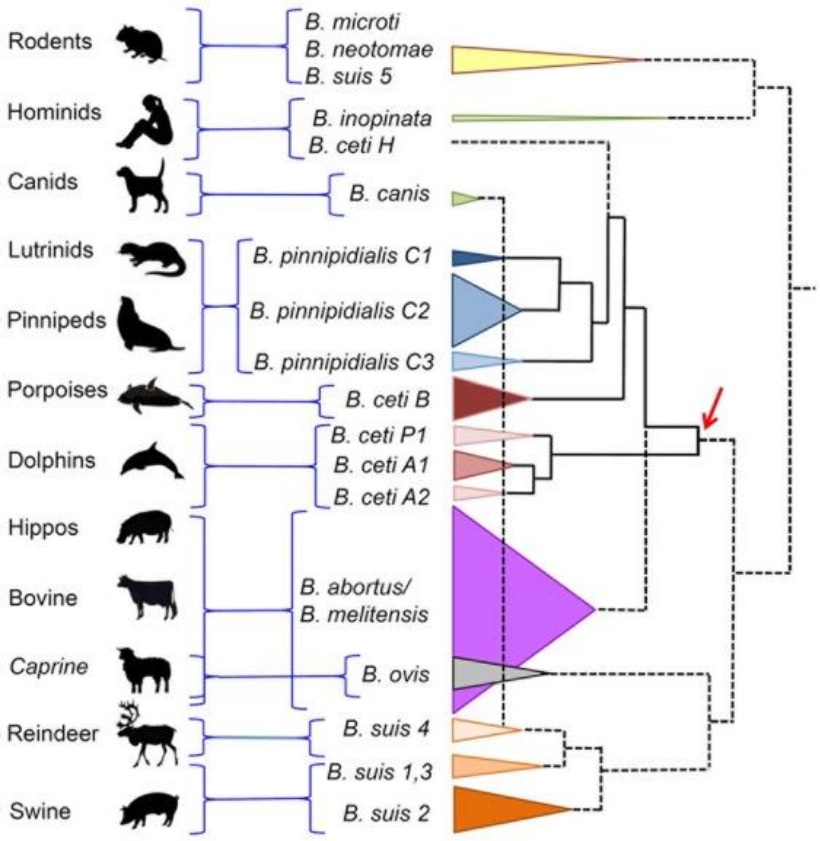

Figure 3. Dispersion of *Brucella* species and their preferred host mammal. *Brucella* cladogram was estimated from MLVA-16 published values (http://minisatellites.u-psud.fr/MLVAnet/login.php?&largeur=1680). The dispersion of the various *Brucella* species is depicted as cones proportional to the number of strains analyzed. The arrow indicates the proposed dispersion of the clade that gave origin to *B. ceti* strains. Notice that according to this proposal, the *B. ceti* B porpoise type is closer to the *B. pinnipedialis* C clusters than to the *B. ceti* dolphin types A1, A2, and P1. *B. suis* biovar 2 also has affinity for hares (lagomorphs) (adapted from (Guzmán-Verri et al., 2012)).

2.3 A furtive pathogen hiding inside

Brucella spp. are often referred to as facultative intracellular parasites, but it would be more appropriate to term them "facultatively extracellular intracellular parasites" (Moreno & Moriyon, 2002). Indeed, even if they are relatively easy to cultivate on rich media, these bacteria are almost exclusively found intracellularly inside their host (Moreno & Moriyón, 2006). During their dissemination, *Brucella* are briefly released in the environment, unlike other Rhizobiales such as *Bartonella* which are transmitted by

a vector. Accordingly, the genome of *Brucella* spp. is approximately three times bigger than the genome of *Bartonella* spp. (Teyssier et al., 2004).

2.3.1 An intracellular and furtive pathogen

Brucella are able to survive and replicate inside a variety of host cells. These bacteria notably successfully replicate inside professional phagocytes such as macrophages or dendritic cells (Archambaud et al., 2010). On the one hand, these phagocytes provide *Brucella* with a replicative niche protected from components of the immune system such as antibodies and complement, and on the other hand, *Brucella* use these cells as vehicles for their systemic dissemination (Roop et al., 2009). *Brucella* also invade and replicate inside placental trophoblasts in pregnant mammals (Moreno, 2014).

Many intracellular pathogens evolve towards genomic reduction after long periods of coevolution with their hosts (Yu et al., 2009). As mentioned previously, the genome of *Brucella* is relatively big in comparison with other intracellular pathogens (Teyssier et al., 2004). Indeed, *Brucella* have broad biosynthetic abilities and are notably prototrophic for all amino acids (Wattam et al., 2012). This ability of *Brucella* to synthesize essential building blocks on its own could be correlated with its furtive infection style (Teyssier et al., 2004). Indeed, unlike bacteria with reduced genomes that are entirely dependent on their host, *Brucella* do not overexploit their host cells. Accordingly, *Brucella* are able to persist for a long time inside a host and to escape the immune system.

2.3.2 The journey inside macrophages

The mechanism underlying the entry of *Brucella* into macrophages and dendritic cells is still unclear. Nevertheless, interactions with the O-chain of smooth lipopolysaccharide (S-LPS) and lipid rafts have been suggested to be required for successful replication and survival inside the cells (Naroeni & Porte, 2002). Rough mutants which lack the O-chain do not enter via the lipid rafts and were reported to be rapidly degraded by phagosome-lysosome fusion (Porte et al., 2003). Following successful entry into its host cell, *Brucella* is enclosed in a membrane-bound compartment named *Brucella*-containing vacuole (BCV). In macrophages and epithelial cells, the BCV transiently and sequentially interacts with the endocytic pathway, resulting in the acquisition of markers of the early and late endosomes (Figure 4) (Celli et al., 2003; Starr et al., 2008). The BCV also undergoes acidification to pH 4-4.5, but lysosomal hydrolases have never been detected inside the BCV, suggesting that interactions between BCV and lysosomes are restricted, although not completely inhibited (Celli, 2015). BCV acidification is determinant for further survival of *Brucella* inside the cell because it provides a signal for the induction of a major virulence factor, the VirB type IV secretion system (Starr et al., 2008). This apparatus allows *Brucella* to reach its replicative niche. Indeed, following BCV acidification and subsequent *virB* expression, the BCV segregates from the endosomal pathway and undergoes sustained interaction with the ER (Figure 4). After approximately 12 h post-infection, *Brucella* eventually replicates inside ER-derived vacuoles bearing the ER

markers (calreticulin, calnexin and Sec61β) in most cell types tested so far (Celli et al., 2003; Starr et al., 2008).

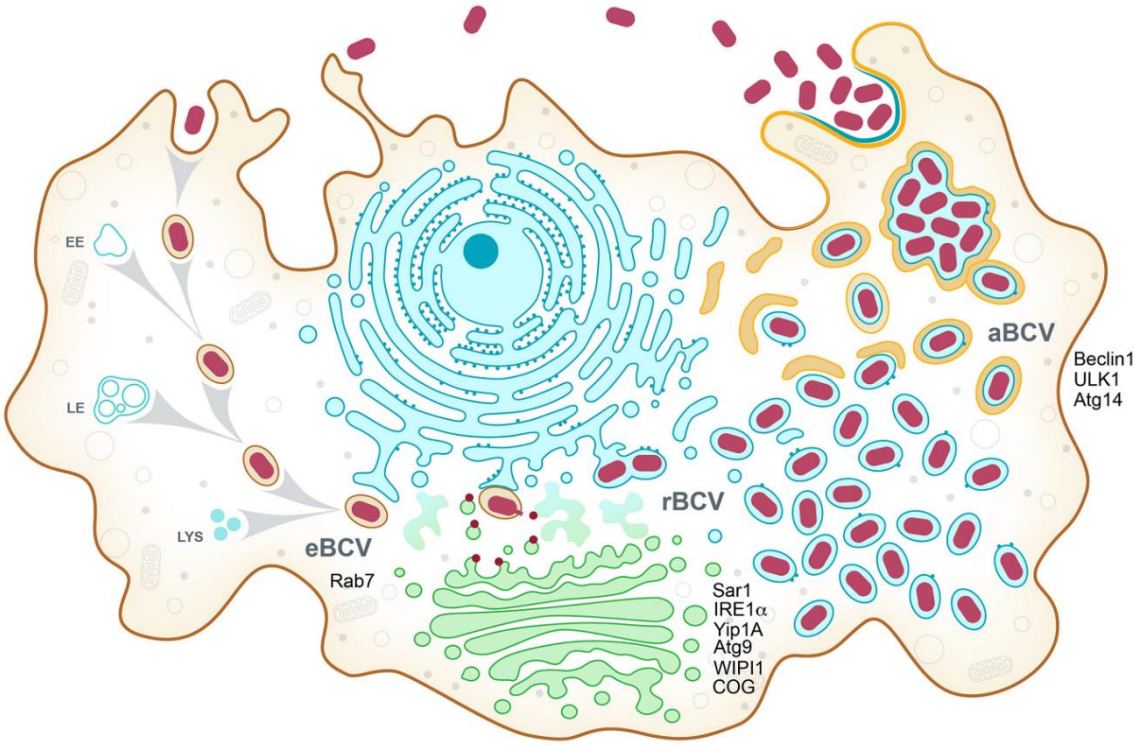

Figure 4. Model of the *Brucella* intracellular cycle in macrophages. Following phagocytic uptake by macrophages, *Brucella spp*. reside in the first 8 to 12 h post infection within a membrane-bound vacuole that undergoes endosomal maturation via sequential interactions with early (EE) and late (LE) endosomes and lysosomes (LYS) to become an acidified, endosomal *Brucella*-containing vacuole (eBCV). The host small GTPase Rab7 contributes to eBCV maturation, which provides physicochemical cues promoting expression of the VirB Type IV secretion system (T4SS), which translocates effector proteins (red) that mediate eBCV interactions with ER exit sites and acquisition of ER and Golgi-derived membranes. These events lead to the biogenesis of replication permissive, ER-derived BCVs, called replicative BCVs (rBCVs). The host proteins Sar1, IRE1α, Yip1A, Atg9, WIPI1 and the COG complex contribute to rBCV biogenesis. Bacteria then undergo extensive replication in rBCVs between 12 and 48 h post-infection, after which rBCVs are captured within autophagosome-like structures in a VirB T4SS-dependent manner, to become autophagic BCVs (aBCVs). The aBCV formation requires the host autophagy proteins Beclin1, ULK1 and Atg14. The aBCVs harbor features of autolysosomes and are required for bacterial egress and new cycles of intracellular infections (Celli, 2019).

Brucella egress and the cell-to-cell spreading relies on the final transition of the rBCV into an autophagic compartment, called the autophagic BCV (aBCV) (Starr et al., 2012).

Brucella intracellular trafficking can be roughly divided into two distinct phases: one non-proliferative and one replicative. During the first phase of the infection, *Brucella* traffics along the endocytic pathway, interacting with endosomes (Celli et al., 2003; Starr et al., 2008). This phase is characterized by growth arrest of the bacteria and their blockage in the G1 step of their cell cycle (Deghelt et al., 2014). The second step of infection is characterized by proliferation of *Brucella* in ER-derived vacuoles. This biphasic trafficking has been observed in professional phagocytes such as macrophages, as well as in HeLa cells. Because the trafficking of *Brucella* has been well characterized in HeLa cells and seems to recapitulate what was observed in RAW 264.7 macrophages, although with slightly different kinetics, HeLa cells are often considered as a good cellular model of infection as these cells are easier to manipulate for microscopy experiments (Celli, 2015).

During the non-proliferative phase, *Brucella* endure harsh conditions including exposure to reactive oxygen species (ROS) and nutrient starvation (Roop et al., 2009). Accordingly, the stringent response regulator Rsh, which synthesizes the alarmone guanosine tetra- or penta-phosphate ((p)ppGpp) in response to amino acid starvation, is required during infection of macrophages by *B. melitensis* and *B. abortus* (Dozot et al., 2006; Van der Henst et al., 2020). The stringent response is also proposed to participate in the regulation of the expression of the major virulence factor of *Brucella*, VirB (Dozot et al., 2006). This finding emphasize the importance of sensing the environment for successful replication inside host cells. Besides, nutritient starvation might be an important signal for *Brucella* to control virulence factors.

3. HOW DO BACTERIA STAY IN SHAPE?

Along their cell cycle, bacterial cells double their size before they eventually divide. The cellular envelope must grow in order to increase in size and finally divide to generate daughter cells, while maintaining the same morphology for generations. A fundamental determinant of cell shape is the peptidoglycan (PG).

3.1 Peptidoglycan structure and synthesis

The PG confers strength to the cell wall and maintains cell shape and size. It protects bacteria from osmotic pressure and environmental stressors. PG is composed of polysaccharide strands connected covalently by peptide bridges and forms a net-like structure that surrounds the cell. In Gram-negative bacteria, the PG cell wall is located in the periplasmic space between the outer and inner membranes (Figure 5). The synthesis of PG will be briefly explained as it was described in the model bacterium *E. coli*.

The elongation of PG starts with the cytoplasmic formation of a disaccharide precursor consisting in two amino sugars, N-acetylglucosamine (NAG) and N-acetylmuramic acid (NAM), the latter being decorated with a pentapeptide composed of L-alanine (L-Ala), D-glutamic acid (D-Glu), meso-diaminopimelic acid (mDAP) and two D-alanines (D-Ala) (Figure 5) (Labischinski et al., 1979). This precursor is attached to the carrier lipid undecaprenyl pyrophosphate and is called lipid II in its lipid-linked form. The lipid II is then flipped across the inner membrane.

In the periplasm, the disaccharide unit of lipid II is first incorporated into an existing glycan strand by a β-1,4 glycosidic bond in a process called transglycosylation. The transglycosylase activity is performed by class A PBPs (Sauvage et al., 2008). Class A and class B PBPs connect the neighboring strands by peptide bridges via D,D-transpeptidation (Figure 5). The DD-transpeptidases catalyze the formation of a covalent bond between the fourth residue of one peptide and the third residue of another chain (4 → 3 cross-links) (Labischinski et al., 1979). In *E. coli*, DD-transpeptidases catalyze the formation of a covalent bond between the free amino group of mDAP at position 3 of one pentapeptide and the carboxyl group of D-alanine on position 4 of the neighboring strand (Figure 5). Class B PBPs are also called monofunctional PBPs as they only perform transpeptidation reactions. In *E. coli*, the monofunctional PBP2 is dedicated to elongation whereas another monofunctional PBP, PBP3 (also called FtsI), is specifically involved in division (Den Blaauwen et al., 2003; Weiss et al., 1999).

LD-transpeptidases (Ldts) form 3 → 3 cross-links (Figure 5) that represent ~5–15 % of the peptide cross-links in *E. coli* (Glauner et al., 1988; Magnet et al., 2008). This percentage of 3 → 3 and 4 → 3 cross-links varies between bacterial species (Cochrane & Lohans, 2020; Zhao et al., 2017). The transpeptidation reactions provide a strong mesh that will define the shape of the cell.

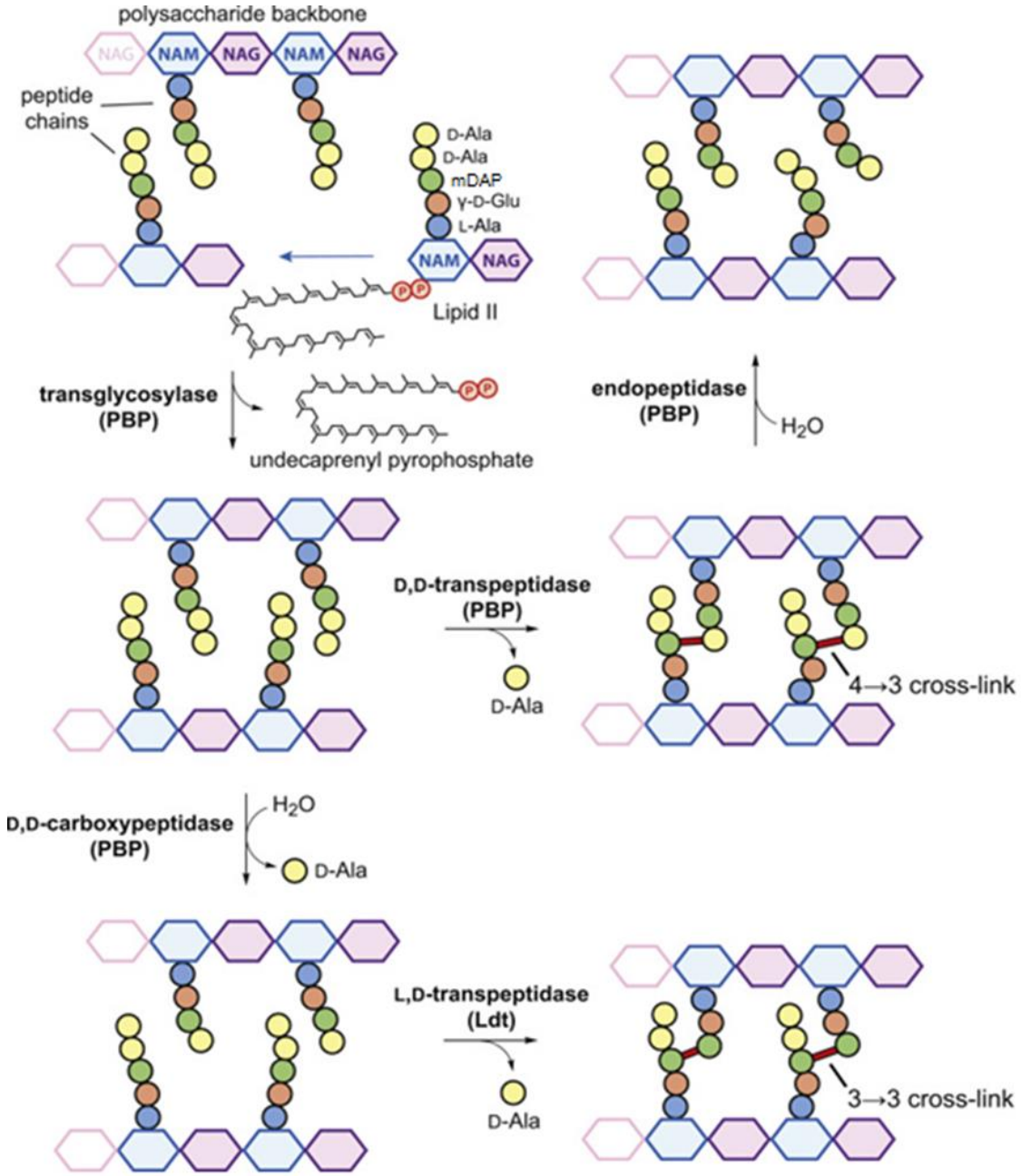

Figure 5. Overview of the roles of penicillin-binding proteins and LD-transpeptidases in bacterial PG synthesis and degradation. Penicillin-binding proteins (PBPs) with transglycosylase activity incorporate the disaccharide core of lipid II into a growing glycan strand. Then, the transpeptidase domain of a PBP may form 4 → 3 cross-links between peptide strands (DD-transpeptidase activity). Other PBPs cleave these cross-links (endopeptidase activity), or cleave the terminal D-Ala residue from the peptide (DD-carboxypeptidase activity). The product of the carboxypeptidase may then be accepted by LD-transpeptidases (Ldts), forming 3 → 3 peptide cross-links. The peptidoglycan shown here represents a form occurring primarily in Gram-negative bacteria, in which the pentapeptide chain bears a meso-diaminopimelic (mDAP) residue in the third position. NAM and NAG refer to *N*-acetylmuramic acid and *N*-acetylglucosamine, respectively (adapted from Cochrane & Lohans, 2020).

The class C PBPs include carboxypeptidases and endopeptidases, which can further modify the PG structure by hydrolytically removing the terminal residue of the peptide chain and cleaving the peptide cross-links, respectively (Figure 5).

3.2 Peptidoglycan incorporation during growth and division

In the majority of bacteria, elongation and division are performed by two distinct machineries, the elongasome and the divisome. These two machineries share some similarities. They are both associated with cytoskeletal proteins and they consist on the one hand of enzymes that synthesize the cytoplasmic precursors of the PG and on the other hand of the periplasmic PBPs that perform transglycosylation and transpeptidation reactions. Both the elongasome and the divisome also comprise PG hydrolases that allow the insertion of new PG by breaking the existing bonds in a tightly controlled way. PG expansion relies on a complex balance between remodeling, recycling and elongation.

3.2.1 The classical picture

During growth, the most studied Gram-negative bacterium *E. coli* incorporates new PG along the sidewalls of the cell. The elongasome is scaffolded by the actin homologue MreB, which forms filaments in an ATP-dependent way (van den Ent et al., 2014). MreB acts as a platform together with MreC, MreD, RodA and RodZ to guide the incorporation of the new PG (White & Gober, 2012). This multiprotein complex links the cytoplasmic MurA → G proteins, that synthesize the PG precursors, with the periplasmic PBPs that proceed to PG elongation. The elongasome comprises two PBPs that are specific to elongation: the monofunctional transpeptidase PBP2 and the bifunctional (transpeptidase and transglycosylase) PBP1A (Figure 6 A) (Typas et al., 2011). More recently, it was shown that RodA also have a transglycosylase activity, and works in concert with PBP2 in *E. coli* to elongate glycan chains (Meeske et al., 2016; Rohs et al., 2018).

The assembly of the divisome is roughly divided in two steps. The first step consists in the formation of the Z-ring at mid-cell by the tubulin prokaryotic homologue FtsZ (Lutkenhaus, 2007). FtsA, ZipA, EzrA, and the Zap proteins anchor the Z-ring to the inner membrane, and are referred to as “early division proteins” (Figure 6 B) (Aarsman et al., 2005). The septum formation is led by the contraction of the Z-ring, and is accompanied by the synthesis of septal PG by the so-called “late division proteins”. The monofunctional PBP3 transpeptidase is specifically involved in septal PG synthesis (Weiss et al., 1999). MurJ and FtsW both contribute to the translocation of the lipid II from the cytoplasm to the periplasmic space. Althought FtsW was initially thought to be a flippase, it appears that MurJ is more likely to fulfil this function (Egan et al., 2020). Instead, FtsW, a RodA homologue, also has a glycosyltransferase activity and would also contribute to PG elongation during division, together with PBP3 (Taguchi et al., 2019). Another PBP, the bifunctional transglycosylase/transpeptidase PBP1B contributes to septal PG synthesis (Bertsche et al., 2006). The coordinated action of these division proteins, together with multiple other Fts proteins (Figure 6 B) allow the generation of two identical daughter cells.

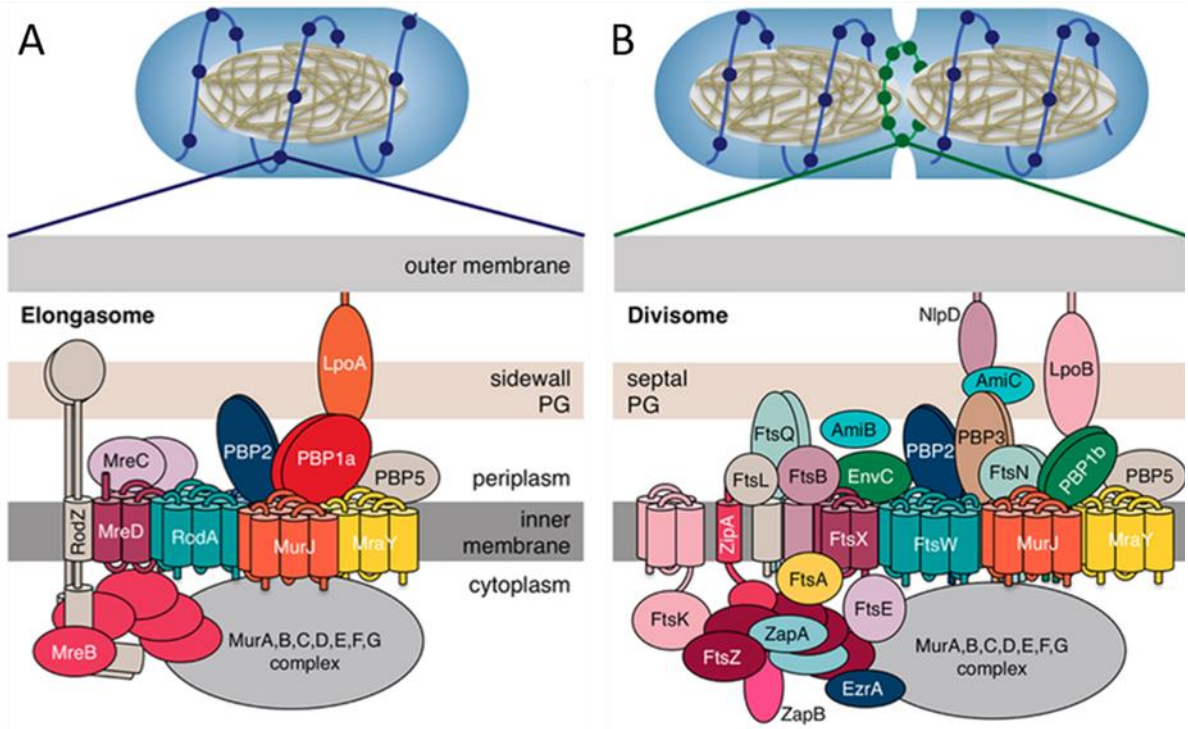

Figure 6. Complexes responsible for peptidoglycan synthesis during lateral elongation and division. A. The elongasome protein complex forms at the lateral sidewalls and facilitates sidewall expansion. The elongasome tracks along the lateral sidewall (see blue line). B. The divisome protein complex forms at the midcell and facilitates septation. The divisome tracks along the midcell (see green line).Copyright 2016 eLife Sciences Publications (https://creativecommons.org/licenses/by/4.0/) (adapted from (Dik, 2018 #145))

3.2.2 A different growth mode in the Rhizobiales: unipolar growth

Many rod-shaped bacteria including *E. coli* grow by lateral insertion of new material along the sidewalls, in a so-called “dispersed elongation” mode of growth (Figure 7 A). In contrast, bacteria can also synthesize new cell wall material in spatially restricted zones, leading to polar or zonal growth. Bacteria such as *Corynebacterium* (Daniel & Errington, 2003) and *Mycobacterium* (Chauhan et al., 2006) display bipolar growth (Figure 7 C). Some representative members from the Rhizobiales such as *Agrobacterium tumefaciens, Sinorhizobium meliloti* and *Brucella abortus* grow only from one pole (Figure 7 B) (Brown et al., 2012).

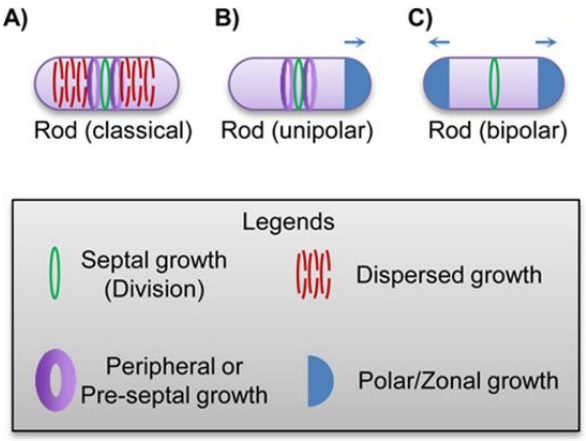

Figure 7. Different ways of generating a rod. **A.** The dispersed elongation model in which new material is uniformly incorporated into the side wall (Red dashed rings). In *E. coli* and *C. crescentus*, a specialized type of growth called pre-septal growth also contributes to elongation (Purple bands). **B.** Unipolar growth elongates the cell body in a "budding" fashion (Blue cap). In *A. tumefaciens*, pre-septal elongation occurs and defines the future sites of active polar growth (Purple bands). **C.** Some Actinobacteria species elongate the cell body in a bi-polar fashion (Blue caps) (adapted from (Jiang et al., 2015)).

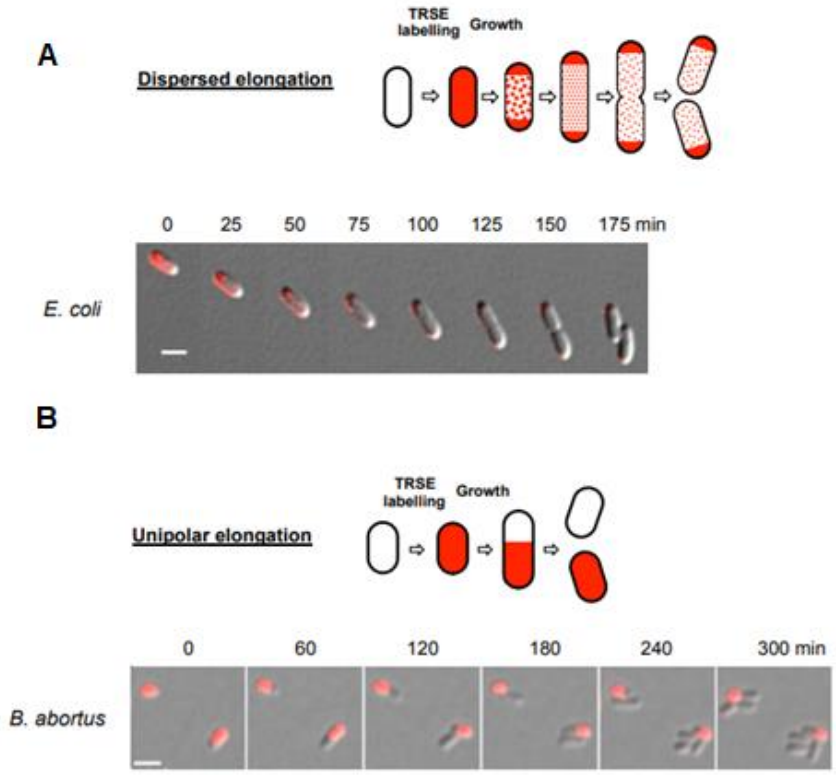

Figure 8. Comparison between dispersed and unipolar elongation. Model and time-lapse microscopy of dispersed elongation monitored by Texas red-X succinimidyl ester (TRSE) labeling in *E. coli* (A), in comparison to unipolar growth in *B. abortus* (B) (adapted from (Brown et al., 2012)).

The existence of a unipolar growth mode was discovered by comparing the growth pattern of *E. coli* with *A. tumefaciens* and several other members of the Rhizobiales (including *B. abortus*) after treatment with Texas red-X succinimidyl ester (TRSE), a dye which supposedly binds covalently to the amine groups of cell surface proteins (Brown et al., 2012). When *E. coli* is growing by dispersed elongation, new unlabeled material is inserted homogeneously along the sidewalls, leading to a dilution of the TRSE labeling (Figure 8). In contrast, during elongation in Rhizobiales, new unlabeled material is inserted only at one pole, namely the new pole, whereas the main body of the cell remains inert. The two generated daughter cells are therefore asymmetrical, as one of them displays a completely new envelope and the other one consists of "old" cell envelope material. The use of fluorescent D-amino acids (FDAAs) such as HADA to visualize the sites of nascent PG incorporation revealed the same growth patterns in *A. tumefaciens* (Kuru et al., 2012) (Figure 9).

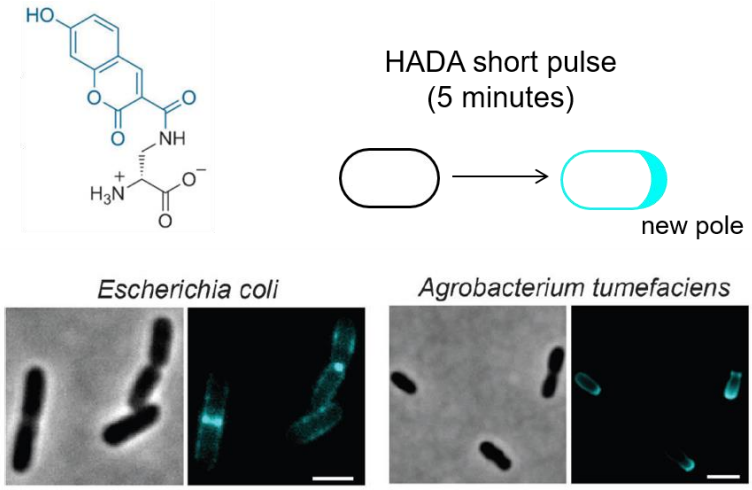

Figure 9. Short pulse-labeling of PG insertion sites with HADA. Polar insertion of HADA labels the new pole. *E. coli* shows dispersed insertion of PG along the sidewalls or at constriction sites at midcell. In *A. tumefaciens*, new PG is inserted at the growing pole and/or at the constriction site (adapted from (Kuru et al., 2012)).

As explained in the previous section, the mechanisms of elongation and division have been extensively characterized in *E. coli* and other model species growing by dispersed elongation. The picture is however much less clear in polar growing bacteria.

In Gram-positive bacteria from the phylum Actinobacteria, which comprises *Streptomyces* and *Corynebacteria*, the polar protein DivIVA provides a platform for polar PG elongation. DivIVA would recognize negative membrane curvature and organize the elongation machinery in growing poles (Flärdh, 2003; Fuchino et al., 2013; Hempel et al., 2008; Kang et al., 2008; Letek et al., 2009). Strikingly, Rhizobiales lack most actors from the elongasome including MreB, MreC, MreD and RodA (Margolin, 2009). In the Rhizobiales, the identity of a polar scaffolding protein for PG elongation remains uncertain. A potential candidate for this function would be the polar-organization protein PopZ, a polar protein which is conserved in that group. PopZ was shown to be localized at the growing pole and then relocalized to the newly generated growing poles directly after division in *A. tumefaciens* (Grangeon et al., 2015). PopZ is also crucial for cell cycle and polarity in *C. crescentus* (Ebersbach et al., 2008).

In contrast to *E. coli*, inhibition of cell division in *A. tumefaciens* either resulting from thermosensitive mutants or after treatment with antibiotics targeting components of the divisome results in branches instead of filamentation, which is typically observed in

E. coli (Fujiwara & Fukui, 1974; Latch & Margolin, 1997a). These branches probably result from the duplication of one or several growth poles. A similar branching phenotype was also observed in a *B. abortus* CtrA depletion strain (Figure 10) (Francis et al., 2017). CtrA is an essential master regulator of cell cycle progression, exclusively present in Alphaproteobacteria and well conserved among them (Brilli et al., 2010). Many direct targets of this transcription factor have been identified by chromatin immunoprecipitation followed by deep sequencing (ChIP-seq) (Francis et al., 2017), but the molecular mechanism underlying division in *B. abortus* remains largely undetermined.

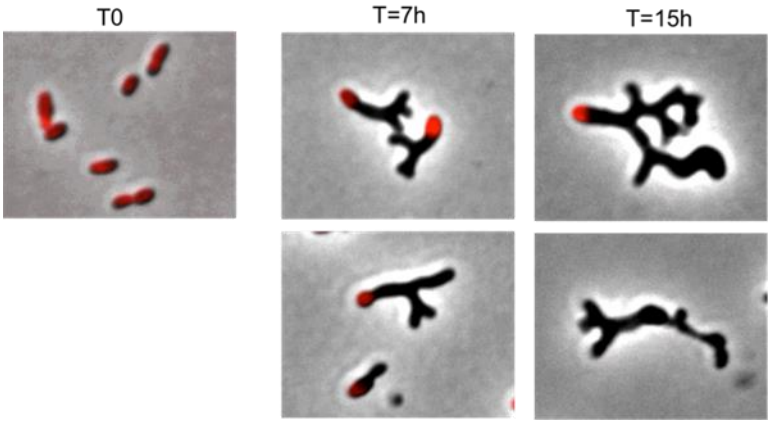

Figure 10. CtrA depletion generates cell division defects in *B. abortus*. CtrA depletion strain labeled with TRSE and grown without IPTG for 7 and 15 h forms branches. TRSE binds covalently to the bacterial cell surface. Growth occurring after TRSE labeling results in the incorporation of unlabeled envelope material (adapted from (Francis et al., 2017)).

In comparison with *E. coli*, the PG of Rhizobiales comprises a higher percentage of 3 → 3 cross-links (more than 50 % in *A. tumefaciens* against 5 to 15 % in *E. coli*), that are formed by Ldts. Accordingly, *B. abortus* and *A. tumefaciens* encode an important number of genes coding for Ldts. There could be a correlation between the high proportion of 3 → 3 cross-links and polar growth (Brown et al., 2012).

A. tumefaciens and *B. abortus* also lack the PBP2 which is associated with PG elongation in *E. coli*. The genome of *A. tumefaciens* contains genes predicted to encode four bifunctional PBPs (PBP1A, PBP1B1, PBP1B2, and PBP1C) and two monofunctional PBPs (PBP3A and PBP3B) (Cameron et al., 2014). It was suggested that PBP1A would be dedicated to polar elongation, and PBP3A and PBP3B would be required for division. Indeed, PBP1A is localized at the growing pole during most of the cell cycle, whereas PBP3A and PBP3B are localized at mid-cell during division (Cameron et al., 2014).

B. abortus only encodes one predicted monofunctional PBP, *pbp3* or *ftsI,* located in a "division and cell wall" genomic cluster. FtsI was localized both at elongation and division sites in *B. abortus* (Mike Deghelt, PhD thesis, 2014).

3.3 Peptidoglycan hydrolases: the cell's tailors

Cell separation is a very complex process that ultimately leads to the generation of two daughter cells from one initial bacterium. Septum cleavage during division requires the coordinated and controlled activity of enzymes that synthesize and hydrolyze PG. This

process is particularly dangerous because it requires the hydrolysis of the PG, which could cause cell lysis if not tightly regulated, because of the turgor pressure.

3.3.1 Classes of peptidoglycan hydrolases

There are three main classes of PG hydrolyzing enzymes. Lytic transglycosylases (1) cleave the glycosidic bonds between NAM and NAG sugars. Amidases (2) cleave the amide bond between NAM and the peptide side chain, and finally endopeptidases and carboxypeptidases (3) hydrolyze peptide bonds within and between the peptide side chains (Figure 11).

In *E. coli*, PG cleavage during cell separation is mostly performed by three amidases, AmiA, AmiB and AmiC. A mutant lacking all three amidases displays a cell-chaining phenotype (Heidrich et al., 2001). To ensure that amidases are only active during cell separation, they are kept inactive by an auto-inhibitory loop (Rocaboy et al., 2013). Interaction of the amidases with the LytM factors EnvC and NlpD causes a conformational change that allows the activation of the amidase and the resulting hydrolysis of the peptide side chains (Uehara et al., 2009). The LytM factors EnvC and NlpD are catalytically inactive endopeptidases that are themselves recruited to the division site by FtsN and FtsEX (Cook et al., 2020; Rocaboy et al., 2013; Schmidt et al., 2004).

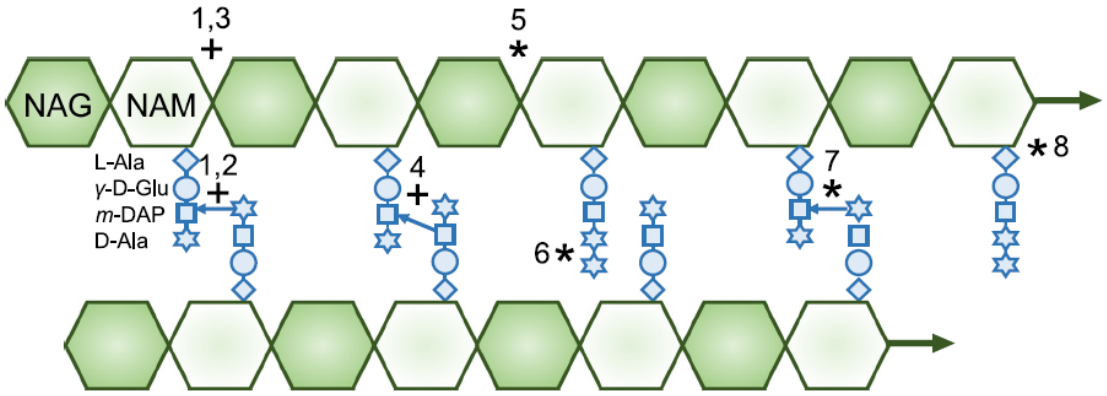

Figure 11. Summary of *E. coli* extracellular peptidoglycan enzymes and their activities. Schematic of the PG cell wall depicting major synthesis reactions (numbered 1 to 4 and indicated by a plus symbol) and autolysis reactions (numbered 5 to 8 and indicated by an asterisk) and associated enzymes. Essential enzymes are shown in italic type. m-DAP, *meso*-diaminopimelic acid (adapted from (Mueller & Levin, 2020)).

While amidases perform cell separation in *E. coli,* most endopeptidases are connected with cell elongation in that species. Three endopeptidases (MepS, MepM and MepH) are redundantly essential in *E. coli,* depletion of all three resulting in lysis (Singh et al., 2012). One of these endopeptidases, MepS, is subject to degradation by the periplasmic protease Prc (Singh et al., 2015). Proteolytic degradation is one way to regulate the activity of PG hydrolases.

3.3.2 The many functions of PG hydrolases

PG hydrolases not only ensure proper separation of bacterial cells (Goley et al., 2010; Heidrich et al., 2001; Uehara et al., 2009), they also contribute to PG elongation (Singh et al., 2012), PG recycling (Jacobs et al., 1995) and the insertion of structures that span across the cell envelope, including flagella and secretion systems (Scheurwater et al., 2008; Vollmer et al., 2008).

As usual, what is known for *E. coli* is not necessarily true for other Gram-negative bacteria. The alphaproteobacterium *C. crescentus* for example has only one amidase, AmiC, and its absence does not affect the morphology or growth of the bacterium (Zielinska et al., 2017). AmiC is also the only periplasmic amidase of *A. tumefaciens* and *S. meliloti,* members of the Rhizobiales. In these two bacterial species, AmiC seems to be important for proper cell shape and for polarity, rather than being only involved in septal PG hydrolysis as in *E. coli* (Figueroa-Cuilan et al., 2021; Krol et al., 2021). Overall, PG hydrolases have only been investigated very recently in Rhizobiales, and many questions remain to be addressed regarding their role in polar growth and division.

A general feature of bacterial PG hydrolases is their important redundancy. *E. coli* for example encodes at least 35 PG hydrolases (van Heijenoort, 2011). Bacterial cells probably use different PG hydrolases depending on the environmental conditions (Egan et al., 2020; Mueller & Levin, 2020). *In E. coli*, the DD-carboxypeptidase PBP5 is crucial for cell shape maintenance in normal laboratory conditions. In acidic conditions however, another DD-carboxypeptidase, PBP6B, becomes a major factor for cell shape (Peters et al., 2016). Among the three DD-endopeptidases of *Vibrio cholerae,* namely ShyA, ShyB and ShyC, ShyB is specifically overexpressed in conditions of zinc starvation. The two other endopeptidases ShyA and ShyC are not functional in those conditions (Murphy et al., 2019). The ShyB homologue in *A. baumannii*, ZrlA, is also upregulated upon zinc starvation. Importantly, this endopeptidase is also required for colonization and dissemination in a murine model of pneumonia (Lonergan et al., 2019). These examples illustrate the importance of redundancy in the periplasmic PG hydrolases, which are exposed to fluctuating environmental conditions.

3.4 Other factors that influence bacterial shape

Even though there are major DNA-encoded factors that determine cell shape, bacteria can still modulate their shape in response to their environment. The enteric pathogen

Campylobacter jejuni transitions from a helical shape to coccoid shape under unfavorable conditions (Frirdich et al., 2019). Peptidoglycan-modifying enzymes, namely the carboxypeptidases Pgp1 and Pgp2 and the amidase AmiA are involved in this transition, and therefore can modify the virulence properties of the bacterium, as the helical shape is required for proper host colonization (Frirdich et al., 2019; Frirdich et al., 2014). Interestingly, the pathogenic bacterium *Legionella pneumophila* undergoes a transition from a rod shape to a filamentous shape to evade macrophage killing (Prashar et al., 2013).

In *B. melitensis*, a *rsh* deletion mutant displays morphological alterations such as abnormal swelling and branching (Dozot 2006). This finding is consistent with the fact that ppGpp blocks DNA replication, and therefore cell cycle in *B. abortus* (Van der Henst et al., 2020), as it was observed with the dimorphic bacteria *C. crescentus* (Lesley & Shapiro, 2008).

Mutations affecting functions that are *a priori* even less related to bacterial cell wall can also dramatically affect cell shape. For example, mutations in the histidine biosynthesis pathway induce a cell division inhibition resulting in filamentous phenotype in *E. coli* and *S. typhimurium*. This filamentous phenotype was only observed in certain conditions, namely high temperature and a high-glucose containing medium (Cano et al., 1998; Frandsen & D'Ari, 1993; Murray & Hartman, 1972). In this case, the effect of the mutation in a histidine biosynthetic gene is most probably indirectly affecting the shape of *S. typhimurium*. A possible explanation for the inhibition of cell division, would be that impaired histidine biosynthesis, which is connected to purine biosynthesis, would lead to nucleotide imbalance and as a result mutations (Gibert & Casadesús, 1990). Accordingly, cell division is blocked by the so-called SOS response when DNA is damaged (Radman, 1975). DNA damage results in the accumulation of SulA and a resulting blockage of cell division (Radman, 1975). This possibility was however ruled out in *Salmonella*, as *sulA* expression does not seem to be upregulated in histidine biosynthesis mutants (Gibert & Casadesús, 1990). The mechanism by which the histidine biosynthesis pathway leads to an inhibition of division remains therefore unexplained.

4. HISTIDINE, A METABOLIC CROSSROAD

The imidazole ring side chain of histidine confers this amino acid aromatic properties. Besides, histidine is the only amino acid to have a pK_a closest to the physiological pH (pK_a ~6). As a result, it can switch from an unprotonated to a protonated state under neutral pH conditions (Nelson & Cox, 2017). The imidazole side chain of histidine also confers this amino acid with the ability to bind transition metal ions (Sundberg & Martin, 1974).

This amino acid is essential for mammals, but most plants, bacteria and fungi are able to synthesize it (Kulis-Horn et al., 2014). Whereas biosynthesis of NEAA is generally simple and involves few reactions, EAA biosynthesis is generally more complex.

4.1 Histidine biosynthesis pathway

The histidine biosynthesis pathway has been extensively studied in *E. coli* and its close relative *Salmonella typhimurium* (Brenner & Ames, 1971) as well as in plants (Stepansky & Leustek, 2006). The five first steps of the pathway lead to the formation of imidazole glycerol phosphate (IGP), which will be further converted to histidine by four other enzymatic steps, and 5-amino-1-(5-phospho-D-ribosyl)imidazole-4-carboxamide (AICAR), an intermediate of the *de novo* purine biosynthesis (Figure 12).

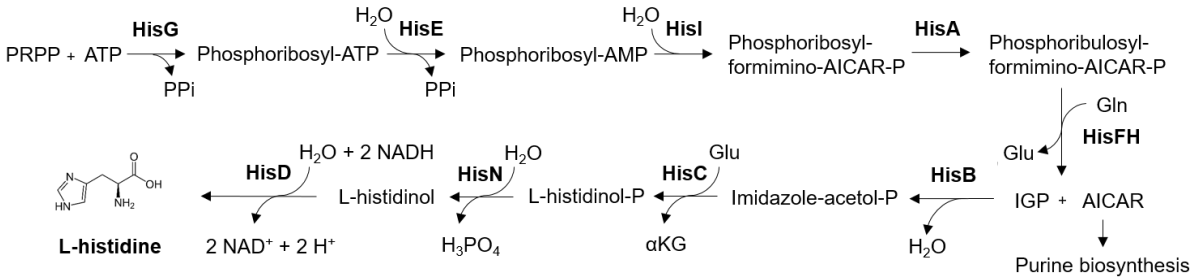

Figure 12. Schematic representation of histidine biosynthetic pathway. AICAR, 5-amino-1-(5-phospho-D-ribosyl)imidazole-4-carboxamide; IGP, Imidazole Glycerol Phosphate; αKG, α-ketoglutarate; PRPP, phosphoribosylpyrophosphate.

4.2 Genomic organization of the histidine biosynthesis genes

In *S. typhimurium* and *E. coli*, all histidine biosynthesis genes are concentrated in one operon and are therefore expressed and regulated as a single unit (Martin, 1963). In most other bacteria however, the organization of histidine biosynthesis genes is different. In all alphaproteobacteria, five of the *his* genes (*hisBHAFE*) are clustered together, and in some cases together with open reading frame(s) of unknown function (Fani et al., 2005). The other genes of the pathway are dispersed on the genome, and in *Brucella suis*, *B. melitensis* and *B. abortus*, some genes are even scattered on different chromosomes (Figure 13) (Fani et al., 2005). The histidine biosynthetic genes of *B. abortus* are listed in Table 1. In *S. typhimurium* and *E. coli,* the sixth step of the pathway is catalysed by a bifunctional enzyme encoded by the *hisNB* gene. This enzyme comprises imidazoleglycerol-phosphate dehydratase activity at the C-terminus and histidinol-phosphate phosphatase activity at the N-terminus, catalyzing the eighth step of biosynthesis. This gene fusion seems to be restricted again to the

enterobacteria, since in most other bacteria and lower eukaryotes both activities are encoded by separated genes (Alifano et al., 1996).

Table 1. Histidine biosynthesis genes in *B. abortus*.

Gene	ORF	Function
hisA	BAB1_2085	Phosphoribosyl-formimino-AICAR-P isomerase (EC 5.3.1.16)
hisB	BAB1_2082	Imidazoleglycerol-phosphate dehydratase (EC 4.2.1.19)
hisC	BAB1_1988	Imidazole acetol phosphate aminotransferase (EC 2.6.1.9)
hisD	BAB1_0285	Histidinol dehydrogenase (EC 1.1.1.23)
hisE	BAB1_2087	PR-ATP pyrophosphohydrolase (EC 3.6.1.31)
hisF	BAB1_2086	Cyclase
hisG	BAB2_0183	ATP phosphoribosyl transferase (EC 2.4.2.17)
hisH	BAB1_2084	Glutamine amidotransferase
hisI	BAB1_1098	PR-AMP cyclohydrolase (EC 3.5.4.19)
hisN	BAB2_0044	Histidinol-phosphate-phosphatase (EC 3.1.3.15)
hisS	BAB2_0181	Histidine-tRNA ligase
hisZ	BAB2_0182	ATP phosphoribosyl transferase regulatory subunit

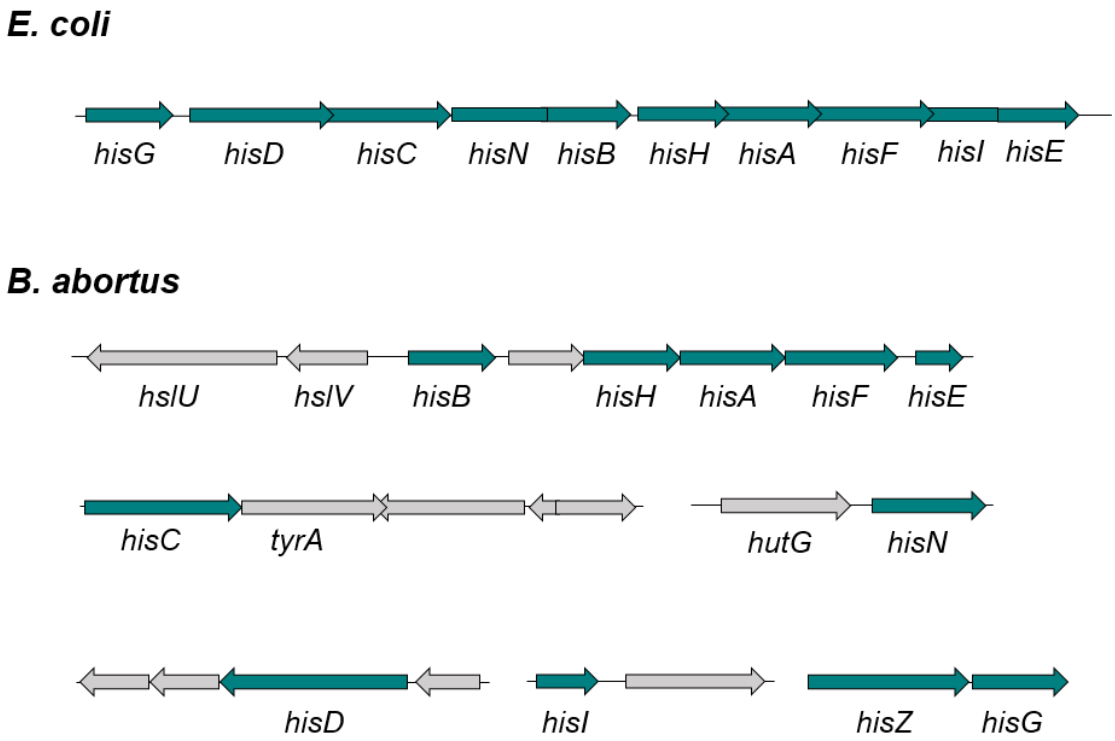

Figure 13. Genomic organization of histidine biosynthetic genes in *E. coli* and *B. abortus*. In *E. coli*, all the *his* genes are clustered into a same operon. Some *his* genes are clustered together, also with a gene of unknown function in *B. abortus.* The other genes are scattered throughout the genome.

4.3 Regulation of histidine biosynthesis

The metabolic cost of histidine biosynthesis is the third highest in all proteinogenic amino acids. Each molecule of histidine costs 41 ATP equivalents for the cell, therefore regulation of histidine biosynthesis is crucial to prevent waste of energy (Brenner & Ames, 1971). There are several ways to regulate the histidine biosynthesis.

First, feedback inhibition of HisG, the first enzyme of the pathway, limits the flow of intermediates through the pathway. The end product histidine acts as noncompetitive inhibitor of HisG so that the pathway is rapidly shut down when histidine levels are high (Alifano et al., 1996; Martin, 1963).

The second layer of regulation governs the intracellular concentration of biosynthetic enzymes. In *E. coli* and *S. typhimurium*, the transcription of the *his* operon is under the control of the stringent response (Winkler & Ramos-Montañez, 2009). The effector of the stringent response, the “alarmone” guanosine tetraphosphate (ppGpp) or guanosine pentaphosphate (pppGpp) is synthesized by RelA in response to amino acid starvation (Chatterji & Ojha, 2001). The pp(p)Gpp alarmone represses the translation machinery by interfering with transcription of ribosomal and transfer RNA (rRNA and tRNA) (Traxler et al., 2008). On the other hand, pp(p)Gpp upregulates the transcription of most amino acid biosynthesis genes, including histidine (Chatterji & Ojha, 2001).

The concentration of histidine biosynthetic enzymes is also regulated by a mechanism called transcription attenuation. The biosynthesis of histidine which was initially characterized in *E. coli* and *S. typhimurium* has been a model to study this process (Winkler & Ramos-Montañez, 2009). Transcriptional attenuation allows the coordination of the expression of the *his* structural genes with the availability of charged histidyl-tRNA (Box 1).

Box 1. Transcriptional attenuation regulates the histidine biosynthetic genes in *S. enterica* (adapted from (Chevance et al., 2014)). The 5’ regulatory region of the *his* operon codes for a short leader peptide of 16 amino acids, containing 7 consecutive histidine residues. This leader peptide is followed by a transcription terminator : the attenuator. **A.** When histidyl-tRNA levels are high, the leader peptide is rapidly translated by ribosomes. Transcription of the *his* structural genes is blocked by the formation of the E:F attenuator stem-loop. **B.** Limited availability in histidyl-tRNA slows down the leader peptide translation and results in ribosome stalling, which in turn promotes the formation of an alternative anti-terminator RNA secondary structure. Inhibition of the attenuator formation allows transcription of the *his* operon. **C.** Under conditions where transcription from the *his* promoter is not coupled to translation, the E:F attenuator is formed and prevents transcription of the *his* structural genes (Johnston et al., 1980).

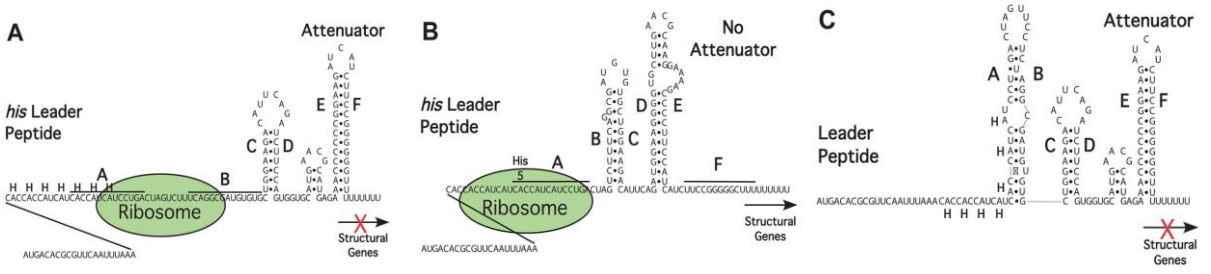

4.4 Histidine utilization pathway

When histidine is in excess, many bacteria are able to degrade this amino acid for energy generation. The histidine utilization pathway (hut) is widespread among bacteria including *B. abortus* (Figure 14 A), even though it is absent in the model organism *E. coli* (Bender, 2012). This pathway leads to the formation of ammonia, glutamate and a one-carbon compound (formate or formamide) (Figure 14 B). Among eukaryotes, the presence of a complete hut pathway is spotty. It is however present in all vertebrates (Bender, 2012). In *B. abortus*, the *hut* operon is regulated by HutC. HutC represses transcription of the *hut* genes under conditions where urocanate (the first intermediate of histidine degradation pathway) levels are low. When urocanate levels increase, its interaction with HutC promotes the dissociation of HutC from the *hut* promoter (Sieira et al., 2010). As a result, the *hut* genes are expressed and allow the degradation of histidine for energy generation.

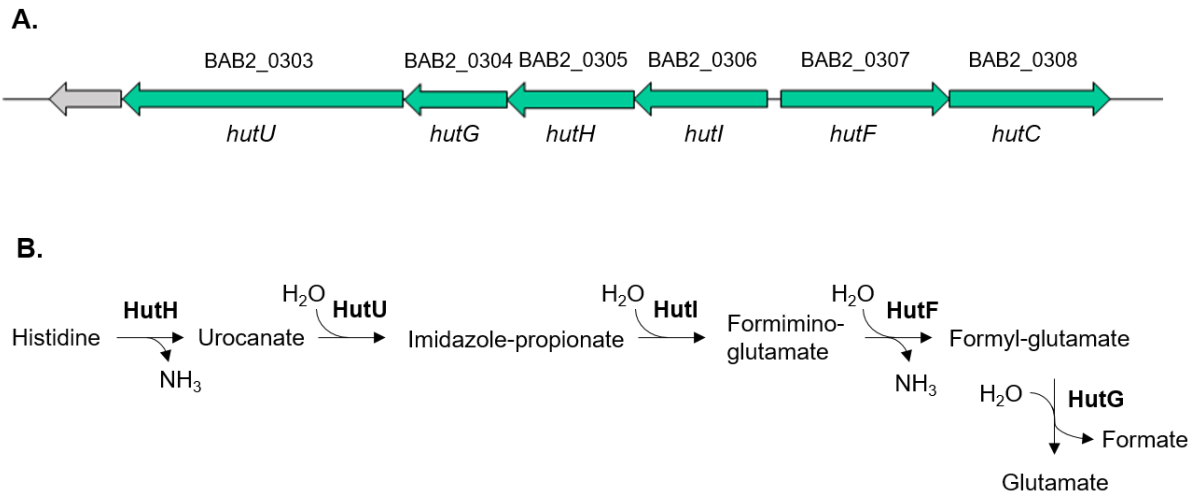

Figure 14. Genetic organization of the *hut* gene cluster in *B. abortus* and deduced metabolic pathway for the degradation of L-histidine.

4.5 Histidine transport

Some bacteria encode a histidine transporter within the *hut* operon. *Acinetobacter baumannii* and *Pseudomonas putida* for example possess a *hutT* gene clustered within the *hut* operon. HutT belongs to the amino acid-polyamine-organocation (APC) family of secondary transporters (Wirtz et al., 2021). *B. abortus* encodes a *hutT* homologue in its genome (BAB1_0055), but it is not found within the *hut* operon but instead is curiously found next to the *virB* operon. In enterobacteria, the main histidine transporter is the ABC-type transporter HisJMPQ (Ames, 1985; Ardeshir & Ames, 1980). Overall, bacteria appear to have a variety of transporters capable of transporting histidine with varying specificity and affinity for histidine (Zhang et al., 2012).

4.6 Histidine metabolism and virulence

Even though histidine biosynthesis and catabolism are essential for bacterial growth in general, there are cases where histidine metabolism can be specifically linked with virulence.

The opportunistic Gram-negative bacterial pathogen *Acinetobacter baumannii* is a frequent cause of nosocomial infections and is associated with various infectious diseases including bloodstream infections, urinary tract infections, wound infections and pneumonia. Paradoxically, both *A. baumannii* mutants in histidine biosynthesis and utilization showed decreased virulence in mice models of pneumonia (Lonergan et al., 2020; Martinez-Guitian et al., 2019). On the one hand, survival rate of mice infected with a *hisF* deletion mutant was higher than for mice infected with the WT strain, suggesting that *hisF* is required for persistence in lungs (Martinez-Guitian et al., 2019). On the other hand, a *hutH* deletion mutant is severely attenuated in intranasally infected mice. Since the enzyme HutH allows *A. baumannii* to acquire nitrogen from histidine, bioavailable histidine in the lung could be an important nitrogen source during infection (Lonergan et al., 2020).

Intriguingly, in *B. abortus*, both histidine utilization and biosynthesis are also somehow connected to virulence. First, the repressor of the Hut pathway HutC is able to bind to the *virB* promoter and to coactivate the expression of the Type IV secretion system (Sieira et al., 2010). Importantly, urocanate also favors the induction of virulence genes including the *virB* operon by VjbR, an important regulators of virulence factors in *Brucella* (Kleinman et al., 2017). As a matter of fact, urocanate also promote VjbR-dependent expression of *btaE* (Kleinman et al., 2017), a polar adhesin identified in *B. suis* (Ruiz-Ranwez et al., 2013). Second, a *B. suis* transpositional mutant in *hisD,* the gene coding for the enzyme catalyzing the last step of the histidine biosynthesis pathway, was shown to be attenuated inside THP-1 human macrophages (Kohler et al., 2002). Thanks to this discovery, inhibitors of HisD have been developed to block *Brucella* replication (Joseph et al., 2007). More recently, Tn-seq experiments in *B. abortus* and *B. melitensis* also unveiled several histidine biosynthesis genes as required during infection of RAW 264.7 murine macrophages (Sternon et al., 2018) and for intranasally infected mice (George Potemberg, PhD thesis) (Figure 15).

Overall, many questions remain concerning the role of histidine metabolism in the virulence of *B. abortus*, and have never been addressed so far.

In the airborne fungal pathogen *Aspergillus fumigatus,* it was shown that HisB or IGPD, the sixth enzyme of the biosynthesis pathway, is essential for virulence (Dietl et al., 2016). Indeed, an auxotrophic *hisB* deletion mutant was attenuated in several virulence models including mice pulmonary infection. In this work, the role of histidine in metal homeostasis was also highlighted, since the *hisB* mutant was more sensitive to both metal excess and starvation. Considering that vertebrate hosts have evolved sophisticated mechanisms to either intoxicate pathogens with toxic metal ions or to deprive them from crucial metals, the role of histidine in metal homeostasis could be particularly relevant during the infection process (Dietl et al., 2016).

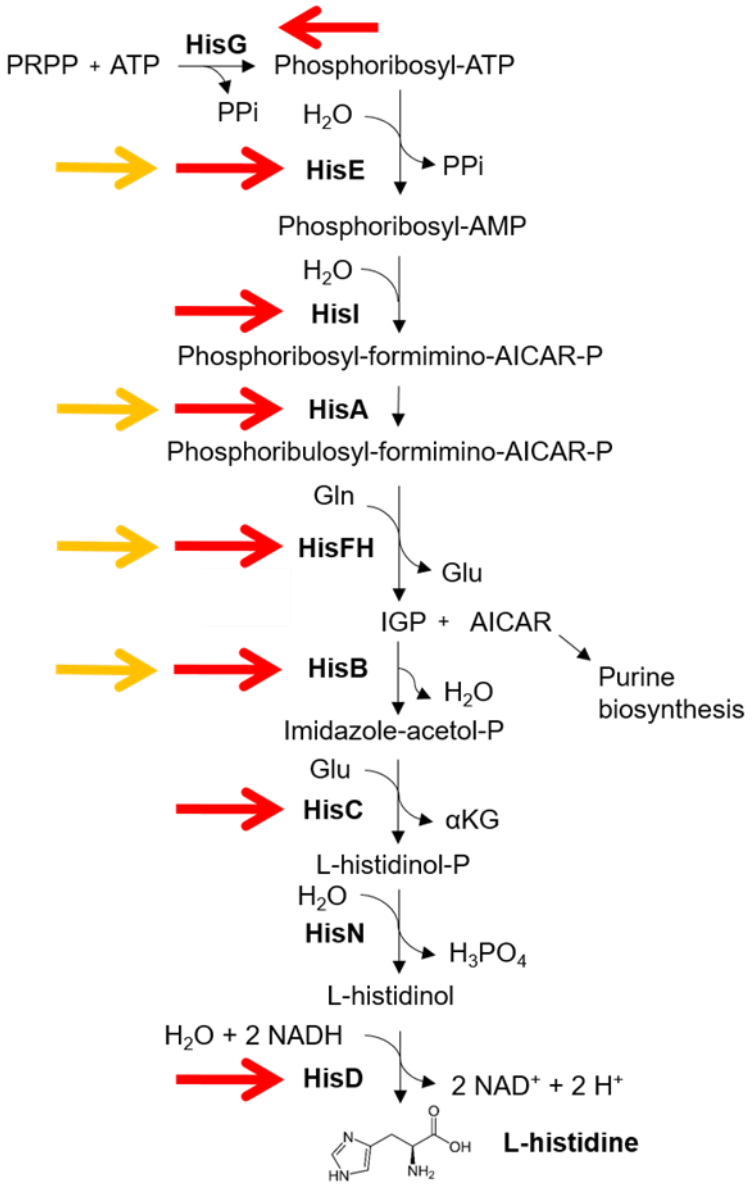

Figure 15. Several genes from the histidine biosynthesis pathway are required for *B. abortus* infection of RAW 264.7 macrophages and mice. Red arrows indicate genes that are required for replication inside macrophages at 24 h post infection (Sternon et al., 2018). Yellow arrows indicate genes that are required at 2 and 5 days post-infection in an intra-nasal lung mice infection model.

5. METAL HOMEOSTASIS IN BACTERIA

Metals are essential for life. Metal cofactors are indispensable for many central bioenergetic and biogeochemical processes on earth, which include respiration, photosynthesis and nitrogen fixation. The three most important metals for metabolism are iron, manganese (Mn) and zinc (Chandrangsu et al., 2017). Both environmental and pathogenic bacteria are exposed to situations of metal imbalance. Even though bacteria possess sophisticated systems to maintain metal homeostasis, mammalian hosts have evolved many ways to sequester essential metals and in parallel to intoxicate pathogens with metals.

5.1 Metals and immunity

Mammalian hosts fight against pathogenic bacteria by sequestering key metals for their survival. Most of the iron is not bioavailable for bacteria as it is bound by transferrin and hemoglobin (Palmer & Skaar, 2016). Neutrophils that are recruited in places of infection also release calprotectin, which sequesters zinc and Mn (Damo et al., 2013). In response to infection by intracellular bacteria, neutrophils and macrophages also deplete the phagosome of Mn and iron thanks to the natural resistance–associated macrophage protein 1 (Nramp1) (Gunshin et al., 1997) (Figure 16).

Even though metal starvation is well established as a defense mechanism against pathogens, it is becoming clearer that metal intoxication also actively takes place during infection to fight against invading pathogens. Activated macrophages accumulate copper inside the phagocytic vacuole in response to stimulation with interferon-γ (INF-γ). INF-γ induces the expression of copper transport protein 1 (CTR1) to import extracellular copper inside the cytoplasm where it is shuttled by the chaperone ATOX1 to the ATP7A transporter at the membrane of the phagolysosome (Kim et al., 2012; White et al., 2009; Wolschendorf et al., 2011) (Figure 16). The expression of ATP7A is also induced by INF-γ (White et al., 2009). Copper resistance has been associated with virulence in intravacuolar pathogens such as *Salmonella enterica* (Achard et al., 2010) and *Mycobacterium tuberculosis* (Ward et al., 2010; Wolschendorf et al., 2011).

The accumulation of zinc inside phagocytic vacuoles may also contribute to kill intracellular bacteria. The intramacrophagic vacuole containing *M. tuberculosis* is flooded with zinc. Accordingly, the zinc export system CtcP is required for *M. tuberculosis* survival inside macrophages (Botella et al., 2011). Zinc was found to accumulate in metal-containing vesicles that possibly fuse with the phagocytic vacuole within the macrophage (Kapetanovic et al., 2016) (Figure 16).

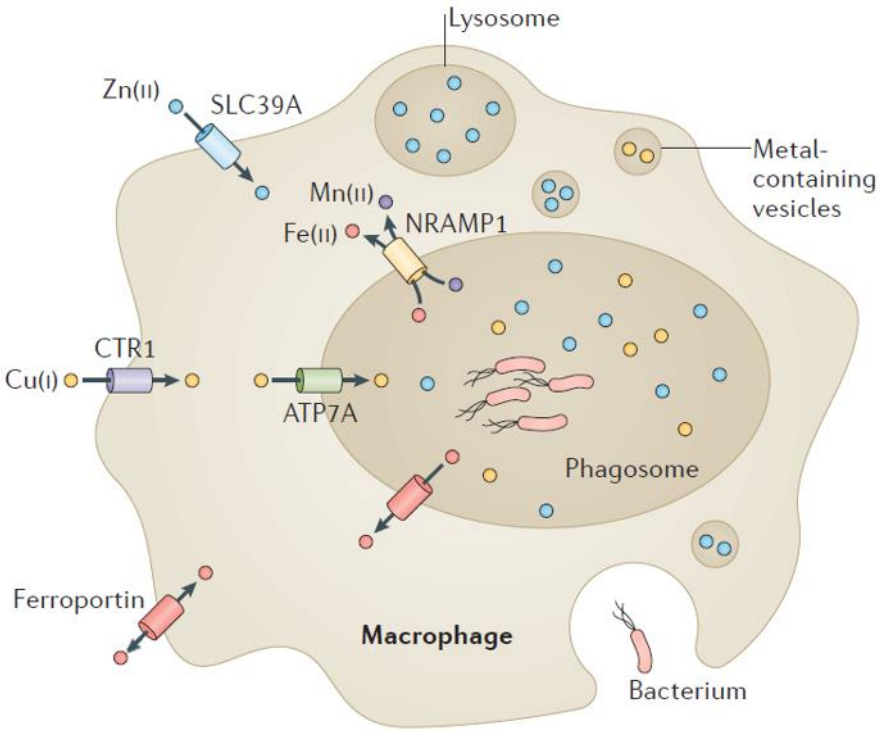

Figure 16. Metal homeostasis during macrophage infection**.** Macrophages employ various strategies to disrupt bacterial metal homeostasis. NRAMP1 and ferroportin deplete the phagosome of iron (Fe(II)) and manganese (Mn(II)). Conversely, CTR1 and ATP7A allow copper (Cu(I)) poisoning of bacteria inside the phagosome. Zinc (Zn(II)) may accumulate intracellularly by entering through the SLC39A family of Zn transporters. Besides, Zn could also possibly accumulate inside the phagosome by fusion of the latter with metal-containing vesicles within the macrophage (adapted from (Chandrangsu et al., 2017)).

5.2 Coping with metal toxicity

There are several layers of protection for bacteria to resist toxic concentrations of metals. The fastest way to prevent metal toxicity before any transcriptional regulation takes place is to buffer metal ions in the cytoplasm. Metal buffering is generally ensured by small molecules such as glutathione or derived molecules such as bacillithiol, which is responsible for zinc buffering in *Bacillus subtilis* (Ma et al., 2014). Some bacteria and many eukaryotes express cysteine-enriched small proteins called metallothioneins which buffer zinc (Maret, 1994). Alternatively, histidine was identified as a possible zinc buffer in *Acinetobacter baumannii* (Nairn et al., 2016). Cytosolic copper could also potentially be buffered by methionine in *E. coli* (Fung et al., 2013), as well as glutathione in *Streptococcus pneumoniae* (Potter et al., 2012).

When metal ions reach toxic levels, bacteria induce the expression of a set of specific genes that will precisely respond to the toxic metal. This response typically involves the expression of efflux systems as well as proteins involved in the storage and sequestration of metals.

The response to copper is relatively well conserved in proteobacteria, and consists of a core *cue* (copper efflux) regulon (Giachino & Waldron, 2020). This regulon consists of a copper-responsive metalloregulatory protein, CueR, that up-regulates the expression of *copA* and *cueO* when copper concentration increases (Outten et al., 2000). CopA is a copper efflux P-type ATPase (Rensing et al., 2000). The periplasmic multicopper oxidase CueO oxidizes the highly reactive cuprous ion (Cu(I)) to the more biologically inert cupric ion (Cu(II)) in the presence of oxygen (Outten et al., 2001). The *cue* regulon also involves *copZ*, coding for a cuprochaperone in *E. coli* (Figure 17) (Meydan et al., 2017).

Most *S. enterica* serotypes also harbor a duplicated homologous version of the *cue* regulon, the *gol* regulon (Figure 17) (Osman et al., 2013; Osman et al., 2010). In these strains, the CueR homologue GolS transcriptionally regulates GolT, a CopA homologue and GolB, a putative CopZ-like cuprochaperone found in the cytoplasm (Giachino & Waldron, 2020). Furthermore, a supplementary cuprochaperone was identified in the periplasm of *S. enterica*, CueP (Osman et al., 2010; Pontel & Soncini, 2009). CueP itself accepts copper pumped out by GolT or CopA (Fenlon & Slauch, 2017). Presumably, the expanded anti-copper arsenal of *S. enterica* could be an adaptation to survival inside macrophages (Achard et al., 2010; Giachino & Waldron, 2020).

E. coli and *S. enterica* possess a second Cu efflux system, the Cus system (copper sensing) (Figure 17). The *cus* regulon is controlled by the two-component system CusSR (Gudipaty & McEvoy, 2014), and activates the expression of the *cusCFBA* operon when copper levels are elevated (Outten et al., 2001). The *cusCBA* genes code for the resistance, nodulation and division (RND) proton-cation antiporter CusCBA (Grass & Rensing, 2001), whereas CusF is a periplasmic cuprochaperone (Franke et al., 2003). As a matter of fact, all known copper-requiring enzymes in enterobacteria are localized in the cell envelope (Giachino & Waldron, 2020). Unlike the Cue system, the Cus system could play an essential role for copper efflux under anaerobic conditions (Outten et al., 2001).

The *pco* genomic island has been isolated from feces of pigs fed with copper and has spread to both *E. coli* and *S. enterica* (Figure 17) (Giachino & Waldron, 2020; Tetaz & Luke, 1983). Similarly to the two previous systems, the *pco* locus comprises a copper-sensitive system named PcoSR, a periplasmic cuprochaperone PcoC and a multi-copper oxidase PcoA (Osman & Cavet, 2011). PcoA is predicted to work in concert with PcoB, an outer membrane protein whose function in copper resistance remains unclear (S. Gillet, PhD thesis, 2019), and is still under investigation.

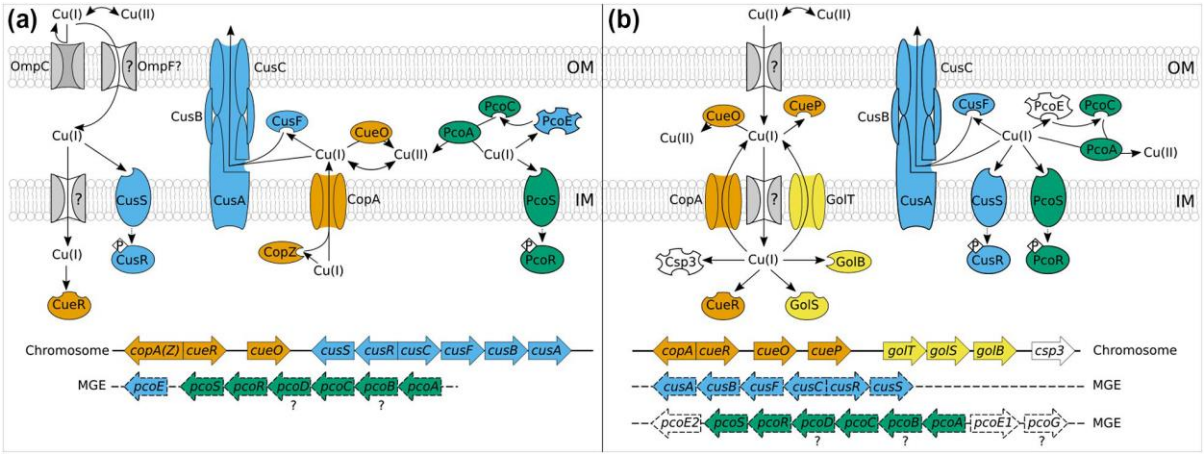

Figure 17. Copper homeostasis in *E. coli* and *S. enterica*. (a) In *E. coli*, three systems, Cue (orange), Cus (blue) and Pco (green), control Cu^{+} levels in the cytoplasm and periplasm. These systems contain sensory elements: CueR, CusSR and PcoSR respectively. Cu is actively exported from the cytoplasm and the periplasm by two efflux pumps, CopA and CusCBA respectively. In addition, high-affinity cuprochaperones, CopZ and CusF, bind Cu(I) in the cytoplasm and in the periplasm, respectively. In the periplasm, Cu detoxification is carried out by a multi-copper oxidase, CueO. The Pco system includes one multicopper oxidase, PcoA and periplasmic chelators, PcoC and PcoE. (b) In *S. enterica*, the homologous *gol* regulon (yellow) is a duplicate of the *cue* regulon and contains the efflux pump GolT, a chaperone GolB in the cytoplasm and the transcriptional regulator GolS. The *cus* system is not present on the chromosome but can be supplied by mobile genetic elements (MGE) (adapted from (Giachino & Waldron, 2020)).

5.3 Consequences of metal intoxication

When their concentrations reach a certain threshold, metals are toxic for all cells. Toxicity is mostly caused by mismetallation, or the ability of the metal in excess to compete with other metals in metalloproteins, thereby perturbing their activities. Outside of bacterial cells, the electron transport chain is an important target of metals such as zinc, cadmium or cobalt (Beard et al., 1995; Chandrangsu et al., 2017). Zinc can also interfere with Mn import by competing with Mn within the Mn-specific PsaA importer (McDevitt et al., 2011). Mechanisms of metal toxicity also involve the displacement of iron-sulfur clusters. Notably, the primary cause of copper toxicity in *E. coli* is the replacement of iron by copper in iron-sulfur cluster proteins in branched-chain amino acid biosynthesis (Macomber & Imlay, 2009).

Besides mismetallation, metals can also promote reactive oxygen species (ROS) generation. Iron and copper can react with H_2O_2 and O_2 to generate highly reactive hydroxyl radicals, potentially able to oxidize DNA, lipids and proteins (Espírito Santo et al., 2008; Grass & Rensing, 2001).

5.4 Metal homeostasis and virulence of *B. abortus*

As an intracellular pathogen, *B. abortus* is potentially exposed to both metal starvation and poisoning.

Unlike *M. tuberculosis* which has to cope with zinc poisoning during infection of macrophages, it seems that *B. abortus* is rather struggling with zinc starvation during infection. Indeed, mutations in the genes coding for the ZnuABC zinc import system lead to decreased replication of *Brucella* in macrophages and mice (Box 2) (Kim et al., 2004; Yang et al., 2006). In contrast to the Znu zinc uptake system, the zinc exporter ZntA is not essential for *Brucella* virulence (Sheehan, Budnick, Roop, et al., 2015). ZntA is an ATP-dependent zinc exporter which is transcriptionally induced when zinc reaches toxic concentrations by the MerR family regulator ZntR (Box 2) (Hantke, 2001). Deletion of the regulator ZntR leads to attenuation of *B. abortus* in a mouse model of infection. It was hypothesized that in the Δ*zntR* mutant, *zntA* is overproduced because it is derepressed. This would lead to zinc starvation by leakage of zinc through the overproduced export system during infection (Sheehan, Budnick, Roop, et al., 2015). Overall, zinc seems to be a rather limiting element for *B. abortus* inside macrophages.

The Mn-specific transporter MntH is also determinant for the virulence of *B. abortus* inside macrophages and mice (Anderson et al., 2009), suggesting that this micronutrient is essential for *Brucella* during infection.

B. abortus genome comprises homologues of several genes related to copper resistance such as *cueR*, *copA*, *copZ*, *cueO*, *fixI*, *senC* and *pcuC* (Figure 18). Only the homologue of CueO, named BmcO for *Brucella* multi-copper Oxidase, has been investigated functionally in *Brucella melitensis* (Wu et al., 2015). A *bmcO* deletion mutant appeared to be more sensitive to $CuCl_2$, indicating that it contributes to copper tolerance. This Δ*bmcO* was however not attenuated in murine macrophages (Wu et al., 2015). Transposon insertion in the sequence of the *copA* gene resulted in attenuation inside RAW 264.7 macrophages (Sternon et al., 2018).

Copper is however an important cofactor for the SodC Cu-Zn superoxide dismutase and the CcoN subunit of the cytochrome *c* oxidase, from the electron transport chain (Roop & Caswell, 2017).

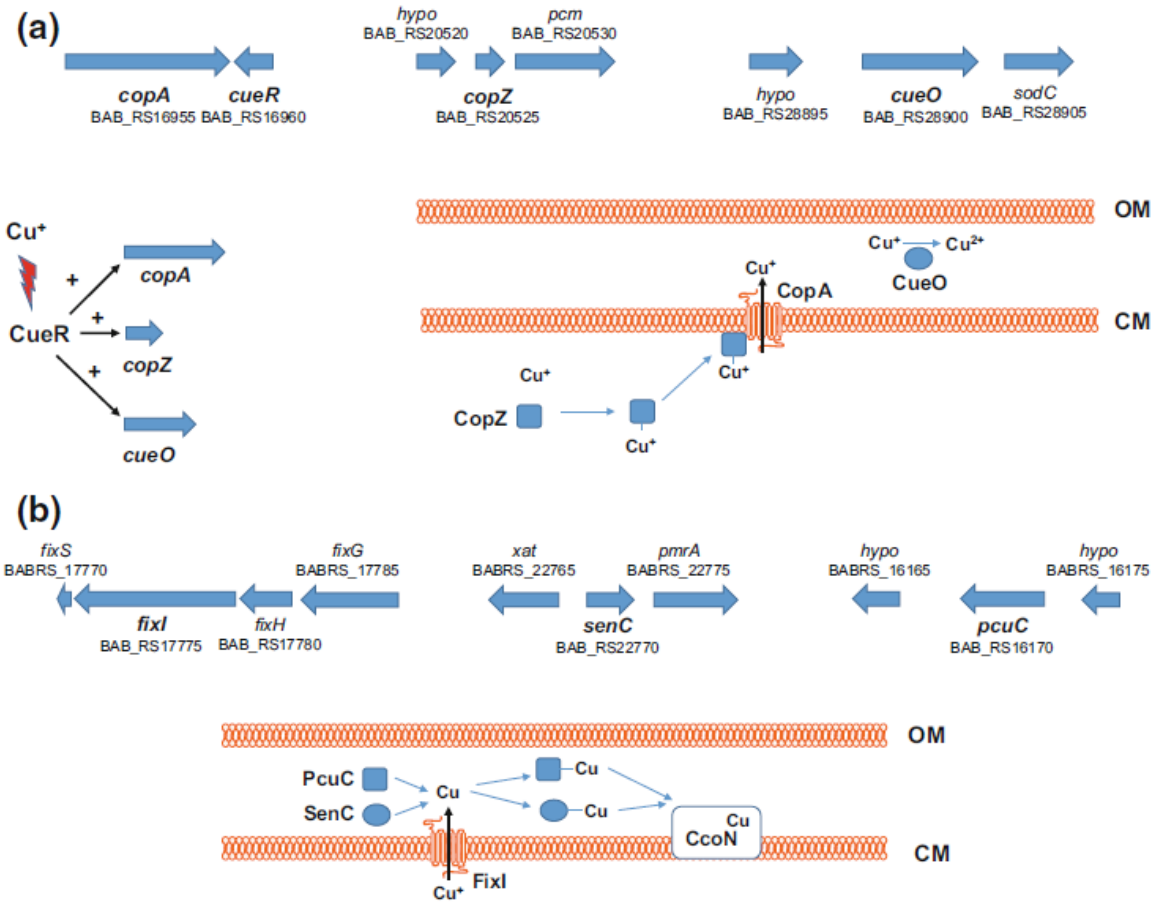

Figure 18. Putative roles of different *Brucella* proteins involved in the response to copper toxicity. (a) CopA, CueO, CopZ and CueR. (b) PcuC, FixI and SenC. CM: cytoplasmic membrane; OM: outer membrane; CcoN: subunit N of *cbb*$_3$-type cytochrome *c* oxidase (from (Roop & Caswell, 2017)).

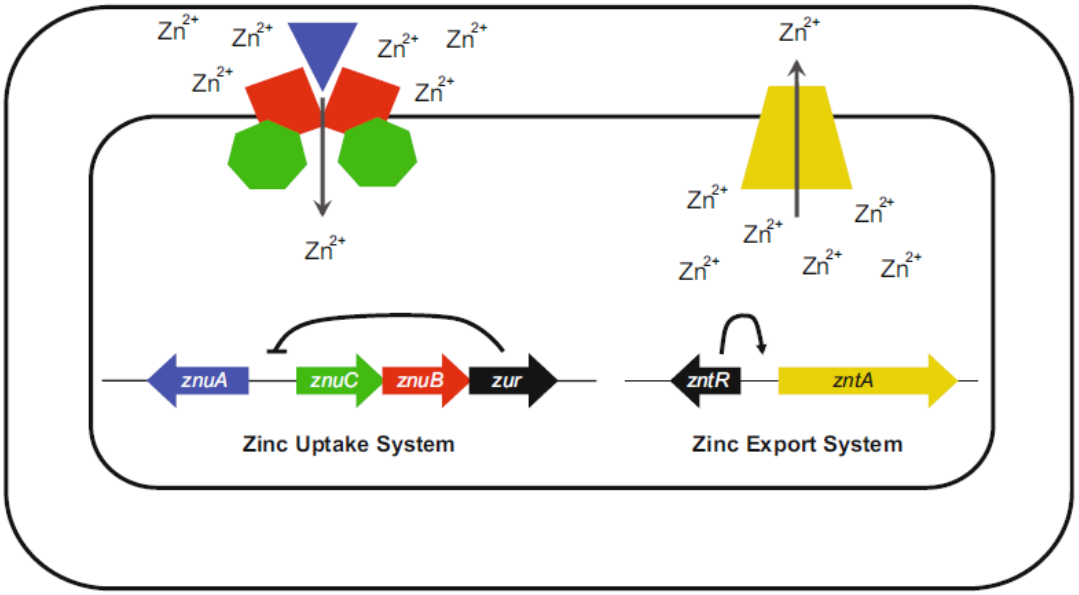

Box 2. Intracellular levels of zinc are precisely controlled by zinc uptake and export systems. Genetic regulation is mediated by two different zinc-responsive regulatory proteins, called Zur and ZntR. In low zinc-conditions, Zur activates the expression of the *znuABC* locus, which encodes the high-affinity zinc transporter ZnuABC. Conversely, ZntR activates the expression of the exporter ZntA in high-zinc conditions (adapted from (Roop & Caswell, 2017)).

OBJECTIVES

The aim of this thesis is to understand why *B. abortus* requires histidine during infection. The nature of the BCV remains so far largely unknown. The metabolic sensing of histidine or its degradation product could play a role in the intracellular trafficking of *Brucella*. Indeed, the major virulence factor of *Brucella*, the type IV secretion system, is itself regulated by a repressor of the histidine utilization pathway (Sieira et al., 2010) (see Introduction, section 4.4). To get some insights into which nutrients are present or absent in the BCV, and which ones are crucial or not for *Brucella*, auxotroph strains are interesting tools. For instance, the histidine biosynthesis pathway is predicted to be essential for *B. abortus* to survive inside RAW 264.7 macrophages, whereas the biosynthesis of several other amino acids seems to be dispensable (Sternon et al., 2018). **Furthermore, histidine auxotroph mutants have unexpected properties related to cell morphology and copper homeostasis, and might be useful to reveal essential processes at play in *B. abortus,* and yet never described.**

First, we will try to understand how a mutation in the histidine biosynthesis pathway can affect cell morphology in *B. abortus*. We will concentrate on PG since it is a crucial factor for cell morphology determination (see Introduction, section 3). Bacteria encode many enzymes involved in PG synthesis, hydrolysis and recycling. In Gram-negative bacteria such as *B. abortus*, these enzymes that modify PG are found inside the periplasm. In this work, we will use different tools to stain the PG and other envelope components of *Brucella* in order to try and understand how histidine metabolism could affect PG remodeling, in particular during cell separation in *B. abortus*.

Second, an important property of histidine is its ability to coordinate metal ions. Interestingly, several intracellular pathogens have to face copper poisoning, a response induced by infected host cells to get rid of the invading bacteria (White et al., 2009) (see Introduction, section 5). We will therefore investigate the capacity of histidine auxotroph mutants to react to metal excess and starvation, with a focus on copper homeostasis.

RESULTS

The results part of this thesis is divided into three main sections.

First, we include a manuscript that regroups the majority of the data obtained concerning cell separation in *B. abortus*. Supporting information is also provided, and comprise supplementary figures and tables.

Second, we included a section comprising additional data related to cell separation.

Finally, a third section includes results obtained about the role of histidine in copper homeostasis in *B. abortus*.

1. MANUSCRIPT

A histidine auxotroph mutant is defective for cell separation and allows the identification of crucial factors for cell division in *Brucella abortus*

Agnès Roba, Elodie Carlier, Pierre Godessart, Cerine Naili and Xavier De Bolle*.

Research Unit in Biology of Microorganisms, Narilis, University of Namur, B-5000 Namur, Belgium.

*Corresponding author.

Email: xavier.debolle@unamur.be

Author Contributions: XDB and AR designed research. AR performed all experiments, unless stated otherwise, EC made cellular infections and fluorescence microscopy, PG and CN set up the CRISPRi applied to B. abortus and generated the depletion strains. AR and XDB wrote the paper.

Competing Interest Statement: Disclose any competing interests here.

Classification: Biological sciences, Microbiology

Keywords: Cell division, peptidoglycan, *Brucella*

Abstract

The pathogenic bacterium *Brucella abortus* invades and multiplies inside host cells. To grow inside host cells, *B. abortus* requires a functional histidine biosynthesis pathway. Here, we show that a *B. abortus* histidine auxotroph mutant also displays an unexpected chaining phenotype. The intensity of this phenotype varies according to the culture medium and is exacerbated inside host cells. Chains of bacteria consist of contiguous peptidoglycan, and likely result from the defective cleavage of peptidoglycan at septa. Genetic suppression of the chaining phenotype unearthed two essential genes with a role in *B. abortus* cell division, *dipM* and *cdlP*. Loss of function of *dipM* and *cdlP* generates swelling at the division site. While DipM is strictly localized at the division site, CdlP is localized at the growth pole and the division site. Altogether, the unexpected chaining phenotype of a *hisB* mutant allowed the discovery of new crucial actors in cell division in *B. abortus*.

Significance Statement

Brucella abortus is a pathogenic bacterium from the order Rhizobiales, and is responsible for one of the world's major zoonoses. Mechanisms that take place during growth and division in this bacterium are essential, largely uncharacterized, and are very different from what is known in model bacteria such as *Escherichia coli*. In this work, we highlight the importance of histidine biosynthesis for *Brucella* to proliferate inside host cells. We also show that a histidine auxotroph displays a chaining phenotype caused by inadequate peptidoglycan splitting during cell separation. We identified two division factors, DipM and CdlP, which suppress the cell separation defect in the histidine auxotroph. Thus, histidine metabolism has a pivotal role in both *Brucella abortus* pathogenicity and fundamental processes such as cell division.

Main Text

Introduction

The alphaproteobacterial order Rhizobiales comprise a great diversity of bacteria in terms of shape and lifestyle. They include plant symbionts (*Rhizobium*) and pathogens (*Agrobacterium*), free-living bacteria (*Ochrobactrum*) and animal pathogens (*Bartonella, Brucella*) (Batut et al., 2004). Bacteria from the genus *Brucella* are able to infect a broad range of vertebrates and are responsible for a worldwide zoonosis known as brucellosis (Whatmore & Foster, 2021). *Brucella abortus* is a Gram negative

facultative intracellular pathogen which causes sterility and abortion in cattle and a debilitating febrile illness sometimes referred to as Malta fever in humans (Georgios Pappas et al., 2006). This bacterium displays some characteristics of the alphaproteobacteria, such as cell cycle regulation by CtrA (Francis et al., 2017), and unipolar growth which was also observed in other Rhizobiales such as *Agrobacterium tumefaciens* and *Sinorhizobium meliloti* (Brown et al., 2012). Unipolar growth is characterized by two main steps along the cell cycle, incorporation of new cell envelope components at the new pole and cell division. Many genes of *B. abortus* have been predicted to be involved in cell division by homology with *Escherichia coli* or *Caulobacter crescentus* (Sternon et al., 2018), however their function has not been characterized so far.

Brucella abortus can invade, and survive and proliferate inside host cells including macrophages, where it resides in a membrane-bound compartment known as the *Brucella*-containing vacuole (BCV). During the first hours of infection, *B. abortus* initially traffics through an acidic vacuole derived from the endocytic pathway (Starr et al., 2008). Then, it manages to reach the endoplasmic reticulum, inside which it will proliferate (Celli et al., 2003). Unlike many other intracellular bacteria that have coevolved for a long time with their eukaryotic host, *B. abortus* has not undergone a major genome reduction and retains broad biosynthetic abilities (Batut et al., 2004). Notably, *B. abortus* is prototrophic for all 20 amino acids. Recently, the ability of *B. abortus* to survive and grow inside the infection model RAW 264.7 macrophages was investigated by Tn-seq (Sternon et al., 2018). Genes required during infection of this model host cell were identified, and the histidine biosynthesis pathway genes, including *hisB*, were predicted to be essential for intracellular proliferation.

To investigate the importance of histidine biosynthesis for *B. abortus* during infection, we characterized the ability of auxotrophic *hisB* mutants to proliferate inside HeLa cells. Surprisingly, besides showing a decreased intracellular proliferation, loss of function *hisB* mutants exhibited a chaining morphology inside HeLa cells. Characterization of this chaining morphology revealed that it was due to a cell separation defect, originating from incomplete PG cleavage during late division. Overexpression of two putative cell division factors, a DipM endopeptidase homologue and a periplasmic protease that was renamed CdlP, suppressed the chaining phenotype of the *hisB* mutant. Localization and depletion of these two essential factors confirmed their role in cell division in *B. abortus*.

Results

The auxotrophic mutants Δ*hisB* and *hisB*$_{E17Q}$ replicate less efficiently inside host cells. HisB is the sixth enzyme involved in the histidine biosynthesis pathway (Fig. S1 A). It is the first enzyme of the pathway to be specifically dedicated to histidine biosynthesis, as the five first enzymes also contribute to the generation of 5-aminoimidazole-4-carboxamide ribonucleotide (AICAR), a metabolic intermediate of the purine biosynthesis pathway (Fig. S1 A). HisB is a dehydratase that generates imidazole-acetol-phosphate from imidazole glycerol phosphate (IGP). In frame deletion of *hisB* makes *B. abortus* auxotrophic for histidine since it does not affect growth in in Plommet erythritol (PE) minimal medium supplemented with 1 mM histidine, but it renders the bacterium unable to grow in PE without histidine (Fig. S1 B). The growth defect of this auxotrophic mutant can be fully rescued by *in trans* expression of *hisB* (Fig. S1 B). Using site-directed mutagenesis, we produced a catalytically inactive mutant of *B. abortus hisB, hisB*$_{E17Q}$, by replacing glutamate 17 in HisB with a glutamine (Figure S1 B). This point mutation phenocopies *hisB* deletion in terms of growth (Fig. S1 B). We then evaluated the ability of these mutants and the complemented Δ*hisB* mutant to replicate inside HeLa cells. The Δ*hisB* and *hisB*$_{E17Q}$ mutations strongly affect intracellular proliferation at 24 h and 48 h post infection (Fig. 1). This replication defect inside HeLa cells can be rescued either by genetic complementation, or by the addition of 10 mM histidine in the HeLa cell culture medium. These results suggest that *B. abortus* relies on *de novo* histidine biosynthesis for intracellular replication.

The *hisB* mutants display chaining morphology inside HeLa cells. Very surprisingly, besides being attenuated inside HeLa cells, the Δ*hisB* and *hisB*$_{E17Q}$ mutants also show a striking chaining morphology at 24 h post infection (Fig. 2). The addition of 10 mM histidine to the HeLa cell culture medium restores both intracellular replication and normal morphology of the mutants. This finding supports the idea that histidine is not only required for intracellular proliferation of the brucellae but also for their normal morphology within the intracellular environment. is required for proliferation but also for normal morphology. We then checked whether the chains were formed inside the host cells, or formed prior to

contact with host cells and then internalized as such. Before infection, bacteria were stained with eFluor (Cell Proliferation Dye eFluor™ 670), a dye which covalently binds to the bacterial surface and was previously used to show unipolar growth in *B. abortus* (Vassen et al., 2019). After bacteria were stained with eFluor, they were washed and then incubated with HeLa cells. At 4 h and 24 h post infection, cells were fixed and stained with anti-*Brucella* (S-LPS) antibodies to detect all intracellular bacteria (Fig. S2). Therefore, bacteria that were immunolabeled but were negative for eFluor have been newly generated inside host cells. At 4 h post infection, intracellular *Brucella* are mostly isolated and positive for eFluor, regardless of the genotype. At 24 h post infection, WT as well as *hisB* mutant strains appeared to derive from only one or two "mother" cells stained with eFluor. This indicates that *hisB* mutant chains are indeed formed by the brucellae replicating after entry into HeLa cells, likely due to a problem of cell division.

Chaining phenotype intensity varies with the culture medium *in vitro*. When the Δ*hisB* strain was cultured in TSB, the usual rich medium used for *B. abortus*, a very low percentage of chaining bacteria was observed under the microscope (Fig. 3 A and B). However, the proportion of chains increased when the bacteria were grown in Heart Infusion broth (HI), another rich medium, or in Gerhardt's minimal medium supplemented with 0.1 % casamino acids (GCA) (Fig. 3 C and D). The nature of the culture media strongly affected the morphology of Δ*hisB* mutant, but not the morphology of the WT *B. abortus*. Although GCA and HI are very different media, they both generated chaining phenotypes but the length distribution is very different between these two media. The ability to reproduce the chaining phenotype in culture offers the opportunity to investigate its generation.

Chaining is generated by uncleaved peptidoglycan at cell division sites. Typically, chaining morphology is due to a defect of cell separation, the last step of cell division (Heidrich et al., 2002; Uehara et al., 2009). Division defects in bacteria belonging to the order Rhizobiales lead to many different aberrant morphologies, such as branching, elongated and spherical cells (Latch & Margolin, 1997b). Since *B. abortus* is growing in a unipolar fashion like all other Rhizobiales investigated so far (Brown et al., 2012), we investigated how new cell wall material was inserted inside chaining bacteria. First, bacteria were stained with eFluor, then they were washed and then allowed to grow for 5 h in HI medium without eFluor, thus newly generated envelope appears as unstained. Then, we performed a short pulse labeling with the fluorescent D-amino acid HADA to highlight newly inserted peptidoglycan (PG) (Kuru et al., 2012) (Fig. S3). Constriction sites and growing poles appear in blue (HADA), whereas older envelopes, typically in "mother" cells are labeled in far red (eFluor). The combination of these two dyes shows us that new cell wall material is still incorporated in a unipolar fashion inside the chains. The eFluor labeled either a terminal pole of the chains or an internal segment within the chains (Fig. S3). Strikingly, the vast majority of contacts between cells within the chains are also labeled with HADA (Fig. S3), which could be due to either incomplete division or closely associated new (growing) poles. This raised two possible hypotheses for the generation of chains, either bacteria are still connected by continuous PG, which is not completely split at division sites, or PG splitting is complete and bacteria remain connected by their outer membrane. As it is possible to highlight chains with connected PG by the imaging of sacculi (Yakhnina & Bernhardt, 2020), we purified sacculi of the different strains and checked if they are still forming chains. We checked that these purified sacculi bind wheat germ agglutinin and a monoclonal antibody recognizing *Brucella* PG, but not a monoclonal antibody directed against lipopolysaccharide, which indicates that outer membrane has been removed (Fig. S4). When Δ*hisB* or *hisB*$_{E17Q}$ mutants were grown in HI, in the conditions where chaining phenotype is easily observable, the sacculi obtained are still forming chains, which confirms that these chains of bacteria are made of connected peptidoglycan. Accordingly, late division steps that normally lead to final separation of the cells seem to be compromised in a strain with a deleted or catalytically dead *hisB*.

Suppression of the *hisB* chaining phenotype. Considering the lack of knowledge regarding the repertoire of enzymes digesting PG in *B. abortus,* we first performed a bioinformatic analysis to identify and classify putative PG hydrolyzing enzymes encoded by the *B. abortus* genome. Predicted PG hydrolases were identified based on homology with *A. tumefaciens* and *Caulobacter crescentus* PG hydrolases and thanks to the "HyPe" tool, a software designed to identify PG hydrolases (Sharma et al., 2016). We compared the list of genes obtained with two sets of data acquired previously, the first being predicted essential identified by Tn-seq data analysis (Sternon et al., 2018) and the second being direct target genes of the cell division regulator CtrA identified by ChIP-seq analysis (Francis et al., 2017) (Table S1). Only two of these genes were potentially essential (BAB1_0907 and BAB1_1773), while

three others (including BAB1_0931) were considered “low fitness”, suggesting that loss of function of the gene could be tolerated but would compromise growth and/or survival. An obvious candidate to be an important division factor in *B. abortus* is BAB1_0907, the homolog of DipM in *C. crescentus* since this gene is proposed to be both essential and regulated by CtrA (BAB1_0907 was thus renamed *dipM*). We decided to check whether overexpression of this *B. abortus dipM* gene would compensate the chaining phenotype of Δ*hisB,* by integrating $dipM_{Ba}$ on a medium-copy plasmid. We also tested the overexpression of the essential LysM domain-containing protease BAB1_1773 and the only periplasmic amidase BAB1_0931, which is almost essential. Overexpression of *dipM* and BAB1_1773 but not BAB1_0931 significantly reduces chaining, as indicated by cell length measurements (Fig. 4). The data obtained with *dipM* overexpression are consistent with a PG separation defect in the chains, and they suggest that BAB1_1773, a conserved lipoprotein of unknown function displaying a LysM domain and a predicted M48 protease domain, could also be involved in cell division. BAB1_1773 was thus renamed *cdlP* (**c**ell **d**ivision **L**ysM-containing **p**rotease).

DipM and CdlP are involved in cell divison. DipM and CdlP are both predicted to contain a PG-binding domain called LysM (Fig. 5 A and D). Since it is expected that cell division proteins will be localized at constriction sites, we fused DipM and CdlP with the fluorescent protein mNeonGreen (mNG). Both fusion proteins were found to localize at cell septa, in WT as well as the Δ*hisB* mutant strain, further supporting the role of these proteins in cell division (Fig. 5 B and E, Fig. S5). DipM localization is restricted at midcell in dividing bacteria (Fig. 5 B), whereas CdlP appears to be localized both at septa and at the growing pole (Fig. 5 E, Fig. S6). As both *dipM* and *cdlP* are predicted to be essential, we used a anhydrotetracycline (AHTC)-inducible CRISPR-intereference (CRISPRi) system to deplete the corresponding gene products. Depletion of DipM leads to the generation of large bulges at midcell, very similar to what was observed when *B. abortus* is treated with the antibiotics aztreonam and cephalexin which target the division machinery in *E. coli* (Fig. 5 C) (Eberhardt et al., 2003). Depletion of CdlP also generates bulges at midcell, although smaller than when DipM is depleted (Fig. 5 F). HADA staining highlights the abnormally large midcell bands observed in CdlP depleted cells, in comparison with a strain expressing CdlP at normal levels (Fig. 5 F).

Discussion

Division defects in Rhizobiales usually lead to very diversified morphologies, such as branches, spheres, bulges or the generation of buds (Francis et al., 2017; Latch & Margolin, 1997b). Here, we identified a characteristic chaining phenotype related to cell division, although originating from an *a priori* unrelated function, *i.e.* histidine biosynthesis. This unusual morphology phenotype allowed us to identify essential actors of cell division, DipM and CdlP, which have not been characterized yet in *B. abortus*.

In this work, we propose that the chaining phenotype is due to incompletely digested PG at septa in *hisB* defective cells. On the one hand, PG sacculi extracted from Δ*hisB* mutant conserved the chaining morphology (Fig. S4). On the other hand, overexpression of two essential proteins predicted to be PG-associated suppressed the chaining phenotype. We could also show by fusing DipM and CdlP with mNG that both enzymes are localized at the constriction site in dividing cells, both in the WT and Δ*hisB* mutant (Fig. S5).

DipM is a M23 family endopeptidase, a family of enzymes cleaving bonds between amino acids of the stem peptide of the PG. DipM was shown to be involved in PG remodeling during cell division in *C. crescentus* (Moll et al., 2010). In distant organisms such as cyanobacteria, DipM was also found to be involved in cell separation, and is even conserved in chloroplasts of some algae, where it also allows division through PG digestion (Miyagishima et al., 2014). More recently, it was shown that the homologue of DipM in *Agrobacterium tumefaciens* ($DipM_{At}$) is likely to have broader functions than just the direct hydrolysis of PG to promote cell separation (Figueroa-Cuilan et al., 2021). Indeed, catalytic residues of the active site of $DipM_{At}$ are not conserved, similarly to their homologues in *E. coli*, EnvC and NlpD. In *E. coli*, these two factors do not have endopeptidase activity on their own but instead activate the amidases (AmiA, AmiB and AmiC) that are responsible for PG splitting (Uehara et al., 2010). In $DipM_{Ba}$, only two out of the four canonical catalytic residues are conserved (Figure S7), meaning that it is most probably inactive as an endopeptidase (Bochtler et al., 2004; Figueroa-Cuilan et al., 2021).

Finding interacting partners of DipM$_{Ba}$ could help in deciphering its exact function in *B. abortus*. Unlike DipM$_{At}$ and CdlP, DipM$_{Ba}$ seems to be located only at the constriction site, and not at the growing pole (Figure 5) (Figueroa-Cuilan et al., 2021). In *C. crescentus*, DipM septal localization was shown to be dependent on its LysM domain, which is also present in DipM$_{Ba}$ (Moll et al., 2010). Additionally, it would be worth to investigate the function of other endopeptidases in *B. abortus* (Table S1) and in particular BAB1_1846, that is also predicted to be directly regulated by the cell division activator CtrA.

The CdlP lipoprotein is predicted to be a zinc-dependent M48 protease. CdlP is both localized at constriction sites and growing poles in *B. abortus.* CdlP displays homologues in several genera of Rhizobiales like *Agrobacterium*, *Sinorhizobium*, *Phyllobacterium*, *Mesorhizobium* and *Bartonella,* suggesting that it could have co-evolved with unipolar growth. CdlP possesses a PG-binding LysM domain. The M48 peptidase domain of CdlP displays many homologues including BepA in *E. coli* (Narita et al., 2013) (Daimon et al., 2017) and Oma1, a negative regulator of mitochondrial fusion in humans (Murata et al., 2020). As a protease, CdlP is probably participating in PG remodeling by acting on other actors of cell division, and not directly on PG. For instance, CdlP could activate otherwise inactive PG hydrolases. CdlP could also inactivate negative regulators of division by proteolysis. Indeed, Oma1 is involved in mitochondrial fission, by cleaving Opa1, a positive regulator of mitochondrial fusion (25). Overall, the role of this metalloprotease in division and unipolar growth is a promising area of research for the future.

A common feature of CdlP, endopeptidases and amidases in general is that all these enzymes depend on zinc as a cofactor, and histidine is most often the metal binding residue (Vermassen et al., 2019). The ability of histidine to complex metal has already been demonstrated (Nairn et al., 2016). It is tempting to speculate that our *hisB* mutants would have impaired metal homeostasis, which could in turn locally affect the activity of some key periplasmic metalloenzymes involved in PG splitting.

Histidine metabolism has been already associated with filamentation phenotypes in *Escherichia coli* and *Salmonella enterica* serovar Typhimurium (Frandsen & D'Ari, 1993; Murray & Hartman, 1972). In those two bacterial species, division was inhibited when HisFH enzymes were overproduced, for reasons that remain unclear (Cano et al., 1998; Frandsen & D'Ari, 1993). Based on our results, we cannot exclude that the accumulation of IGP, the product of HisFH and the substrate of HisB (Figure S1) could be responsible for the phenotype of the *B. abortus hisB* mutants. However, in *Mycobacterium smegmatis,* histidine auxotroph mutants in almost the whole biosynthesis pathway genes exhibited a filamentation phenotype, all of which could be rescued by histidine supplementation, suggesting a link between cell division inhibition and histidine limitation in this particular case (de Wet et al., 2020).

Maintaining bacterial cell wall integrity during division is challenging. Characterizing the chaining phenotype of a *B. abortus* histidine auxotroph allowed us to identify two new periplasmic proteins required for normal cell division. These proteins, DipM and CdlP, are conserved in alphaproteobacteria and even more distantly in chloroplast and mitochondria. A deeper investigation of the molecular mechanisms involved in PG hydrolysis during cell division is needed to understand how a mutation in an *a priori* unrelated metabolic pathway is able to affect this crucial and well controlled process, which is still largely underinvestigated in bacterial pathogens such as *B. abortus*.

Materials and Methods

Bacterial strains, media and strains construction. *E. coli* strains were grown in Luria-Bertani medium at 37°C. Derivatives of the *B. abortus* 544 Nal^R strain were cultivated in TSB rich medium (3% Bacto Tryptic Soy Broth) at 37°C. Alternatively, the rich medium Heart Infusion Broth (HI) was used to grow *B. abortus.* Two defined media were also used for *B. abortus*, Plommet Erythritol (PE) (Plommet, 1991) composed of 7 g/L K_2HPO_4, 3 g/L KH_2PO_4, 0.1 g/L $Na_2S_2O_3$, 5 g/L NaCl, 0.2 mg/L nicotinic acid, 0.2 mg/L thiamine, 0.04 mg/L pantothenic acid, 0.01 g/L $MgSO_4$, 0.01 mg/L $MnSO_4$, 0.1 mg/L $FeSO_4$, 0.1 µg/L biotin and 2 g/L erythritol, and Gerhardt medium (Gerhardt & Wilson, 1948), composed of 30 g/L glycerol, 5 g/L lactate, 5 g/L glutamate, 10 g/L K_2HPO_4, 0.1 g/L $Na_2S_2O_3$, 7.5 g/L NaCl, 0.4 mg/L nicotinic acid, 0.2 mg/L thiamine, 0.2 mg/L pantothenic acid, 0.5 g/L $(NH_4)_2SO_4$, 0.01 g/L $MgSO_4$, 0.01 mg/L $MnSO_4$, 0.1 mg/L $FeSO_4$, 0.1 µg/L biotin. For the growth measurements in PE, the *B. abortus* strains were first grown overnight in TSB, next they were diluted to reach an exponential phase, then they were

washed twice with PBS and diluted to reach an OD_{600nm} of 0.1 in PE (with or without 1 mM histidine). Antibiotic concentrations are the following: ampicillin, 100 µg/ ml; kanamycin, 10 or 50 µg/ml (10 µg/ml is chosen when *kan*^{R} marker is integrated in a chromosome of *B. abortus*); chloramphenicol, 20 µg/ml; nalidixic acid, 25 µg/ml; gentamicin, 50 µg/ml. The strains and plasmids used in this study are listed in SI Appendix, Tables S2 and S3, respectively. Details of their construction can be found in the SI Appendix text.

CRISPR-interference. The CRISPRi plasmids (pJMP1039, pJMP1339, pJMP1356 and pJMP1339) were bought from Addgene (see Table S3) and were a gift from Carol Gross, Jason Peters & Oren Rosenberg. The pJMP1339t2 was constructed by Gibson Assembly (see SI appendix for more details). Single guide RNAs (sgRNAs) were designed with Benchling and chosen on the minus strand of the target promoter, then assembled on the *Bsa*I sites of the pJMP1339t_2 as detailed by the authors (Banta et al., 2020). Cloning steps until conjugation with *Brucella* were made as described by Banta and colleagues (37). Primers that will be transcribed to sgRNA were hybridized by adding 1 µL of each primer (100 µM) to 5 µl of CutSmart 10X buffer (NEB) and scaled up to 50 µL with ddH_2O. The mix was then heated at 95 °C for 5 min and let cool down at room temperature (RT) for 15 min. Annealed oligos were diluted 40 times and 2 µl were used for ligation with the *Bsa*I restricted plasmid.

HeLa cells culture and infection. HeLa cells (from the Centre d'Immunologie de Marseille-Luminy, Marseille, France) were cultivated at 37°C and in a 5 % CO_2 atmosphere in DMEM (Invitrogen) supplemented with 10 % fetal bovine serum (Gibco), 0.1 g/l non-essential amino acids and 0.1 g/l sodium pyruvate (Invitrogen). For the infections, HeLa cells were seeded in 24-well plates (on coverslips for immunolabeling) at a concentration of 6.10^4 cells/ml. On the day of the infection, an overnight culture of *B. abortus* was diluted in DMEM to reach a MOI (multiplicity of infection) of 300. Bacteria were added to HeLa cells and the 24-well plates were centrifuged at 400 *g* for 10 min at RT. Cells were then incubated at 37°C in a 5 % CO_2 atmosphere for 1 h. Cells were washed twice in PBS and fresh medium supplemented with 50 µg/ml gentamicin was added to kill extracellular bacteria. For CFU counts, at the different time points (2 h, 5 h, 24 h and 48 h after infection) cells were washed twice in PBS, and then lysed with PBS with 0.1% Triton X-100 for 10 min at RT. Dilutions were then spotted (20 µl) onto TSB agar, incubated at 37 °C and colony-forming units were counted. The CFU number was calculated per ml of lysate (0.5 ml per well). When indicated, 10 mM histidine was added in the medium at the beginning of the infection.

Immunolabeling of infected HeLa cells. Cells were washed three times with PBS, then fixed in 2 % paraformaldehyde (PFA) for 20 min at RT and permeabilized in PBS 0.1 % Triton X-100 (Prolabo) for 10 min. Primary and secondary antibodies were diluted in PBS containing 0.1 % Triton X-100 and 3 % bovine serum albumin (BSA, Sigma-Aldrich). The immunodetection of intracellular *B. abortus* was made with a A76-12G12 monoclonal antibody (Cloeckaert et al., 1992) (hybridoma culture supernatant not diluted) followed by goat anti-mouse secondary antibodies coupled to Alexa 488 or Texas red diluted 500 times (Sigma Aldrich). The coverslips were washed three times with PBS, then once with ddH_2O and mounted with Mowiol (Sigma).

PG isolation for morphology analysis. An overnight culture of around 7.5 mL of *B. abortus* in HI medium was pelleted (4,600 *g*, 2.5 min), resuspended in 1 mL PBS and then inactivated for 1 h at 80°C. Cells were pelleted again for 10 min at 10,000 *g* and then heated for 3 h in 1 mL 5 % SDS at 95°C. Cells were washed three times with PBS and then 2 µl were dropped on an agarose pad (1% PBS agarose) for microscopy.

eFluor and PG labelling. Exponential phase bacteria were washed (4,600 *g*, 2.5 min) twice with PBS resuspended in eBioscience™ Cell Proliferation Dye eFluor™ 670 (eFluor, Invitrogen) at a final concentration of 5 µM in PBS. After 15 min of incubation at RT with shaking and protected from light, bacteria were washed twice and resuspended either in DMEM or in HI, for the generation of chains inside host cells or in growth medium, respectively. For PG labeling, after 5 h of growth in HI, bacteria were short pulse labeled for 5 min with 7-hydroxycoumarin 3-carboxylic acid coupled to 3-amino-D-alanine (HADA) (12) at a final concentration of 500 µM in HI, protected from the light. Cells were pelleted and resuspended in 70 % ice cold ethanol. After 15 min of incubation on ice, cells are washed 3 times with PBS before being observed by fluorescence microscopy.

Microscopy and analysis. Bacteria were observed on 1 % agarose PBS pad with an inverted microscope Nikon Eclipse Ti2 (oil objective 100x, CFI plan Apo Lambda DM 100XH 1.45/0.13 mm). Pictures were acquired with an Orca Flash 4.0 V3 (Hamamatsu). All images were analyzed with MicrobeJ, a plug-in of ImageJ (Ducret et al., 2016; Schneider et al., 2012). For length quantification, only isolated bacteria were analyzed and disrupted bacteria as well as cell aggregates were excluded from the analysis. For strains labelled with eFluor, only bacteria possessing a unique polar eFluor signal were used to construct a demographic representation.

Acknowledgments

We are grateful to Marty Roop and Jean-Jacques Letesson for their advices in the writing of this manuscript. We thank Stéphane Vincent and his team for the synthesis of HADA, Neeraj Dhar for advices regarding mNeonGreen, as well as Mathieu Waroquier, Françoise Tilquin and Aurélie Mayard for their technical assistance. This research has been funded by grants from the *Fonds de la Recherche Scientifique-Fonds National de la Recherche Scientifique* (FRS-FNRS, http://www.fnrs.be) (PDR Brucell-cycle T.0060.15, and PDR Single cell analysis of *Brucella* growth T.0058.20) to X. De Bolle. The work was also supported by a grant from Actions de Recherche Concertée 17/22-087 from the *Fédération Wallonie-Bruxelles* of Belgium. Agnès Roba and Pierre Godessart hold a PhD fellowship from FRS-FNRS (Aspirant and FRIA, respectively). We thank the University of Namur for logistic support.

References

1. J. Batut, S. G. Andersson, D. O'Callaghan, The evolution of chronic infection strategies in the alpha-proteobacteria. *Nat Rev Microbiol* **2**, 933-945 (2004).
2. A. M. Whatmore, J. T. Foster, Emerging diversity and ongoing expansion of the genus *Brucella*. *Infect Genet Evol* **92**, 104865 (2021).
3. G. Pappas, P. Papadimitriou, N. Akritidis, L. Christou, E. V. Tsianos, The new global map of human brucellosis. *The Lancet Infectious Diseases* **6**, 91-99 (2006).
4. N. Francis *et al.*, CtrA controls cell division and outer membrane composition of the pathogen *Brucella abortus*. *Mol Microbiol* **103**, 780-797 (2017).
5. P. J. Brown *et al.*, Polar growth in the Alphaproteobacterial order Rhizobiales. *Proc Natl Acad Sci U S A* **109**, 1697-1701 (2012).
6. J. F. Sternon *et al.*, Transposon Sequencing of *Brucella abortus* Uncovers Essential Genes for Growth In Vitro and Inside Macrophages. *Infect Immun* **86** (2018).
7. T. Starr, T. W. Ng, T. D. Wehrly, L. A. Knodler, J. Celli, *Brucella* intracellular replication requires trafficking through the late endosomal/lysosomal compartment. *Traffic* **9**, 678-694 (2008).
8. J. Celli *et al.*, *Brucella* evades macrophage killing via VirB-dependent sustained interactions with the endoplasmic reticulum. *J Exp Med* **198**, 545-556 (2003).
9. C. Bisson *et al.*, Crystal Structures Reveal that the Reaction Mechanism of Imidazoleglycerol-Phosphate Dehydratase Is Controlled by Switching Mn(II) Coordination. *Structure* **23**, 1236-1245 (2015).
10. V. Vassen *et al.*, Localized incorporation of outer membrane components in the pathogen *Brucella abortus*. *EMBO J* **38** (2019).
11. C. Heidrich, A. Ursinus, J. Berger, H. Schwarz, J. V. Holtje, Effects of multiple deletions of murein hydrolases on viability, septum cleavage, and sensitivity to large toxic molecules in *Escherichia coli*. *J Bacteriol* **184**, 6093-6099 (2002).
12. T. Uehara, T. Dinh, T. G. Bernhardt, LytM-domain factors are required for daughter cell separation and rapid ampicillin-induced lysis in *Escherichia coli*. *J Bacteriol* **191**, 5094-5107 (2009).
13. J. N. Latch, W. Margolin, Generation of buds, swellings, and branches instead of filaments after blocking the cell cycle of *Rhizobium meliloti*. *Journal of bacteriology* **179**, 2373-2381 (1997).
14. E. Kuru *et al.*, In Situ probing of newly synthesized peptidoglycan in live bacteria with fluorescent D-amino acids. *Angew Chem Int Ed Engl* **51**, 12519-12523 (2012).
15. A. A. Yakhnina, T. G. Bernhardt, The Tol-Pal system is required for peptidoglycan-cleaving enzymes to complete bacterial cell division. *Proc Natl Acad Sci U S A* **117**, 6777-6783 (2020).

16. A. K. Sharma, S. Kumar, H. K, D. B. Dhakan, V. K. Sharma, Prediction of peptidoglycan hydrolases- a new class of antibacterial proteins. *BMC Genomics* **17**, 411 (2016).
17. C. Eberhardt, L. Kuerschner, D. S. Weiss, Probing the catalytic activity of a cell division-specific transpeptidase in vivo with beta-lactams. *J Bacteriol* **185**, 3726-3734 (2003).
18. A. Moll, S. Schlimpert, A. Briegel, G. J. Jensen, M. Thanbichler, DipM, a new factor required for peptidoglycan remodelling during cell division in *Caulobacter crescentus*. *Mol Microbiol* **77**, 90-107 (2010).
19. S. Y. Miyagishima, Y. Kabeya, C. Sugita, M. Sugita, T. Fujiwara, DipM is required for peptidoglycan hydrolysis during chloroplast division. *BMC Plant Biol* **14**, 57 (2014).
20. W. M. Figueroa-Cuilan *et al.*, Diversification of LytM Protein Functions in Polar Elongation and Cell Division of *Agrobacterium tumefaciens*. *Frontiers in Microbiology* **12** (2021).
21. T. Uehara, K. R. Parzych, T. Dinh, T. G. Bernhardt, Daughter cell separation is controlled by cytokinetic ring-activated cell wall hydrolysis. *EMBO J* **29**, 1412-1422 (2010).
22. M. Bochtler, S. G. Odintsov, M. Marcyjaniak, I. Sabala, Similar active sites in lysostaphins and D-Ala-D-Ala metallopeptidases. *Protein Sci* **13**, 854-861 (2004).
23. S. Narita, C. Masui, T. Suzuki, N. Dohmae, Y. Akiyama, Protease homolog BepA (YfgC) promotes assembly and degradation of beta-barrel membrane proteins in *Escherichia coli*. *Proc Natl Acad Sci U S A* **110**, E3612-3621 (2013).
24. Y. Daimon *et al.*, The TPR domain of BepA is required for productive interaction with substrate proteins and the beta-barrel assembly machinery complex. *Mol Microbiol* **106**, 760-776 (2017).
25. D. Murata *et al.*, Mitochondrial Safeguard: a stress response that offsets extreme fusion and protects respiratory function via flickering-induced Oma1 activation. *EMBO J* **39**, e105074 (2020).
26. A. Vermassen *et al.*, Cell Wall Hydrolases in Bacteria: Insight on the Diversity of Cell Wall Amidases, Glycosidases and Peptidases Toward Peptidoglycan. *Front Microbiol* **10**, 331 (2019).
27. B. L. Nairn *et al.*, The Response of *Acinetobacter baumannii* to Zinc Starvation. *Cell Host Microbe* **19**, 826-836 (2016).
28. N. Frandsen, R. D'Ari, Excess histidine enzymes cause AICAR-independent filamentation in *Escherichia coli*. *Mol Gen Genet* **240**, 348-350 (1993).
29. M. L. Murray, P. E. Hartman, Overproduction of hisH and hisF gene products leads to inhibition of cell division in *Salmonella*. *Canadian Journal of Microbiology* **18**, 671-681 (1972).
30. D. A. Cano, C. Mouslim, J. A. Ayala, F. García-del Portillo, J. Casadesús, Cell Division Inhibition in *Salmonella typhimurium* Histidine-Constitutive Strains an ftsI-Like Defect in the Presence of Wild-Type Penicillin-Binding Protein 3 Levels. *J Bacteriol.* **180**, 5231-5234 (1998).
31. T. J. de Wet, K. R. Winkler, M. Mhlanga, V. Mizrahi, D. F. Warner, Arrayed CRISPRi and quantitative imaging describe the morphotypic landscape of essential mycobacterial genes. *Elife* **9** (2020).
32. M. Plommet, Minimal requirements for growth of *Brucella suis* and other *Brucella* species. *Zentralblatt für Bakteriologie* **275**, 436-450 (1991).
33. P. Gerhardt, J. B. Wilson, The nutrition of Brucellae: growth in simple chemically defined media. *Journal of bacteriology* **56**, 17-24 (1948).
34. A. B. Banta, A. L. Enright, C. Siletti, J. M. Peters, A High-Efficacy CRISPR Interference System for Gene Function Discovery in *Zymomonas mobilis*. *Appl Environ Microbiol* **86** (2020).
35. A. Cloeckaert, I. Jacques, P. de Wergifosse, G. Dubray, J. N. Limet, Protection against *Brucella melitensis* or *Brucella abortus* in mice with immunoglobulin G (IgG), IgA, and IgM monoclonal antibodies specific for a common epitope shared by the *Brucella* A and M smooth lipopolysaccharides. *Infect Immun* **60**, 312-315 (1992).
36. C. A. Schneider, W. S. Rasband, K. W. Eliceiri, NIH Image to ImageJ: 25 years of image analysis. *Nat Methods* **9**, 671-675 (2012).
37. A. Ducret, E. M. Quardokus, Y. V. Brun, MicrobeJ, a tool for high throughput bacterial cell detection and quantitative analysis. *Nat Microbiol* **1**, 16077 (2016).

Figures and Tables

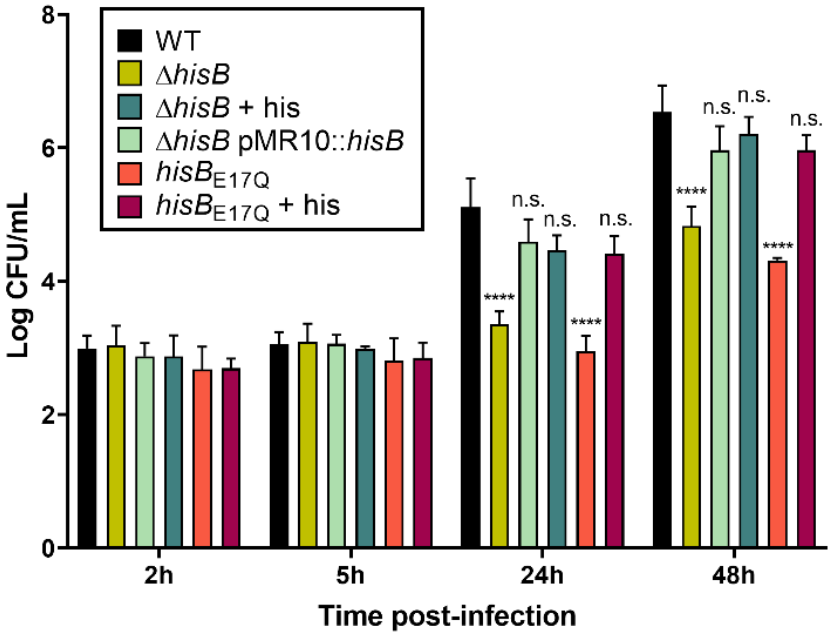

Figure 1. Functional HisB is required for *B. abortus* intracellular replication. Intracellular replication of WT, deletion mutant Δ*hisB*, catalytically dead mutant *hisB*$_{E17Q}$ and the complemented Δ*hisB* mutant was assessed by enumerating colony-forming units (CFU) after 2, 5, 24 and 48 h post infection of HeLa cells. When indicated, 10 mM histidine was added in the medium at the beginning of the infection. Data represents mean ± SD of biological triplicates. Statistical significance between results for a given strain and those for the WT was determined by two-way ANOVA followed by Dunnett's multiple comparison test (n.s., not significant; **** $P < 0.0001$).

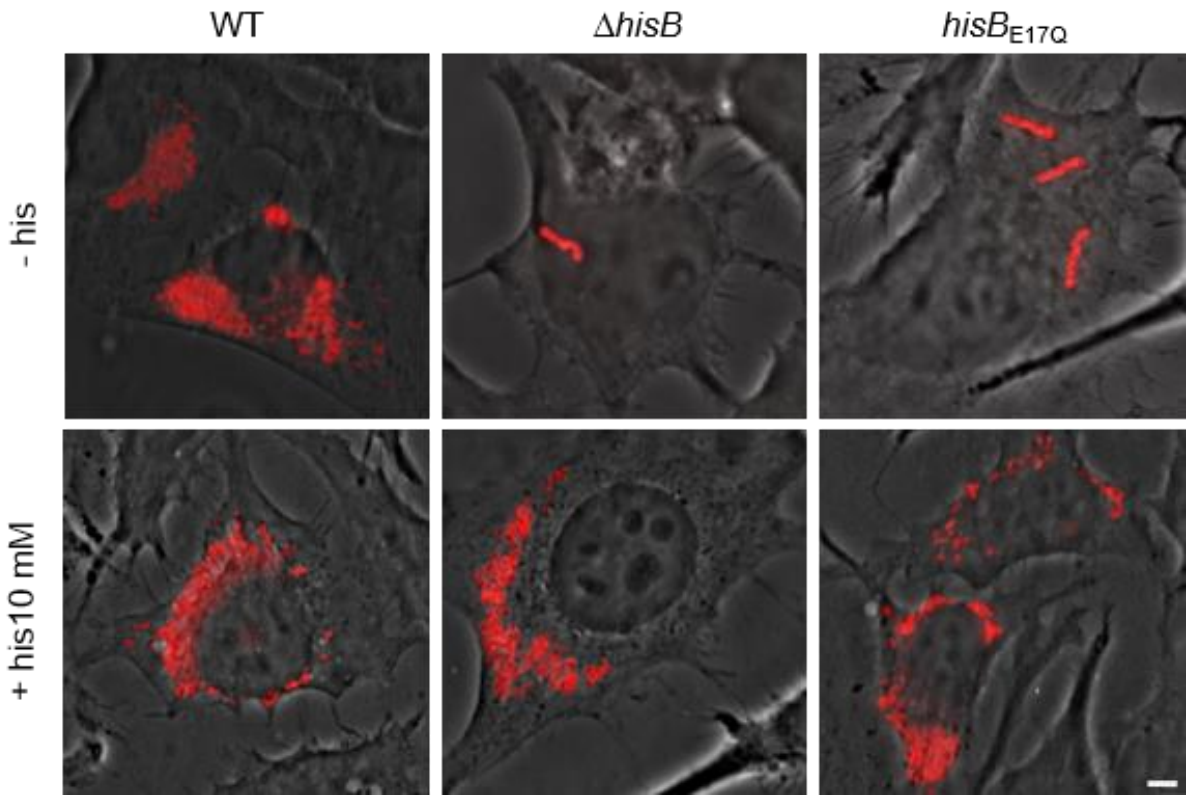

Figure 2. Morphology of *B. abortus hisB* deletion and catalytic mutants during infection of HeLa cells. Immunofluorescence microscopy of HeLa cells infected for 24 h with WT, Δ*hisB* or $hisB_{E17Q}$ strains. Phase contrast images were merged with anti-*Brucella* (S-LPS) staining (red) to detect intracellular bacteria. Chaining morphology was observed in 97.5 % (*n* = 80) and 98.9 % (*n* = 93) of infected cells with Δ*hisB* and $hisB_{E17Q}$, respectively. This percentage falls down to 20 % (*n* = 73) and 8.4 % (*n* = 60) when histidine is added to the medium during the infection. (Scale bar: 5 µm).

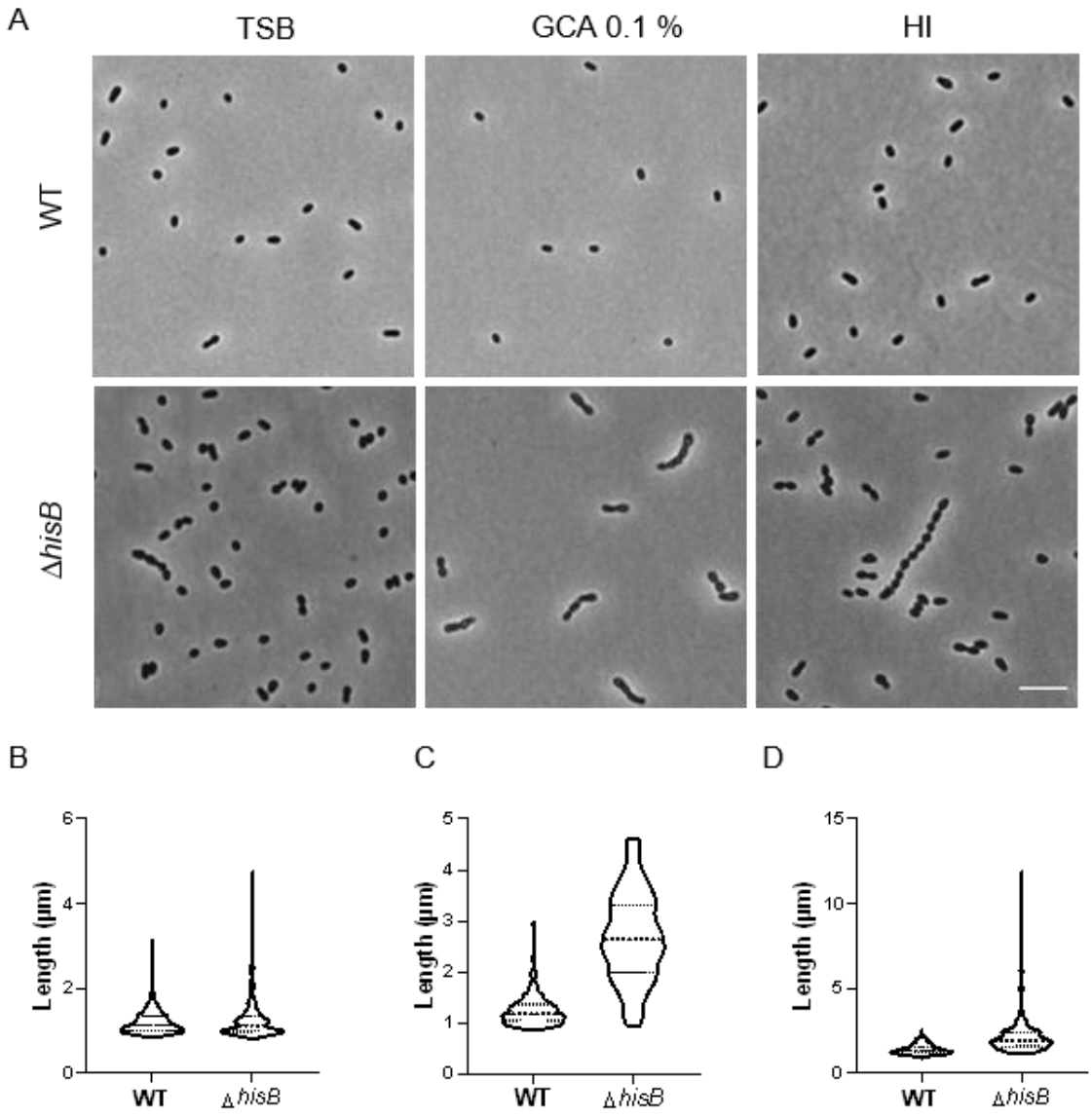

Figure 3. Cell morphology of the *B. abortus* Δ*hisB* mutant is dependent on growth conditions. (A) Morphology of WT and an isogenic Δ*hisB* mutant grown in rich medium (TSB), minimal medium (Gerhardt + 0.1 % Casamino Acids) and another rich medium (HI). Scale bar: 5 µm. Bottom panels indicate cell length distribution ($100 < n < 450$) depending on corresponding growth conditions (B–D). The length axis was adapted to chain length in each culture condition.

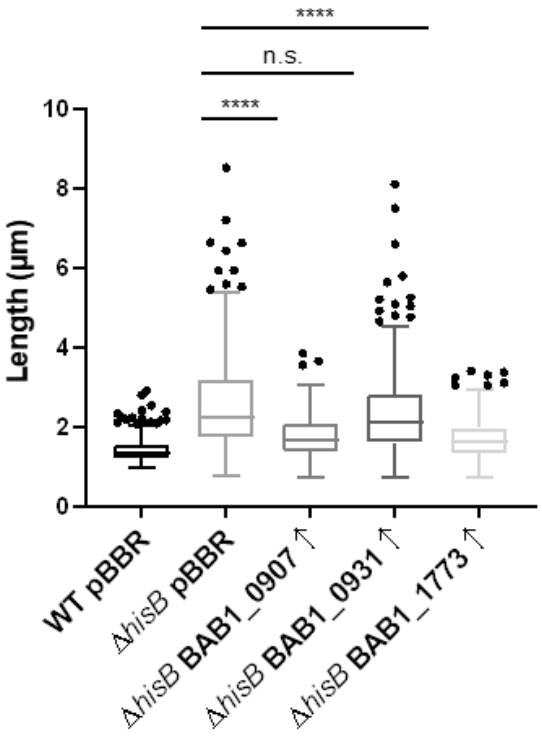

Figure 4. Length distribution of WT (n = 314), Δ*hisB* (n = 296), and Δ*hisB* strains overexpressing BAB1_0907 (n = 339), BAB1_0931 (n = 263) and BAB1_1773 (n = 290). All strains were grown in HI with chloramphenicol, with the WT and Δ*hisB* carrying an empty pBBR1 vector whereas overexpression strains carry a pBBR1 vector with the corresponding genes. Distributions were analyzed using Dunn's multiple comparison tests after Kruskal–Wallis. **** $P < 0.0001$.

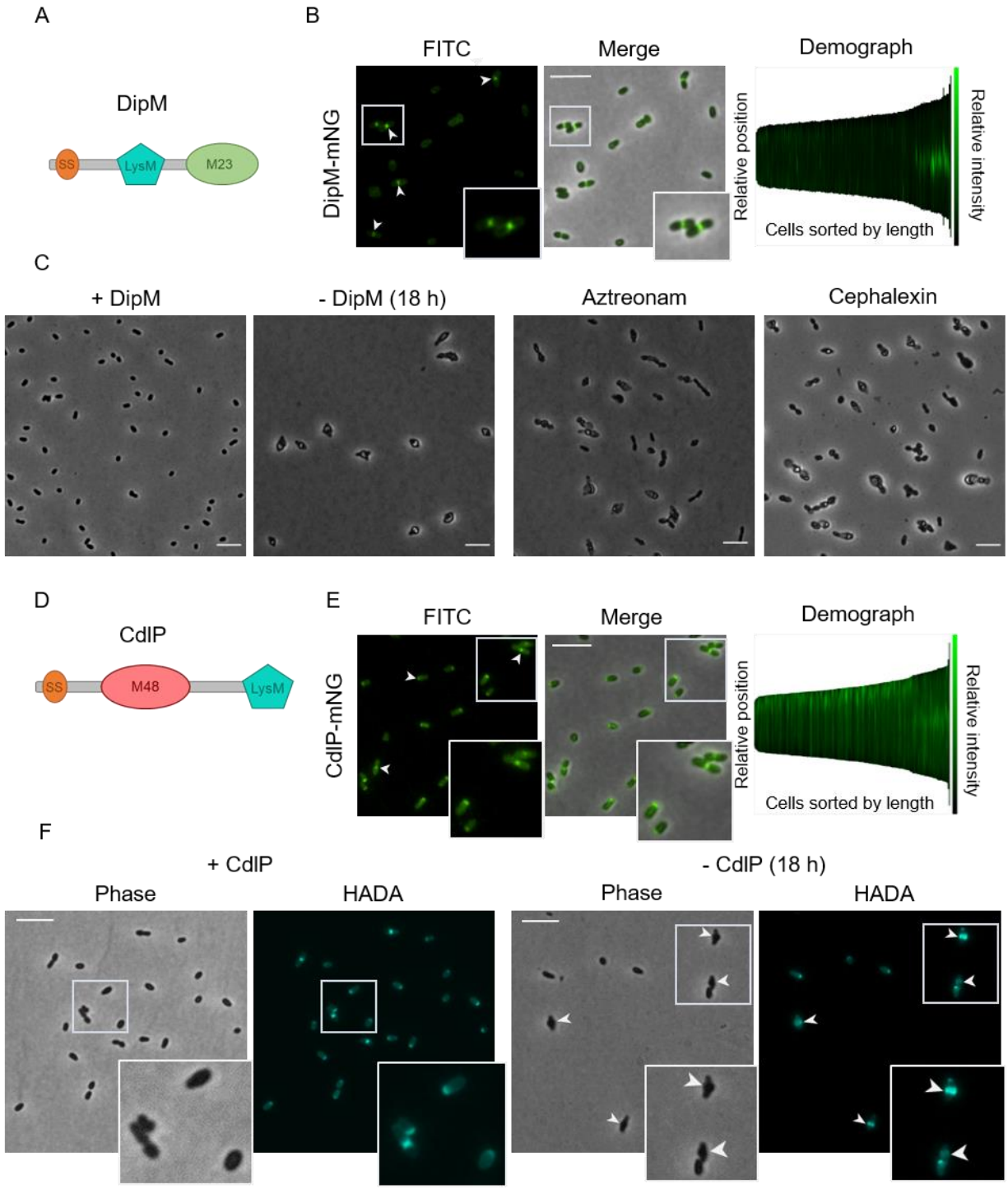

Figure 5. DipM and CdlP are involved in cell division in *B. abortus*. Schematic of the domain organization of DipM (A) and CdlP (D). Both comprise a LysM domain and a predicted lipoprotein signal sequence (SS). Overnight cultures of *B. abortus* strains bearing the DipM-mNG (B) or CdlP-mNG (E) fusion were imaged on agarose pads by phase contrast and fluorescence microscopy. Arrows show midcell and/or polar localization. Demographic representation of mNG localization was obtained after bacteria were sorted by cell length and show midcell localization of DipM in dividing cells (*N* = 246) (B) and polar and midcell localization of CdlP (*N* = 216) (E). (C) Phase contrast images of DipM-depleted cells after 18 hours of growth in the presence of anhydrotetracycline (AHTC) (left panels), or after 18 hours of growth in the presence of 100 µg/ml of aztreonam and cephalexin (right panels). (F) Phase contrast and fluorescence images of CdlP-depleted cells after 18 hours of growth in the presence of AHTC, and after HADA labelling. Arrows show bulges at midcell. Scale bars: 5 µm.

Supporting information

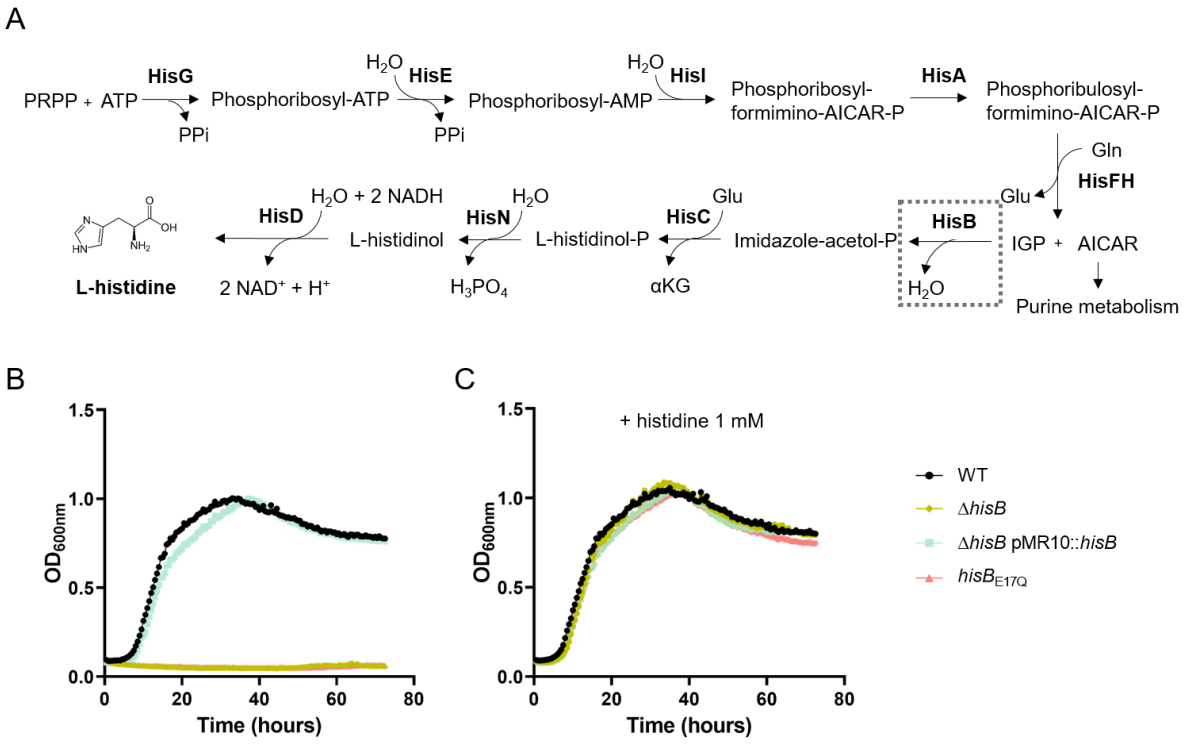

Figure S1. *B. abortus hisB* mutants are auxotrophic for histidine. (*A*) Schematic representation of histidine biosynthetic pathway in *B. abortus*. IGP, Imidazole Glycerol Phosphate; αKG, α-ketoglutarate; PRPP, phosphoribosylpyrophosphate. (*B, C*) Growth kinetics of *B. abortus* WT and the indicated strains in PE with or without 1 mM histidine. The pMR10 is a low copy plasmid. Data are representative of biological triplicates.

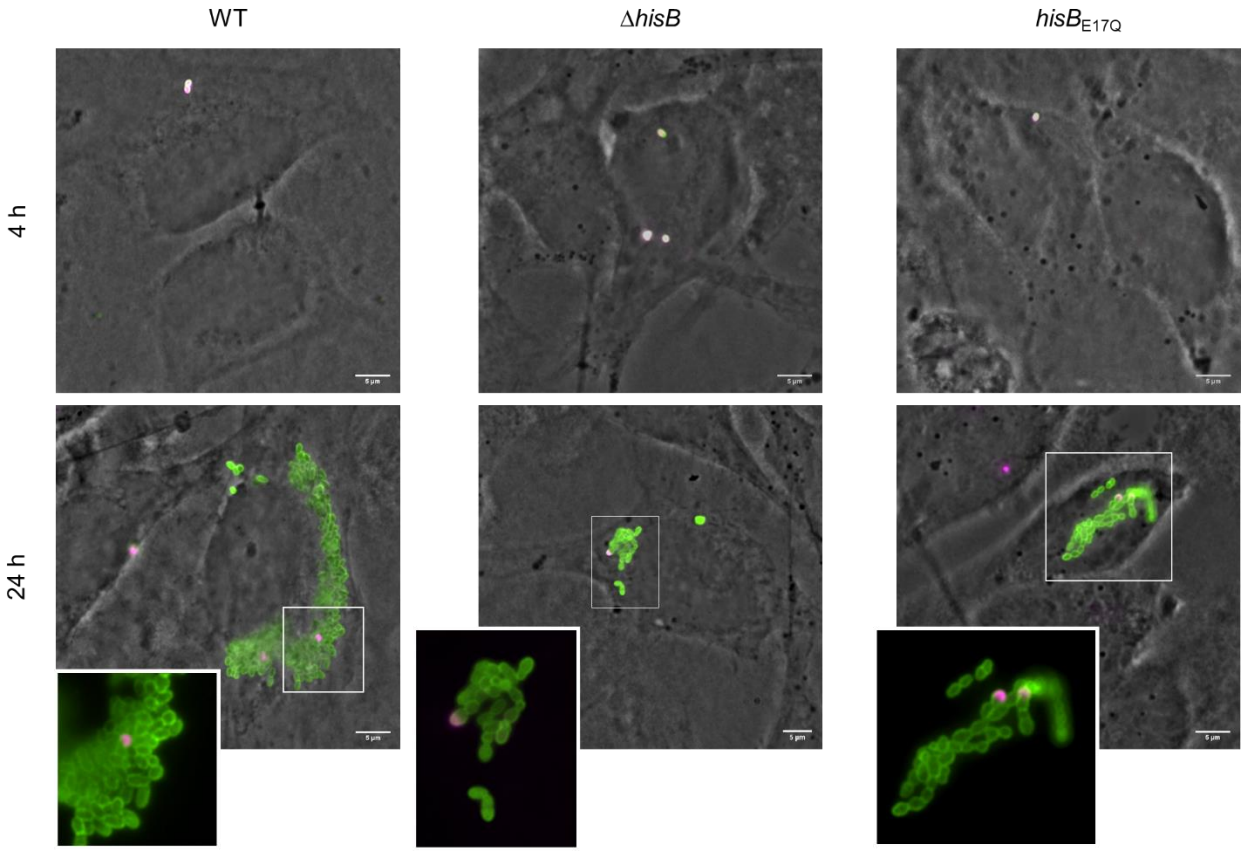

Figure S2. Chains are newly generated inside host cells. Immunofluorescence microscopy of HeLa cells infected for 4 and 24 h with WT, Δ*hisB* or *hisB*$_{E17Q}$ strains. HeLa cell were infected with eFluor-labeled bacteria, then at the indicated time points, cells were fixed and labeled with anti-*Brucella* (S-LPS) staining (green) to detect intracellular bacteria. Scale bar: 5 µm.

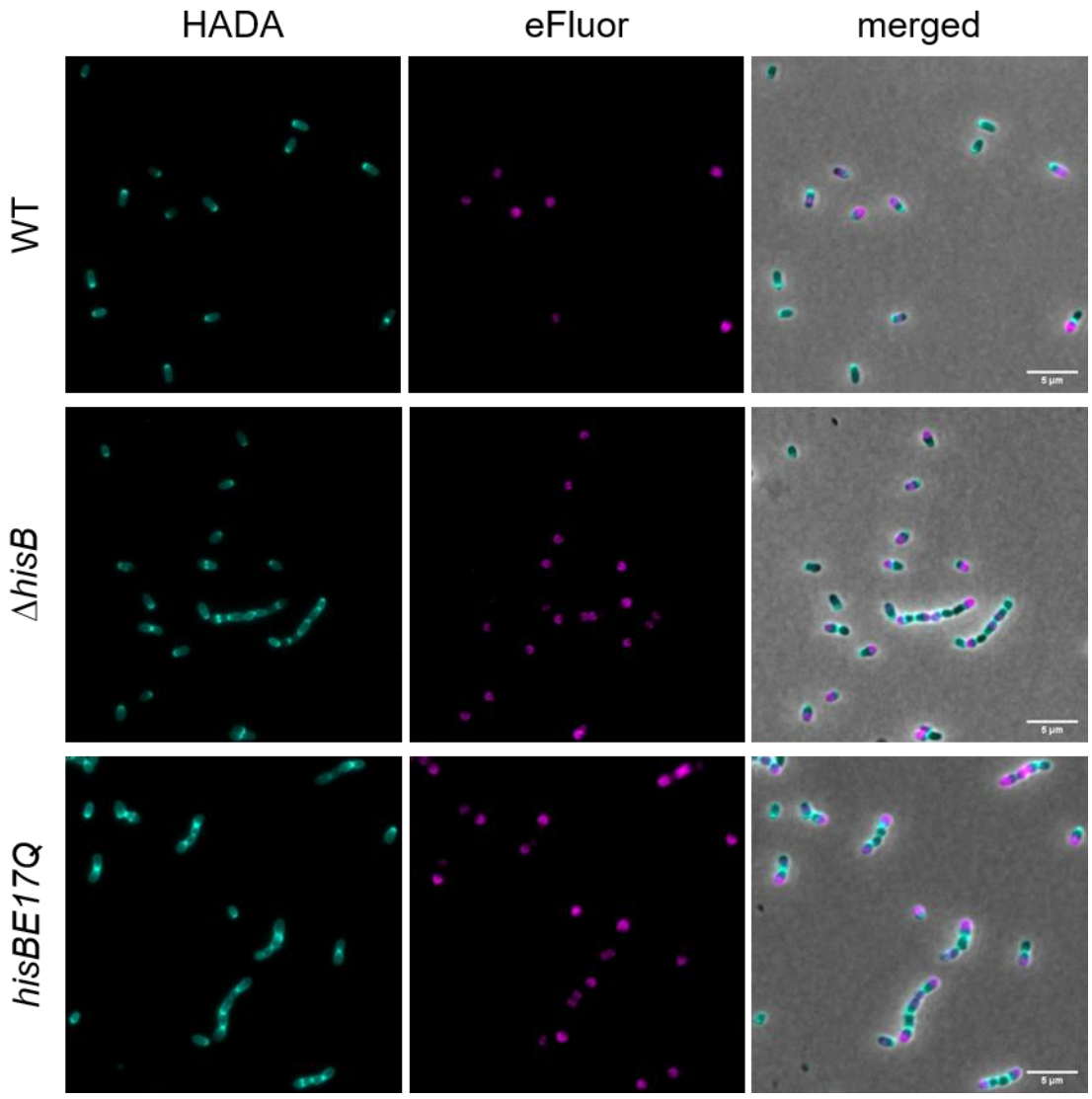

Figure S3. Unipolar insertion of PG in WT and chaining mutants. Short pulse labelling with the fluorescent D-amino acid HADA was performed on eFluor-labeled bacteria after 5 h of growth in HI without any labeling. Scale bars: 5 µm.

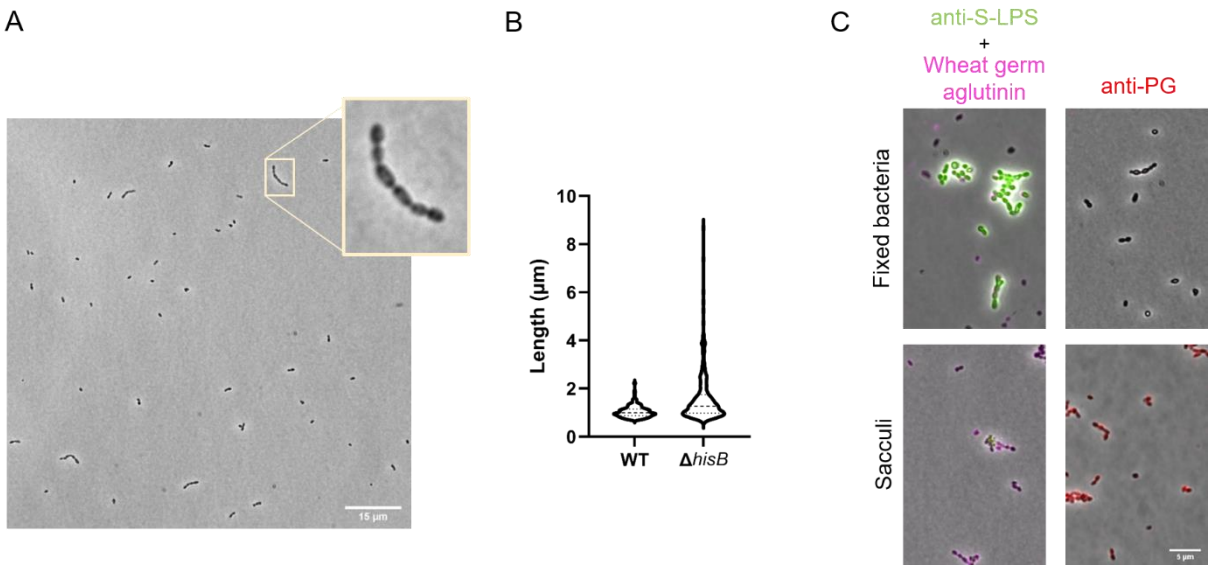

Figure S4. Δ*hisB* mutant chaining phenotype is due to septal PG splitting defect. (*A*) Images of PG sacculi isolated from Δ*hisB* cells grown in HI. Scale bar: 15 µm. (*B*) Comparison of the length distribution of sacculi isolated from WT or Δ*hisB.* (*C*) Images of fixed intact Δ*hisB* cells and purified PG sacculi, labeled either with anti-S-LPS antibodies (green) and Alexa 647-conjugated WGA (pink) or with anti-PG antibodies (red). Scale bar: 5 µm.

Table S1. Putative PG hydrolases predicted from the genome of *B. abortus*. *B. abortus* genome was examined using the BLAST server and the « HyPe » tool (http://metabiosys.iiserb.ac.in/hype/) (Sharma et al., 2016) to identify and classify novel PG hydrolases.

Type	Locus Tag[a]	Signal P[b]	Essentiality in *B. abortus*[c]	CtrA target[d]	Conserved domains[e]	Family, type or class[f]	Equivalent in *C. crescentus*/*A. tumefaciens*[g]
Amidase	BAB1_0931	Periplasmic Sec/SpI	**"Low fitness"**		AMIN, Ami3	Type3	AmiC (CC_1876)
	BAB1_1462	Cytoplasmic	Not essential		Ami2	Type2	AmpD (CC_2567)
Endopeptidase	BAB1_0907 / DipM	Periplasmic Sec/SpII	**Essential**	yes	LysM	Peptidase M23/M37	DipM (CC_02075)
	BAB1_0703	Cytoplasmic	Not essential			Peptidase M23/M37	LdpA (CC_1872)
	BAB1_1866	Cytoplasmic	Not essential			Peptidase M23/M37	LdpD (CC_3034)
	BAB1_1846 / EnvC	Periplasmic Sec/SpI	Not essential	yes		Peptidase M23/M37	LdpF (CC_3434)
	BAB2_1008 / MepA	Periplasmic Sec/SpI	Not essential			Peptidase M74	MepA (Atu_0186)
Carboxypeptidase	BAB1_1010	Periplasmic Sec/SpI	Not essential		2x PBP5 domain (C-terminal) ; transmembrane region (N-terminal)	DacC superfamily	PBP5 (Atu_1499)
	BAB2_0257	Cytoplasmic	Not essential		Transmembrane region	AmpC transpeptidase superfamily (class C)	AmpC (Atu_0929)
	BAB2_0287	Cytoplasmic	Not essential			D-aminopeptidase	Atu_2513
	BAB1_1193	Periplasmic Sec/SpI	**"Low fitness"**	yes		D-alanyl-D-alanine carboxypeptidase	DacC (Atu_1505)
	BAB1_1094	Periplasmic TAT	Not essential	yes	DacC, SPOR	D-alanyl-D-alanine carboxypeptidase	Atu_2321
	BAB1_2037	Periplasmic Sec/SpI	**"Low fitness"**		DacC	D-alanyl-D-alanine carboxypeptidase	Atu_3634
Lytic transglycosylases	BAB1_0666	Cytoplasmic	Not essential			Slt70	SdpA (CC_1194)
	BAB1_1461	Periplasmic Sec/SpI	Not essential		Transmembrane region	Lyz-like	SdpC (CC_2416)
	BAB2_1100 / MltE	Periplasmic Sec/SpI	Not essential			MltE superfamily	Atu_0572
	BAB1_1836	Periplasmic Sec/SpI	Not essential			Lyz-like	
	BAB1_2076 / MltA	Periplasmic	Not essential			MltA superfamily	MltA (Atu_0009)
	BAB1_0028 / MltB2	Periplasmic Sec/SpI	Not essential		Transmembrane region	Lyz-like, MltB	MltB1 (Atu_0092)
	BAB1_1466 / MltB1	Periplasmic Sec/SpI	Not essential			Lyz-like, MltB	MltB2 (Atu_2122)
	BAB1_1836	Periplasmic Sec/SpI	Not essential			Lyz-like	MltB3 (Atu_2489)
	BAB2_0069	Periplasmic Sec/SpI	Not essential	yes	Transmembrane region	Lyz-like, MltB2	MltB4 (Atu_3779)
	BAB1_0064	Periplasmic Sec/SpII	Not essential			MltE superfamily	Atu_2117
	BAB1_1227	Periplasmic Sec/SpII	Not essential			Lyz-like	Atu_2451
	BAB1_1531	Periplasmic Sec/SpI	Not essential		Transmembrane region	Lyz-like, MltE	Atu_3093
	BAB2_0068 / VirB1	Periplasmic	Not essential			Lyz-like	Atu_6167
Others	BAB1_1773/ CdlP	Periplasmic Sec/SpII	**Essential**		LysM	Zinc dependent protease M48	Atu_2710
	BAB1_1465	Periplasmic Sec/SpII	Not essential		GH25 muramidase	GH25 muramidase 1	Atu_2121

Columns indicate [a] the locus tag of the gene in the genome of *B. abortus* 2308 strain, plus the canonical name when available, [b] putative localization of the protein based on Signal P 5.0 (Almagro Armenteros et al., 2019), [c] essentiality of the gene based on Tn-seq data (Sternon et al., 2018), [d] putative direct regulation by CtrA based on ChIP-seq data (Francis et al., 2017), [e] conserved domains and [f] protein family name based on CDD database and SMART (Letunic & Bork, 2017), and [g] *C. crescentus* and *A. tumefaciens* homologues gathered using BLAST. Lyz-like, lysozyme-like domain family.

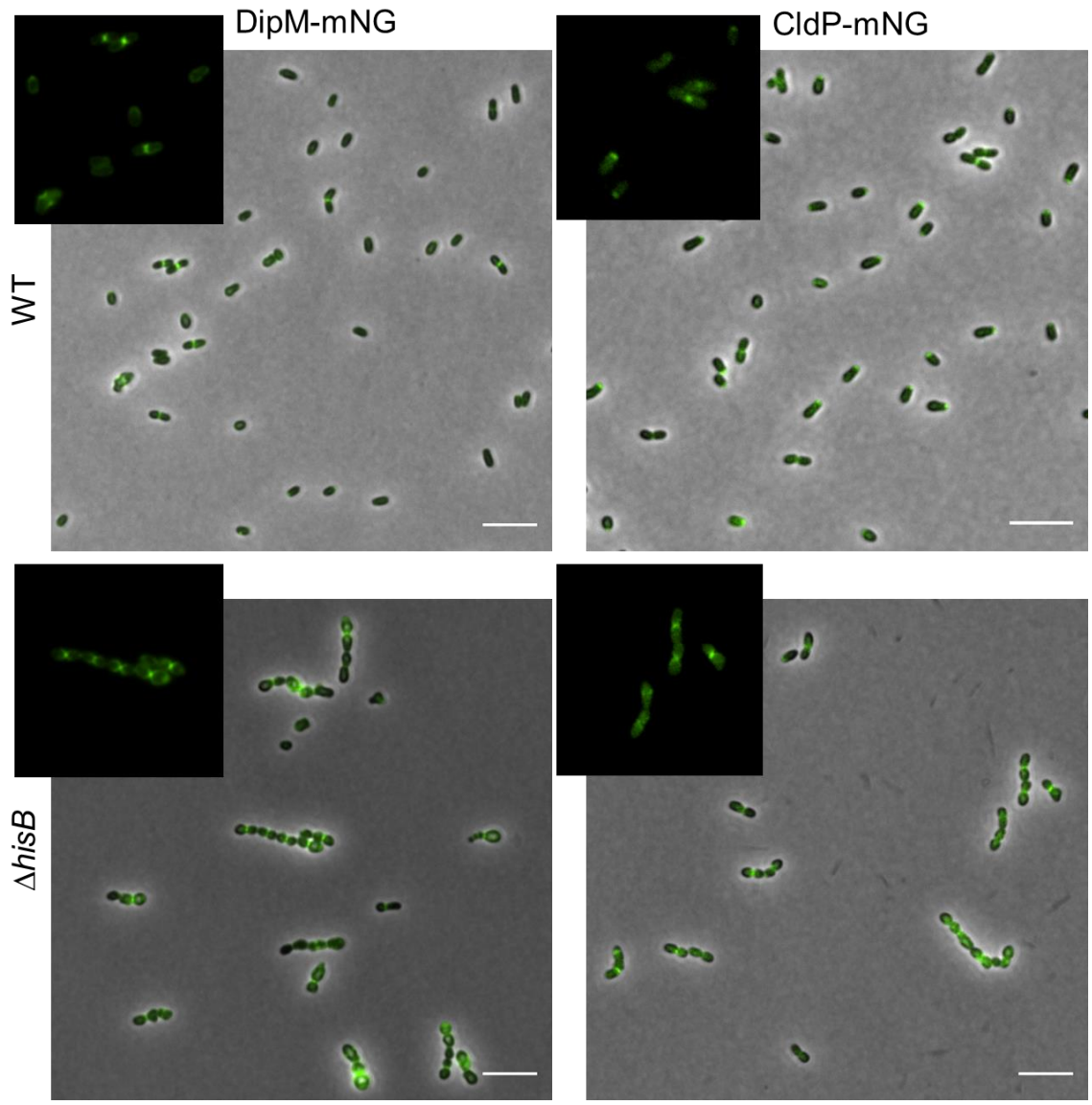

Figure S5. DipM and CldP display septal localization in WT and Δ*hisB* mutant. Cells expressing DipM-mNG or CldP-mNG were grown in HI to stationary phase and imaged by phase contrast and fluorescence microscopy. Scale bar: 5 µm.

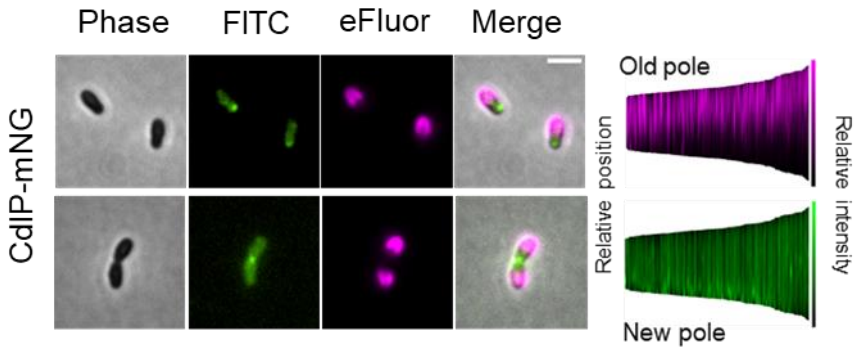

Figure S6. CdlP is localized at the growing pole. Phase contrast and microscopy images of the *cdlP-mNG* strain. Overnight cultures were diluted to an OD_{600nm} of 0.2 and stained with eFluor, and afterwards were allowed to grow in fresh TSB medium for 2 hours. Demographic representation of mNG localization, after bacteria were sorted by cell length and oriented with the the eFluor signal on top of the demograph, corresponding to the old pole. *N* = 214 (three biological replicates). Scale bar: 2 µm.

```
Atu1832          NRMDPFLGRPALHTGIDFRAETGADVKSTGAGKVTVAENS-GGYGNMVEIDHGQGVSTRF 370
DipMCc           VKG-----TGQRNDGLNIRAPQGTPVLSSADGEIAYAGNQVPTFGNLVLVKHADGWVTAY 550
DipMBa           QRE-----GTSVSDGIDIMVPEGTPVKAAENGVVIYAGDGLKEFGQTVLIRHDNGLVTVY 374
DipMAt           DNV-----EGSRNDGINISVPEGTPIKAAENGVVIYAGNGLKQLGNTVLVRHDDGKVTVY 485
                  .           *:::    *  :  :  * :  *       *: * : * :*  * :

Atu1832          GHLSAILVRAGDRVEAGDVIGRAGSTGRSTGPHVHYEVRRNDT------PVDPMRYLIAG 424
DipMCc           AHLSSTNVKMRQQVKQGEQLGTVGATGGVNEPQLHFEMRYAPTVKDKAKPVDPALVLPR- 609
DipMBa           GHNSQIMVQRGQKVRRGEEIAKSGMSGNAKSPKLHFEVRKNSA------PVNPTKYLES- 427
DipMAt           GNAANLDVQRGQKVQRGQTIATSGMTGSAKRPQVHFEVRKDAT------PVNPSGFLE-- 537
                 .: :   *:  : *  .: :.  * :*  .  ::*:*:*           *:*   :
```

Figure S7. Sequence alignment of DipM from *C. crescentus* and selected Rhizobiales species. The active site of Atu1832, a catalytically active endopeptidase of *A. tumefaciens* contains four chelating residues (in red and boxed), forming two active site patterns HXXXD and HXH. $DipM_{Ba}$ comprise two of out these four residues and $DipM_{Cc}$ and $DipM_{At}$ only have one conserved residue. *Cc, Caulobacter crescentus*; *Ba, Brucella abortus*; *At, Agrobacterium tumefaciens*.

Table S2. Strains used in this work.

Strains	Relevant characteristics	Source
Brucella abortus		
544 WT	Nal^R	J.-M. Verger, INRA, Tours, FR
544 Δ*hisB*		This study
544 $hisB_{E17Q}$		This study
544 Δ*hisB* pMR10::*hisB*	Kan^R	This study
544 Δ*hisB* pBBR::BAB1_0907		This study
544 Δ*hisB* pBBR::BAB1_0931		This study
544 Δ*hisB* pBBR::BAB1_1773		This study
544 WT pBBR-MCS1::empty		This study
544 Δ*hisB* pBBR-MCS1::empty		This study
544 WT BAB1_0907-mNG		This study
544 Δ*hisB* BAB1_0907-mNG		This study
544 WT BAB1_1773-mNG		This study
544 Δ*hisB* BAB1_1773-mNG		This study
544 DipM -		This study
544 CdlP -		This study
Escherichia coli		
DH10B	F- endA1 recA1 galE15 galK16 nupG rpsL ΔlacX74 Φ80lacZΔM15 araD139 Δ(ara,leu)7697 mcrA Δ(mrr-hsdRMS- mcrBC) λ	Invitrogen
S17.1	M294::RP4-2 (Tc::Mu)(Km::Tn7)	
BW 25141	F-, Δ(araD-araB)567, ΔlacZ4787(::rrnB-3), Δ(phoB-phoR)580, λ-, galU95, ΔuidA3::pir+, recA1, endA9(del-ins)::FRT, rph-1, Δ(rhaD-rhaB)568, hsdR514	From L. Van Melderen Lab
MFD pir	F- λ- ilvG- rfb-50 rph-1 RP4-2-Tc::[ΔMu1::aac(3)IV-ΔaphA-Δnic35-ΔMu2::zeo] ΔdapA::(erm-pir) ΔrecA	From R. Hallez (RH2845)

Table S3. Plasmids used in this work.

Name	Relevant characteristics	Source
pNPTS138	Cloning suicide vector bearing sacB, Kn^R	M. R. K. Alley, Imperial College of Science, London, UK
pMR10	Cloning vector, Kn^R	C.D. Mohr and R.C. Roberts, Stanford University
pBBR MCS1	Cloning vector, Cm^R	(Elzer et al., 1995)
pMR10::*hisB*	Complementation of *hisB* deletion, Kan^R	this study
pBBR::BAB1_0907	Overexpression of *dipM*	this study
pBBR::BAB1_0931	Overexpression of BAB1_0931	this study
pBBR::BAB1_1773	Overexpression of *cdlP*	this study
pNPTS-Δ*hisB*	Deletion of *hisB*	this study
pNPTS-*hisB*$_{E17Q}$		this study
pNPTS-dipM-mN		this study
pNPTS-cldP-mNG		this study
pJMP1039	Amp^R	Initial CRISPRi plasmid (Addgene Plasmid #119239)
pJMP1356	Amp^R, Cm^R	Initial CRISPRi plasmid (Addgene Plasmid #119276)
pJMP1339	Amp, Kan^R	Initial CRISPRi plasmid (Addgene Plasmid #119271)

Table S4. Primes used in this work.

N#	Name	Sequence	Purpose
1	F1-*hisB*	cgtaattgccgccggaac	Primers for *hisB* deletion
2	R1-*hisB*	**cttgagcgac**cagcggtcataggctttcc	
3	F2-*hisB*	**atgaccgctg**gtcgctcaagggctaaagc	
4	R2-*hisB*	tcgatttccgccgatatgc	
5	Fup-*hisB*	ctttcgacgatgatattgtg	primers used to check *hisB* deletion
6	Rdown-*hisB*	tcaatacggtatcgttcag	
7	F-compl-*hisB*	gagcgaaacctgtccatc	*hisB* complementation
8	R-compl-*hisB*	ggaaaggctttagcccttg	
9	F2-*hisB*-E17Q	ccaag**CAG**acgagtattgccgtttccgtcgatc	$hisB_{E17Q}$ point mutation
10	R1-*hisB*-E17Q	gcaatactcgt**CTG**cttggtggagcgttc	
11	F-907-BamHI	**acgcGGATCC**aggaaaagatgcgcgtc	BAB1_0907 (*dipM*) overrexpression
12	R-907-XhoI	**ccgCTCGAG**ggcttggaaaaaccatgc	
13	F-931-BamHI	**acgcGGATCC**actgactgcgatgcatctg	BAB1_0931 overrexpression
14	R-931-XhoI	**ccgCTCGAG**cgaaaaactatccgccgctg	
15	F-1773-BamHI	**acgcGGATCC**ctgttccaaaggcgtccttg	BAB1_1773 (*cdlP*) overrexpression
16	R-1773-XhoI	**ccgCTCGAG**gcgggattggaaatcaatcc	
17	F-SpeI-end-907	**ctagACTAGT**tgcctacgtcgtgaagag	907-mNeonGreen fusion
18	R-end-907-linker-KpnI	**ccgCTCGAGcccGGTACC**ggtgattccagatatttggtcgg	
19	F-kpnI-linker-mNG	**cggGGTACCgggCTCGAGcggc**ggcggtggcgactac	
20	R1-mNGssATG	**gaaactgttac**ttatcagttcatccatgccca	
21	F2-down-907	**aactgtataagtaa**cagtttcagcaggaaaaaatg	
22	R2-down-907-NheI	**ctaGCTAGC**tgaccagcttgtggacaatacc	
23	F-speI-end-1773	**ctagACTAGT**gaagcctatacgggcttcc	1773-mNeonGreen fusion
24	R-end-1773-linker-kpnI	**ccgCTCGAGcccGGTACC**ggttcgctgatgatcttcacgc	
25	R1-mNG-down-1773	**tgaaaatgc**tttacttatacagttcatccatgccca	
26	F2-down-1773	**gtataagtaa**agcattttcagcgggggg	
27	R2-down-1773-NheI	**ctaGCTAGC**atccggtgaaccggtttgc	
28	pJMP1339t2-sgBAB1-0907 REV	**tagt**gaacgattgcgacattccgc	DipM depletion
29	pJMP1339t2-sgBAB1-0907 FWD	**aaac**gcggaatgtcgcaatcgttc	
30	pJMP1339t2-sgBAB1-1773 FWD	**tagt**gcatataaattgtgagacaca	CdlP depletion
31	pJMP1339t2-sgBAB1-1773 REV	**aaac**tgtgtctcacaatttatatgc	

References

1. A. K. Sharma, S. Kumar, H. K, D. B. Dhakan, V. K. Sharma, Prediction of peptidoglycan hydrolases- a new class of antibacterial proteins. *BMC Genomics* **17**, 411 (2016).
2. J. J. Almagro Armenteros *et al.*, SignalP 5.0 improves signal peptide predictions using deep neural networks. *Nat Biotechnol* **37**, 420-423 (2019).
3. J. F. Sternon *et al.*, Transposon Sequencing of *Brucella abortus* Uncovers Essential Genes for Growth In Vitro and Inside Macrophages. *Infect Immun* **86** (2018).
4. N. Francis *et al.*, CtrA controls cell division and outer membrane composition of the pathogen *Brucella abortus*. *Mol Microbiol* **103**, 780-797 (2017).
5. I. Letunic, P. Bork, 20 years of the SMART protein domain annotation resource. *Nucleic Acids Research* **46**, D493-D496 (2017).
6. P. H. Elzer *et al.*, In vivo and in vitro stability of the broad-host-range cloning vector pBBR1MCS in six *Brucella* species. *Plasmid* **33**, 51-57 (1995).

2. ADDITIONAL RESULTS

2.1 Possible links between zinc homeostasis and cell separation

Surprisingly, we found out that the *B. abortus* parental strain was also displaying chains when exposed to relatively high amounts of zinc (1 to 2 mM), but not to copper (Figure 19). This phenotype was quantified by measuring the length of a high number of bacteria ($326 < N < 890$) that were exposed or not to zinc (Figure 20). The distribution of lengths of the parental strain exposed to zinc is significantly higher compared to unexposed bacteria and tends to resemble the one of the Δ*hisB* mutant (Figure 20). Interestingly, the presence of the metal chelator EDTA strikingly prevents chain formation in the Δ*hisB* mutant. We confirmed that the chains observed in the WT strain exposed to zinc were also made of contiguous PG by purifying and labeling the sacculi (Figure 21). Overall, it suggests that chaining is connected with zinc homeostasis. However, these observations have been only made in the rich medium HI and could not be reproduced in other media such as GCA or TSB.

It was reported that the endopeptidase of *S. aureus* LytU was inhibited at high zinc concentrations (Raulinaitis et al., 2017). This could be a possible explanation for the observation that *B. abortus* WT strain is chaining in the presence of high zinc concentrations. This is also consistent with the fact the Δ*hisB* mutant does not show any chains in the presence of EDTA, assuming that histidine could be a zinc buffer, and that in the Δ*hisB* mutant zinc ions would tend to accumulate. This mutant would be less able to buffer zinc ions, which would then accumulate and impede endopeptidase(s) activity, or another PG digestion activity that would be sensitive to high zinc concentration. By chelating excess zinc ions, EDTA would allow these enzymes (e.g. endopeptidases) to perform their function normally.

In *V. cholerae*, the endopeptidase ShyB was shown to be regulated by the zinc starvation regulator Zur (Murphy et al., 2019). This endopeptidase is not expressed under standard laboratory conditions, unlike the two other endopeptidases of *V. cholerae* ShyA and ShyC. However, ShyB is the only active endopeptidase in low-zinc conditions. Very interestingly, the homologue of ShyB in *B. abortus* BAB1_0703, is histidine-enriched (4.67 % histidine enrichment). A deletion mutant of this endopeptidase has no particular phenotype in rich medium, but its morphology becomes dramatically affected upon metal-starvation conditions (Figure 22). Indeed, this mutant forms long and thin filaments upon EDTA exposure, suggesting again a problem of cell separation, and probably several other defects, in these conditions.

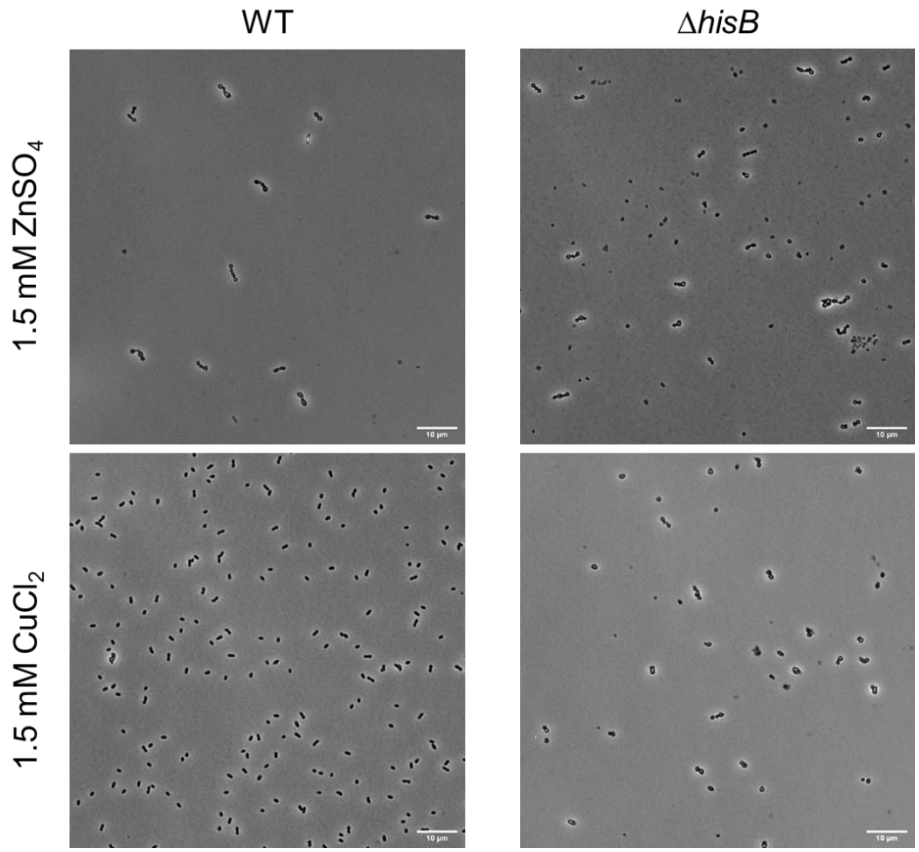

Figure 19. Zinc exposure generates chaining phenotype. *B. abortus* WT or Δ*hisB* mutant strain were incubated overnight in HI in the presence of 1.5 mM $ZnSO_4$ or $CuCl_2$ and then imaged with phase contrast microscopy. Scale bars: 10 µm.

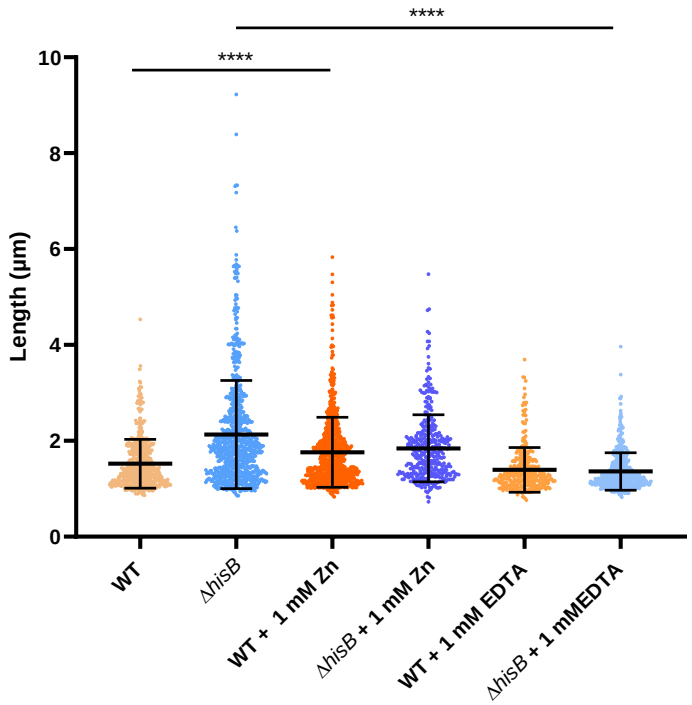

Figure 20. Length distribution of *B. abortus* WT and Δ*hisB* depends on zinc concentration. Cells were grown overnight in HI containing either 1 mM $ZnSO_4$ or 1 mM EDTA, then imaged with phase contrast microscopy. Length was measured and plotted for every condition (WT: *N* = 548, Δ*hisB: N* = 890, WT + Zn: *N* = 829, Δ*hisB* + Zn: *N* = 400, WT + EDTA: *N* = 327, Δ*hisB* + EDTA: *N* = 527). Distributions were analysed using Dunn's multiple comparison tests after Kruskal–Wallis. **** $P < 0.0001$.

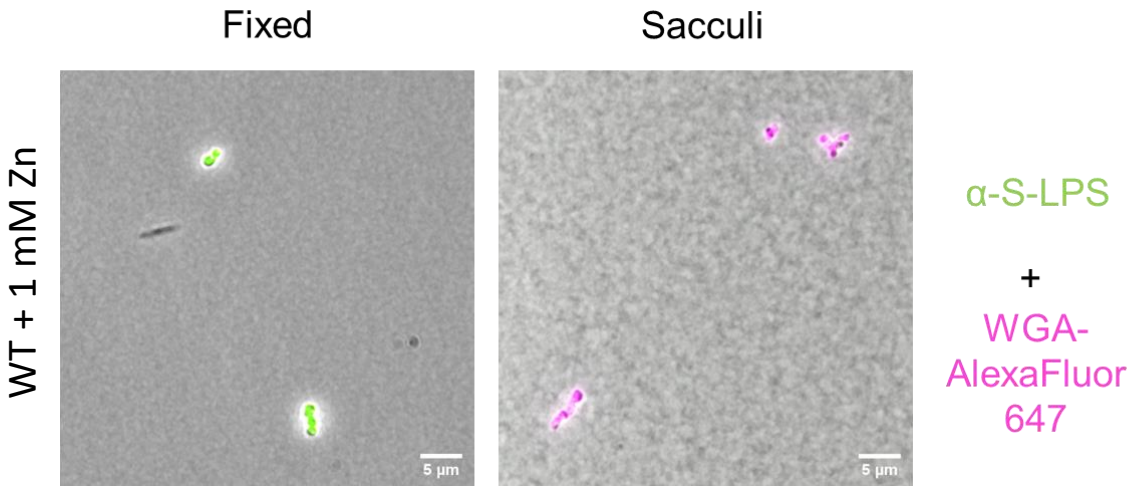

Figure 21. Sacculi extracted from chaining bacteria generated upon zinc exposure keep their morphology. *B. abortus* WT strain was grown overnight in HI in the presence of 1 mM $ZnSO_4$ and was either fixed with PFA or sacculi were extracted from the culture. Both fixed bacteria and sacculi were labeled with S-LPS antibodies (green) and Alexa 647-conjugated WGA (pink). Scale bar: 5 µm

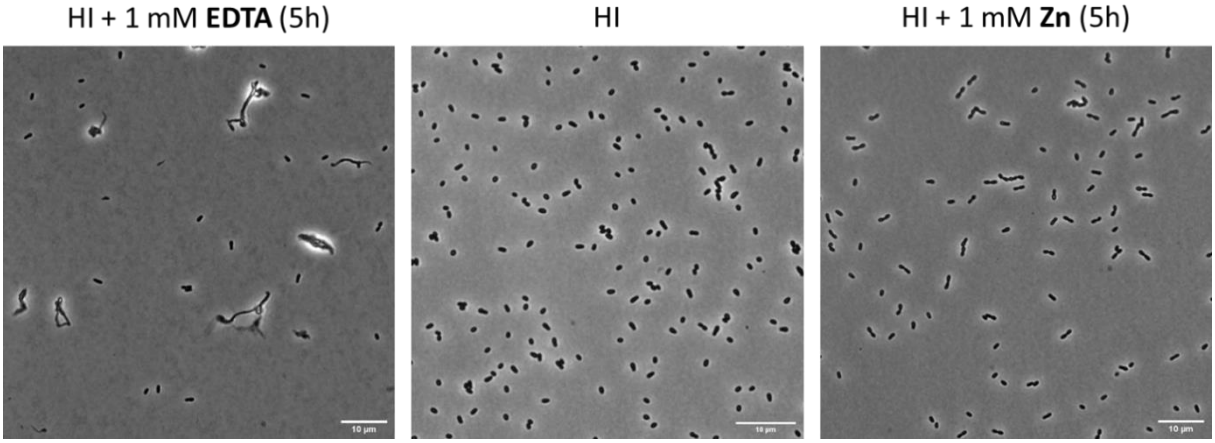

Figure 22. *BAB1_0703* deletion mutant shows a strong cell separation defect in the presence of the metal chelator EDTA. Δ*BAB1_0703* strain was grown overnight in HI and then was exposed either to 1 mM EDTA or to 1 mM $ZnSO_4$ for 5 hours. Scale bars: 10 µm.

2.2 Chaining phenotype is probably not linked with S-LPS or with IGP accumulation

We wondered whether LPS could be involved in the cell contacts inside the chains. Since rough mutants usually tend to adhere better and form clusters or aggregates, we wondered whether patches of rough LPS (R-LPS) could be enriched at cell contact places. To this end, we stained our Δ*hisB* mutant with an antibody against R-LPS (Figure 23), that does not recognize S-LPS. We could not see any consistent enrichment of R-LPS in between the cells. Besides, a Δ*hisB* was generated in the Δ*gmd* background, a mutant that is not able to produce O chain and thus S-LPS, and whose envelope is therefore completely made of R-LPS. The absence of S-LPS did not prevent the formation of chains nor did it increase their frequency, further demonstrating that the composition of the external leaflet of the outer membrane is probably not linked with the chaining phenotype.

To investigate whether the accumulation of IGP could somehow cause chaining, we constructed a strain that overexpresses *hisF* and *hisH*, the enzymes that both generate IGP, the substrate of HisB (Figure 12, Introduction). The coding sequences for these enzymes being in an operon which also comprises *hisA*, we cloned the three genes in a medium-copy pBBR overexpression vector (*hisHAF*). The WT strain overexpressing these three genes, and supposedly accumulating IGP, was observed under the microscope, and showed many strange morphological aberrations (Figure 24). However, these aberrations are very different from the chaining phenotype that we observed with the Δ*hisB* mutant.

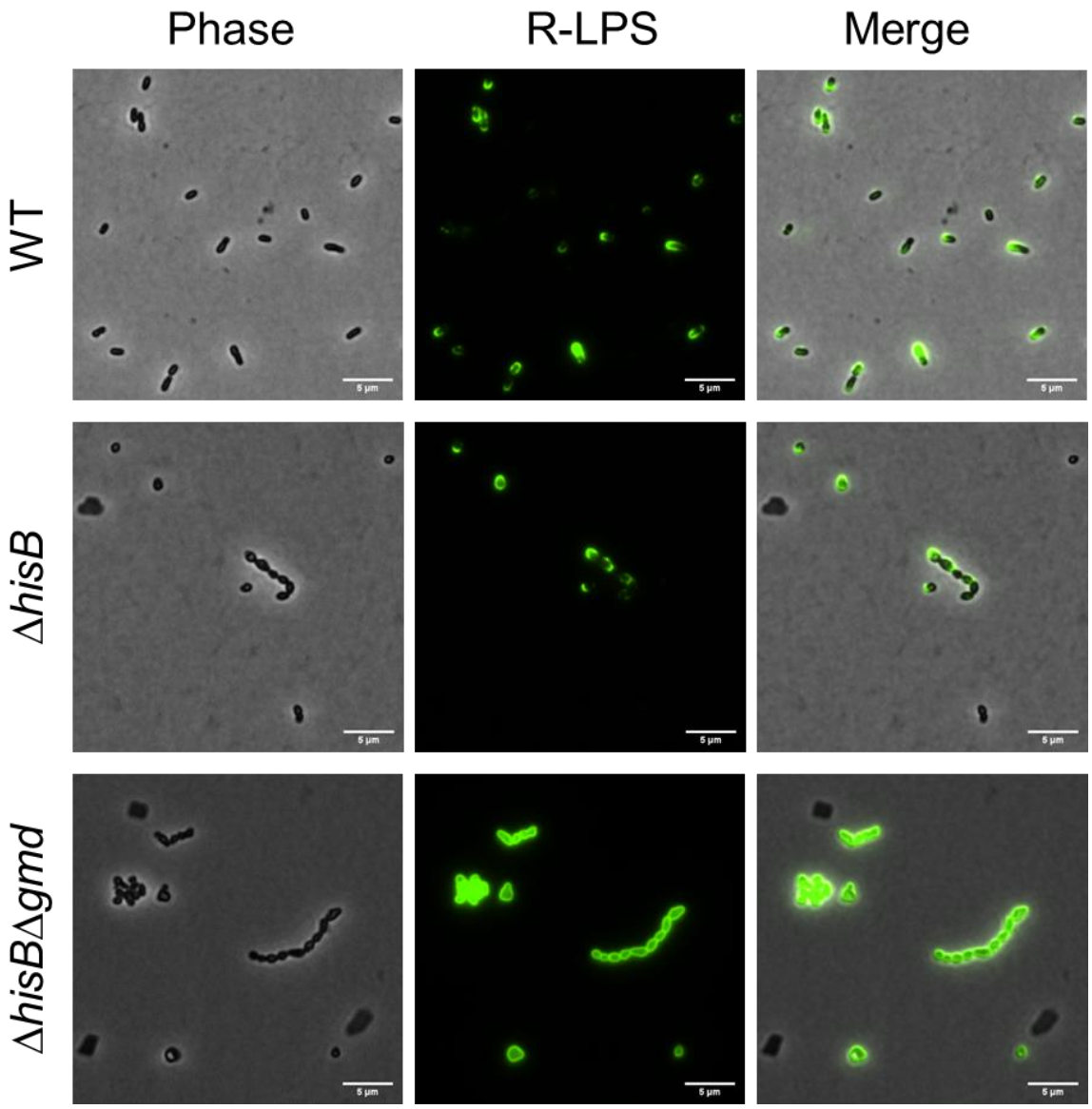

Figure 23. The absence of S-LPS does not affect chaining generation. *B. abortus* WT, Δ*hisB* and the rough mutant Δ*hisB*Δ*gmd* were grown in HI overnight and labeled with monoclonal antibody (A68 3F3 D5) against rough LPS (R-LPS). Scale bars: 5 µm.

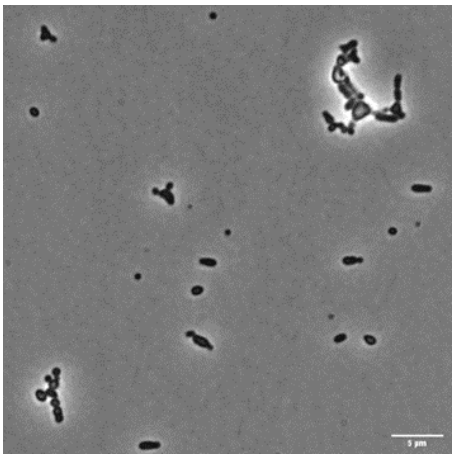

Figure 24. Overexpression of *hisHAF* generates morphological alterations differing from chains. *B. abortus* WT strains bearing *hisHAF* genes under a P_{lac} promoter from a medium-copy pBBR plasmid (in the absence of the Lac repressor) were grown overnight in HI and imaged with phase contrast microscopy. Scale bar: 5 µm.

3. HISTIDINE AND COPPER HOMEOSTASIS

3.1 Histidine-enriched proteins are associated with metals in *B. abortus*

Lack of endogenous histidine production in histidine auxotrophs should have an impact on protein synthesis, and we formulate the hypothesis that protein enriched in His codons may be more affected by a limitation in the histidine pool in the cell. In order to identify the proteins that are the most affected by the reduced histidine availability, a bioinformatic analysis on the *B. abortus* 2308 strain predicted proteome was carried out. Damien Devos (CABD, Sevilla, Spain) helped us to set up a program able to calculate the proportion of histidyl residues in each protein sequence of *B. abortus*. Only 85 out of the 2941 predicted proteins have a proportion of histidine residues above 5 % (Figure 25). An important number of the proteins with a high histidine percentage have a predicted function related to metal homeostasis or use metal as cofactors (Table 2). This finding is consistent with the fact that histidine can coordinate metal ions. However, the link between histidine biosynthesis and metal homeostasis remains to be investigated, even in model bacteria. Considering that metal homeostasis is also at the heart of host-pathogen interactions and that our histidine auxotroph mutants are attenuated in several models of infection, we decided to test different phenotypes related to metal acquisition or resistance in our auxotroph mutants.

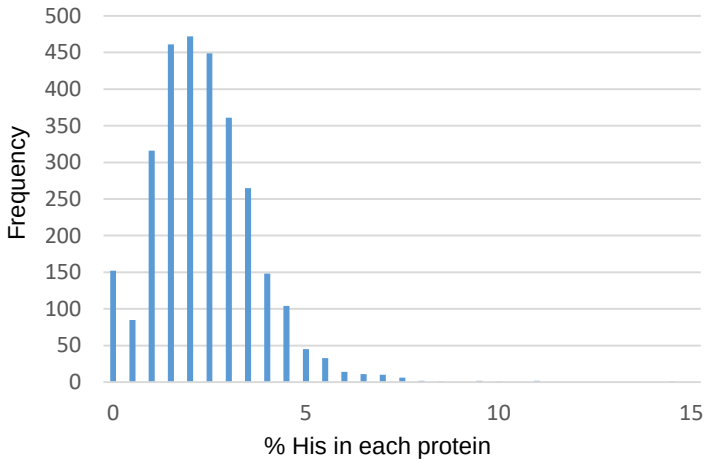

Figure 25. Histidine frequency in the proteome of *B. abortus* 2308**.** Histidine frequency in each protein in the *B. abortus* 2308 proteome was computed *via* a bioinformatic program developed by Damien Devos (CABD, Sevilla, Spain). For each protein sequence, it counts the number of the amino acid histidine (represented by H in the sequence) and calculates the percentage of histidine in the sequence in order to illustrate the enrichment of proteins in histidine. An arbitrary threshold value of 5 % was established. Only 85 out of 2941 predicted proteins (thus 2.9 %) have a proportion of His residues >5 %.

Table 2. Histidine enrichment in *Brucella abortus* strain 2308 proteome

Tag	%H[a,b]	Name[c]	Functions
BAB1_0301	14.04	UreE *	Nickel donor during urease metallocenter assembly
BAB1_1974	10.74	QueD	7-cyano-7-deazaguanine biosynthesis and purine metabolism
BAB_RS33715	10.53	Uncharacterized protein	Unknown
BAB_RS22295	9.68	CbtB *	Cobalt transporter subunit
BAB2_0432	9.09	NikR *	Transcriptional repressor of the nikABCDE operon
BAB_RS32835	9.09	Uncharacterized protein	Unknown
BAB2_0246	8.44	GTP-binding protein *	Cobalamin synthesis
BAB2_1080	7.72	ZnuC *	Energy coupling in ZnuABC zinc uptake transport system

BAB1_2027	7.69	BolA-like protein	DNA-binding regulator and stress-induced morphogen
BAB1_1818	7.37	Usg protein	Unknown
BAB2_0964	7.32	GAF/GGDEF domain protein	Diguanylate cyclase
BAB_RS33725	7.29	Uncharacterized protein	Unknown
BAB1_1173	7.19	LpxA	Lipid A biosynthesis
BAB1_0771	7.14	Zinc finger domain *	Unknown
BAB1_0174	7.06	Lactoylglutathione lyase	Methylglyoxal detoxification
BAB2_0545	6.96	RibH2	Riboflavin biosynthesis
BAB1_1743	6.94	Uncharacterized protein	Unknown
BAB1_2036	6.92	GTP-binding protein	Cobalamin synthesis protein
BAB1_2175	6.90	Irr *	Ferric uptake regulation
BAB_RS25890	6.90	Uncharacterized protein	Unknown
BAB_RS21185	6.78	Uncharacterized protein	Unknown
BAB1_1754	6.78	YdcH family protein	Unknown
BAB1_1347	6.73	Serine hydrolase (ydeN)	Esterase activity
BAB_RS17660	6.56	Superoxyde dismutase	Superoxide dismutase activity
BAB_RS22375	6.52	Serine hydrolase family protein	Esterase activity
BAB1_1991	6.45	Gamma-glutamylcyclotransferase	Glutathione catabolic process
BAB_RS17240	6.41	Uncharacterized protein	Unknown
BAB1_1668	6.38	Fur *	Ferric uptake negative regulation
BAB1_1476	6.37	Alpha.beta hydrolase	Lipid transport and metabolism
BAB2_0535	6.36	SodC	Superoxide dismutase activity: radicals elimination
BAB2_1079	6.29	ZnuA *	ZnuABC zinc uptake transport system
BAB_RS32250	6.25	Uncharacterized protein	Unknown
BAB2_1082	6.21	Zur *	Fe^{2+} or Zn^{2+} uptake regulation
BAB1_0161	6.17	DUF1150 family protein	Unknown
BAB1_0497	6.16	CoxC Cytochrome c oxydase III	Aerobic electron transport chain
BAB1_0751	6.15	Uncharacterized protein	Unknown
BAB2_0644	5.91	Metal-dependent hydrolase *	Hydrolase activity
BAB1_0714	5.88	Damage-inducible protein DinB	Unknown
BAB1_0518	5.85	MutY adenine glycosylase	Adenine glycosylase active on G-A mispairs
BAB1_0556	5.83	Uncharacterized protein	Unknown
BAB1_0042	5.79	Cytochrome o ubiquinol oxidase subunit IV	Electron transport
BAB1_1716	5.78	RuvC	Nuclease activity; Holliday junction intermediates resolution
BAB1_0456	5.70	Histone deacetylase family	Deacetylase activity
BAB1_1899	5.69	VOC family protein	Glyoxalase/Bleomycin resistance protein/dioxygenase
BAB1_1689	5.63	Uncharacterized protein	Unknown
BAB1_1732	5.63	2Fe-2S ferredoxins, iron-sulfur binding protein	Unknown
BAB1_1828	5.63	Uncharacterized protein	Unknown
BAB1_1189	5.57	Uncharacterized protein	Unknown
BAB2_0495	5.56	Uncharacterized protein	Unknown
BAB_RS22085	5.52	Uncharacterized protein	Unknown
BAB1_1001	5.48	Uncharacterized protein	Unknown
BAB1_1755	5.48	Uncharacterized protein	Unknown
BAB2_1068	5.48	Class II aldolase/adducin, N-terminal:ATP/GTP-binding site	Carbohydrate transport and metabolism
BAB2_1145	5.45	Sulfatase	Sulfuric ester hydrolase activity
BAB2_0505	5.44	Lectin-like protein BA14k	Immunoglobulin-binding and hemagglutination properties, virulence (LPS biosynthesis)
BAB2_0534	5.43	CueO *	Copper oxidation
BAB2_1016	5.41	Universal stress protein (Usp)	Stress survival

BAB1_0814	5.38	Uncharacterized protein	Unknown
BAB1_0135	5.36	Uncharacterized protein	Unknown
BAB1_1617	5.35	Gfo/Idh/MocA family oxidoreductase	Dehydrogenase activity
BAB1_1581	5.33	Metallo-phosphoesterase *	Hydrolase activity
BAB1_1297	5.32	DUF2218 domain-containing protein	Unknown
BAB1_1495	5.26	Antifreeze protein, type I	Subzero environment survival
BAB1_1904	5.26	GCN5-related N-acetyltransferase	Acetyltransferase activity
BAB1_0041	5.26	Cytochrome c oxidase, subunit III	Aerobic electron transport chain
BAB1_1568	5.26	Aspartyl/asparaginyl beta-hydroxylase	Unknown
BAB1_0573	5.23	Helix-turn-helix transcriptional regulator	Transcriptional regulator
BAB1_0856	5.19	BolA-like protein	DNA-binding regulator and stress-induced morphogen
BAB1_1666	5.19	Pseudouridine synthase	Pseudouridine synthesis from uracil
BAB1_1284	5.18	Cold-shock DNA-binding domain	DNA binding at low temperature
BAB1_1277	5.16	PAS domain-containing protein	Unknown
BAB1_1219	5.15	DJ-1/PfpI family protein	Peptidase activity
BAB1_2161	5.15	TrmB	N(7)-methylguanine-tRNA biosynthesis
BAB1_1632	5.13	Uncharacterized protein	Unknown
BAB1_0085	5.13	YncA	Amino acid transport and metabolism
BAB2_0777	5.11	GntR family	DNA-binding transcriptional regulator
BAB2_0326	5.10	PurU	IMP biosynthesis via *de novo* pathway
BAB1_0926	5.10	AroQ	Chorismate biosynthesis
BAB1_0051	5.09	DUF1775 domain-containing protein	Unknown
BAB_RS33345	5.08	Uncharacterized protein	Unknown
BAB2_0897	5.08	Gfo/Idh/MocA family oxidoreductase	Dehydrogenase activity
BAB2_0170	5.06	YdcH family protein	Unknown
BAB1_1355	5.03	CREC-EF hand family protein	Calcium binding
BAB1_0961	5.00	Uncharacterized protein	Unknown
BAB2_0802	5.00	PIG-L family deacetylase	Deacetylase activity

Proteome fasta file was downloaded from NCBI and submitted by Oak Ridge National Laboratory. The bioinformatic program used was developed by Damien Devos (CABD, Sevilla, Spain). It reads the fasta file and, for each protein sequence, counts the number of the amino acid histidine (represented by H in the sequence). It also calculates the percentage of histidine in the sequence in order to illustrate the enrichment of proteins in histidine.

[a] % H indicates the percentage of histidine in the amino acid sequence of the protein.

[b] Proteins with a histidine percentage equal to or greater than 5 % are found in the table above. A minority of the protein has a histidine enrichment above 5 % and these proteins could be more strongly impacted by histidine starvation caused by mutations in the biosynthetic pathway. Only 85 out of 2941 predicted proteins (thus 2.9%) have a proportion of His residues > 5 %.

[c] Proteins whose function is known and is related with metal homeostasis and metal binding are indicated with an *.

3.2 Histidine auxotroph mutants are more sensitive to copper toxicity, but not to metal starvation

Copper is a heavy metal toxic at high concentrations. It is notably used by macrophages to fight against invading pathogens. Four auxotroph deletion mutants from different histidine biosynthesis genes replicate less efficiently inside RAW 264.7 macrophages compared to WT *B. abortus* (Figure 26). Those mutants are not able to grow in minimal medium in the absence of any amino acids but grow very similarly to the WT in TSB rich medium (Figure 27). We decided to explore how our histidine auxotroph mutants would behave when exposed to high concentrations of copper.

First, the auxotroph mutants were grown for 48 h in TSB in the presence of 1.6 and 2 mM $CuSO_4$, concentrations at which the *B. abortus* parental strain is still able to grow (Figure 28). At both copper concentrations, all auxotroph mutants showed a growth defect compared to the WT, meaning that they are more sensitive to copper. The Δ*hisA* mutant was particularly affected, but already showed a slight growth defect in rich medium compared to WT and other mutants (Figure 27 B). The Δ*hutH* mutant was also tested for copper sensitivity. Since this mutant does not have the first enzyme of the histidine degradation pathway, it is expected to accumulate histidine. In the conditions that we tested, namely in rich medium supplemented with different concentrations of $CuSO_4$, this mutant tolerates copper just as well as the parental strain.

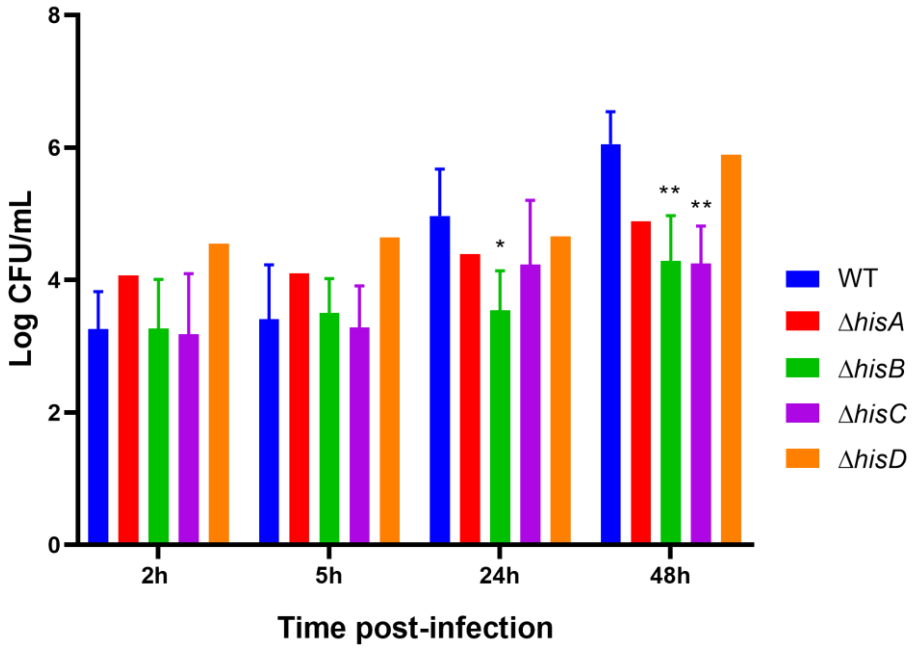

Figure 26. Histidine biosynthesis is required for *B. abortus* intramacrophagic replication. Intracellular replication of WT and Δ*hisA*, Δ*hisB*, Δ*hisC* and Δ*hisD* deletion mutants was assessed by enumerating colony-forming units after 2, 5, 24 and 48 h post infection. Data represents mean of biological triplicates ± SD, or mean of technical triplicates from a single biological replicate. Statistical significance between results for a given strain and those for the WT was determined by two-way ANOVA followed by Dunnett's multiple comparison test (*, $P < 0.05$; **, $P < 0.01$).

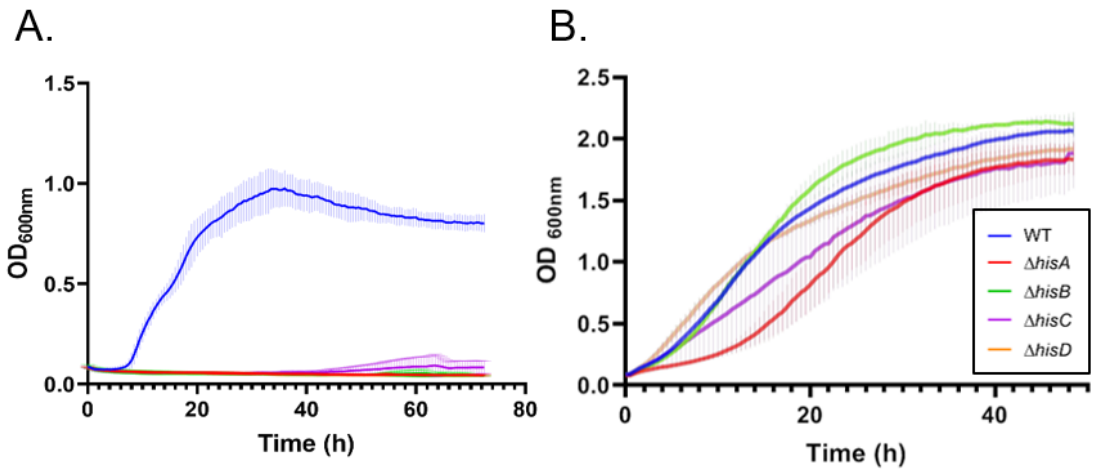

Figure 27. The *his* auxotroph mutants grow similarly to WT *B. abortus* in TSB rich medium, except for the Δ*hisA* mutant, which displays a slower growth at the start of the culture. The optical density (OD) at 600 nm was measured every 30 minutes for 48 hours of growth in PE (A) or in TSB (B). Since there is no histidine in PE, it was expected that Δ*his* mutants do not grow. Data are representative of biological triplicates.

The copper sensitivity phenotype of the *his* auxotroph mutants was rescued with complemented strains (Figure 28). Then, copper sensitivity was confirmed by an agar well diffusion assay. Again, the auxotroph mutants showed a greater sensitivity to copper, which could be rescued by complementation (Figure 29).

Since histidine is known to coordinate metals, it is possible that not only does it prevents metal toxicity, but it could also be used to acquire metals in metal-poor conditions. To test this possibility, we grew some *his* auxotroph mutants in the presence of the metal chelator EDTA, and no difference of growth was observed (Figure 30). To determine whether the increased sensitivity that we observed in our mutants was specific to copper, we also exposed them to another metal which is toxic at high doses, zinc. When exposed to 1 or 2 mM $ZnSO_4$, WT and mutant strains were affected in the same way.

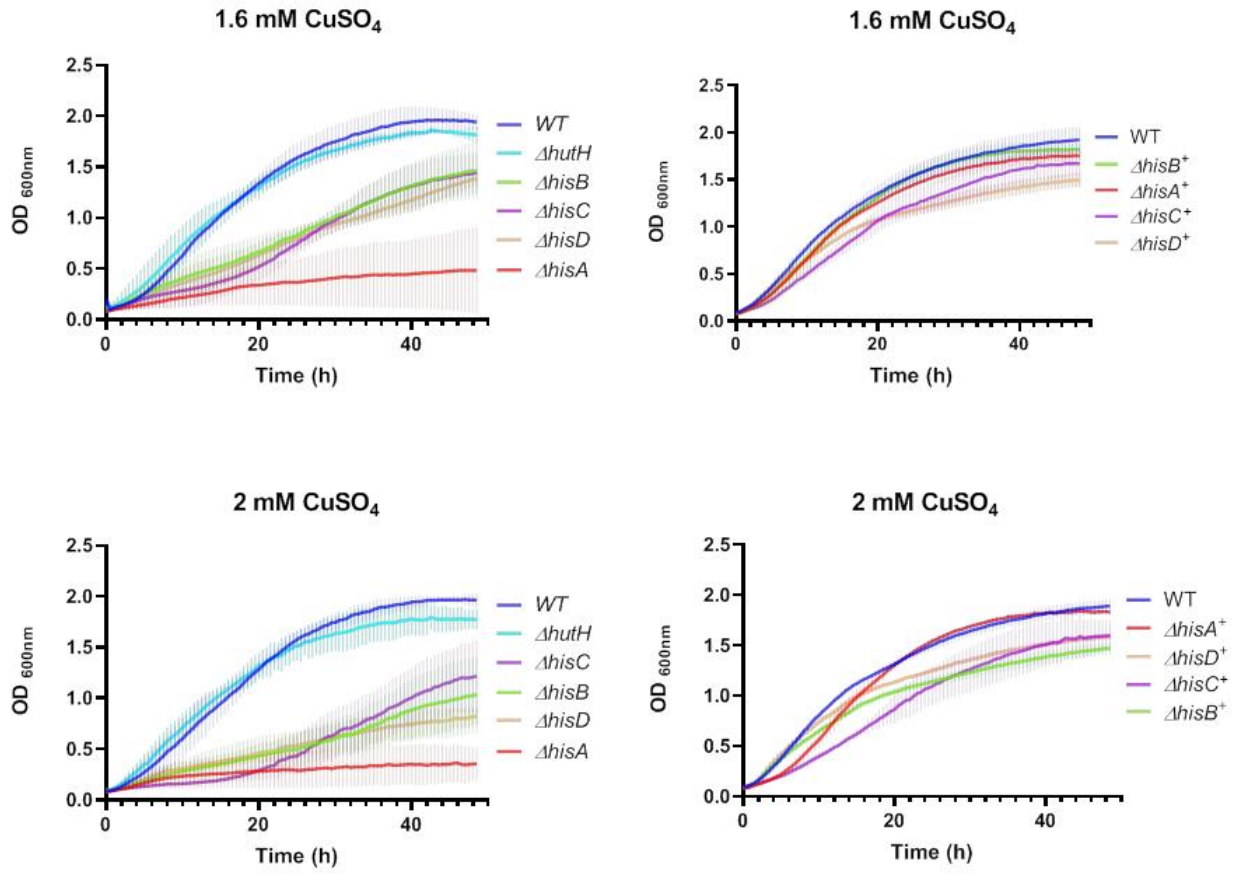

Figure 28. The *his* auxotroph mutants have increased copper sensitivity in liquid medium. WT, *his* mutants (left) and complemented strains (right) were grown in TSB rich medium containing 1.6 or 2 mM of $CuSO_4$. The optical density (OD) at 600 nm was measured every 30 minutes for 48 hours. Data are representative of biological triplicates.

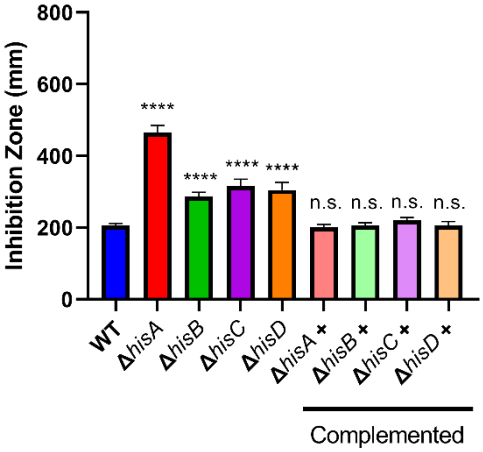

Figure 29. The *his* auxotroph mutants have increased copper sensitivity on solid medium. WT, *his* mutants and complemented strains were tested in an agar well diffusion assay for their sensitivity to toxic levels of copper. The results are plotted as the average diameter (± standard deviation) of the zone of inhibition around an agar well containing 200 mM $CuSO_4$. Results are mean of biological triplicates. Statistical significance between results for a given strain and those for the WT was determined by one-way ANOVA followed by Dunnett's comparison (n.s., not significant; ****, $P < 0.0001$).

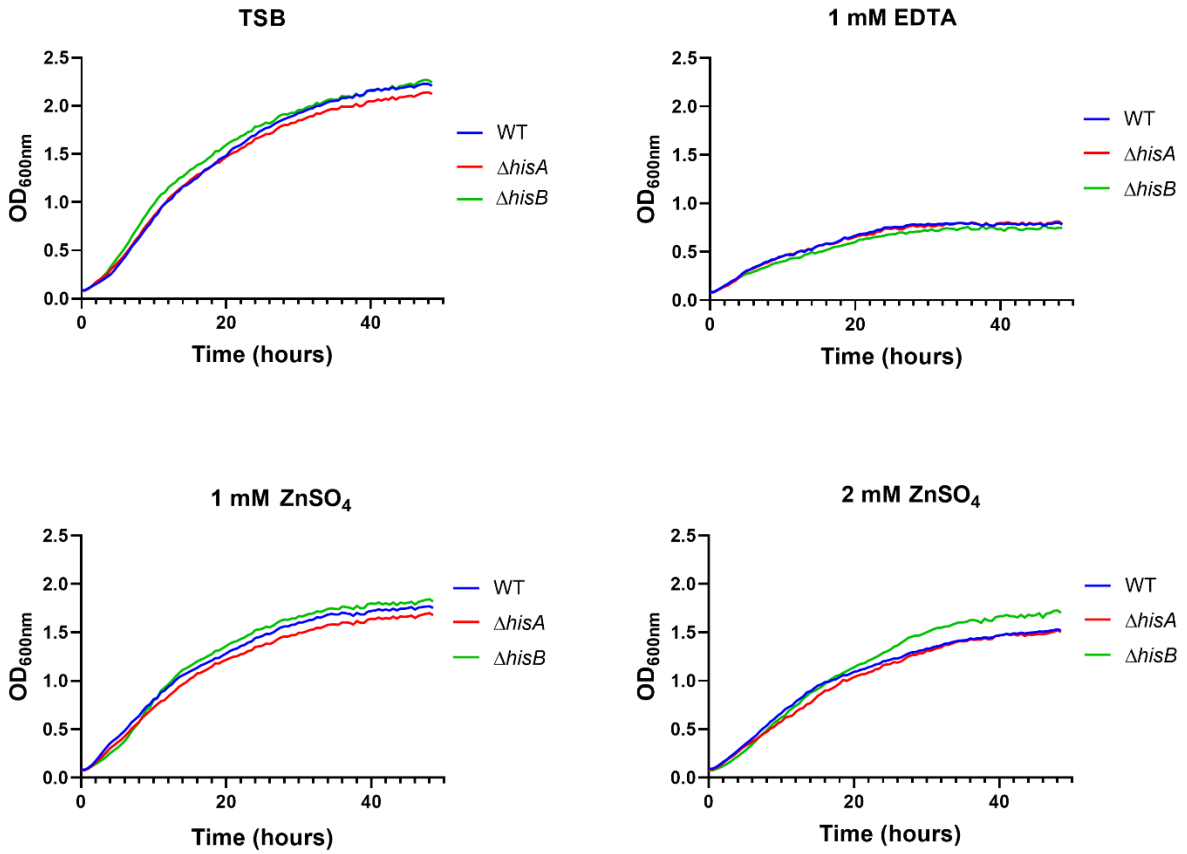

Figure 30. The *his* auxotroph mutants are as sensitive to Zn and EDTA as the WT *B. abortus*. WT, Δ*hisA* and Δ*hisB* mutants were grown in TSB rich medium containing 1 mM EDTA or 1 or 2 mM $ZnSO_4$. The optical density (OD) at 600 nm was measured every 30 minutes for 48 hours. Data are mean of three samples, from one single biological replicate.

3.3 Canonical copper detoxifying enzymes CopA and CueO are not required for copper resistance in *B. abortus*

While the role of histidine biosynthesis in copper homeostasis was rather unexpected, some actors that are classically involved in copper resistance are conserved in *B. abortus* and could be also important for copper tolerance. We deleted two putative actors of copper resistance, the multicopper oxidase CueO and the inner membrane ATPase CopA. To our surprise, in liquid culture medium, both growth curves of Δ*copA* and Δ*cueO* were similar to the WT strain when exposed to increasing concentrations of $CuSO_4$, except at very high copper concentration where a slight growth delay is observed for both mutants (4.6 mM) (Figure 31). A disk diffusion assay did not reveal any sensitivity to copper when comparing the mutants with the WT (Figure 32). Therefore, it seems that in the conditions of copper toxicity that we tested so far, histidine biosynthesis is more critical than CopA and CueO.

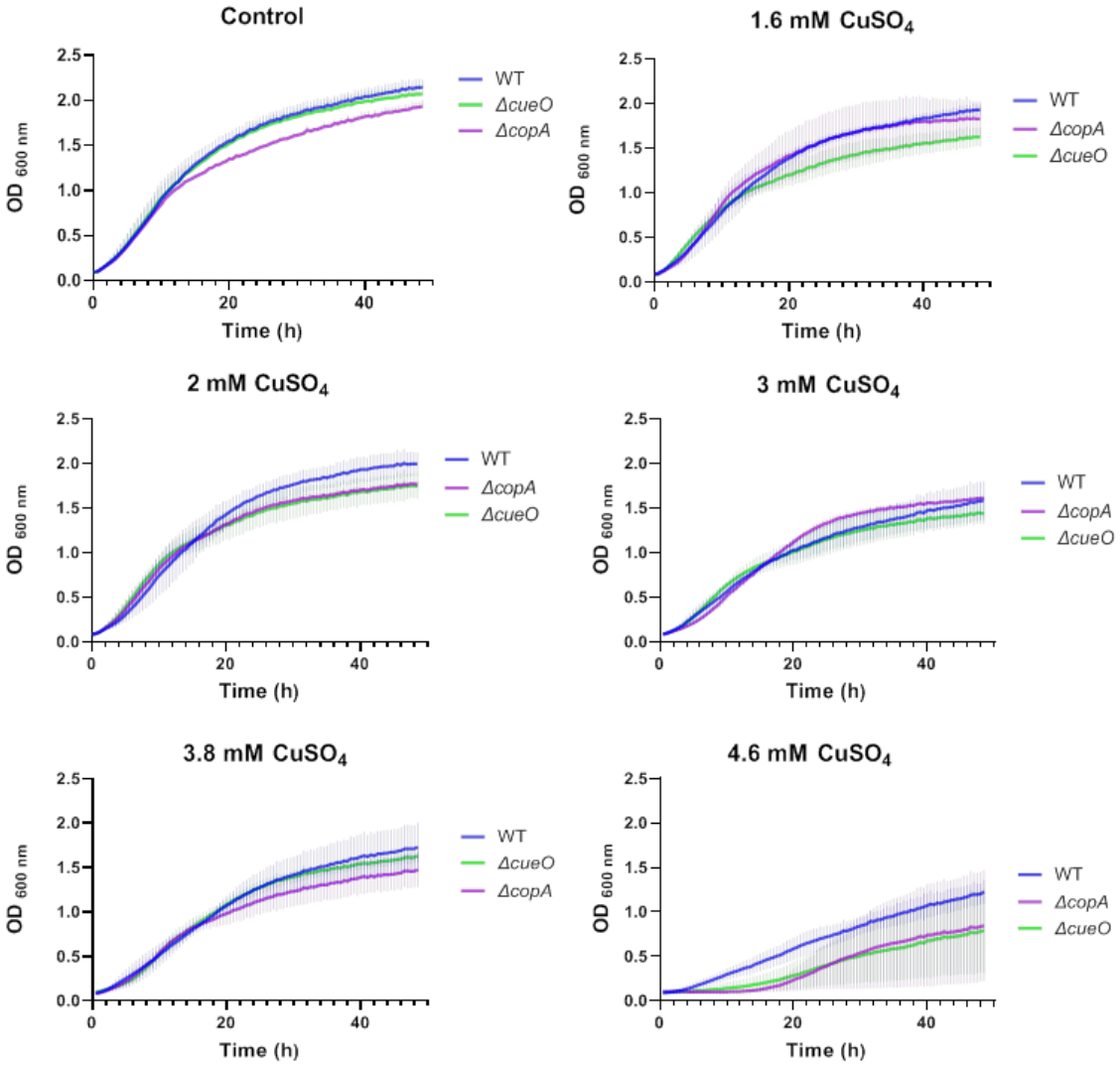

Figure 31. The *cueO* and *copA* genes are not required for copper resistance in liquid medium. WT, Δ*cueO* and Δ*copA* strains were grown in TSB rich medium containing the indicated concentrations of $CuSO_4$. The optical density (OD) at 600 nm was measured every 30 minutes for 48 hours. Data are representative of biological triplicates.

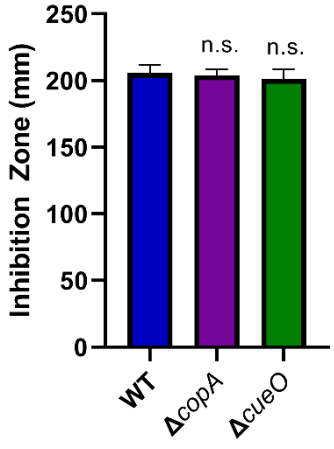

Figure 32. *cueO* and *copA* are not required for copper resistance in solid medium. WT, Δ*cueO* and Δ*copA* strains were tested in an agar well diffusion assay for their sensitivity to toxic levels of copper. The results are plotted as the average diameter (± standard deviation) of the zone of inhibition around an agar well containing 200 mM $CuSO_4$. Results are expressed as the mean of biological triplicates. Statistical significance between results for a given strain and those for the WT was determined by one-way ANOVA followed by Dunnett's comparison (n.s., not significant).

3.4 Spontaneous secondary mutations suppress copper sensitivity in the four *his* mutants

Higher copper sensitivity of the *his* mutants was also observed on solid medium. Indeed, on TSB plates containing 2 mM $CuSO_4$, all mutants have a strong growth defect. Interestingly, after several days at 37°C, some colonies appeared on the copper-containing plates. We streaked isolated colonies from this plate where the four mutants were plated (Δ*hisA*, Δ*hisB,* Δ*hisC and* Δ*hisD*) on new copper-containing plates to check that they were indeed resistant to copper. We selected 25 resistant clones that were designated "suppressor" mutants. Their genomic DNA was purified and then analysed by whole-genome sequencing.

A total of 29 mutations were identified among the suppressors. Seven of them were recurring in different suppressors (Table 3), suggesting that they have not been acquired independently but rather were already present in the parental strains. Thus, only the unique mutations were retained and investigated. 22 mutations were then retained in total (Table 4). A first mutation was identified on the first chromosome, inside the *vtlR* gene. VtlR is a LysR-family transcriptional regulator which is associated with virulence (Sheehan, Budnick, Blanchard, et al., 2015). It was shown to regulate a small RNA which is also required for virulence, AbcR2 (Sheehan, Budnick, Blanchard, et al., 2015). Besides, *vtlR* gene is found upstream a gene encoding a thioredoxin reductase. This mutation is leading to an amino acid change: glutamine to glycine. The second mutation was found on the second chromosome, and results in the replacement of a lysine for an asparagine in the *lysK* sequence, coding for the essential lysine–tRNA ligase. Two other mutations were found in *pdhA* and *pdhB*, which code for the E1 components of the pyruvate dehydrogenase complex, an enzymatic step which links the glycolysis and the Krebs cycle. The *pdhA* gene was previously found to be essential for *B. abortus* (Sternon et al., 2018). Very unexpectedly, except for these mutations, the 15 remaining SNPs all appeared within the same operon: the *opp* operon (BAB2_0699-BAB2_0703, Table 3). Opp, for oligopeptide transport, is composed of 5 genes. The first two, *oppA1* and *oppA2*, are periplasmic proteins predicted to bind short peptides. The two following genes *oppB* and *oppC* are permeases and the last one *oppD/F* codes for the ATP-hydrolyzing subunits. Strikingly, only the two first genes are targeted by mutations (Figure 33). Among all these SNPs

within the *opp* operon (in Table 3), some lead to amino acid changes (in green) while others do not, and are therefore referred to as silent mutations (in grey). In the case of the B10 suppressor, the first mutation generates a stop codon (in red), thus rendering the 3 following mutations silent, since the translation reading frame is interrupted. It is thus likely that in the B10 suppressor, OppA1 lost its function compared to the parental strain. We confirmed that 3 selected suppressors, A1, B10 and C6, are more resistant to copper compared to their parental strains by agar well diffusion assay (Figure 34).

Table 3. Shared SNPs mutations.

	Suppressors					
Suppressors[a]	**Position[b]**	**Type[c]**	**Ref.[d]**	**Alt.[e]**	**Gene[f]**	
A1, A2	chr2. 696738	snp	T	C	BAB2_0700 & 0701	Opp operon
B7, B8, B12, D7	chr2. 694270	complex	ATG	CTC	BAB2_0699	OppA1
	chr2. 695907	complex	TCT	CCG	BAB2_0700	OppA2
B7, B8, B9, B10, B12, C8, D7	chr2. 695019	deletion TA -> T missing			BAB2_0699	OppA1
C3, C4, C5, C6, C8	chr1. 1419703	del	TA	T	BAB1_1460 & 2215	Intergenic region
C4, D5	chr1. 1122459	del	GCGCCGT	G	BAB1_1150	AceF
B4, C6	chr2. 766953	complex mutation missing			BAB2_0775	Hypothetical protein

The SNP analysis program used was usegalaxy.org, using Snippy tool. The program aligns the reads given by the sequencing to a reference genome, here *Brucella abortus* 544. The output given is a table showing the different SNPs appearing in the suppressors.

[a] The name of the suppressor with the letter of the *his* mutant to which it refers as well as a number related to the colony streaked (e.g. A1 corresponds to the first colony of the suppressors found for *hisA*).

[b] Refers to the position on the chromosome.

[c] SNP type. Del: deletion.

[d] Ref. Sequence found in the genome of the reference mutant for the suppressor: *ΔhisA, ΔhisB, ΔhisC* and *ΔhisD.*

[e] Alt. Sequence found in the genome of the suppressor.

[f] Locus tag where SNP is found.

Table 4. Unique SNP mutations

	Suppressors				
Mutant[a]	**Suppr.[b]**	**Position[c]**	**Amino acid change[d]**	**Gene[e]**	
ΔhisA	**A1**	chr1. 1472668	Gln -> Lys	BAB1_1517	LysR21
	A2	chr1. 936216		BAB1_0955 & 0956	Intergenic region
ΔhisB	**B1**	chr2. 695058	60 bp deletion	BAB2_0699	OppA1
	B4	chr1. 460842		BAB2_0464 & 0465	Intergenic region
	B9	chr2. 695451	Glu -> Gln	BAB2_0700	OppA2
		chr2. 695457	Ser -> Thr		
		chr2. 695468	Arg-Ile -> Arg-Leu		
		chr2. 695483			
		chr2. 695489			
	B10	chr2. 694185	Stop	BAB2_0699	OppA1
		chr2. 694191	Glu -> Lys		
		chr2. 694200	Asp->Tyr		
		chr2. 694219	Ser-Gly -> Phe-Cys		
ΔhisC	**C5**	chr2. 444440	Lys->Asn	BAB2_0447	LysK
		chr2. 745096		BAB2_0748 & 0749	Intergenic region
	C6	chr2. 693379	Potential promoter region	BAB2_0698 & 0699	OppA1
	C8	chr2. 693942		BAB2_0699	OppA1
		chr2. 693957			
		chr2. 693966			
		chr2. 695612	Lys -> Asn	BAB2_0700	OppA2
ΔhisD	**D4**	chr1. 1124993	1 bp deletion	BAB1_1152	PdhA
	D6	chr1. 1124208	Stop	BAB1_1151	PdhB

The SNP analysis program used was usegalaxy.org, using Snippy tool. The program aligns the reads given by the sequencing to a reference genome, here *Brucella abortus* 544 WT. The output given is a table showing the different SNPs appearing in the sequenced genome of the suppressors.

[a] The different *his* mutants constructed in the lab.

[b] The name of the suppressor with the letter of the *his* mutant to which it refers as well as the number of the isolated clone.

[c] Refers to the position on the chromosome

[d] Green: SNP leading to an amino acid change, Grey: silent SNP and Red: SNP leading to stop codon.

[e] Locus tag where SNP is found.

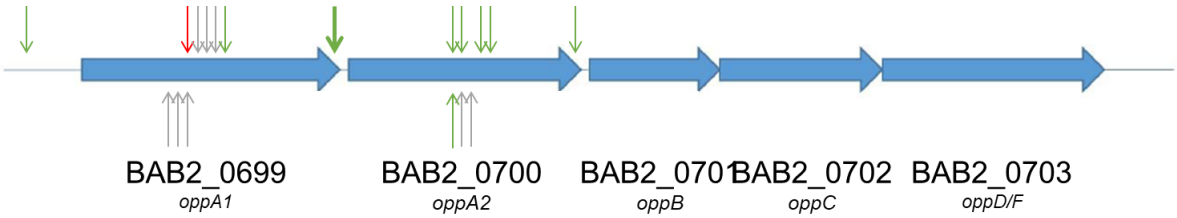

Figure 33. Localisation of SNPs on the opp operon. Each arrow represents the SNP position. Green arrows represent SNPs leading to amino acid changes, grey arrows represent silent SNPs and red arrow represents STOP codon. The 60 bp deletion is represented by a green arrow at the end of BAB2_0699.

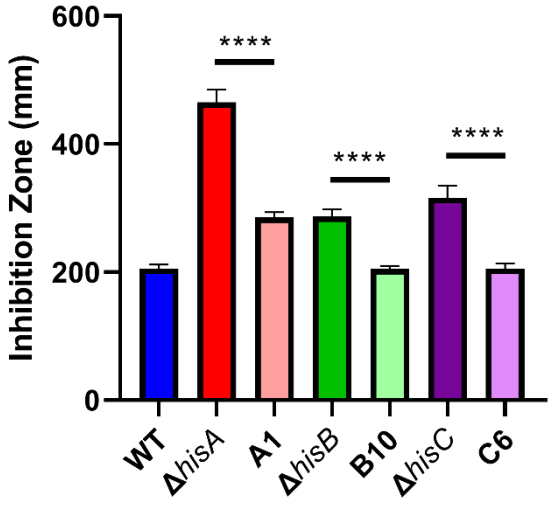

Figure 34. The suppressors A1, B10 and C6 are resistant to copper compared to their parental strains. WT, Δ*hisA,* Δ*hisB* and Δ*hisC* and the suppressor strains A1, B10 and C6 were tested in an agar well diffusion assay for their sensitivity to toxic levels of copper. The results are plotted as the average diameter (± standard deviation) of the zone of inhibition around an agar well containing 200 mM $CuSO_4$. Results are expressed as the mean of biological triplicates. Statistical significance between results for suppressors and those for their parental strains was determined by t-test (****, $P < 0.0001$).

DISCUSSION

As an intracellular pathogen *B. abortus* has evolved adaptations to survive in hostile conditions which include acidic pH, nutrient limitation (Roop et al., 2009) and also possibly metal poisoning, as it was shown with other intravacuolar pathogens (Chandrangsu et al., 2017). Whereas some intracellular bacteria have become increasingly dependent on their host for nutrient acquisition, *B. abortus* preserves broad biosynthetic abilities. Among the numerous biosynthesis pathways that *B. abortus* possesses, the histidine biosynthesis pathway appears to be crucial for proliferation inside host cells. In this work, we provide some answers to the following question: why does *Brucella* need to synthesize histidine during infection?

1. ABOUT THE LINK BETWEEN HISTIDINE BIOSYNTHESIS AND MORPHOLOGY

In the first part of this work, we found out that histidine biosynthesis might be related to an *a priori* unrelated process: cell division. A Δ*hisB* mutant has a specific chaining phenotype, suggesting that division is affected in that background. Besides, we have shown in the present work that the chaining phenotype of the Δ*hisB* mutant resists a harsh treatment of sacculi extraction. This means that chaining bacteria consists of contiguous PG.

What we however still do not know is to what extent this phenotype is reversible. We have seen that the addition of histidine during the whole infection process rescues the chaining phenotype, but it would be very interesting to see if the addition of histidine in the course of infection would rescue chains that have already been formed. Another very important perspective would be to use live microscopy to monitor how the cells react to the addition of histidine in conditions where chains are already abundant, such as in the rich medium HI for example. A microfluidic device would allow us to both observe the cells in real time, and to inject histidine at certain time points. Determining if this chaining phenotype is reversible or not, which could be achieved with classical agarose pads and time lapse in the presence of histidine, could give us further new insights about how the chains are generated.

Out of four mutants in the histidine biosynthesis pathway that we constructed, only Δ*hisB* presented a chaining phenotype. It is therefore reasonable to think that the morphological aberrations observed in this mutant could be due to the accumulation of the substrate of HisB, IGP. HisB catalyzes the sixth step of the histidine biosynthesis pathway. It is the first step of the pathway to be specifically dedicated to histidine biosynthesis, as the first five steps also contribute to the generation of AICAR, a precursor of purines. Filamentation has been already associated with histidine metabolism in *E. coli* and *S. typhimurium* (Frandsen & D'Ari, 1993; Murray & Hartman, 1972). In particular, division inhibition was observed in strains constitutively expressing *hisFH,* the IGP synthase or the fifth step of the pathway (Figure 12, introduction). This filamentation phenotype has never been really explained, however it seemed to be independent of the flow through the histidine biosynthetic pathway (Flores et al., 1993; Murray & Hartman, 1972). In other words, the division inhibition observed in *E. coli* and

S. enterica serovar Typhimurium is not related to the accumulation of IGP. This filamentation also appeared to be independent of AICAR accumulation (Flores et al., 1993; Frandsen & D'Ari, 1993).

In the present work, we tried to overexpress *hisHAF*, and we observed strong morphological aberrations in that background (Figure 24). Nevertheless, this morphology was very different from the chaining phenotype of the Δ*hisB* mutant. To rule out the involvement of IGP and AICAR in the chaining phenotype that we observed, we could also observe the morphology of WT *B. abortus* cells exposed to high IGP or AICAR levels. Nonetheless, the synthesis of these compounds is highly expensive.

Interestingly, it was recently shown with *Mycobacterium smegmatis* that histidine auxotroph mutants generated by CRISPR-interference exhibited a filamentation phenotype (de Wet et al., 2020). In this study, genes from the whole biosynthesis pathway were knocked down and appeared to form filaments, all of which could be rescued by histidine supplementation. Histidine limitation is likely at the origin of filamentation in this case. If histidine limitation is causing the chaining phenotype in the *B. abortus* Δ*hisB* auxotroph mutant, it would be worthwile to monitor intracellular levels of histidine in this strain in comparison with the WT *B. abortus,* and other histidine auxotroph mutants which do not display a chaining phenotype.

2. THE CHAINING PHENOTYPE OF Δ*HISB* ALLOWS THE IDENTIFICATION OF CELL DIVISION FACTORS IN *B. ABORTUS*

In bacteria, chaining phenotypes are generally related to a defect of cell separation. In particular, unlike filamentation which is generally characterized by the absence of visible constriction sites, chaining is the result of unresolved cell separation, even though constriction was already initiated. One of the key steps of cell separation is the processing of PG by PG hydrolyzing enzymes. This event is potentially dangerous if not well controlled and coordinated. Therefore, PG hydrolyzing enzymes are subject to tight regulation in time and space.

Even though the actors of cell division and cell separation can be easily predicted from *B. abortus* genome by homology with other bacteria, almost none of these actors have been actually characterized so far in *Brucella* (M. Deghelt, PhD thesis, 2014). Given the important redundancy in PG hydrolyzing enzymes, the identification of key actors of cell separation is challenging. Here, we provide evidence that at least two lipoproteins play a crucial role in cell division in *B. abortus*: DipM and CdlP.

These two actors share some interesting features in the light of our work. First, their function related to division seems to be well conserved, even across domains of life. Indeed, there are distant homologues of both DipM and CdlP in some chloroplasts and cyanobacteria, and in mitochondria, respectively (Miyagishima et al., 2014; Murata et al., 2020). In both types of organelles, their function is related with fission. Second, these two cell division factors are zinc-dependent and thirdly they possess a LysM

domain presumably involved in PG binding. Finally, they are both predicted to be essential in *B. abortus* (Sternon et al., 2018).

DipM belongs to the M23 family endopeptidases. These enzymes cleave the peptide bond between two amino acids of the stem peptide of the PG (Małecki et al., 2021) and are therefore used by certain bacteria to compete with other bacteria from a same ecological niche (Baba & Schneewind, 1996) (Heng et al., 2007). In the alphaproteobacteria *C. crescentus, A. tumefaciens* and presumably *B. abortus*, the function of DipM is related to cell division (Figueroa-Cuilan et al., 2021; Goley et al., 2010; Zielinska et al., 2017). Indeed, DipM$_{Ba}$-mNG is localized only at constriction sites. Besides, depletion of DipM$_{Ba}$ leads to the formation of bulges at midcell, very similarly to what is observed after treatment of *B. abortus* with the antibiotics aztreonam and cephalexin, which target specifically FtsI in *E. coli* (also called PBP3, the transpeptidase typically involved in septal PG synthesis) (Eberhardt et al., 2003). The exact activity of DipM$_{Ba}$ in the context of division remains however unclear. Alignment of DipM$_{Ba}$ with DipM homologues in *C. crescentus* and *A. tumefaciens* (DipM$_{Cc}$ and DipM$_{At}$) revealed that in DipM$_{Ba}$, two out of the four conserved catalytic residues of the M23 endopeptidases are substituted (Figure S7). DipM$_{Ba}$ is therefore likely to be inactive in terms of PG hydrolysis. The domain organization of DipM$_{Ba}$ is very similar to the one of NlpD from *E. coli.* It comprises a N-terminal signal peptide, a PG-binding LysM domain, and a C-terminal LytM/M23 peptidase domain (Tsang et al., 2017). The C-terminal LytM domain of NlpD from *E. coli* is degenerated, but it is crucial for activation of the amidase AmiC, which in turn cleaves the linkages attaching the stem peptides to the glycan strands, at the division site (Uehara et al., 2010). Whereas DipM is essential in *B. abortus* and *A. tumefaciens* (Figueroa-Cuilan et al., 2021; Sternon et al., 2018), NlpD deletion is silent in *E. coli* (Uehara et al., 2009). In the *B. abortus* genome, we have only found two amidases, of which only one is predicted to be periplasmic, AmiC. Transposon insertion in the *amiC* gene is predicted to generate a decrease in *B. abortus* fitness (Sternon et al., 2018). In the future, it would be worth investigating the role of this amidase in the context of cell separation, and to test its physical and functional interaction with DipM$_{Ba}$. Interestingly, *dipM$_{Ba}$* is predicted to be regulated by the cell cycle regulator CtrA (Francis et al., 2017). The characterization of this protein which is obviously a key actor of cell division in *B. abortus* paves the way for a better understanding of proper cell division in this bacterium.

The chaining phenotype of *hisB* mutants was also suppressed by the overexpression of a protease that we renamed CdlP (for Cell Division LysM-containing Protease). This protease appeared to be localized both at septa and at growing poles. CdlP shares its M48 protease domain with its distant homologue BepA in *E. coli*. BepA is a peptidase involved in the quality control of LptD, a major component of the outer membrane LPS translocon and was also shown to interact with the β-barrel assembly machinery (BAM) (Daimon et al., 2017; Narita et al., 2013). Assuming that CdlP is able to interact with the BAM machinery like its BepA homologue in *E. coli,* it could link PG synthesis with the insertion of outer membrane β-barrels. Indeed, it was recently shown that outer membrane β-barrels and PG synthesis are both incorporated at growing poles and at

the division site in *B. abortus* (Vassen et al., 2019). Nevertheless, we found another BepA homologue in the *B. abortus* genome: BAB1_0928. In closely related genera of the Rhizobiales such as *Agrobacterium, Sinorhizobium, Phyllobacterium, Mesorhizobium* and *Bartonella* homologues of CdlP exist but have never been characterized so far. Intriguingly, apart from BepA, another distant homologue of CdlP includes a mitochondrial protein, Oma-1. This metalloprotease is involved in mitochondrial fission, by cleaving Opa1, a positive regulator of mitochondrial fusion (Murata et al., 2020). It is tempting to speculate that CdlP also participates in PG remodeling during division and/or polar growth by cleaving negative regulators of cell division, similarly to how Oma-1 functions in mitochondria (Murata et al., 2020). It is also possible that CdlP activates other PG hydrolases that are otherwise inactive. The role of this metalloprotease in division and unipolar growth is a promising area of research for the future.

3. POSSIBLE ORIGINS OF THE CHAINING PHENOTYPE

3.1 An effect of the environment on the chaining phenotype

The morphology of a *hisB* deletion or loss of function mutant is differentially affected depending on the environment of *Brucella*. In Gerhardt's defined minimal medium supplemented with 0.1 % casamino acids (GCA 0.1 %), we can observe a high percentage of short chains, whereas in the rich medium HI we observe a moderate percentage of chains which can be sometimes very long. The bacterium *Deinococcus indicus* exhibits different morphologies, including multi-cell chains, depending on the amino acid availability in the culture medium (Chauhan et al., 2019). Differences in cross-linkage and composition of the PG was probably at the origin of morphological variations in this bacterium. It is therefore possible that the PG composition and/or cross-linking would differ between WT and the *hisB* mutant, depending in which culture media *B. abortus* is grown (TSB, HI or GCA). Mass spectrometry analysis of the PG should be performed to verify the nature of the PG of the *hisB* mutant in different culture media. Besides, it would be worth to have a precise measure of amino acid contents in the different media we used. Equally, it would be worth to grow the Δ*hisB* mutant in minimal medium with each amino acid individually, and see which amino acid, or combination of amino acids rescues the chaining phenotype.

The chaining phenotype was remarkable inside HeLa cells, at 24 h post-infection, where a very high percentage of infecting bacteria displayed chaining structures. To be able to identify the parameters that contribute to generate this phenotype during infection, it would be imperative first to localize in which compartment the *hisB* mutants are found inside HeLa cells or macrophages. Since intracellular replication of the mutants is compromised in both cell types, the *hisB* mutant could either fail to reach its replicative niche in the ER, or it could reach the ER but cannot find enough histidine molecules there. Since the *hisB* histidine auxotroph mutants still grow between 24 and 48 hours of infection in both macrophages and HeLa cells, it is likely that the *hisB* mutants are indeed able to reach the ER, where histidine is probably limiting. This possibility however remains to be confirmed by immunolabeling of the BCV markers

for the *hisB* mutant at 24 hours of infection. Antibodies against the ER marker calnexin and the endosomal marker LAMP-1 could be used to confirm the *hisB* mutant intracellular localization (Luizet et al., 2021). Indeed, we cannot exclude the possibility that *hisB* mutant could be growing – although in a delayed way – inside acidic compartments.

Besides, other infection models, such as activated macrophages or mice, should be used to confirm the importance of histidine biosynthesis for the intracellular survival of *Brucella*. Imaging the Δ*hisB* mutant in those different infection models would also be very informative, and would help us to gain knowledge on how the environment influence the chaining phenotype of Δ*hisB.*

3.2 The effects of metals on the bacterial envelope

At toxic levels, metals primarily affect the surface and the envelope of bacteria. In Gram-negative bacteria, metals penetrate inside the periplasm. It was shown recently in *E. coli*, that copper affects cell envelope biogenesis and stability by interfering with LD-transpeptidase (Ldt) activity (Peters et al., 2018). Copper also inhibits the metallo-β-lactamase NDM-1 in *E. coli*, thereby increasing its susceptibility to the carbapenems ertapenem and meropenem (Djoko et al., 2018). Presumably, the inhibition of these enzymes would be caused by the binding of copper ions to the catalytic cysteine residues of the Ldts, and possibly also of the metallo-β-lactamase of *E. coli* (Peters et al., 2018).

In terms of morphology, we have not observed any visible effects of copper exposure on any *B. abortus* strains, either WT or *his* auxotrophs. However, we have seen that when the *B. abortus* WT strain is exposed to zinc, it displays a chaining morphology which is conserved even after sacculi extraction. This observation led us to formulate the hypothesis that a problem of zinc homeostasis could be at the origin of the chaining phenotype of the *hisB* mutant. Besides, the presence of the metal chelator EDTA significantly reduced chaining in the Δ*hisB* mutant, further suggesting a role for zinc in the chaining phenotype. Those two observations were also intriguing considering that many PG hydrolyzing enzymes are zinc-dependent.

Remarkably, two histidines are responsible for the catalytic activity of the M23 family endopeptidases (which includes DipM and at least three other enzymes in *B. abortus* – see Table S1, Results part I). The catalytic mechanism of the enzymes of this family involves a zinc ion, which is coordinated by two histidines and an aspartate, and two catalytic histidines (Grabowska et al., 2015). In the M23 family endopeptidase of *Staphylococcus aureus* LytU, it was shown that a second zinc ion can inhibit the activity of the enzyme by binding to the catalytic histidine residues (Raulinaitis et al., 2017). An increase in zinc concentration could therefore result in the inhibition of endopeptidases by binding to their catalytic histidines. To test this hypothesis, we could measure zinc periplasmic contents using inductively coupled plasma-mass spectrometry (ICP-MS) in the WT and Δ*hisB* strain.

The mechanism of zinc toxicity mostly involves mismetallation (Palmer & Skaar, 2016). Notably, Mn-metalloenzymes would be particularly sensitive to zinc mismetallation (Martin et al., 2017). Thereby, bacterial zinc poisoning in the cytoplasm would inhibit the Mn-utilizing glycolytic enzymes phosphofructokinase and glyceraldehyde-3-phosphate dehydrogenase, as it was observed for *Streptococcus pyogenes* (Ong et al., 2015). Besides, zinc would also prevent Mn uptake by binding to the solute-binding protein PsaA of a Mn-specific ABC transporter in *Streptococcus pneumoniae* (McDevitt et al., 2011). Remarkably, HisB itself is a Mn-dependent enzyme. Therefore, an alternative explanation for zinc-induced chaining morphology in WT *B. abortus* would be that zinc inhibits HisB activity by mismetallation, thereby inducing the same morphology as a *hisB* deletion or catalytically dead mutant. In this case, the chaining phenotype would be linked with the activity of HisB *per se*. Since we only saw this chaining phenotype with Δ*hisB* and not the other mutants from the histidine biosynthesis pathway, it is possible that HisB harbors a "moonlighting" function which has yet to be discovered, but which is probably linked with cell division, or at least related to PG. As a reminder, HisB forms a large 24-mer complex, with each subunit binding a Mn ion (Bisson et al., 2015). We could expect this oligomeric protein to have another non-canonical function inside the cell, in addition to its function in histidine biosynthesis. The localization of HisB inside *B. abortus* cells could provide some information about a potential moonlighting function.

4. HISTIDINE: A METAL BUFFER?

Whereas the chaining morphology was only observed in *hisB* mutants, this mutant and all other *his* auxotroph mutants showed an increased susceptibility to copper. To cope with fluctuating metal environments, a first-line mechanism is the buffering of metal ions by small molecules. Afterwards, sophisticated sequestration systems and uptake or efflux pumps come into play. These systems are usually under the control of transcriptional regulators which are responsible to either metal excess or starvation. They allow a fine-tuned response to cope with metal excess or starvation, but are somehow delayed in time, unlike buffering systems which are already present before metal poisoning or starvation (Chandrangsu et al., 2017).

To our knowledge, the evidence of a role for histidine as an intracellular buffer to protect against copper was never demonstrated. A *hisB* auxotroph mutant in the fungal airborne pathogen *Aspergillus fumigatus* was shown to be more sensitive to both heavy metal excess and starvation (Dietl et al., 2016). The nematode *C. elegans* is like most animals naturally auxotrophic for histidine. In this worm however, mutations that negatively affect the histidine ammonia lyase (HALY-1), the first enzyme of the histidine degradation pathway, result in increased resistance to zinc and nickel. Animals mutated in *haly-1* gene presented higher levels of histidine. Presumably, higher levels of histidine prevent toxicity by allowing the chelation of heavy metals such as zinc or nickel (Murphy et al., 2011). In the present work, a deletion mutant of the histidine ammonia lyase gene of *B. abortus* (*hutH*) was also generated, but it did not present any increased resistance to copper in the conditions that we tested. It is for example

possible that *hutH* is not expressed in the conditions that we tested. Interestingly, in *C. crescentus*, it was recently shown that the complete histidine utilization pathway was downregulated in response to copper stress, suggesting an increased need for histidine in these conditions (Maertens et al., 2021).

The role of histidine as a buffer for zinc has been well established in *A. baumannii* (Nairn et al., 2016). During infection by *A. baumannii*, host cells use calprotectin to sequester zinc and starve the invading pathogen. The response of *A. baumannii* to zinc starvation involves the activation of the transcriptional regulator *zur* (Hood et al., 2012). This transcription factor induces the expression of the high-affinity zinc transporter ZnuABC, but also of a GTPase named ZigA (Zur-induced GTPase A). The gene coding for ZigA is interestingly found adjacent to the *hut* operon in *A. baumannii*. The *hut* operon includes *hutH*, coding for the histidine ammonia lyase. This enzyme actually depends on zinc for proper activity, and is likely activated by ZigA, which would act as a zinc metallochaperone (Nairn et al., 2016). Interestingly, according to the authors of this study, HutH would help increasing zinc availability by degrading histidine, which under normal conditions is bound to zinc ions in the form of a histidine-zinc labile pool.

The evidence that histidine could be a buffer for copper in *B. abortus* is suggested by the fact that the *his* auxotroph mutants are all more sensitive to copper. Those mutants were however not more sensitive to high zinc concentrations nor to zinc-starvation mimicking conditions. In the future, it would be interesting to monitor the expression of the *hut* operon upon copper exposure, in rich and minimal medium.

5. THE FUNCTION OF OPP IN COPPER HOMEOSTASIS

Our speculation that histidine could act as a buffer for copper ions was supported by the identification of numerous suppressive mutations inside the *opp* operon. Opp stands for Oligopeptide Permease, and is an ATP-binding cassette (ABC) transporter of the inner membrane.

It is likely that Opp would serve as an amino acid or oligopeptide importer, and therefore would allow the uptake of histidine, either as a free amino acid or inside short peptides. In that respect, mutations in the periplasmic proteins OppA1 and OppA2 could increase the affinity of the importer for histidine and thereby increase the cell ability to buffer copper ions intracellularly. Radiolabeled histidine (for example tritiated histidine) could be used to test whether the uptake of histidine is increased or not in the suppressors.

Another possibility would be that Opp accidentally imports copper, and therefore loss of function mutations in *oppA1* or *oppA2* reduce Opp-dependent copper permeability. In plants, it was indeed shown that ABC transporters are involved in the import of metals complexed with glutathione, metallophores or amino acids (Lubkowitz, 2006). To test this other possibility, copper levels inside the cytoplasm of suppressors should be compared with their parental strain (the *his* auxotroph mutants), as well as the WT *B. abortus* by ICP-MS.

Strikingly, all the suppressive mutations were exclusively found in the two periplasmic proteins of the Opp system, OppA1 and OppA2. Importantly, one of these mutations (suppressor B10, Table 4) leads to a stop codon in the coding sequence of OppA1, suggesting that loss of function of this protein provides an advantage for copper resistance. Accordingly, the B1 suppressor presents a 60 base-pair deletion inside the *oppA1* coding sequence. Deletion of the *oppA1* gene could therefore potentially improve copper tolerance. According to the two possibilities evoked previously, OppA1 could either prevent histidine uptake or favor copper import. To distinguish between these two possibilities, we should measure the uptake of tritiated histidine in a *oppA1* deletion background. The intracellular levels of copper could also be measured by ICP-MS in that same background, in comparison with the WT and *his* auxotroph strain(s). Another suppressive mutation (suppressor C6, Table 4) was found upstream of the *oppA1* coding sequence, thus presumably in its promoter region. The expression of *oppA1* and *oppA2* should be measured in that background, in comparison with the WT and Δ*hisC* strains.

A last hypothesis would be that Opp actually exports histidine outside of the cells, and that histidine exerts its protective function from outside, and not in the cytoplasm. Until now and to the best of our knowledge, Opp transporters only import peptides. However, the versatility of the ABC transporters, that can for example flip molecules like LPS through the inner membrane, suggests that this hypothesis is worth being tested anyway (Mi et al., 2017).

6. ABOUT THE RELEVANCE OF METAL POISONING DURING INFECTION

Studying the response of *B. abortus* to copper would make even more sense if we had the evidence that *B. abortus* actually faces metal intoxication during infection. One way to answer this question would be to interfere with copper transport inside macrophages, for example by modulating the copper transporter ATP7A expression, which was shown to be responsible for accumulating copper inside pathogen-containing phagolysosomes (White et al., 2009). Macrophage cell lines either knocked-out for this transporter or transfected with small interfering RNAs against the *ATP7A* gene could be infected with the WT and *his* mutant strains. If the *his* auxotroph mutants recover their ability to proliferate inside macrophages when ATP7A is knocked-down or knocked-out (KO), it could mean that not only *B. abortus* faces copper intoxication inside macrophages, but also that histidine is important to face copper during infection. This possibility could be further demonstrated by infecting WT or ATP7A KO macrophages with Δ*cueO* and Δ*copA* mutants, which have already been constructed. Transposon insertion in the sequence of the *copA* gene resulted in attenuation inside RAW 264.7 macrophages (Sternon et al., 2018). Unexpectedly, according to our results, CopA is not involved in copper resistance in *B. abortus*. However, the conditions that *Brucella* encounters during infection are different than just rich medium supplemented with copper. Especially inside the endocytic BCV, *Brucella* probably additionally faces nutrient starvation and oxidative stress (Roop et al., 2009). In nutrient replete conditions, buffering molecules such as histidine could provide a first barrier

against the toxic effects of copper, and would render CopA dispensable for copper tolerance. Testing Δ*cueO* and Δ*copA* sensitivity to copper in minimal medium could be a first way to test this hypothesis. CueO was already characterized in *Brucella melitensis* and renamed BmcO for *Brucella* multicopper oxidase (Wu et al., 2015). Interestingly, it was shown that BmcO was induced upon copper exposure, and that a Δ*bmcO* deletion mutant was more sensitive to copper than the parental strain in minimal medium. However, BmcO was not essential for replication inside J774.A1 macrophages. Besides, to further test the possibility that *Brucella* encounters copper during infection, Δ*copA* and Δ*cueO* mutants should be constructed in *his* auxotroph background, and their intracellular proliferation should be monitored. Because we know that several mutations in *oppA1* and *oppA2* suppress copper sensitivity of the *his* auxotroph mutants, it would be also interesting to compare the suppressors and their parental strains for intracellular multiplication inside macrophages as well.

7. CONLUSION

In this work, we provide new evidence that histidine biosynthesis is connected with crucial processes for the biology and pathogenesis of *B. abortus*, cell separation and metal homeostasis (Figure 35).

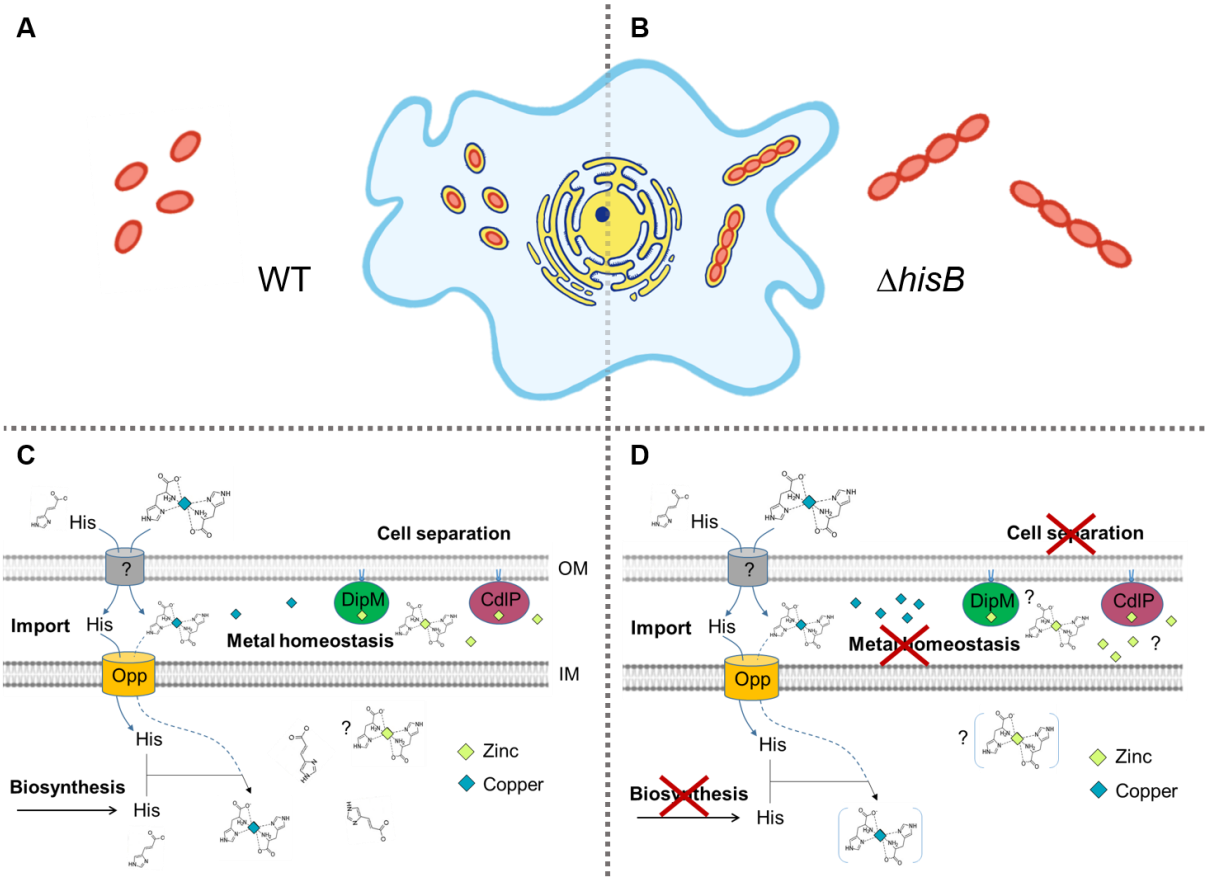

Figure 35. WT (**A.**) and Δ*hisB* (**B.**) *B. abortus* morphology in culture and HeLa cells. Putative mechanism to explain the role histidine biosynthesis in cell separation and metal homeostasis in the WT (**C.**) and how impaired histidine biosynthesis affects these two processes in the Δ*hisB* mutant (**D.**).

ADDITIONAL MATERIALS AND METHODS

1. BACTERIAL STRAINS AND GROWTH

All *E. coli* strains used during this work were grown in Luria-Bertani (LB) medium. Two different strains were used: DH10B for plasmid constructions and S17-1, a conjugative strain, for the mating with *Brucella*. The strain of *B. abortus* used in our experiment is *B. abortus* 544 Nal^R and was cultivated in Tryptic Soy Broth (TSB) rich medium.

Depending on the plasmid used for constructions, different antibiotics were used at the following concentrations: ampicillin (100 µg/ml), chloramphenicol (20 µg/ml), kanamycin (50 µg/ml), nalidixic acid (25 µg/ml).

2. STRAINS CONSTRUCTION

To generate Δ*hisA*, Δ*hisC*, Δ*hisD*, Δ*copA*, Δ*cueO* and Δ*hutT* mutants, the coding sequence was removed by homologous recombination. Regions of about 500 – 600 base pairs upstream and downstream the target gene were amplified using the primer couples: F1/R1 for the upstream region and F2/R2 for the downstream region for each deletion mutant. The two resulting fragments were fused together by joint PCR. Afterwards, the resulting fusion was inserted in an *Eco*RV-linearized pNPTS138 plasmid and was transformed in DH10B *E. coli*. Then, the plasmid was purified and checked by sequencing thereafter. The plasmid was transformed in S17-1 *E. coli* and then introduced to *B. abortus* 544 Nal^R (our "WT" control) by mating. The acquisition of the plasmid by *Brucella* after mating was selected thanks to the kanamycin resistance cassette of the pNPTS138 vector and the resistance of this strain of *Brucella* to nalidixic acid. The loss of the plasmid which would eventually lead to the deletion or a return to WT genotype was selected on sucrose thanks to the *sacB* counter-selection marker of the vector. Deletion strains were identified by diagnostic PCR.

Deletion strains Δ*hisA*, Δ*hisC* and Δ*hisD* were complemented with pMR10 carrying the deleted gene. Complementation plasmids were obtained by amplification of the genes with a region of 400 base pairs upstream the coding sequence, digestion of the PCR product and the pMR10 plasmid with *Bam*HI/*Xba*I and then ligation of the insert in the same direction as the *E. coli lac* promoter of the vector.

3. RAW 264.7 CULTURE AND INFECTION

RAW 264.7 macrophages (from ATCC) were cultivated at 37°C and in a 5 % CO_2 atmosphere in DMEM (Invitrogen) supplemented with 10 % fetal bovine serum (Gibco). For the infections, RAW 264.7 macrophages were seeded in 24-well plates at a density of 1.10^5 cells/ml. On the day of the infection, an overnight culture of *B. abortus* was diluted in DMEM to reach a MOI (multiplicity of infection) of 50. Bacteria were added to the cells and the 24-well plates were centrifuged at 400 g for 10 min at room temperature (RT). Cells were then incubated at 37°C in a 5 % CO_2 atmosphere for 1 h. Cells were washed twice in PBS and fresh medium supplemented with 50 µg/ml gentamicin was added to kill extracellular bacteria. Cells were washed twice in PBS at the different time points (2 h, 5 h, 24 h and 48 h after infection) and then lysed with PBS with 500 µl 0.1 % Triton X-100 for 10 min. Dilutions were then spotted (20 µl) onto TSB agar, incubated at 37 °C and colony-forming units (CFU) were counted.

4. AGAR WELL DIFFUSION ASSAYS

500 µl of the bacterial suspensions were mixed with 4.5 ml TSB soft agar (0.7 % agar), and then spread on a regular TSB agar plate. After the soft agar had dried, a well was dug with the upper part of a 200 µl pipet tip and carefully removed. 100 µl of a 200 mM $CuSO_4$ solution were then poured in the agar well. After 4 days at 37°C, the inhibition zone around each well was measured in mm.

5. BIOINFORMATIC ANALYSIS

Proteome fasta file was downloaded from NCBI and submitted by Oak Ridge National Laboratory. The bioinformatic program used was developed by Damien Devos (CABD, Sevilla, Spain). It reads the fasta file and, for each protein sequence, counts the number of the amino acid histidine (represented by H in the sequence). It also calculates the percentage of histidine in the sequence in order to illustrate the enrichment of proteins in histidine. An arbitrary threshold value of 5 % was established and proteins with a percentage equal to or greater than 5 are found in Table 2. Only 85 out of 2941 predicted proteins (thus 2.9 %) have a proportion of His residues > 5 %.

6. SUPPRESSOR ISOLATION, SEQUENCING AND MAPPING

For all four Δ*his* mutants, 29 isolated colonies formed on 1.6 or 2 mM $CuSO_4$ plates after 4 to 5 days were streaked on new TSB agar 1.6 and 2 mM $CuSO_4$ plates to confirm colonie formation and putative suppressive mutations leading to a suppressor phenotype. Among the 29 clones, 21 were still resistant to copper on the new plates and were grown overnight and stored. In order to extract genomic DNA (gDNA), bacteria were first inactivated. In order to do so, bacterial cultures of around 7.5 ml were centrifuged at 7,000 rpm for 5 minutes. After, supernatants were removed and bacterial pellets were resuspended in 300 µl of PBS. Then, bacteria were inactivated at 80°C during at least 1 hour. Afterwards, 100 µl of SDS 10 % were added. The gDNA extraction was achieved following manufactural instructions of the Macherey-Nagel™ NucleoSpin™ Tissue Kit. Bacterial SNP sequencing was performed by BIO, part of Pathology and Genetics Institute (http://www.bio-be.be/biopharma-croservices/). SNP sequencing analysis was carried out on Galaxy.org (https://usegalaxy.org/) with Snippy tool.

Table 6. Strains used in this study.

Name	Strains	Antibiotic resistance
Δ*hisA*	*B. abortus* 544	Nal
Δ*hisB*	*B. abortus* 544	Nal
Δ*hisC*	*B. abortus* 544	Nal
Δ*hisD*	*B. abortus* 544	Nal
Δ*hutH*	*B. abortus* 544	Nal
Δ*hisA* pMR10::*hisA*	*B. abortus* 544	Kan, Nal
Δ*hisB* pMR10::*hisB*	*B. abortus* 544	Kan, Nal
Δ*hisC* pMR10::*hisC*	*B. abortus* 544	Kan, Nal
Δ*hisD* pMR10::*hisD*	*B. abortus* 544	Kan, Nal
Δ*copA*	*B. abortus* 544	Nal
Δ*cueO*	*B. abortus* 544	Nal

Table 7. Primers used in this study.

Name	5'-3' Sequence
F1-hisA	cccatgaaagcggcatatcg
R1-hisA-bis	catcgtaaagttgaggcgcacgcattgac
F2-hisA-bis	tgcgcctcaactttacgatggccgcatcg
R2-hisA	tgctatcaacggaccggatcg
F1-hisC	aacgcactttcgccttcatg
R1-hisC	gtgagggcgggtaggtttctgcatgtcggtc
F2-hisC	agaaacctacccgccctcacagaatttctg
R2-hisC	ccttgttgtgcaggcagac
F1-hisD	ctgcatcatcgtgcacaagg
R1-hisD	ccctcataggccatgcggacactccttca
F2-hisD	gtccgcatggcctatgagggaccatgactgc
R2-hisD	ggcgattgtcgagtgacag
F1-hutT	cgcaaactcgccttctatgc
R1-hutT	agaagcacgagtattcatgcaagcgcctc
F2-hutT	gcatgaatactcgtgcttctgggcattgc
R2-hutT	attgggcgaccaagatgc
F1-copA	CCCTATCGGTGATTGGGTC
R1-copA	GCTCAGAACGCATGGCAATCCCTTTCGTG
F2-copA	GATTGCCATGCGTTCTGAGCAATGCCTTG
R2-copA	GAAGCGAACAGGTCGAAC
F1-cueO	GTGAAAGGGGGCTTTCTC
R1-cueO	AAACGGTCACGGCGGGTAATTCCAGTCATG
F2-cueO	ATTACCCGCCGTGACCGTTTGAGAGCAAGG
R2-cueO	AAGAGCCGGTACGATCTTGC
F-compl-hisA-Xba1	CTAGTCTAGAtcggcctttcgctcattgc
R-compl-hisA-BamH1	acgcGGATCCgcggccatctttcacatcgag
F-compl-hisC	ccctatagccgcacacag
R-compl-hisC	cgaagtggattgtggacatttg
F-compl-hisD-Xba1	CTAGTCTAGAtgcgcttttgggctgcaag
R-compl-hisD-BamH1	acgcGGATCCttgggaacgtcggcagtcatg

OTHER CONTRIBUTIONS IN PUBLISHED ARTICLES

nature COMMUNICATIONS

ARTICLE

https://doi.org/10.1038/s41467-019-12516-8 OPEN

Occurrence and repair of alkylating stress in the intracellular pathogen *Brucella abortus*

Katy Poncin[1,2], Agnès Roba[1], Ravikumar Jimmidi[3], Georges Potemberg[1], Antonella Fioravanti[4,5], Nayla Francis[1], Kévin Willemart[1], Nicolas Zeippen[1], Arnaud Machelart[1,6], Emanuele G. Biondi[4], Eric Muraille[7,8], Stéphane P. Vincent[2] & Xavier De Bolle[1*]

It is assumed that intracellular pathogenic bacteria have to cope with DNA alkylating stress within host cells. Here we use single-cell reporter systems to show that the pathogen *Brucella abortus* does encounter alkylating stress during the first hours of macrophage infection. Genes encoding direct repair and base-excision repair pathways are required by *B. abortus* to face this stress in vitro and in a mouse infection model. Among these genes, *ogt* is found to be under the control of the conserved cell-cycle transcription factor GcrA. Our results highlight that the control of DNA repair in *B. abortus* displays distinct features that are not present in model organisms such as *Escherichia coli*.

[1] URBM, Narilis, University of Namur, Namur, Belgium. [2] Sir William Dunn School of Pathology, University of Oxford, South Parks Road, Oxford OX1 3RE, UK. [3] Unité de Chimie Organique, University of Namur, 61 rue de Bruxelles, 5000 Namur, Belgium. [4] Unité de Glycobiologie Structurale et Fonctionnelle, UMR 8576 CNRS, Université de Lille, 50 Avenue Halley, Villeneuve d'Ascq, France. [5] VIB,Vrije Universiteit Brussel, Pleinlaan 2, 1050 Brussels, Belgium. [6] Université de Lille, CNRS, INSERM, CHU Lille, Institut Pasteur de Lille, U1019, UMR 8204, Center for Infection and Immunity of Lille, Lille, France. [7] IMM, 31 Chemin Joseph Aiguier, 13009 Marseille, Aix-Marseille Université, Marseille, France. [8] Laboratoire de Parasitologie, Faculté de Médecine, Université Libre de Bruxelles, Brussels, Belgium. *email: xavier.debolle@unamur.be

On DNA, alkylating stress typically results in aberrant methylation patterns. Many positions of DNA can be targeted and these modifications range from innocuous to mutagenic or cytotoxic[1,2]. Alkylating agents are ubiquitous in the environment and also have endogenous and dietary sources[3,4].

Three main endogenous sources of alkylating agents are reported in living organisms: (1) the ubiquitous methyl-donor *S*-adenosylmethionine (SAM)[5], (2) lipid peroxidation-derived alkylating agents[6], and (3) N-nitroso compounds resulting from the nitrosation of metabolites and being either direct alkylating agents or requiring metabolic activation[7–9]. SAM is often cited as the primary cause of endogenous alkylation, but its role has probably been overestimated in prokaryotic cells. Indeed, a 100-fold change of SAM levels was achieved experimentally without causing any change in the mutation rate of *Escherichia coli*[10]. Additionally, lipid peroxidation predominantly occurs on poly-unsaturated fatty acids[11], which are rarely present in bacteria[12,13]. Prokaryotic cells are thus considered to face marginal lipid-derived alkylating stress. In fact, in *E. coli*, the majority of the spontaneous mutations resulting from alkylating stress was found to be generated via the endogenous formation of N-nitroso compounds[7,14].

One question that remains unanswered is whether alkylating agents are produced by immune cells to fight intracellular pathogens. Of relevance, macrophages and neutrophils are known to produce N-nitroso compounds[15,16]. However, the occurrence of alkylating stress on intracellular bacteria has not been detected as yet. It has been hypothesized that N-nitroso compounds could be differentially produced in subcellular compartments[17], suggesting that vacuoles containing bacteria may also be prone to accumulating such compounds. Indeed, many intracellular bacteria first travel through an endosomal-derived vacuole, before reaching their replicative compartment[18], as in *Brucella abortus*, the causative agent of brucellosis in animals and Malta fever in humans[19,20]. This class III α-proteobacterium is known to enter host cells to form an endosomal *Brucella*-containing vacuole (eBCV), which becomes acidified to a pH of 4.0–4.5, suggesting that the eBCV undergoes normal endosomal maturation process, with the acquisition of the LampI marker[21,22]. Later, in most cell types, the bacterium reaches the endoplasmic reticulum, its replicative niche (rBCV)[19,23,24].

Both prokaryotic cells and eukaryotic cells are competent for N-nitrosation reactions. In eukaryotic cells, the production of N-nitroso compounds is dependent on an acidic pH and the intracellular concentration of reactive nitrogen species (RNS)[15,25]. However, in *E. coli*, a side reaction of nitrate reductases leads to the N-nitrosation of amines at a neutral pH[7]. Three classes of *E. coli* mutants have been shown to be deficient in nitrosation: (1) *narG*, encoding the catalytic subunit of nitrate reductase A; (2) *fnr*, encoding a pleotropic activator that influences the expression of the *narGHIJ* operon; and (3) *moa*, the mutant with the strongest nitrosation deficiency, probably because the enzyme is involved in the synthesis of a molybdopterin cofactor, required by all three *E. coli* nitrate reductases[7]. Importantly, the endogenous production of N-nitroso compounds is known to be more important in anaerobic and resting *E. coli*[26]. In this respect, during the first hours of infection, while still inside the eBCV, *B. abortus* is known to be blocked in the G1 stage of its cell cycle, characterized by a non-growing and non-replicating state[27].

In the late 1970s, a specific response to alkylating stress was described in vitro for *E. coli*[28]. This system was called "adaptive response" and is based on the detection of a methylphosphotriester (meP3ester) modification on DNA by the Ada[29]. Most bacteria possess an Ada-based adaptive response, with some variation in the target genes and their genomic organization[1]. In *E. coli*, *ada* is stochastically expressed to produce on average only one Ada protein per generation[30]. The detected meP3ester group is captured on the cysteine 38 (C38) residue of Ada, which becomes active as a transcription factor, upregulating the expression of a series of genes coding for proteins dedicated to the repair of alkylated DNA. These proteins comprise Ada itself, which can also directly repair O^6-methylguanine and O^4-methylthymine via the capture of the methyl group by the C321 residue of Ada; the dioxygenase AlkB, involved in the direct repair of the mutagenic lesions N^1-methyladenine and N^3-methylcytosine, as well as the DNA glycosylase AlkA, which removes the most cytotoxic lesion N^3-methyladenine via the base excision repair (BER) pathway[31]. The *aidB* gene is also over-expressed by the adaptive response, but its function still remains elusive[32,33]. There are also two proteins constitutively produced and independent of the adaptive system, namely the methyltransferase Ogt, which has a C139 residue with similar function than the C321 of Ada, and the glycosylase TagA, which is functionally similar to AlkA[31]. Importantly, other DNA repair pathways can be involved in repairing alkylated DNA. For instance, in *E. coli*, the SOS pathway—which is repressed by LexA under non-stress conditions—is activated early following alkylating stress, before the adaptive response takes over[34].

Here, we demonstrate that a weak alkylating stress occurs when *B. abortus* is inside its eBCV in a macrophage cell line. We also show that genes responsible for the response against alkylating stress are required by *B. abortus* to survive following mice intranasal infection. Our data indicate that *B. abortus* does not possess a functional Ada-based adaptive system, but instead relies on redundant repair pathways, partially dependent on the methylation-sensitive transcription factor GcrA and the SOS response, to cope with alkylating stress and subvert potentially mutagenic host environments.

Results

Conservation of alkylated DNA repair genes in bacteria. We rationalized that if most intracellular bacteria face alkylating stress, there would be a significant conservation of some alkylated DNA repair genes. We found that many intracellular bacteria, including obligate pathogens such as *Chlamydia pneumoniae* and *Coxiella burnetii*, have genes homologous to some of known DNA repair genes (Fig. 1). Note that *Brucella* species are predicted to be particularly well equipped against alkylating stress (Fig. 1 and Supplementary Fig. 1).

Alkylation stress is encountered by *Brucella* inside host cells. Until now, strategies to detect the presence of alkylating stress inside host cells have been based on the survival of alkylation-specific DNA repair enzymes. These approaches have been uninformative, probably because repair systems are redundant, or because the stress is too weak to be detected by CFU counting[35,36]. Here, we took advantage of the ability of the auto-regulated Ada protein from *E. coli* to detect meP3ester groups on DNA[37] to create a transcription-based fluorescent reporter system. As the *ada* gene is in operon with *alkB* in *E. coli*[38], we replaced *alkB* with a superfolder *gfp* on a medium-copy plasmid (Fig. 2a). A mutated version of the reporter system was used as a negative control, in which a C38A mutation was introduced in Ada to prevent the protein from capturing meP3ester groups.

The reporter system was first tested with the alkylating agent methyl methane sulfonate (MMS) in *E. coli* and in *Salmonella enterica* biovar Typhimurium, which does not possess an Ada-based functional adaptive system[39]. In both bacteria, the reporter system was activated only in the presence of MMS and only with the functional version of *E. coli* Ada (Supplementary Fig. 2). In *B.*

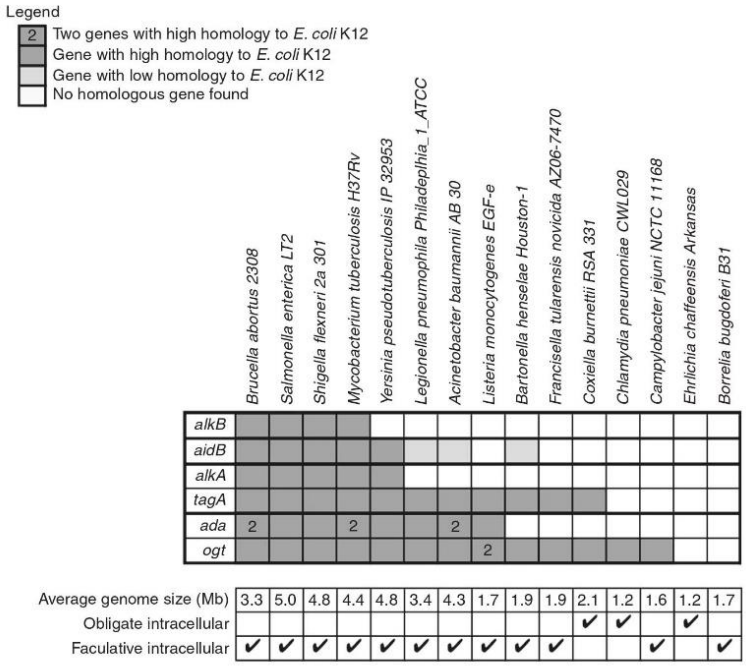

Fig. 1 Conservation of genes coding for alkylated DNA repair proteins. Genes were grouped by function. Homology was calculated based on *E. coli* K12 genome (www.patricbrc.org/). In the case of *aidB*, genes annotated as acyl-coA dehydrogenase with e-value between 10^{-29} and 10^{-44} were considered as genes with low homology and genes with e-value lower than 10^{-133} were considered as genes with high homology

abortus, the reporter was more active in exponential phase cultures compared to stationary phase cultures (Supplementary Fig. 3a). The emitted fluorescence was also dependent on the time of exposure and concentration of MMS (Supplementary Fig. 3b). To check that the reporter system was not affected by the endogenous Ada production in *B. abortus*, the mean fluorescence intensity of the system in a *B. abortus* Δ*ada1* Δ*ada2* background was compared with results in a wild-type (WT) background. No statistical difference could be observed between the two experiments, supporting the notion that endogenous Ada proteins do not affect the activation of the reporter system (Supplementary Fig. 3c).

The reporter system was then tested at the single-cell level during infection of RAW 264.7 macrophages. The first time point was 5 h PI, which corresponds to the end of the first phase of the infection, when *B. abortus* is not growing and blocked in a G1-like phase inside the eBCV[27]. The second time point chosen was at 24 h PI, when the bacteria are actively growing inside the rBCV[27]. The ratio between the mean fluorescence intensities of the functional reporter system and the non-functional version was calculated, and the level of fluorescence was significantly ($p < 0.01$) higher at 5 h PI than at 24 h PI (Fig. 2b, Supplementary Fig. 3d). This suggests that bacteria encounter alkylating stress inside host cells, but mainly during the initial phase of the infection.

To investigate the potential mutagenic properties of the intracellular eBCV environment compared to other conditions, we sequenced the genome of several individual clones of *B. abortus* before and after infection of RAW 264.7 macrophages at 6 and 48 h, and after early infection of mice (60 h), as well as after a similar number of generations in liquid culture (48 h). The genomes of five individual clones resulting from these different conditions were sequenced and subsequent analyses indicated that the number of mutations was not increased in the infection conditions compared to the culture (Supplementary Fig. 4).

N-nitrosation events occur inside the eBCV. One of the main sources of alkylating agents is the N-nitrosation of metabolites[8]. Since the content of the eBCV is unknown, we developed a new tool to investigate the presence of N-nitrosation in this compartment. Succinimidyl ester groups have been successfully employed to label the outer membrane of bacteria with fluorescent molecules[27,40]. Besides, Miao et al.[41] established a highly specific probe emitting fluorescence upon N-nitrosation. The two techniques were combined to create a N-nitrosation-sensitive probe that was covalently attached to the surface of *B. abortus*, allowing us to follow whether N-nitrosation occurs inside the eBCV, before the growth of bacteria[27] (Fig. 3a).

Labeled bacteria were first tested for their fluorescence in presence of KNO_2, which generates the NO donor N_2O_3 in aqueous solution (Supplementary Fig. 5a). Autofluorescence of non-labeled *B. abortus* was also compared to the fluorescence of labeled bacteria in the absence of KNO_2 (Supplementary Fig. 5a). Results demonstrate that the probe emits fluorescence when N-nitrosated, as expected. Next, RAW 264.7 macrophages were infected with labeled bacteria and mean fluorescence intensities were calculated at 5 h post infection at the single-cell level (Fig. 3b, Supplementary Fig. 5b, c). As a negative control, the same experiment was conducted in the presence of 163 µM of ascorbate in the cell culture medium, as this concentration of antioxidant is known to inhibit N-nitrosation reactions in RAW 264.7 macrophages[42]. We observed that about a quarter (23.3 %) of the bacterial population was subjected to N-nitrosation inside

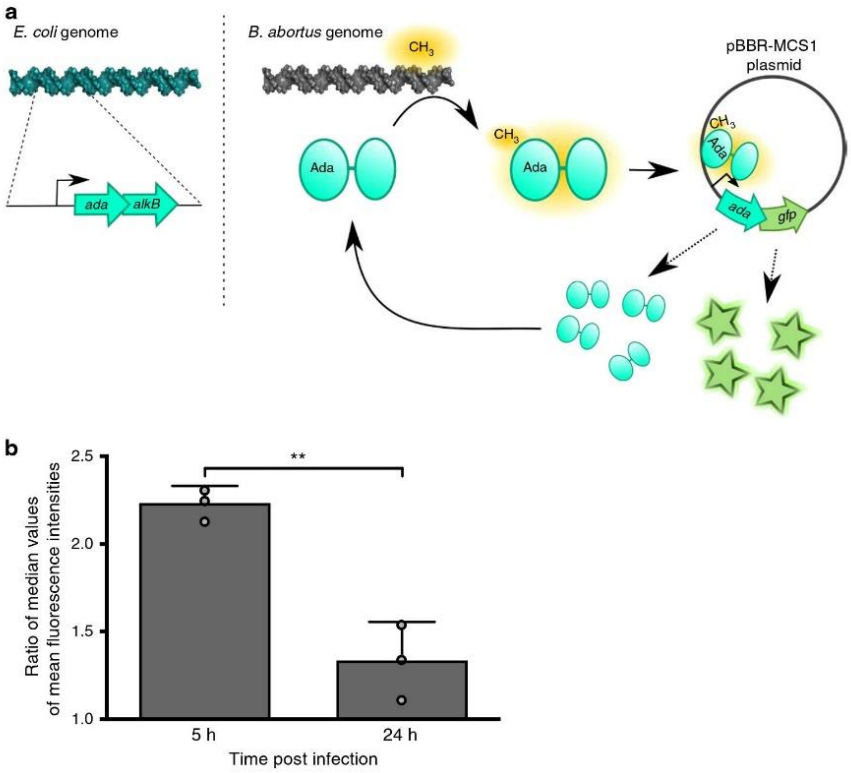

Fig. 2 Reporter system for alkylation stress. **a** Schematic representation of the reporter system. The sequence corresponding to $ada_{E.\ coli}$ and its promoter were cloned into a pBBR-MCS1 plasmid and a superfolder *gfp* was inserted downstream $ada_{E.\ coli}$. This plasmid (pBBR-p_{ada}-*ada-gfp*) was transferred to *B. abortus*. When $Ada_{E.\ coli}$ detects a methylphosphotriester group on *B. abortus* DNA, it activates the expression of its own promoter, which leads to an accumulation of $Ada_{E.\ coli}$ and GFP. Note that a mutation in $ada_{E.\ coli}$ (C38A) leads to the abrogation of its ability to bind methylphosphotriester. **b** Bacteria carrying either the pBBR-p_{ada}-*ada-gfp* reporter system or its mutated version (ada^{C38A}) were used to infect RAW 264.7 macrophages and mean fluorescence intensities (FITC channel) were calculated at 5 or 24 h post infection ($n = 60$). Ratio of median values (ada/ada^{C38A}) were plotted for biological triplicates. Error bars correspond to standard deviation. Student's *t*-test was performed with $p < 0.01$ (**). Source data are provided as a Source Data file

the eBCV. Importantly, the addition of ascorbate markedly decreased the proportion of positive labeled bacteria (Fig. 3b, Supplementary Fig. 5c), indicating that N-nitrosation reactions can effectively be prevented by antioxidants. LampI labeling of BCVs confirmed that most *B. abortus* were in the endosomal stage (eBCV) of the infection at that time point (Supplementary Fig. 5d).

We also investigated the presence of alkylating stress due to the endogenous production of N-nitroso compounds. To do so, the $Ada_{E.\ coli}$-based reporter system was tested in different genetic backgrounds (WT, Δ*narG*, and Δ*moaA*) at 5 h post infection. The deletion of *narG* alone was not sufficient to reduce alkylating stress, whereas it was the case with the Δ*moaA* strain (Fig. 3c). Notably, the addition of 163 µM of ascorbate to the cell culture medium did not significantly reduce the extent of alkylating stress, suggesting that external N-nitrosation is not responsible for alkylating stress in these conditions. Overall, this indicates that during RAW 264.7 infection, alkylating stress is mainly produced endogenously by *B. abortus* metabolism.

Key actors against alkylating stress in *B. abortus*. To evaluate which DNA repair genes are required by *B. abortus* to counteract alkylating stress, deletion strains were constructed and plated on rich medium supplemented with alkylating agents (Fig. 4). Mutants were constructed for genes predicted to encode proteins involved in direct repair, BER, HR, nucleotide excision repair (NER), and mismatch repair (MMR). Two strains were also included as negative controls: the triple mutant Δ*mutM* Δ*mutY* Δ*mutT*, required for DNA repair following oxidative stress, and the Δ*virB* strain, lacking the *B. abortus* type IV secretion system. These strains were tested for their survival against the S_N1 agent methylnitronitrosoguanidine (MNNG) that reacts with DNA in two main steps via a unimolecular nucleophilic substitution, and the S_N2 agent MMS, which reacts in one step with biomolecules[43,44] (Fig. 4).

Interestingly, some genes were required against MMS only, such as *alkB* and the BER genes. A *B. abortus* Δ*xthA*1 endonuclease mutant had been previously reported to be sensitive to MMS[45], although the function of XthA2 remains unclear. Here, we show that XthA1 is the major endonuclease, since its deletion was sufficient to confer sensitivity to MMS, whereas it was not the case for the deletion of *xthA2*. However, the double mutant was approximately a hundred-fold more sensitive than the single Δ*xthA*1 (Fig. 4), indicating that the genes have partially redundant functions. Similarly, the Δ*alkA* mutant was not affected by MMS, while the Δ*tagA* mutant displayed a 35-fold decrease in bacterial survival recovery. The Δ*tagA* Δ*alkA* mutant

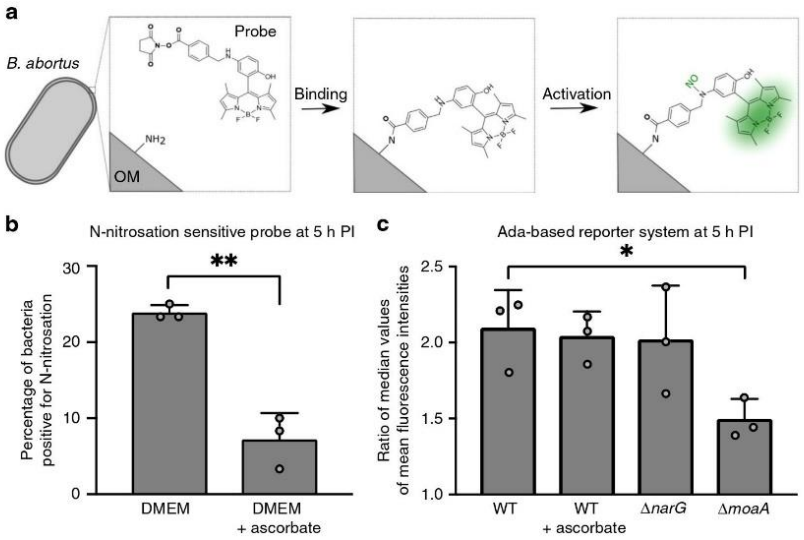

Fig. 3 Production of N-nitroso compounds inside host cells. **a** Schematic representation of the N-nitrosation-sensitive probe reacting with primary amine from *B. abortus* outer membrane (OM), and subsequently being activated by NO. **b** Evaluation of exogenous N-nitrosation by calculating the percentage of positive labeled bacteria. Bacteria were labeled with the N-nitrosation-sensitive probe and used to infect RAW 264.7 macrophages. Mean fluorescence intensities were calculated at 5 h post infection ($n = 60$) and values above 100 were considered as positive. The addition of 163 μM of ascorbate to the cell culture medium at time 0 was used to inhibit N-nitrosation. Experiments were done in biological triplicates. Error bars correspond to standard deviation. Student's *t*-test was performed with $p < 0.01$ (**). Source data are provided as a Source Data file. **c** Evaluation of endogenous N-nitroso compounds formation via the alkylation-sensitive reporter system. The $Ada_{E.\ coli}$-based reporter system was used in three genetic backgrounds (WT, Δ*narG*, and Δ*moaA*) and in the presence of ascorbate (for the WT background only). Bacteria carrying either the pBBR-p_{ada}-*ada-gfp* reporter system or its mutated version (*ada*^{C38A}) were used to infect RAW 264.7 macrophages and mean fluorescence intensities were calculated at 5 h post infection ($n = 60$). Ratio of median values (*ada*/*ada*^{C38A}) was plotted for biological triplicates. Error bars correspond to standard deviation. A Student's *t*-test was performed with a $p < 0.05$ (*). Source data are provided as a Source Data file

Function		TSB	MNNG	MMS
	WT	1,95E + 08	2,12E + 08	1,80E + 08
DR	Δ*ada*1	1,43E + 08	1,48E + 08	1,30E + 08
	Δ*ada*2	1,77E + 08	1,73E + 08	1,33E + 08
	Δ*ada*1 Δ*ada*2	1,52E + 08	9,56E + 07	8,68E + 07
	Δ*ada*1 Δ*ada*2 Δ*ogt*	1,87E + 08	7,93E + 05	4,99E + 04
	Δ*ogt*	1,90E + 08	9,26E + 06	7,48E + 04
	Δ*alkB*	1,52E + 08	1,30E + 08	2,07E + 07
BER	Δ*tagA*	1,72E + 08	1,57E + 08	4,95E + 06
	Δ*tagA* Δ*alkA*	1,70E + 08	1,23E + 08	2,03E + 03
	Δ*alkA*	1,75E + 08	1,25E + 08	1,40E + 08
	Δ*xthA*1	1,72E + 08	1,63E + 08	1,22E + 07
	Δ*xthA*2	2,15E + 08	1,65E + 08	1,43E + 08
	Δ*xthA*1 Δ*xthA*2	1,58E + 08	1,60E + 08	1,08E + 05
HR	Δ*recA*	1,40E + 08	2,13E + 07	9,90E + 04
NER	Δ*uvrA*	2,13E + 08	2,17E + 08	1,32E + 08
MMR	Δ*mutS* Δ*mutL*	2,57E + 08	2,19E + 08	1,91E + 08
Others	Δ*mutM* Δ*mutY* Δ*mutT*	2,18E + 08	1,70E + 08	1,40E + 08
	Δ*virB*	2,32E + 08	2,53E + 08	1,38E + 08

Survival + −

Fig. 4 Survival of DNA repair mutants against alkylating agents in vitro. Deletion strains were plated on rich medium (TSB) supplemented or not with alkylating agents (35 μM of MNNG or 2.5 mM of MMS). Data shown here are the mean values of colony forming units for biological triplicates. DR stands for direct repair, BER for base excision repair, HR for homologous recombination, NER for nucleotide excision repair, and MMR for mismatch repair. The category "others" comprises 8-oxo-dG repair (*mutM mutY mutT*) and the type IV secretion system (*virB*) as negative controls. Source data are provided as a Source Data file

was more markedly sensitive, with a decrease in CFU of 5 orders of magnitude compared to the control condition (Fig. 4). This result indicates that AlkA and TagA share an overlapping function, which is crucial for survival in the presence of MMS in *B. abortus*, as it is the case in *E. coli*[46]. The Δ*recA* mutant was also strongly affected by MMS (as described previously[47]), but only slightly in the presence of MNNG (Fig. 4). The Δ*ogt* mutant is particularly noteworthy, as it appeared to be very sensitive to MMS exposure. The triple mutant Δ*ada*1 Δ*ada*2 Δ*ogt* was only marginally more attenuated than the single Δ*ogt* mutant against MMS, and slightly more against MNNG (Fig. 4). This indicates that the presence of Ogt is a key factor for *B. abortus* survival against alkylating agents in these conditions, unexpectedly more than the two Ada proteins compared to the *E. coli* model. At the protein level, $Ogt_{B.\ abortus}$ is predicted to be 33% identical to $Ogt_{E.\ coli}$ with the conservation of the methyl-acceptor C139 residue (Supplementary Fig. 6a). In *B. abortus*, the residue corresponding to $Ogt_{E.\ coli}$ S134 is a proline (Supplementary Fig. 6a). Remarkably, in *E. coli*, the mutation of S134 into a proline confers broader substrate specificity to the protein by increasing the size of its active site[48], so this could explain why Ogt seems to be the major actor amongst the three methyltransferases of *B. abortus*.

The two genes predicted to code for Ada also possess conserved C38 and C321 residues (Supplementary Fig. 6b). Nevertheless, the deletion of the *ada1* and *ada2* genes did not change drastically the sensitivity of *B. abortus* to alkylating agents (Fig. 4), Questioning whether the Ada proteins are functioning as transcription factors. Quantitative reverse transcription polymerase chain reaction (RT-qPCR) experiments were performed on *B. abortus* in the presence or absence of MMS, and several DNA repair genes were compared for their mRNA levels in these conditions (Fig. 5). Interestingly, the mRNA levels of the two *ada* genes were not statistically increased after MMS exposure. In fact, the only overexpressed alkylation-specific genes were *alkA* and *tagA*, which are predicted to code for proteins of similar function. The absence of induction of the *ada* genes (Fig. 5) and their marginal role in coping with alkylating stress in vitro (Fig. 4) suggest that *B. abortus* does not rely on a classical Ada-dependent adaptive system to subvert alkylating stress. It has been proposed that the absence of an adaptive response in *S. enterica* serovar Typhimurium could be due to the lack of an acidic residue in position 106th[39]. Similarly, in *B. abortus*, the corresponding position is occupied by either a N116 (Ada1) or a V105 (Ada2) (Supplementary Fig. 6b), so this could also explain why *B. abortus* does not possess a functional Ada-based adaptive system.

Another gene that was overexpressed upon MMS exposure was *lexA* (Fig. 5). Interestingly, the early accumulation of the SOS repressor LexA is a marker of the activation of the SOS response, because *lexA* itself is part of its early regulon to prevent an uncontrolled over-activation of the SOS response[49]. To determine which genes are part of the SOS regulon in *B. abortus* under alkylating stress, the fold induction of several genes was compared after MMS exposure in the WT and *lexA* overexpression (pBBRMCS1-p_{lac}-*lexA*) strains. In the overexpression strain, *lexA* itself was not further induced by MMS exposure, as its level of transcription was probably already maximal (Supplementary Fig. 7). Importantly, neither *tagA* nor *alkA* were significantly differentialy induced by MMS in the two conditions (Supplementary Fig. 7), indicating that their induction is dependent of a yet unknown factor. Among the two error-prone DNA polymerases of *B. abortus*, the *imuABC* operon[50] had a drop of induction upon *lexA* overexpression, in contrast to *dinB*, which encodes DNA polymerase IV (Supplementary Fig. 7). Of note, in α-proteobacteria, a few genes are downregulated following the activation of the SOS response[51,52]. In *B. abortus*, our results suggest that it could also be the case for the NER endonuclease *uvrA*, as it was further induced in the *lexA*-overexpressing strain (Supplementary Fig. 7). Importantly, RecA is suspected to constitutively trigger a basal SOS response in *B. abortus*, even under non-stress conditions[53], which could explain the relatively low induction of many potential target genes in our experiment.

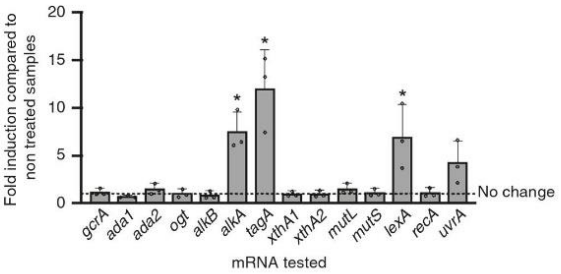

Fig. 5 Gene expression following MMS treatment. RT-qPCR was performed on exponential phase *B. abortus* cultured in rich medium for 5 h in the presence or absence of 2.5 mM MMS. Experiments were performed three times and mean values were compared between the stressed and non-stressed conditions. Error bars represent standard deviation. Student's *t*-test was performed on data with minimum 1.5-fold induction ($p < 0.05$, *). Source data are provided as a Source Data file

Involvement of GcrA against alkylation stress in vitro. One striking characteristic of *ogt* is the presence, right after the start codon, of a GANTC motif. This sequence is known to be a site of epigenetic regulation in α-proteobacteria[54]. Indeed, GANTC sites have been shown to be methylated by CcrM in a cell-cycle-dependent manner in the α-proteobacterium *Caulobacter crescentus*[55,56], and probably also in *B. abortus*[57,58]. Interestingly, the gene coding for the alkylation-specific DNA repair AlkB protein is regulated throughout the cell cycle in *C. crescentus*[59] and in this bacterium, *alkB* mRNA levels drop by more than two-fold in a GcrA depleted strain[60]. Since the cell cycle-dependent transcription factor GcrA is known to be modulated by methylated GANTC sites on *C. crescentus* DNA[60,61], we identified the ortholog of *gcrA* in *B. abortus* (BAB1_0329), a gene previously shown to be essential[62]. ChIP-seq analysis of GcrA was performed to identify its targets in *B. abortus*. As many as 232 hits were found for the first chromosome of *B. abortus*, and 110 for the second one (available at https://figshare.com/articles/Summary_of_whole_genome_sequencing_for_B_abortus/9747653). This high number of targets is consistent with GcrA being associated with the housekeeping sigma factor (σ^{70}), similarly to *C. crescentus*[60]. Among GcrA targets, several genes are involved in DNA repair (*ogt, lexA, uvrA*, and *mutL* but also *aidB*) (Fig. 6a). Compared to the rest of the chromosomes, we found a significantly higher (4.4- and 4.7-fold in chromosomes I and II, respectively) frequency of GANTC sites in the peaks of this ChIP-seq ($p < 0.001$ according to a Poisson distribution), which is consistent with methylation-dependent binding of GcrA in *B. abortus*.

To test if genes involved in DNA repair are regulated by GcrA, we constructed a strain with IPTG-inducible GcrA factor (Δ*gcrA* pBI-*gcrA*). In the absence of IPTG, the Δ*gcrA* pBI-*gcrA* strain mainly formed Y-shaped bacteria within the first 6 h of growth, indicating that their division was impaired. Texas Red succinimidyl ester (TRSE) labeling[40] also suggested that bacterial growth was also slower at later time points (Fig. 6b). After 3 h in the absence of IPTG, the bacteria were efficiently depleted from

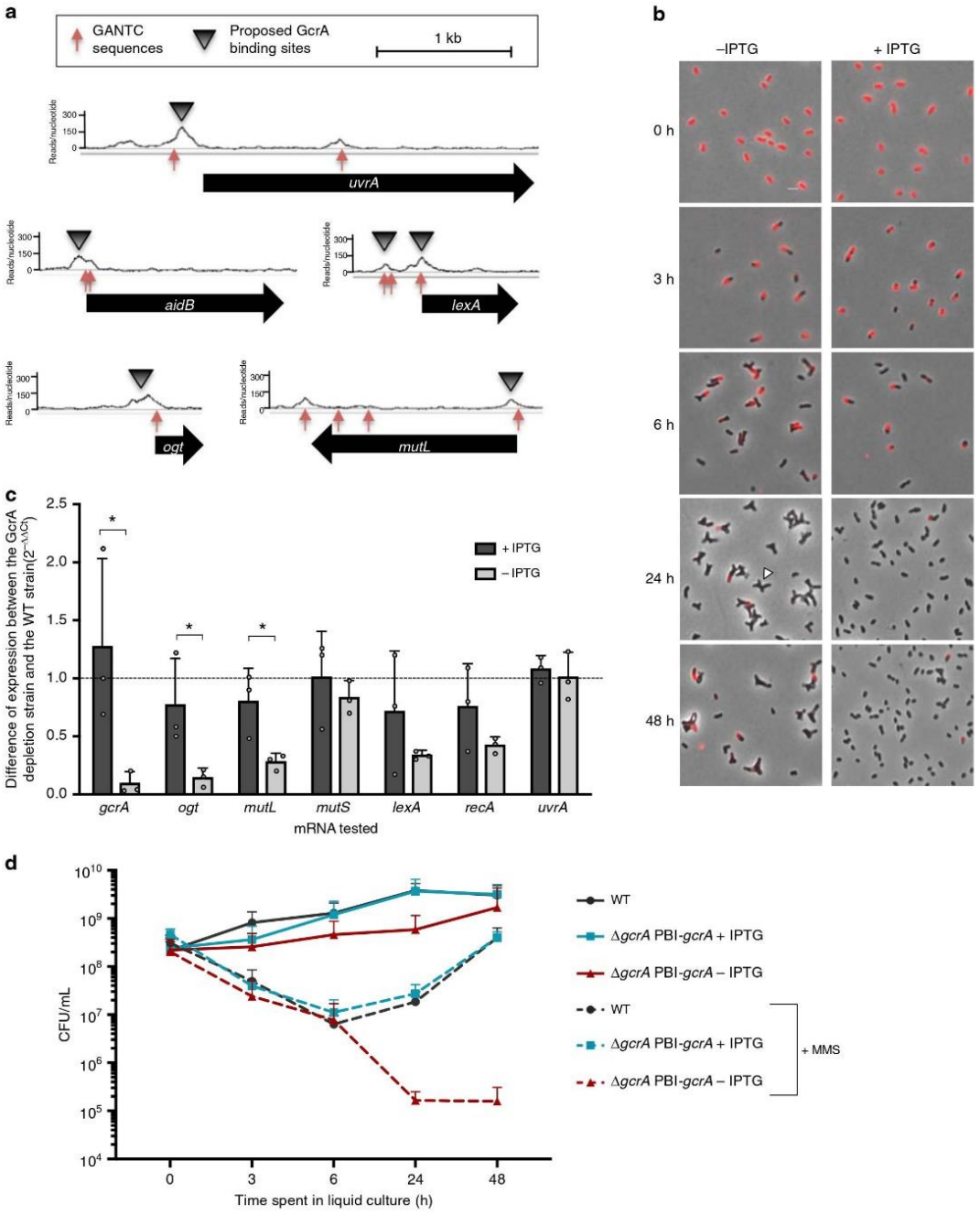

leftover GcrA, as demonstrated by western blot analysis (Supplementary Fig. 8a). RT-qPCR was performed on DNA repair genes after culturing *B. abortus* Δ*gcrA* pBI-*gcrA* in the presence or absence of IPTG. This confirmed that GcrA regulates the expression of *ogt* and *mutL* (Fig. 6c). Of note, the induction of *lexA* still occurred after MMS exposure in the absence of GcrA (Supplementary Fig. 8b), indicating that the activation of the SOS response under exogenous stress is regulated through a GcrA-independent mechanism.

The WT and GcrA-depleted strains were grown in liquid medium supplemented or not with IPTG and/or MMS to test whether the presence of GcrA is crucial for survival and growth in alkylating conditions. Aliquots were taken at different time points and plated on rich media supplemented with IPTG to assess bacterial survival. As seen with TRSE labeling (Fig. 6b), the Δ*gcrA* pBI-*gcrA* strain cultured without IPTG was almost not multiplying but did survive (at least up to 2 days) as bacteria were recovered following plating on media supplemented with IPTG

Fig. 6 Targets and functions of the transcription factor GcrA. **a** GcrA-binding sites detected by ChIP-seq. The number of reads per nucleotide is plotted for five promoter regions enriched by GcrA pull-down. **b** GcrA depletion generates growth and division defects in *B. abortus*. Bacteria were labeled with TRSE to covalently bind Texas Red to amine groups present at the bacterial surface. Non-labeled area thus correspond to newly incorporated envelope material. Grown in rich medium in the presence of IPTG (+IPTG), bacteria have a normal morphology. Upon IPTG removal (−IPTG), bacteria elongate (3 h), then form branches (6 h). At 24 h post IPTG removal, many bacteria present Y-shapes or more complex branched phenotypes (white arrow). **c**Gene expression in the GcrA-depleted strain. The mRNA levels of several genes coding for DNA repair proteins were calculated through RT-qPCR experiments for the GcrA-depleted strain. As predicted by ChIP-seq experiment, *ogt* and *mutL* expression are both affected by the absence of GcrA (−IPTG). The expression of the other genes was not statistically different (Student's *t*-test) between the two conditions (±IPTG) ($n = 3$). Source data are provided as a Source Data file. **d** Survival of GcrA-depleted strain in the presence of in vitro alkylating stress. Bacteria were cultured in liquid medium supplemented or not with IPTG and in the presence or absence of 5 mM of MMS. Samples were taken after 0, 3, 6, 24, and 48 h of culture and plated on rich medium supplemented with IPTG. Colony-forming units were counted to evaluate survival. Error bars represent standard deviation ($n = 3$). Source data are provided as a Source Data file

(Fig. 6d). When bacteria were cultured in the presence of MMS, both strains first underwent a strong drop of CFU, independent of IPTG. Subsequently, both the WT and the Δ*gcrA* pBI-*gcrA* strains were able to overcome the stress and recovered with time if supplemented with IPTG (Fig. 6d). When *B. abortus* was depleted of GcrA, bacteria were unable to recover (Fig. 6d), indicating that the presence of GcrA is required for *B. abortus* to efficiently cope with high exogenous alkylating stress.

Individual repair pathways are required for long-term infections. Three strains (Δ*ada*1 Δ*ada*2 Δ*ogt*, Δ*alkA* Δ*tagA*, and Δ*alkB*) which displayed increased sensitivity to alkylating stress in vitro (Fig. 4) were tested during the infection of RAW 264.7 macrophages but failed to show attenuation (Supplementary Fig. 9). Similarly, an *aidB* mutant had previously been shown to be unaffected in infection[63]. Other DNA repair mutants were also tested but none of them was attenuated in this model of infection (Supplementary Fig. 9).

According to RT-qPCR data, GcrA is involved in the regulation of at least two DNA repair pathways: direct repair through *ogt* and MMR through *mutL* (Fig. 6c). In RAW 264.7 macrophages, it was observed that the GcrA depleted strain maintained a stable number of CFU until 24 h post infection, before dropping at 48 h post infection (Fig. 7). This indicates that GcrA is required for survival in this model of infection. However, this attenuation might not be only due to the disruption of DNA repair pathways, as GcrA also regulates many other functions, which will require further investigation.

The Ada-based reporter system allowed us to determine that the alkylating stress occurring on *B. abortus* inside RAW 264.7 macrophages is very low. In addition, our assays have all focuses on early infection times. One possibility is that alkylation stress could be more important at later time points inside host cells and/or in more physiological infection conditions. For example, a *B. abortus* Δ*recA* mutant was previously shown to be attenuated in a mouse infection model[47] even though we could not detect any attenuation in RAW 264.7 macrophages (Supplementary Fig. 9). Therefore, we tested several mutant strains in an intranasal mice infection model[64] at 12 and 28 days (Fig. 8). In the lungs, there was a striking attenuation at both time points for the alkylation-specific direct repair Δ*ada*1 Δ*ada*2 Δ*ogt* mutant and the glycosylase (Δ*alkA* Δ*tagA*) deficient strain. The double endonuclease Δ*xthA*1 Δ*xthA*2 mutant and the MMR Δ*mutL* Δ*mutS* mutant were also strongly attenuated. In spleen, the defects were mild, with the BER mutants being the most affected (Fig. 8).

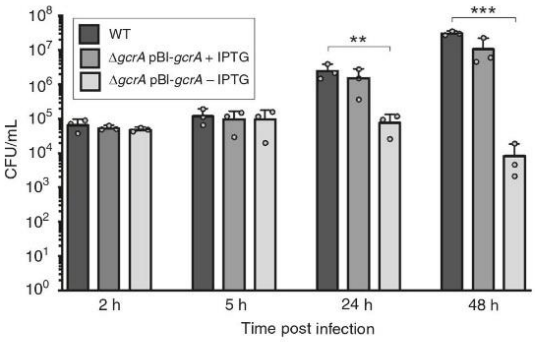

Fig. 7 Infection of RAW 264.7 macrophages with the GcrA depleted strain. Colony-forming units were counted after 2, 5, 24, and 48 h post infection for the WT and the GcrA depleted strains incubated with or without IPTG (+IPTG or −IPTG, respectively). Error bars represent standard deviations ($n = 3$). A Scheffe statistical analysis reveals that, in the absence of IPTG, the GcrA-depleted strain is attenuated at 24 ($p < 0.01$, **) and 48 h ($p < 0.001$, ***) post infection in this cell type. Source data are provided as a Source Data file

Discussion

Many environmental and pathogenic bacteria possess an adaptive system against alkylating stress[1], indicating that this stress is widespread in the environment. Nevertheless, before this study, it was not known whether intracellular bacteria also face alkylation during infection. Here, we show that the intracellular pathogen *B. abortus* faces alkylation stress during infection, with functional DNA repair pathways for alkylation damage required in a mice model of infection, and that the control of the genes involved in the repair of alkylated DNA is different from the one reported in *E. coli*.

To investigate the occurrence of alkylating stress at early time points of infection, we developed a fluorescence-based reporter system to follow the occurrence of the stress on bacterial DNA at the single-cell level. To understand the source of alkylating stress, a probe was designed to be covalently attached at the bacterial surface and report N-nitrosation events occurring inside the eBCV. The combination of those two approaches allowed us to determine that alkylating stress occurs inside the eBCV mainly via the bacterial metabolism. Indeed, the addition of ascorbate, which quenches N-nitrosation on the bacterial surface, was not able to decrease alkylation damage detected with the Ada-based reporter. Moreover, the deletion of *moaA*, which is involved in the biosynthesis pathway of the molybdenum cofactor, decreased the intensity of alkylating stress. *B. abortus* possesses a single nitrate reductase, so it is likely that the phenotype of the *moaA* mutant comes from the simultaneous deficiency of Nar and other enzymes dependent on the molybdenum cofactor[7]. It could be the case of MSF, a nitrate–nitrite antiporter, as well as FdnG, a formate dehydrogenase involved in nitrate respiratory chain[65]. Importantly, the occurrence of external N-nitrosation events is relevant for alkylating stress only if metabolites are present in the

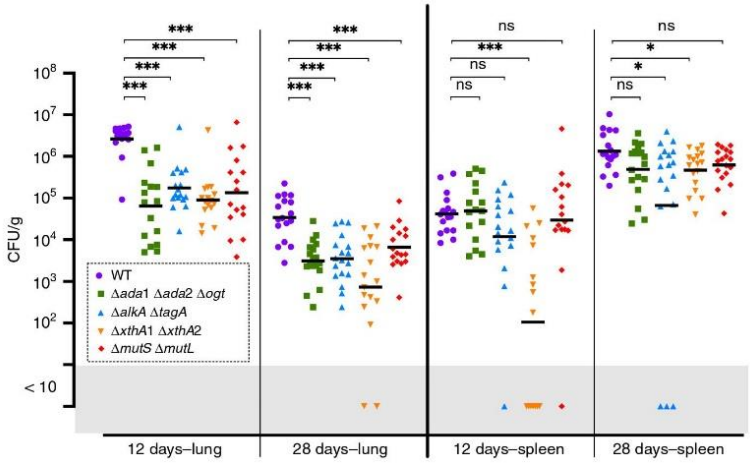

Fig. 8 Intranasal mice infection with *B. abortus* DNA repair deletion strains. Wild-type C57BL/6 mice received 2×10^4 CFU of *B. abortus*, as indicated in the section "Methods". The mice were sacrificed at the selected time post infection. The data represent the number of CFU g^{-1} of lung and spleen. These results are representative of two independent experiments with, in the same order than in the figure, $n = 9+8, 8+8, 9+8, 8+8, 8+8$ mice at 12 days and $n = 9+8, 9+9, 9+9, 9+8, 9+9$ mice at 28 days. Black lines correspond to mean values. A Mann–Whitney test was performed with $p > 0.05$ (ns non significant), $p < 0.05$ (*) and $p < 0.001$ (***). Source data are provided as a Source Data file

environment. Indeed, alkylating stress is generated by those modified metabolites, and not by N-nitrosation per se[66]. It has been proposed that the eBCV is deficient in metabolites[67,68], which could explain why host cells do not produce detectable exogenous alkylating agents. Another important point is that N-nitrosation reactions are dependent on RNS levels[25] and *B. abortus* is known to be very weakly immunogenic, as it prevents proinflammatory responses in macrophages and neutrophils[69]. In addition, *B. abortus* possesses a gene coding for a nitric oxide reductase, involved in detoxification of NO and nitrate respiration, which is required and overexpressed by the bacterium early during infection[68,70,71]. One interesting hypothesis is that by avoiding exogenous sources of alkylating stress, *B. abortus* generates weak endogenous stress. Indeed, as *B. abortus* activates its nitrate respiration/denitrification pathway inside host cells, it must probably also generate endogenous N-nitroso compounds and hence endogenous alkylating agents. Importantly, alkylating stress does not induce a linear dose response in organisms[72], which could explain why DNA repair mutants were not attenuated during macrophage infection, but was attenuated in the more physiologicaly and relevant intranasal mouse infection model.

E. coli deals with alkylating stress through various and dynamically regulated DNA repair pathways. Indeed, in the model developed by Uphoff[34], *E. coli* mainly relies on damage tolerance (via the SOS response) and constitutive repair (via TagA and Ogt), before the adaptive response takes over after prolonged alkylating stress. Our data indicate that *B. abortus* has a different strategy to cope with this stress. First, we found that an Ada-based adaptive system is absent in *B. abortus*, similarly to some other α-proteobacteria[59,73]. Nevertheless, *B. abortus* does possess the ability to induce the expression of both *alkA* and *tagA* upon alkylating agent exposure, via a yet unknown mechanism. Secondly, we showed that, through the SOS response, the genes coding for the error-prone DNA polymerase *imuABC* were also overexpressed in conditions of high alkylating stress. Finally, *B. abortus* was found to rely on the essential and well-conserved transcription factor GcrA to control the expression of a series of genes involved in DNA repair, including *mutL* and *ogt*. The GcrA depleted strain was impaired for division, growth, and virulence, suggesting that it plays a role in *B. abortus* cell cycle regulation. Of note, in *B. abortus*, the promoter of *tagA* is directly bound by CtrA, another conserved cell cycle regulator[57]. In *E. coli*, *ada* is known to be overexpressed in the stationary phase, independent of the methylation of its C38 residue but through the activity of the alternative sigma factor RpoS[7]. Since there appears to be no *rpoS* homolog in *B. abortus* and other α-proteobacteria[74], it is tempting to speculate that these bacteria have selected systems in which cell cycle regulators control DNA repair. A previous report[53] also indicates that genes of the SOS regulon have a high basal expression in *B. abortus*, which could be an additional way to ensure sufficient protection against endogenously produced stress. Interestingly, the absence of genome replication inside the eBCV also constitutes a direct advantage against genotoxic stresses, as DNA adducts do not fix mutations so long as replication has not occurred. Another characteristic of GcrA in *C. crescentus* is its ability to sense CcrM-dependent methylation on DNA[61]. Knowing that this epigenetic mark is cell cycle regulated in *C. crescentus*[75] and probably also in *B. abortus*[57,58], there could be a functional link between both damage-induced and epigenetic methylation.

This study provides new insights into a stress that was, until now, only hypothetically associated with intracellular bacterial pathogens. The discovery of alkylating stress on intracellular *B. abortus* suggests that other bacteria transiting through similar compartments could also be exposed to such a stress. Future investigations along these lines could generate a better understanding of host–pathogen interactions at the molecular level.

Methods

Bacterial strains and media. *E. coli* strains DH10B (Thermo Fisher Scientific) and S17-1 (ref. [76]) were grown in Luria-Bertani (LB) medium at 37 °C. *B. abortus* 544 Nal^R strain (Obtained from J.-M. Verger and M. Grayon, Institut National de la Recherche Agronomique, Laboratoire de Pathologie Infectieuse et d'Immunologie, Nouzilly, France) and its derivatives were grown in either 2YT-rich medium (1% yeast extract, 1.6% peptone, 0.5% NaCl) or TSB-rich medium (3% Bacto tryptic soy broth) at 37 °C. Antibiotics were used at the following concentrations: ampicillin, 100 μg mL^{-1}; kanamycin, 10 μg mL^{-1} with integrative plasmids or 50 μg mL^{-1} with replicative plasmids; chloramphenicol, 20 μg mL^{-1}; nalidixic acid, 25 μg mL^{-1}; rifampicin, 20 μg mL^{-1}; gentamicin, 10 or 50 μg mL^{-1} as indicated. When required, isopropyl β-D-1-thiogalactopyranoside (IPTG) was used at a concentration of 1 mM in bacterial culture and at 10 mM in the culture medium during cellular infections.

B. abortus deletion strains were constructed by allelic exchange, via pNPTS138 vectors (M. R. K. Alley, Imperial College of Science, London, UK) carrying a kanamycin resistance cassette and a sucrose sensitivity cassette[27]. Briefly, we selected bacteria which had integrated the plasmid containing upstream and downstream sequences (about 750 bp each) of our target gene by plating them on kanamycin-containing agar plates, then performed a counterselection on 5% sucrose-containing agar plates without kanamycin to allow plasmid curing. To confirm gene deletion, PCR was performed on colonies that were kanamycin-negative and sucrose-resistant with primers targeting sequences upstream and downstream of the plasmid-containing sequences. Note that in the case of the Δ*xthA2* strain, 204 nucleic acids were kept on each side of the gene, as there was a previous report that the full deletion of the gene was not feasible[45]. Primers, plasmids and ORF of the studied genes are listed in Supplementary Data 1.

B. abortus GcrA-depleted strain was constructed similarly than the CtrA-depleted strain[57]. Briefly, the p_{lacI}-*lacI*-p_{lac} sequence was amplified from the pSRK-Kan plasmid[77] using Phusion High-Fidelity DNA Polymerase (New England BioLabs). The PCR product was then cloned into a pBBRMCS1 plasmid using *Sac*I and *Bam*HI restriction enzymes. This modified pBBRMCS1 is referred to as pBI. The *gcrA* coding sequence was amplified form *B. abortus* 544 genome with Phusion High-Fidelity DNA Polymerase (New England BioLabs) and then cloned into pBI using *Bam*HI and *Kpn*I enzymes in order to orient the insert opposite to the p_{lac} promoter already present in pBBRMCS1. This final plasmid (pBI-*gcrA*) was transferred to *B. abortus* by mating, after inserting the deletion plasmid (pNPTS138-Δ*gcrA*), then *gcrA* was removed from the chromosome of *B. abortus* as described above.

The *lexA* sequence was amplified from *B. abortus* 544 genome with primers listed in Supplementary Data 1 and the PCR product was ligated into a pBBRMCS1 plasmid after *Apa*I and *Bam*HI restiction, generating the pBBRMCS1-p_{lac}-*lexA* final plasmid.

Cloning of the reporter system for alkylating stress. The p_{ada}-$ada_{E.\ coli}$ sequence, including the start codon of $alkB_{E.\ coli}$, was amplified from *E. coli* DH10B with Phusion High-Fidelity DNA Polymerase (New England BioLabs) using primers listed in Supplementary Data 1. A superfolder *gfp* coding sequence (Supplementary Note 1), with a *Xho*I sequence after the start codon and a *Pst*I sequence after the stop codon, was adapted to fit the codon usage of *B. abortus* 2308 (http://www.kazusa.or.jp/codon/) and ordered as gBlocks gene fragment (Integrated DNA Technologies). Both DNA products were cloned into a pBBRMCS1 plasmid using *Pst*I, *Xho*I, and *Spe*I restriction enzymes in a triple ligation to orient the p_{ada}-$ada_{E.\ coli}$-*gfp* fusion opposite to the p_{lac} promoter of pBBRMCS1.

Synthesis of N-nitrosation-sensitive probe and binding conditions. The probe was designed based on Mio et al.[41], with the addition of a succinimidyl ester group in order to allow the binding of the probe on amines at the bacterial surface. The characterization of the probe can be found in Supplementary Note 2.

One milliliter of bacteria (DO_{600} 0.5) was centrifuged at 7000 r.p.m. for 2 min and washed twice in phosphate buffered saline (PBS). They were incubated for 1 h at 37 °C with the probe (10 µM) in 1 mL of PBS supplemented with 100 µL of $NaHCO_3$ 1 M (pH 8.4). Bacteria were then washed three times with PBS and used either for RAW 264.7 infection or for experiments in culture. For experiments in culture, labeled bacteria were left for 1 h on wheel in the dark with 1 M of KNO_2 (Thermo Fisher scientific) and 20 µL of HCl 3 M, before to be washed twice with PBS and fixed with paraformaldehyde (PFA) 2% for 20 min at 37 °C.

Texas Red succinimidyl ester labeling. One milliliter of bacteria (DO_{600} 0.5) was centrifuged at 7000 r.p.m. for 2 min and washed twice in PBS. Bacteria were resuspended in 1 mL of PBS and incubated with Texas Red succinimidyl ester (TRSE) at a final concentration of 1 µg mL^{-1} (Invitrogen) for 15 min at room temperature. Bacteria were then washed three times with PBS.

RAW 264.7 macrophage culture and infection. RAW 264.7 macrophages (ATCC) were cultured at 37 °C in the presence of 5% CO_2 in DMEM (Invitrogen) supplemented with 4.5 g L^{-1} glucose, 1.5 g L^{-1} $NaHCO_3$, 4 mM glutamine, and 10% fetal bovine serum (Gibco). RAW 264.7 macrophages were seeded in 24-well plates (with coverslips for immunolabeling) at a concentration of 10^5 cells per mL and left in the incubator overnight. The next morning, late exponential phase cultures of *Brucella* (DO_{600} 06–0.9) were washed twice in PBS in order to remove antibiotics and traces of growth medium, then they were prepared in DMEM at a multiplicity of infection of 50. During that step, IPTG or ascorbate was added to the culture medium if required. Bacteria and cells were centrifuged at 400 *g* for 10 min at 4 °C and then incubated for 1 h at 37 °C with 5% CO_2 atmosphere before to be washed twice with PBS and then incubated in medium supplemented with 50 µg mL^{-1} of gentamicin to kill extracellular bacteria. One hour later, the medium was replaced by fresh medium supplemented with 10 µg mL^{-1} of gentamicin.

Immunolabeling of infected RAW 264.7 macrophages. Cells were washed twice in PBS before to be fixed for 20 min in 2% PFA pH 7.4 at 37 °C. They were then left in PBS in the dark at 4 °C overnight before to be permeabilized in PBS with 0.1% Triton X-100 (Prolabo) for 10 min. Cells were incubated for 45 min with primary antibodies in PBS containing 0.1% Triton X-100 and 3% (w/v) bovine serum albumin (BSA, Sigma-Aldrich). Next, cells were washed three times in PBS before to be incubated with secondary antibodies in PBS containing 0.1% Triton X-100 and 3% BSA. For LampI labeling experiments, the primary antibodies consisted in homemade anti-*Brucella* rabbit polyclonal antibodies[27] and anti-LampI rat antibodies (1D4B; Developmental Studies Hybridoma Bank, University of Iowa), and the secondary antibodies consisted in goat anti-rabbit antibodies coupled to Pacific Blue (Invitrogen, cat. no. P10994) and goat anti-rat antibodies coupled to Alexa Fluor 647 (Invitrogen, cat. no. A21247). For all other experiments, we used anti-*Brucella* LPS primary antibodies (A76-12G12, undiluted hybridoma culture supernatant[78]) and goat anti-mouse secondary antibodies coupled to Texas Red (1:500) (Invitrogen, cat. no. T862). Coverslips were washed three times in PBS, once in ddH_2O and then mounted on Mowiol (Sigma).

Microscopy and analyses of fluorescence. We used a Nikon Eclipse E1000 (objective ×100, plan Apo) microscope connected to a ORCA-ER camera (Hamamatsu). The Hg lamp was set with ND filter at 4. Bacteria in culture (2 µL) were observed with the phase contrast on PBS-agarose (1%) pads. Bacteria inside host cells were observed with the TxRed channel (or the CFP channel for LampI experiments) (100 ms). The FITC channel (1 s) was used to detect either the N-nitrosation-sensitive probe or the GFP signal of the reporter system. LampI proteins were detected with the APC channel (800 msec). Pictures were encoded with NIS-element software and analyzed with the plug-in MicrobeJ in ImageJ[79]. For bacteria on pads, mean fluorescence intensities (MFI) were obtained as the "mean_c" values with MicrobeJ for individual bacteria. For intracellular bacteria, MFI were obtained by subtracting the background fluorescence (defined here as the average value of fluorescence given by the Pixel Inspection Tool on three points randomly chosen around a bacterium) to the "mean" value of fluorescence obtained for each bacterium with MicrobeJ (see Supplementary Note 3 for a detailed protocol). Note that MFI values were considered as positive for bacteria labeled with the N-nitrosation-sensitive probe when they reached an arbitrary threshold of MFI = 100, as this value is above 86% of the MFI values on labeled bacteria (in blue in Supplementary Fig. 5a), and below 96% of the MFI values for the positive control (labeled bacteria + KNO_2, in orange in Supplementary Fig. 5a).

Chromatin immunoprecipitation with anti-GcrA antibodies. Cultures of 80 mL of *B. abortus* (OD_{600} 0.8) were harvested by centrifugation and proteins were cross-linked to DNA with 10 mM sodium phosphate buffer (pH 7.6) and 1% (v/v) formaldehyde for 10 min at RT and 30 min on ice. Bacteria were centrifuged and washed twice in cold PBS before to be resuspended in lysis buffer (10 mM Tris-HCl pH 7.5, 1 mM EDTA, 100 mM NaCl, 2.2 mg mL^{-1} lysozyme, 20 mL protease inhibitor solution from Roche). Bacteria were lysed, after the addition of 0.1 and 0.5 mm diameter Zirconia/Silica beads (Biospec Products), in the cell Disruptor Genie from Scientific Industries at maximal amplitude (2800) for 25 min at 4 °C. Bacteria were then incubated for 10 min in the presence of ChIP buffer (1.1% Triton X-100, 1.2 mM EDTA, 16.7 mM Tris-HCl pH 8.0, 167 mM NaCl, protease inhibitors). DNA fragments of about 300 base pairs were obtained by sonicating the lysate on ice (Branson Sonifier Digital cell disruptor S-450D 400 W) by applying 15 bursts of 20 s (50% duty) at 30% amplitude. Debris were excluded in the pellet by centrifugation at 14,000 r.p.m. for 3 min. The supernatant was normalized by protein content by measuring the absorbance at 280 nm and 7.5 mg of protein was diluted in 1 mL of ChIP buffer supplemented with 0.01% SDS and pre-cleared in 80 mL of protein A-agarose beads (Roche) and 100 µg BSA. Homemade anti-rabbit polyclonal GcrA antibodies (290.S3) were added to the supernatant (1:1000) and incubated overnight at 4 °C. The mix was then incubated with 80 mL of protein A-agarose beads pre-saturated with BSA for 2 h at 4 °C. Beads were then washed in the following order: once with low salt buffer (0.1% SDS, 1% Triton X-100, 2 mM EDTA, 20 mM Tris-HCl pH 8.1, 150 mM NaCl), once with high salt buffer (0.1% SDS, 1% Triton X-100, 2 mM EDTA, 20 mM Tris-HCl pH 8.1, 500 mM NaCl), once with LiCl buffer (0.25 M LiCl, 1% NP-40, 1% sodium deoxycholate, 1 mM EDTA, 10 mM Tris-HCl pH 8.1), and twice with TE buffer (10 mM Tris-HCl pH 8.1 and 1 mM EDTA) before to be eluted with 500 µL of elution buffer (1% SDS and 0.1 M $NaHCO_3$). The reverse-crosslinking was performed with 500 mL of 300 mM of NaCl overnight at 65 °C. Samples were then treated with Proteinase K (in 40 mM EDTA and 40 mM Tris-HCl pH 6.5) for 2 h at 45 °C and DNA was finally extracted with QIAGEN MinElute kit to be resuspended in 30 µL of Elution buffer.

Illumina MiSeq was used to sequence immunoprecipitated DNA. Data consisted of a number of reads per nucleotide. A *Z*-score for each base pair (i.e. the number of standard deviations from the average) was calculated based on average and variance in a window of 1 million base pairs. A threshold of *Z*-score above 4 was set to consider genomic regions as bound by GcrA. These sequences were mapped to the genome of *B. abortus* 2308 (available at https://www.ncbi.nlm.nih.gov/geo/query/acc.cgi?acc = GSE136733). The GcrA-binding peaks (.txt files) can also be visualized on Artemis (freely available at http://www.sanger.ac.uk/science/tools/artemis) with the genomic sequences (.gb files) available at https://figshare.com/s/0e580305b65f67619d36. To calculate the number of GANTC sequences in ChIP-seq peaks, we extracted peak sequences online with Emboss-extractseq (http://emboss.bioinformatics.nl/cgi-bin/emboss/extractseq) and looked for the presence of GANTC sites with the "pattern matching, dna-pattern" tool on

RSATools[80] (http://embnet.ccg.unam.mx/rsa-tools/) on both strands and with allowing overlapping matches. Results were normalized according to peak size to obtain the number of GANTC sites per kb (GANTC/kb). A similar analysis was performed for whole chromosomes with the "pattern matching, genome-scale dna-pattern" tool on RSATools. Ratios were calculated between data obtained (in GANTC/kb) for the peaks and for the whole chromosomes.

Mouse infection. *Ethics statement*: The Animal Welfare Committee of the Université de Namur (UNamur, Belgium) reviewed and approved the complete protocols for *Brucella* infections (Permit Numbers: 05-558 for intraperitonneal infections and 19-330 for intranasal infections).

Mice were acquired from Harlan (Bicester, UK) and bred in the animal facility of the Gosselies campus of the Université Libre de Bruxelles (ULB, Belgium). For intraperitoneal infections, mice (C57BL/6, 10–12 weeks old females) were injected with a dose of 10^5 CFU per mL of *B. abortus* in 500 µL of PBS. Infectious doses were validated by plating serial dilutions of inoculums. At 60 h post inoculation, mice were euthanized by cervical dislocation. Immediately after being killed, spleens were recovered in PBS with 0.1% Triton X-100 (Sigma) and plated on 2YT agar medium.

For intranasal mouse infection, mice (C57BL/6, 10–12 weeks old, mix of males and females) were anesthetized with a mix of Xylasine (9 mg kg^{-1}) and Ketamine (36 mg kg^{-1}) in PBS before being inoculated by an intranasal injection of 2×10^4 CFU mL^{-1} of *B. abortus*. Confirmation of the infectious doses was done by plating serial dilutions of the inoculums. Mice were sacrificed by cervical dislocation at 12 or 28 days post infection. Immediately after sacrifice, spleen and lungs were crushed and resuspended in PBS 0.1% Triton X-100 (Sigma-Aldrich). The bacterial load was evaluated by serial dilutions in RPMI and plated on TSB agar medium. The CFU were counted after 5 days of incubation at 37 °C. All experiments were done in a Biosafety level 3 facility.

Whole-genome sequencing after infection and liquid cultures. Two liquid cultures of WT *B. abortus* were inoculated in 2YT-rich medium from the same plate. One of them was divided into five subcultures and diluted (1:10) in liquid cultures twice every 24 h, before to be plated. The remaining original liquid culture was used to infect five C57BL/6 mice and RAW 264.7 macrophages. Mice were injected intraperitoneally as described above and were euthanized at 60 h post inoculation to recover spleens. RAW 264.7 macrophages were infected as described above and bacteria were plated at 6 and 48 h post infection. Five streaks were made from five isolated colonies obtained after passage in either liquid cultures, mice, or RAW 264.7 macrophages from different wells. The five streaks served for inoculation of liquid cultures, from which genomic DNA was extracted (NucleoSpin Tissue extraction kit, Macherey-Nagel). Samples were sequenced with the Illumina sequencing technique using NextSeq500 run Mid PE150 after preparing a TruSeq DNA library (performed by Genomics Core Leuven, Belgium). Sequencing hits were mapped on the genome of *B. abortus* 544 and, for each colony, all the nucleotides that were different from the reference strain were compiled in an Excel table (performed by Genomics Core Leuven, Belgium; data available at https://figshare.com/articles/Summary_of_whole_genome_sequencing_for_B_abortus/9747653). Mutations were counted for each isolated colony by excluding regions corresponding to microsatellites and with less than 10 reads.

Reverse transcription followed by quantitative PCR. Bacterial cultures were grown in rich medium to exponential phase (OD_{600} 0.3), washed twice in PBS, and allowed to grow in rich medium supplemented or not with IPTG and/or MMS 2.5 mM (Sigma) for 5 h. Bacteria were washed twice in PBS, then collected by centrifugation, and immediately frozen and stored at −80 °C until processing. RNA was extracted using TriPure isolation reagent (Roche) according to the manufacturer's instructions. Samples were treated with DNase I (Fermentas), then RNA was reverse transcribed with specific primers (Supplementary Data 1), using the High capacity cDNA Reverse Transcription kit (Applied Biosystems). Specific cDNAs were amplified on a LightCycler 96 Instrument (Roche) using FastStart Universal SYBR Green Master (Roche). Results were normalized using 16S RNA as a reference with the $E^{-\Delta\Delta Ct}$ calculation method[81], where E corresponds to the efficiency of the primers (determined by serial dilution).

Colony-forming units counts. For CFU counts after infection, RAW 264.7 macrophages were washed twice in PBS, then lysed with 0.01% Triton X-100 in PBS for 10 min at 37 °C. Several dilutions were plated on TSB supplemented with IPTG when required. Plates were incubated for 3 days at 37 °C.

For CFU counts in culture, wild-type *B. abortus* and GcrA-depleted strain supplemented with IPTG were grown to the mid exponential phase (OD_{600} 0.3–0.6) and normalized to OD_{600} 0.15. Cultures were divided into different aliquots to be tested with or without MMS 5 mM and with or without IPTG. Samples were taken at different time points (3, 6, 20, 24, and 48 h) and plated with serial dilutions on 2YT plates, supplemented with 1 mM IPTG for the depleted strain.

For CFU counts on plates supplemented with MMS or MNNG, 100 µL of bacteria in the mid exponential phase (OD_{600} 0.3–0.6) were plated after normalization to OD_{600} 0.1 of all bacterial cultures. All plates were prepared fresh, 1–2 h before each experiment. MMS was added at a concentration of 2.5 mM in TSB-agar-rich medium during plate preparation. MNNG was prepared in an acetate buffer (pH 5), and then added at a final concentration of 35 µM in TSB-agar-rich medium during plate preparation.

Western blot. Cultures of *B. abortus* in the late exponential phase (OD_{600} 0.7–1) were concentrated to an OD_{600} of 10 in PBS, then inactivated for 1 h at 80 °C. Loading buffer (1:4 of final volume) was added before to heat the sample at 95 °C for 10 min. Ten microliters of sample were loaded on each well of a 12% acrylamide gels. After migration, proteins were transferred with the semi-dry method onto a nitrocellulose membrane (GE Healthcare) which was blocked in PBS supplemented with 0.05% Tween 20 (VWR) and 5% (w/v) milk (Nestlé, foam topping) overnight. The membrane was incubated for 1 h with polyclonal anti-GcrA (290.S3) or monoclonal anti-Omp10 (A68/4B10/F05) primary antibodies (1:1000), then with secondary antibodies coupled to HRP (Dako Denmark) (1:5000), both in PBS 0.05% Tween 1% milk. The membrane was washed three times in PBS before to be revealed with The Clarity Western ECL Substrate (Biorad) and Image Quant LAS 4000 (General Electric).

Statistical analysis. Statistical tests were performed in Excel or in GraphPad Prism version 8.0. All statistical tests were one-sided.

Reporting summary. Further information on research design is available in the Nature Research Reporting Summary linked to this article.

Data availability

ChIP-seq data are available at the GEO database under accession code GSM4056904. The list of mutations for whole genome sequencing experiments is available at figshare [https://figshare.com/articles/Summary_of_whole_genome_sequencing_for_B_abortus/9747653]. The source data underlying Figs. 2b, 3b-c, 4, 5, 6c-d, 7, and 8 and Supplementary Fig. 3b-d, 5a-b, d, 8a-b, 7, and 9 are provided as a Source Data file. All other relevant data supporting the key findings of this study are available within the article and its Supplementary Information file or from the corresponding author upon request.

Received: 22 October 2018; Accepted: 10 September 2019;
Published online: 24 October 2019

References

1. Mielecki, D., Wrzesinski, M. & Grzesiuk, E. Inducible repair of alkylated DNA in microorganisms. *Mutat. Res. Rev. Mutat. Res.* **763**, 294–305 (2015).
2. Fu, D., Calvo, J. A. & Samson, L. D. Balancing repair and tolerance of DNA damage caused by alkylating agents. *Nat. Rev. Cancer* **12**, 104–120 (2012).
3. Catsburg, C. E. et al. Dietary sources of N-nitroso compounds and bladder cancer risk: findings from the Los Angeles bladder cancer study. *Int. J. Cancer* **134**, 125–135 (2014).
4. Zhu, Y. et al. Dietary N-nitroso compounds and risk of colorectal cancer: a case-control study in Newfoundland and Labrador and Ontario, Canada. *Br. J. Nutr.* **111**, 1109–1117 (2014).
5. Rydberg, B. & Lindahl, T. Nonenzymatic methylation of DNA by the intracellular methyl group donor S-adenosyl-L-methionine is a potentially mutagenic reaction. *EMBO J.* **1**, 211–216 (1982).
6. Tudek, B. et al. Lipid peroxidation in face of DNA damage, DNA repair and other cellular processes. *Free Radic. Biol. Med.* **107**, 77–89 (2017).
7. Taverna, P. & Sedgwick, B. Generation of an endogenous DNA-methylating agent by nitrosation in Escherichia coli. *J. Bacteriol.* **178**, 5105–5111 (1996).
8. Sedgwick, B. Nitrosated peptides and polyamines as endogenous mutagens in O6-alkylguanine-DNA alkyltransferase deficient cells. *Carcinogenesis* **18**, 1561–1567 (1997).
9. Guttenplan, J. B. N-nitrosamines: bacterial mutagenesis and in vitro metabolism. *Mutat. Res.* **186**, 81–134 (1987).
10. Posnick, L. M. & Samson, L. D. Influence of S-adenosylmethionine pool size on spontaneous mutation, dam methylation, and cell growth of *Escherichia coli*. *J. Bacteriol.* **181**, 6756–6762 (1999).
11. Bielski, B. H., Arudi, R. L. & Sutherland, M. W. A study of the reactivity of HO2/O2- with unsaturated fatty acids. *J. Biol. Chem.* **258**, 4759–4761 (1983).
12. Nichols, D. S. & McMeekin, T. A. Biomarker techniques to screen for bacteria that produce polyunsaturated fatty acids. *J. Microbiol. Methods* **48**, 161–170 (2002).
13. Winczura, A., Zdzalik, D. & Tudek, B. Damage of DNA and proteins by major lipid peroxidation products in genome stability. *Free Radic. Res.* **46**, 442–459 (2012).
14. Mackay, W. J., Han, S. & Samson, L. D. DNA alkylation repair limits spontaneous base substitution mutations in Escherichia coli. *J. Bacteriol.* **176**, 3224–3230 (1994).

15. Iyengar, R., Stuehr, D. J. & Marletta, M. A. Macrophage synthesis of nitrite, nitrate, and N-nitrosamines: precursors and role of the respiratory burst. *Proc. Natl Acad. Sci. USA* **84**, 6369–6373 (1987).
16. Vermeer, I. T. M. et al. Neutrophil-mediated formation of carcinogenic N-nitroso compounds in an in vitro model for intestinal inflammation. *Toxicol. Lett.* **154**, 175–182 (2004).
17. Espey, M. G., Miranda, K. M., Thomas, D. D. & Wink, D. A. Distinction between nitrosating mechanisms within human cells and aqueous solution. *J. Biol. Chem.* **276**, 30085–30091 (2001).
18. Kumar, Y. & Valdivia, R. H. Leading a sheltered life: intracellular pathogens and maintenance of vacuolar compartments. *Cell Host Microbe* **5**, 593–601 (2009).
19. Pizarro-Cerda, J. et al. *Brucella abortus* transits through the autophagic pathway and replicates in the endoplasmic reticulum of nonprofessional phagocytes. *Infect. Immun.* **66**, 5711–5724 (1998).
20. Moreno, E. & Moriyon, I. The genus *Brucella*. *Prokaryotes* **5**, 315–456 (2006).
21. Porte, F., Liautard, J. P. & Kohler, S. Early acidification of phagosomes containing *Brucella suis* is essential for intracellular survival in murine macrophages. *Infect. Immun.* **67**, 4041–4047 (1999).
22. Starr, T., Ng, T. W., Wehrly, T. D., Knodler, L. A. & Celli, J. *Brucella* intracellular replication requires trafficking through the late endosomal/lysosomal compartment. *Traffic* **9**, 678–694 (2008).
23. Celli, J. et al. *Brucella* evades macrophage killing via VirB-dependent sustained interactions with the endoplasmic reticulum. *J. Exp. Med.* **198**, 545–556 (2003).
24. Sedzicki, J., et al. 3D correlative electron microscopy reveals continuity of Brucella-containing vacuoles with the endoplasmic reticulum. *J. Cell Sci.* **131**, https://doi.org/10.1242/jcs.210799 (2018).
25. Ohshima, H. et al. L-arginine-dependent formation of N-nitrosamines by the cytosol of macrophages activated with lipopolysaccharide and interferon-gamma. *Carcinogenesis* **12**, 1217–1220 (1991).
26. Kunisaki, N. & Hayashi, M. Formation of N-nitrosamines from seconday animes and nitrite by resting cells of Escherichia coli B. *Appl. Environ. Microbiol.* **37**, 279–282 (1979).
27. Deghelt, M. et al. The newborn *Brucella abortus* blocked at the G1 stage of its cell cycle is the major infectious bacterial subpopulation. *Nat. Commun.* **5**, 4366 (2014).
28. Samson, L. & Cairns, J. A new pathway for DNA repair in Escherichia coli. *Nature* **267**, 281–283 (1977).
29. McCarthy, J. G., Edington, B. V. & Schendel, P. F. Inducible repair of phosphotriesters in *Escherichia coli*. *Proc. Natl Acad. Sci. USA* **80**, 7380–7384 (1983).
30. Uphoff, S. et al. Stochastic activation of a DNA damage response causes cell-to-cell mutation rate variation. *Science* **351**, 1094–1097 (2016).
31. Lindahl, T., Sedgwick, B., Sekiguchi, M. & Nakabeppu, Y. Regulation and expression of the adaptive response to alkylating agents. *Annu. Rev. Biochem.* **57**, 133–157 (1988).
32. Bowles, T., Metz, A. H., O'Quin, J., Wawrzak, Z. & Eichman, B. F. Structure and DNA binding of alkylation response protein AidB. *Proc. Natl Acad. Sci. USA* **105**, 15299–15304 (2008).
33. Rippa, V. et al. Preferential DNA damage prevention by the *E. coli* AidB gene: a new mechanism for the protection of specific genes. *DNA Repair (Amst.)* **10**, 934–941 (2011).
34. Uphoff, S. Real-time dynamics of mutagenesis reveal the chronology of DNA repair and damage tolerance responses in single cells. *Proc. Natl Acad. Sci. USA* **115**, E6516–E6525 (2018).
35. Durbach, S. I. et al. DNA alkylation damage as a sensor of nitrosative stress in Mycobacterium tuberculosis. *Infect. Immun.* **71**, 997–1000 (2003).
36. Alvarez, G. et al. Relevance of DNA alkylation damage repair systems in *Salmonella enterica* virulence. *J. Bacteriol.* **192**, 2006–2008 (2010).
37. Sedgwick, B. Molecular signal for induction of the adaptive response to alkylation damage in *Escherichia coli*. *J. Cell Sci. Suppl.* **6**, 215–223 (1987).
38. Kondo, H. et al. Structure and expression of the alkB gene of *Escherichia coli* related to the repair of alkylated DNA. *J. Biol. Chem.* **261**, 15772–15777 (1986).
39. Hakura, A., Morimoto, K., Sofuni, T. & Nohmi, T. Cloning and characterization of the *Salmonella typhimurium ada* gene, which encodes O6-methylguanine-DNA methyltransferase. *J. Bacteriol.* **173**, 3663–3672 (1991).
40. Brown, P. J. et al. Polar growth in the Alphaproteobacterial order Rhizobiales. *Proc. Natl Acad. Sci. USA* **109**, 1697–1701 (2012).
41. Miao, J. et al. Fast-response and highly selective fluorescent probes for biological signaling molecule NO based on N-nitrosation of electron-rich aromatic secondary amines. *Biomaterials* **78**, 11–19 (2016).
42. Kosaka, H., Wishnok, J. S., Miwa, M., Leaf, C. D. & Tannenbaum, S. R. Nitrosation by stimulated macrophages. Inhibitors, enhancers and substrates. *Carcinogenesis* **10**, 563–566 (1989).
43. Beranek, D. T. Distribution of methyl and ethyl adducts following alkylation with monofunctional alkylating agents. *Mutat. Res.* **231**, 11–30 (1990).
44. Smith, M. B. & March, J. March's advanced organic chemistry: reactions, mechanisms, and structure. 6th edition. *J. Med. Chem.* **50**, 2279–2280 (2007).
45. Hornback, M. L. & Roop, R. M. II *The Brucella abortus xthA*-1 gene product participates in base excision repair and resistance to oxidative killing but is not required for wild-type virulence in the mouse model. *J. Bacteriol.* **188**, 1295–1300 (2006).
46. Kaasen, I., Evensen, G. & Seeberg, E. Amplified expression of the tag+ and alkA+ genes in *Escherichia coli*: identification of gene products and effects on alkylation resistance. *J. Bacteriol.* **168**, 642–647 (1986).
47. Tatum, F. M., Morfitt, D. C. & Halling, S. M. Construction of a *Brucella abortus* RecA mutant and its survival in mice. *Microb. Pathog.* **14**, 177–185 (1993).
48. Schoonhoven, N. M., et al. Altering residue 134 confers an increased substrate range of alkylated nucleosides to the *E. coli* OGT protein. *Molecules* **22**, https://doi.org/10.3390/molecules22111948 (2017).
49. Little, J. W. & Mount, D. W. The SOS regulatory system of *Escherichia coli*. *Cell* **29**, 11–22 (1982).
50. Galhardo, R. S., Rocha, R. P., Marques, M. V. & Menck, C. F. An SOS-regulated operon involved in damage-inducible mutagenesis in *Caulobacter crescentus*. *Nucleic Acids Res.* **33**, 2603–2614 (2005).
51. Tapias, A., Fernandez, S., Alonso, J. C. & Barbe, J. *Rhodobacter sphaeroides* LexA has dual activity: optimising and repressing recA gene transcription. *Nucleic Acids Res.* **30**, 1539–1546 (2002).
52. da Rocha, R. P., Paquola, A. C., Marques Mdo, V., Menck, C. F. & Galhardo, R. S. Characterization of the SOS regulon of *Caulobacter crescentus*. *J. Bacteriol.* **190**, 1209–1218 (2008).
53. Roux, C. M. et al. RecA and RadA proteins of *Brucella abortus* do not perform overlapping protective DNA repair functions following oxidative burst. *J. Bacteriol.* **188**, 5187–5195 (2006).
54. Mohapatra, S. S., Fioravanti, A. & Biondi, E. G. DNA methylation in *Caulobacter* and other Alphaproteobacteria during cell cycle progression. *Trends Microbiol.* **22**, 528–535 (2014).
55. Collier, J., McAdams, H. H. & Shapiro, L. A. DNA methylation ratchet governs progression through a bacterial cell cycle. *Proc. Natl Acad. Sci. USA* **104**, 17111–17116 (2007).
56. Kozdon, J. B. et al. Global methylation state at base-pair resolution of the *Caulobacter* genome throughout the cell cycle. *Proc. Natl Acad. Sci. USA* **110**, E4658–E4667 (2013).
57. Francis, N. et al. CtrA controls cell division and outer membrane composition of the pathogen *Brucella abortus*. *Mol. Microbiol.* **103**, 780–797 (2017).
58. Robertson, G. T. et al. The *Brucella abortus* CcrM DNA methyltransferase is essential for viability, and its overexpression attenuates intracellular replication in murine macrophages. *J. Bacteriol.* **182**, 3482–3489 (2000).
59. Colombi, D. & Gomes, S. L. An *alkB* gene homolog is differentially transcribed during the *Caulobacter crescentus* cell cycle. *J. Bacteriol.* **179**, 3139–3145 (1997).
60. Haakonsen, D. L., Yuan, A. H. & Laub, M. T. The bacterial cell cycle regulator GcrA is a sigma70 cofactor that drives gene expression from a subset of methylated promoters. *Genes Dev.* **29**, 2272–2286 (2015).
61. Fioravanti, A. et al. DNA binding of the cell cycle transcriptional regulator GcrA depends on N6-adenosine methylation in *Caulobacter crescentus* and other Alphaproteobacteria. *PLoS Genet.* **9**, e1003541 (2013).
62. Sternon J. F., et al. Transposon sequencing of *Brucella abortus* uncovers essential genes for growth in vitro and inside macrophages. *Infect. Immun.* **86**, e00312 (2018).
63. Dotreppe, D., Mullier, C., Letesson, J. J. & De Bolle, X. The alkylation response protein AidB is localized at the new poles and constriction sites in *Brucella abortus*. *BMC Microbiol.* **11**, 257 (2011).
64. Hanot Mambres, D. et al. Identification of immune effectors essential to the control of primary and secondary intranasal infection with *Brucella melitensis* in mice. *J. Immunol.* **196**, 3780–3793 (2016).
65. Stewart, V. Nitrate respiration in relation to facultative metabolism in enterobacteria. *Microbiol. Rev.* **52**, 190–232 (1988).
66. Archer, M. C. Mechanisms of action of N-nitroso compounds. *Cancer Surv.* **8**, 241–250 (1989).
67. Lamontagne, J. et al. Intracellular adaptation of *Brucella abortus*. *J. Proteome Res.* **8**, 1594–1609 (2009).
68. Lestrate, P. et al. Attenuated signature-tagged mutagenesis mutants of *Brucella melitensis* identified during the acute phase of infection in mice. *Infect. Immun.* **71**, 7053–7060 (2003).
69. Barquero-Calvo, E. et al. *Brucella abortus* uses a stealthy strategy to avoid activation of the innate immune system during the onset of infection. *PLoS ONE* **2**, e631 (2007).
70. Haine, V., Dozot, M., Dornand, J., Letesson, J. J. & De Bolle, X. NnrA is required for full virulence and regulates several *Brucella melitensis* denitrification genes. *J. Bacteriol.* **188**, 1615–1619 (2006).

71. Rossetti, C. A., Galindo, C. L., Garner, H. R. & Adams, L. G. Transcriptional profile of the intracellular pathogen *Brucella melitensis* following HeLa cells infection. *Microb. Pathog.* **51**, 338–344 (2011).
72. Thomas, A. D. et al. Influence of DNA repair on nonlinear dose-responses for mutation. *Toxicol. Sci.* **132**, 87–95 (2013).
73. Kaufman, A. & Walker, G. C. A constitutive O6-methylguanine-DNA methyltransferase of *Rhizobium meliloti*. *Mutat. Res.* **235**, 165–169 (1990).
74. Staron, A. & Mascher, T. General stress response in alpha-proteobacteria: PhyR and beyond. *Mol. Microbiol.* **78**, 271–277 (2010).
75. Stephens, C., Reisenauer, A., Wright, R. & Shapiro, L. A cell cycle-regulated bacterial DNA methyltransferase is essential for viability. *Proc. Natl Acad. Sci. USA* **93**, 1210–1214 (1996).
76. Simon, R., Priefer, U. & Pühler, A. A broad host range mobilization system for in vivo genetic engineering: transposon mutagenesis in Gram negative bacteria. *Bio/Technology* **1**, 784–791 (1983).
77. Khan, S. R., Gaines, J., Roop, R. M. II & Farrand, S. K. Broad-host-range expression vectors with tightly regulated promoters and their use to examine the influence of TraR and TraM expression on Ti plasmid quorum sensing. *Appl. Environ. Microbiol.* **74**, 5053–5062 (2008).
78. Cloeckaert, A., Zygmunt, M. S., Dubray, G. & Limet, J. N. Characterization of O-polysaccharide specific monoclonal antibodies derived from mice infected with the rough *Brucella melitensis* strain B115. *J. Gen. Microbiol.* **139**, 1551–1556 (1993).
79. Ducret, A., Quardokus, E. M. & Brun, Y. V. MicrobeJ, a tool for high throughput bacterial cell detection and quantitative analysis. *Nat. Microbiol.* **1**, 16077 (2016).
80. van Helden, J. Regulatory Sequence Analysis Tools. *Nucleic Acids Res.* **31**, 3593–3596 (2003).
81. Livak, K. J. & Schmittgen, T. D. Analysis of relative gene expression data using real-time quantitative PCR and the 2(-Delta Delta C(T)) Method. *Methods* **25**, 402–408 (2001).

Acknowledgements

We thank members of the URBM and I. Matic for stimulating discussions. We also thank Y. Ashhab for his help regarding ChIP-seq analysis. We thank H. Lavender and C. M. Tang for their careful reading of our manuscript. We thank UNamur (https://www.unamur.be/) for financial and logistic support. This work was funded by The Fédération Wallonie-Bruxelles (ARC 17/22-087) and by the FRS-FNRS "Brucell-cycle" (PDR T.0060.15). K.P., A.M., and G.P. were supported by a FRIA Ph.D. fellowship. A.R. and N.F. held an Aspirant fellowship from FRS-FNRS. This work was also supported by the French Agence Nationale de Recherche (ANR-JCJC-2011-Castacc) (http://www.agence-nationale-recherche.fr/) and the Region Pas-De-Calais (http://www.nordpasdecalais.fr) CPER to A.F. and E.G.B.

Author Contributions

K.P. and X.D.B. wrote the manuscript. R.J. and S.P.V. created and characterized the N-nitrosation sensitive probe. A.M., G.P. and E.M. designed and performed mice infection experiments. K.P. and X.D.B. designed all other experiments, and E.G.B. contributed to the design of the ChIP-seq experiment. K.P., A.R., G.P., A.F., N.F., K.W. and N.Z. performed experiments.

Competing interests

The authors declare no competing interests.

Additional information

Supplementary information is available for this paper at https://doi.org/10.1038/s41467-019-12516-8.

Correspondence and requests for materials should be addressed to X.D.B.

Peer review information *Nature Communications* thanks Elżbieta Grzesiuk, R. Martin Roop II, and the other, anonymous, reviewer(s) for their contribution to the peer review of this work. Peer reviewer reports are available.

Reprints and permission information is available at http://www.nature.com/reprints

Publisher's note Springer Nature remains neutral with regard to jurisdictional claims in published maps and institutional affiliations.

REFERENCES

Aarsman, M. E., Piette, A., Fraipont, C., Vinkenvleugel, T. M., Nguyen-Distèche, M., & den Blaauwen, T. (2005). Maturation of the *Escherichia coli* divisome occurs in two steps. *Mol Microbiol*, *55*(6), 1631-1645. https://doi.org/10.1111/j.1365-2958.2005.04502.x

Achard, M. E., Tree, J. J., Holden, J. A., Simpfendorfer, K. R., Wijburg, O. L., Strugnell, R. A., Schembri, M. A., Sweet, M. J., Jennings, M. P., & McEwan, A. G. (2010). The multi-copper-ion oxidase CueO of *Salmonella enterica* serovar Typhimurium is required for systemic virulence. *Infect Immun*, *78*(5), 2312-2319. https://doi.org/10.1128/iai.01208-09

Alifano, P., Fani, R., Liò, P., Lazcano, A., Bazzicalupo, M., Carlomagno, M. S., & Bruni, C. B. (1996). Histidine biosynthetic pathway and genes: structure, regulation, and evolution. *Microbiol Rev*, *60*(1), 44-69. https://doi.org/10.1128/mr.60.1.44-69.1996

Almagro Armenteros, J. J., Tsirigos, K. D., Sønderby, C. K., Petersen, T. N., Winther, O., Brunak, S., von Heijne, G., & Nielsen, H. (2019). SignalP 5.0 improves signal peptide predictions using deep neural networks. *Nat Biotechnol*, *37*(4), 420-423. https://doi.org/10.1038/s41587-019-0036-z

Ames, G. F.-L. (1985). The Histidine Transport System of *Salmonella typhimurium*. In F. Bronner & A. Kleinzeller (Eds.), *Current Topics in Membranes and Transport* (Vol. 23, pp. 103-119). Academic Press. https://doi.org/https://doi.org/10.1016/S0070-2161(08)60152-5

Anderson, E. S., Paulley, J. T., Gaines, J. M., Valderas, M. W., Martin, D. W., Menscher, E., Brown, T. D., Burns, C. S., & Roop, R. M., 2nd. (2009). The manganese transporter MntH is a critical virulence determinant for *Brucella abortus* 2308 in experimentally infected mice. *Infect Immun*, *77*(8), 3466-3474. https://doi.org/10.1128/iai.00444-09

Archambaud, C., Salcedo, S. P., Lelouard, H., Devilard, E., de Bovis, B., Van Rooijen, N., Gorvel, J. P., & Malissen, B. (2010). Contrasting roles of macrophages and dendritic cells in controlling initial pulmonary *Brucella* infection. *Eur J Immunol*, *40*(12), 3458-3471. https://doi.org/10.1002/eji.201040497

Ardeshir, F., & Ames, G. F. (1980). Cloning of the histidine transport genes from Salmonella typhimurium and characterization of an analogous transport system in *Escherichia coli*. *J Supramol Struct*, *13*(1), 117-130. https://doi.org/10.1002/jss.400130111

Baba, T., & Schneewind, O. (1996). Target cell specificity of a bacteriocin molecule: a C-terminal signal directs lysostaphin to the cell wall of *Staphylococcus aureus*. *EMBO J*, *15*(18), 4789-4797.

Bäckhed, F., Ley, R. E., Sonnenburg, J. L., Peterson, D. A., & Gordon, J. I. (2005). Host-bacterial mutualism in the human intestine. *Science*, *307*(5717), 1915-1920. https://doi.org/10.1126/science.1104816

Banta, A. B., Enright, A. L., Siletti, C., & Peters, J. M. (2020). A High-Efficacy CRISPR Interference System for Gene Function Discovery in Zymomonas mobilis. *Appl Environ Microbiol*, *86*(23). https://doi.org/10.1128/aem.01621-20

Batut, J., Andersson, S. G., & O'Callaghan, D. (2004). The evolution of chronic infection strategies in the alpha-proteobacteria. *Nat Rev Microbiol*, *2*(12), 933-945. https://doi.org/10.1038/nrmicro1044

Beard, S. J., Hughes, M. N., & Poole, R. K. (1995). Inhibition of the cytochrome bd-terminated NADH oxidase system in *Escherichia coli* K-12 by divalent metal cations. *FEMS Microbiol Lett*, *131*(2), 205-210. https://doi.org/10.1111/j.1574-6968.1995.tb07778.x

Bender, R. A. (2012). Regulation of the histidine utilization (hut) system in bacteria. *Microbiol Mol Biol Rev*, *76*(3), 565-584. https://doi.org/10.1128/mmbr.00014-12

Bergman, E. N. (1990). Energy contributions of volatile fatty acids from the gastrointestinal tract in various species. *Physiol Rev*, *70*(2), 567-590. https://doi.org/10.1152/physrev.1990.70.2.567

Bertsche, U., Kast, T., Wolf, B., Fraipont, C., Aarsman, M. E., Kannenberg, K., von Rechenberg, M., Nguyen-Distèche, M., den Blaauwen, T., Höltje, J. V., & Vollmer, W. (2006). Interaction between two murein (peptidoglycan) synthases, PBP3 and PBP1B, in *Escherichia coli*. *Mol Microbiol*, *61*(3), 675-690. https://doi.org/10.1111/j.1365-2958.2006.05280.x

Best, A., & Abu Kwaik, Y. (2019). Nutrition and Bipartite Metabolism of Intracellular Pathogens. *Trends Microbiol*, *27*(6), 550-561. https://doi.org/10.1016/j.tim.2018.12.012

Bisson, C., Britton, K. L., Sedelnikova, S. E., Rodgers, H. F., Eadsforth, T. C., Viner, R. C., Hawkes, T. R., Baker, P. J., & Rice, D. W. (2015). Crystal Structures Reveal that the Reaction Mechanism of Imidazoleglycerol-Phosphate Dehydratase Is Controlled by Switching Mn(II) Coordination. *Structure*, *23*(7), 1236-1245. https://doi.org/10.1016/j.str.2015.05.012

Bochtler, M., Odintsov, S. G., Marcyjaniak, M., & Sabala, I. (2004). Similar active sites in lysostaphins and D-Ala-D-Ala metallopeptidases. *Protein Sci*, *13*(4), 854-861. https://doi.org/10.1110/ps.03515704

Botella, H., Peyron, P., Levillain, F., Poincloux, R., Poquet, Y., Brandli, I., Wang, C., Tailleux, L., Tilleul, S., Charrière, G. M., Waddell, S. J., Foti, M., Lugo-Villarino, G., Gao, Q., Maridonneau-Parini, I., Butcher, P. D., Castagnoli, P. R., Gicquel, B., de Chastellier, C., & Neyrolles, O. (2011). Mycobacterial p(1)-type ATPases mediate resistance to zinc poisoning in human macrophages. *Cell Host Microbe*, *10*(3), 248-259. https://doi.org/10.1016/j.chom.2011.08.006

Brenner, M., & Ames, B. N. (1971). The Histidine Operon and Its Regulation. In H. J. Vogel (Ed.), *Metabolic Regulation (Third Edition)* (pp. 349-387). Academic Press. https://doi.org/https://doi.org/10.1016/B978-0-12-299255-1.50018-3

Brilli, M., Fondi, M., Fani, R., Mengoni, A., Ferri, L., Bazzicalupo, M., & Biondi, E. G. (2010). The diversity and evolution of cell cycle regulation in alpha-proteobacteria: a comparative genomic analysis. *BMC Syst Biol*, *4*, 52. https://doi.org/10.1186/1752-0509-4-52

Brown, P. J., de Pedro, M. A., Kysela, D. T., Van der Henst, C., Kim, J., De Bolle, X., Fuqua, C., & Brun, Y. V. (2012). Polar growth in the Alphaproteobacterial order Rhizobiales. *Proc Natl Acad Sci U S A*, *109*(5), 1697-1701. https://doi.org/10.1073/pnas.1114476109

Cameron, T. A., Anderson-Furgeson, J., Zupan, J. R., Zik, J. J., & Zambryski, P. C. (2014). Peptidoglycan synthesis machinery in *Agrobacterium tumefaciens* during unipolar growth and cell division. *mBio*, *5*(3), e01219-01214. https://doi.org/10.1128/mBio.01219-14

Cano, D. A., Mouslim, C., Ayala, J. A., García-del Portillo, F., & Casadesús, J. (1998). Cell Division Inhibition in *Salmonella typhimurium* Histidine-Constitutive Strains an ftsI-Like Defect in the Presence of Wild-Type Penicillin-Binding Protein 3 Levels. *J Bacteriol.*, *180*(19), 5231-5234. https://doi.org/10.1128/JB.180.19.

Carvalho Neta, A. V., Mol, J. P., Xavier, M. N., Paixão, T. A., Lage, A. P., & Santos, R. L. (2010). Pathogenesis of bovine brucellosis. *Vet J*, *184*(2), 146-155. https://doi.org/10.1016/j.tvjl.2009.04.010

Celli, J. (2015). The changing nature of the *Brucella*-containing vacuole. *Cell Microbiol*, *17*(7), 951-958. https://doi.org/10.1111/cmi.12452

Celli, J. (2019). The Intracellular Life Cycle of *Brucella spp. Microbiology spectrum*, *7*(2). https://doi.org/10.1128/microbiolspec.BAI-0006-2019

Celli, J., de Chastellier, C., Franchini, D. M., Pizarro-Cerda, J., Moreno, E., & Gorvel, J. P. (2003). *Brucella* evades macrophage killing via VirB-dependent sustained interactions with the endoplasmic reticulum. *J Exp Med*, *198*(4), 545-556. https://doi.org/10.1084/jem.20030088

Chandrangsu, P., Rensing, C., & Helmann, J. D. (2017). Metal homeostasis and resistance in bacteria. *Nat Rev Microbiol*, *15*(6), 338-350. https://doi.org/10.1038/nrmicro.2017.15

Chatterji, D., & Ojha, A. K. (2001). Revisiting the stringent response, ppGpp and starvation signaling. *Curr Opin Microbiol*, *4*(2), 160-165. https://doi.org/10.1016/s1369-5274(00)00182-x

Chauhan, A., Lofton, H., Maloney, E., Moore, J., Fol, M., Madiraju, M. V., & Rajagopalan, M. (2006). Interference of *Mycobacterium tuberculosis* cell division by Rv2719c, a cell wall hydrolase. *Mol Microbiol*, *62*(1), 132-147. https://doi.org/10.1111/j.1365-2958.2006.05333.x

Chauhan, D., Srivastava, P. A., Ritzl, B., Yennamalli, R. M., Cava, F., & Priyadarshini, R. (2019). Amino Acid-Dependent Alterations in Cell Wall and Cell Morphology of *Deinococcus indicus* DR1. *Front Microbiol*, *10*, 1449. https://doi.org/10.3389/fmicb.2019.01449

Chevance, F. F., Le Guyon, S., & Hughes, K. T. (2014). The effects of codon context on in vivo translation speed. *PLoS Genet*, *10*(6), e1004392. https://doi.org/10.1371/journal.pgen.1004392

Cloeckaert, A., Jacques, I., de Wergifosse, P., Dubray, G., & Limet, J. N. (1992). Protection against *Brucella melitensis* or *Brucella abortus* in mice with immunoglobulin G (IgG), IgA, and IgM monoclonal antibodies specific for a common epitope shared by the *Brucella* A and M smooth lipopolysaccharides. *Infect Immun*, *60*(1), 312-315. https://doi.org/10.1128/iai.60.1.312-315.1992

Cochrane, S. A., & Lohans, C. T. (2020). Breaking down the cell wall: Strategies for antibiotic discovery targeting bacterial transpeptidases. *European Journal of Medicinal Chemistry*, *194*, 112262. https://doi.org/https://doi.org/10.1016/j.ejmech.2020.112262

Cook, J., Baverstock, T. C., McAndrew, M. B. L., Stansfeld, P. J., Roper, D. I., & Crow, A. (2020). Insights into bacterial cell division from a structure of EnvC bound to the FtsX periplasmic domain. *Proc Natl Acad Sci U S A*, *117*(45), 28355-28365. https://doi.org/10.1073/pnas.2017134117

Daimon, Y., Iwama-Masui, C., Tanaka, Y., Shiota, T., Suzuki, T., Miyazaki, R., Sakurada, H., Lithgow, T., Dohmae, N., Mori, H., Tsukazaki, T., Narita, S. I., & Akiyama, Y. (2017). The TPR domain of BepA is required for productive interaction with substrate proteins and the beta-barrel assembly machinery complex. *Mol Microbiol*, *106*(5), 760-776. https://doi.org/10.1111/mmi.13844

Damo, S. M., Kehl-Fie, T. E., Sugitani, N., Holt, M. E., Rathi, S., Murphy, W. J., Zhang, Y., Betz, C., Hench, L., Fritz, G., Skaar, E. P., & Chazin, W. J. (2013). Molecular basis for manganese sequestration by calprotectin and roles in the innate immune response to invading bacterial pathogens. *Proc Natl Acad Sci U S A*, *110*(10), 3841-3846. https://doi.org/10.1073/pnas.1220341110

Daniel, R. A., & Errington, J. (2003). Control of cell morphogenesis in bacteria: two distinct ways to make a rod-shaped cell. *Cell*, *113*(6), 767-776. https://doi.org/10.1016/s0092-8674(03)00421-5

de la Fuente, J., Antunes, S., Bonnet, S., Cabezas-Cruz, A., Domingos, A. G., Estrada-Peña, A., Johnson, N., Kocan, K. M., Mansfield, K. L., Nijhof, A. M., Papa, A., Rudenko, N., Villar, M., Alberdi, P., Torina, A., Ayllón, N., Vancova, M., Golovchenko, M., Grubhoffer, L., Caracappa, S., Fooks, A. R., Gortazar, C., & Rego, R. O. M. (2017). Tick-Pathogen Interactions and Vector Competence: Identification of Molecular Drivers for Tick-Borne Diseases. *Front Cell Infect Microbiol*, *7*, 114. https://doi.org/10.3389/fcimb.2017.00114

de Wet, T. J., Winkler, K. R., Mhlanga, M., Mizrahi, V., & Warner, D. F. (2020). Arrayed CRISPRi and quantitative imaging describe the morphotypic landscape of essential mycobacterial genes. *Elife*, *9*. https://doi.org/10.7554/eLife.60083

Dean, A. S., Crump, L., Greter, H., Hattendorf, J., Schelling, E., & Zinsstag, J. (2012). Clinical manifestations of human brucellosis: a systematic review and meta-analysis. *PLoS Negl Trop Dis*, *6*(12), e1929. https://doi.org/10.1371/journal.pntd.0001929

Deghelt, M., Mullier, C., Sternon, J. F., Francis, N., Laloux, G., Dotreppe, D., Van der Henst, C., Jacobs-Wagner, C., Letesson, J. J., & De Bolle, X. (2014). G1-arrested newborn cells are the predominant infectious form of the pathogen *Brucella abortus*. *Nat Commun*, *5*, 4366. https://doi.org/10.1038/ncomms5366

Den Blaauwen, T., Aarsman, M. E., Vischer, N. O., & Nanninga, N. (2003). Penicillin-binding protein PBP2 of *Escherichia coli* localizes preferentially in the lateral wall and at mid-cell in comparison with the old cell pole. *Mol Microbiol*, *47*(2), 539-547. https://doi.org/10.1046/j.1365-2958.2003.03316.x

Dietl, A. M., Amich, J., Leal, S., Beckmann, N., Binder, U., Beilhack, A., Pearlman, E., & Haas, H. (2016). Histidine biosynthesis plays a crucial role in metal homeostasis and virulence of *Aspergillus fumigatus*. *Virulence*, *7*(4), 465-476. https://doi.org/10.1080/21505594.2016.1146848

Djoko, K. Y., Achard, M. E. S., Phan, M. D., Lo, A. W., Miraula, M., Prombhul, S., Hancock, S. J., Peters, K. M., Sidjabat, H. E., Harris, P. N., Mitić, N., Walsh, T. R., Anderson, G. J., Shafer, W. M., Paterson, D. L., Schenk, G., McEwan, A. G., & Schembri, M. A. (2018). Copper Ions and Coordination Complexes as Novel Carbapenem Adjuvants. *Antimicrob Agents Chemother*, *62*(2). https://doi.org/10.1128/aac.02280-17

Dozot, M., Boigegrain, R. A., Delrue, R. M., Hallez, R., Ouahrani-Bettache, S., Danese, I., Letesson, J. J., De Bolle, X., & Köhler, S. (2006). The stringent response mediator Rsh is required for *Brucella melitensis* and *Brucella suis* virulence, and for expression of the type IV secretion system virB. *Cell Microbiol*, *8*(11), 1791-1802. https://doi.org/10.1111/j.1462-5822.2006.00749.x

Ducret, A., Quardokus, E. M., & Brun, Y. V. (2016). MicrobeJ, a tool for high throughput bacterial cell detection and quantitative analysis. *Nat Microbiol*, *1*(7), 16077. https://doi.org/10.1038/nmicrobiol.2016.77

Eberhardt, C., Kuerschner, L., & Weiss, D. S. (2003). Probing the catalytic activity of a cell division-specific transpeptidase in vivo with beta-lactams. *J Bacteriol*, *185*(13), 3726-3734. https://doi.org/10.1128/jb.185.13.3726-3734.2003

Ebersbach, G., Briegel, A., Jensen, G. J., & Jacobs-Wagner, C. (2008). A self-associating protein critical for chromosome attachment, division, and polar organization in *Caulobacter*. *Cell*, *134*(6), 956-968. https://doi.org/10.1016/j.cell.2008.07.016

Egan, A. J. F., Errington, J., & Vollmer, W. (2020). Regulation of peptidoglycan synthesis and remodelling. *Nature Reviews Microbiology*, *18*(8), 446-460. https://doi.org/10.1038/s41579-020-0366-3

Elzer, P. H., Kovach, M. E., Phillips, R. W., Robertson, G. T., Peterson, K. M., & Roop, R. M., 2nd. (1995). In vivo and in vitro stability of the broad-host-range cloning vector pBBR1MCS in six *Brucella* species. *Plasmid*, *33*(1), 51-57. https://doi.org/10.1006/plas.1995.1006

Espírito Santo, C., Taudte, N., Nies, D. H., & Grass, G. (2008). Contribution of copper ion resistance to survival of *Escherichia coli* on metallic copper surfaces. *Appl Environ Microbiol*, *74*(4), 977-986. https://doi.org/10.1128/aem.01938-07

Fani, R., Brilli, M., & Lio, P. (2005). The origin and evolution of operons: the piecewise building of the proteobacterial histidine operon. *J Mol Evol*, *60*(3), 378-390. https://doi.org/10.1007/s00239-004-0198-1

Feng, H., Edwards, N., Anderson, C. M. H., Althaus, M., Duncan, R. P., Hsu, Y.-C., Luetje, C. W., Price, D. R. G., Wilson, A. C. C., & Thwaites, D. T. (2019). Trading amino acids at the aphid–*Buchnera* symbiotic interface. *Proceedings of the National Academy of Sciences*, *116*(32), 16003-16011. https://doi.org/10.1073/pnas.1906223116

Fenlon, L. A., & Slauch, J. M. (2017). Cytoplasmic Copper Detoxification in *Salmonella* Can Contribute to SodC Metalation but Is Dispensable during Systemic Infection. *J Bacteriol*, *199*(24). https://doi.org/10.1128/jb.00437-17

Figueroa-Cuilan, W. M., Randich, A. M., Dunn, C. M., Santiago-Collazo, G., Yowell, A., & Brown, P. J. B. (2021). Diversification of LytM Protein Functions in Polar Elongation and Cell Division of *Agrobacterium tumefaciens*. *Frontiers in Microbiology*, *12*. https://doi.org/10.3389/fmicb.2021.729307

Flärdh, K. (2003). Essential role of DivIVA in polar growth and morphogenesis in *Streptomyces coelicolor* A3(2). *Mol Microbiol*, *49*(6), 1523-1536. https://doi.org/10.1046/j.1365-2958.2003.03660.x

Flores, A., Fox, M., & Casadesús, J. (1993). The pleiotropic effects of his overexpression in *Salmonella typhimurium* do not involve AICAR-induced mutagenesis. *Mol Gen Genet*, *240*(3), 360-364. https://doi.org/10.1007/bf00280387

Francis, N., Poncin, K., Fioravanti, A., Vassen, V., Willemart, K., Ong, T. A., Rappez, L., Letesson, J. J., Biondi, E. G., & De Bolle, X. (2017). CtrA controls cell division and outer membrane composition of the pathogen *Brucella abortus*. *Mol Microbiol*, *103*(5), 780-797. https://doi.org/10.1111/mmi.13589

Frandsen, N., & D'Ari, R. (1993). Excess histidine enzymes cause AICAR-independent filamentation in *Escherichia coli*. *Mol Gen Genet*, *240*(3), 348-350. https://doi.org/doi: 10.1007/BF00280385.

Franke, S., Grass, G., Rensing, C., & Nies, D. H. (2003). Molecular analysis of the copper-transporting efflux system CusCFBA of *Escherichia coli*. *J Bacteriol*, *185*(13), 3804-3812. https://doi.org/10.1128/jb.185.13.3804-3812.2003

Frirdich, E., Biboy, J., Pryjma, M., Lee, J., Huynh, S., Parker, C. T., Girardin, S. E., Vollmer, W., & Gaynor, E. C. (2019). The *Campylobacter jejuni* helical to coccoid transition involves changes to peptidoglycan and the ability to elicit an immune response. *Mol Microbiol*, *112*(1), 280-301. https://doi.org/10.1111/mmi.14269

Frirdich, E., Vermeulen, J., Biboy, J., Soares, F., Taveirne, M. E., Johnson, J. G., DiRita, V. J., Girardin, S. E., Vollmer, W., & Gaynor, E. C. (2014). Peptidoglycan LD-carboxypeptidase Pgp2 influences *Campylobacter jejuni* helical cell shape and pathogenic properties and provides the substrate for the DL-carboxypeptidase Pgp1. *J Biol Chem*, *289*(12), 8007-8018. https://doi.org/10.1074/jbc.M113.491829

Fuchino, K., Bagchi, S., Cantlay, S., Sandblad, L., Wu, D., Bergman, J., Kamali-Moghaddam, M., Flärdh, K., & Ausmees, N. (2013). Dynamic gradients of an intermediate filament-like cytoskeleton are recruited by a polarity landmark during apical growth. *Proc Natl Acad Sci U S A*, *110*(21), E1889-1897. https://doi.org/10.1073/pnas.1305358110

Fujiwara, T., & Fukui, S. (1974). Unidirectional growth and branch formation of a morphological mutant, *Agrobacterium tumefaciens*. *J Bacteriol*, *120*(2), 583-589. https://doi.org/10.1128/jb.120.2.583-589.1974

Fung, D. K., Lau, W. Y., Chan, W. T., & Yan, A. (2013). Copper efflux is induced during anaerobic amino acid limitation in *Escherichia coli* to protect iron-sulfur cluster enzymes and biogenesis. *J Bacteriol*, *195*(20), 4556-4568. https://doi.org/10.1128/jb.00543-13

Gerhardt, P., & Wilson, J. B. (1948). The nutrition of *Brucellae*: growth in simple chemically defined media. *Journal of bacteriology*, *56*(1), 17-24. https://doi.org/10.1128/jb.56.1.17-24.1948

Giachino, A., & Waldron, K. J. (2020). Copper tolerance in bacteria requires the activation of multiple accessory pathways. *Mol Microbiol*, *114*(3), 377-390. https://doi.org/10.1111/mmi.14522

Gibert, I., & Casadesús, J. (1990). *sulA*-independent division inhibition in his-constitutive strains of *Salmonella typhimurium*. *FEMS Microbiol Lett*, *57*(3), 205-210. https://doi.org/10.1016/0378-1097(90)90066-y

Glauner, B., Höltje, J. V., & Schwarz, U. (1988). The composition of the murein of *Escherichia coli*. *J Biol Chem*, *263*(21), 10088-10095.

Godfroid, J. (2018). *Brucella spp.* at the Wildlife-Livestock Interface: An Evolutionary Trajectory through a Livestock-to-Wildlife "Host Jump"? *Vet Sci*, *5*(3). https://doi.org/10.3390/vetsci5030081

Goley, E. D., Comolli, L. R., Fero, K. E., Downing, K. H., & Shapiro, L. (2010). DipM links peptidoglycan remodelling to outer membrane organization in *Caulobacter*. *Mol Microbiol*, *77*(1), 56-73. https://doi.org/10.1111/j.1365-2958.2010.07222.x

Grabowska, M., Jagielska, E., Czapinska, H., Bochtler, M., & Sabala, I. (2015). High resolution structure of an M23 peptidase with a substrate analogue. *Sci Rep*, *5*, 14833. https://doi.org/10.1038/srep14833

Grangeon, R., Zupan, J. R., Anderson-Furgeson, J., & Zambryski, P. C. (2015). PopZ identifies the new pole, and PodJ identifies the old pole during polar growth in *Agrobacterium tumefaciens*. *Proc Natl Acad Sci U S A*, *112*(37), 11666-11671. https://doi.org/10.1073/pnas.1515544112

Grass, G., & Rensing, C. (2001). Genes involved in copper homeostasis in *Escherichia coli*. *J Bacteriol*, *183*(6), 2145-2147. https://doi.org/10.1128/jb.183.6.2145-2147.2001

Gray, M. W., Burger, G., & Lang, B. F. (1999). Mitochondrial evolution. *Science*, *283*(5407), 1476-1481. https://doi.org/10.1126/science.283.5407.1476

Gudipaty, S. A., & McEvoy, M. M. (2014). The histidine kinase CusS senses silver ions through direct binding by its sensor domain. *Biochim Biophys Acta*, *1844*(9), 1656-1661. https://doi.org/10.1016/j.bbapap.2014.06.001

Gunshin, H., Mackenzie, B., Berger, U. V., Gunshin, Y., Romero, M. F., Boron, W. F., Nussberger, S., Gollan, J. L., & Hediger, M. A. (1997). Cloning and characterization of a mammalian proton-coupled metal-ion transporter. *Nature*, *388*(6641), 482-488. https://doi.org/10.1038/41343

Guzmán-Verri, C., González-Barrientos, R., Hernández-Mora, G., Morales, J. A., Baquero-Calvo, E., Chaves-Olarte, E., & Moreno, E. (2012). *Brucella ceti* and brucellosis in cetaceans. *Front Cell Infect Microbiol*, *2*, 3. https://doi.org/10.3389/fcimb.2012.00003

Hantke, K. (2001). Bacterial zinc transporters and regulators. *Biometals*, *14*(3-4), 239-249. https://doi.org/10.1023/a:1012984713391

Heidrich, C., Templin, M. F., Ursinus, A., Merdanovic, M., Berger, J., Schwarz, H., de Pedro, M. A., & Höltje, J. V. (2001). Involvement of N-acetylmuramyl-L-alanine amidases in cell separation and antibiotic-induced autolysis of *Escherichia coli*. *Mol Microbiol*, *41*(1), 167-178. https://doi.org/10.1046/j.1365-2958.2001.02499.x

Heidrich, C., Ursinus, A., Berger, J., Schwarz, H., & Holtje, J. V. (2002). Effects of multiple deletions of murein hydrolases on viability, septum cleavage, and sensitivity to large toxic molecules in *Escherichia coli*. *J Bacteriol*, *184*(22), 6093-6099. https://doi.org/10.1128/JB.184.22.6093-6099.2002

Hempel, A. M., Wang, S. B., Letek, M., Gil, J. A., & Flärdh, K. (2008). Assemblies of DivIVA mark sites for hyphal branching and can establish new zones of cell wall growth in *Streptomyces coelicolor*. *J Bacteriol*, *190*(22), 7579-7583. https://doi.org/10.1128/jb.00839-08

Heng, N., Wescombe, P., Burton, J., Jack, R., & Tagg, J. (2007). Bacteriocins: ecology and evolution. *Springer-Verlag*, 45-92.

Hood, M. I., Mortensen, B. L., Moore, J. L., Zhang, Y., Kehl-Fie, T. E., Sugitani, N., Chazin, W. J., Caprioli, R. M., & Skaar, E. P. (2012). Identification of an *Acinetobacter baumannii* Zinc Acquisition System that Facilitates Resistance to Calprotectin-mediated Zinc Sequestration. *PLOS Pathogens*, *8*(12), e1003068. https://doi.org/10.1371/journal.ppat.1003068

Jacobs, C., Joris, B., Jamin, M., Klarsov, K., Van Beeumen, J., Mengin-Lecreulx, D., van Heijenoort, J., Park, J. T., Normark, S., & Frère, J. M. (1995). AmpD, essential for both beta-lactamase regulation and cell wall recycling, is a novel cytosolic N-acetylmuramyl-L-alanine amidase. *Mol Microbiol*, *15*(3), 553-559. https://doi.org/10.1111/j.1365-2958.1995.tb02268.x

Jiang, C., Caccamo, P. D., & Brun, Y. V. (2015). Mechanisms of bacterial morphogenesis: evolutionary cell biology approaches provide new insights. *Bioessays*, *37*(4), 413-425. https://doi.org/10.1002/bies.201400098

Johnston, H. M., Barnes, W. M., Chumley, F. G., Bossi, L., & Roth, J. R. (1980). Model for regulation of the histidine operon of *Salmonella*. *Proc Natl Acad Sci U S A*, *77*(1), 508-512. https://doi.org/10.1073/pnas.77.1.508

Joseph, P., Abdo, M. R., Boigegrain, R. A., Montero, J. L., Winum, J. Y., & Kohler, S. (2007). Targeting of the *Brucella suis* virulence factor histidinol dehydrogenase by histidinol analogues results in inhibition of intramacrophagic multiplication of the pathogen. *Antimicrob Agents Chemother*, *51*(10), 3752-3755. https://doi.org/10.1128/AAC.00572-07

Kamath, P. L., Foster, J. T., Drees, K. P., Luikart, G., Quance, C., Anderson, N. J., Clarke, P. R., Cole, E. K., Drew, M. L., Edwards, W. H., Rhyan, J. C., Treanor, J. J., Wallen, R. L., White, P. J., Robbe-Austerman, S., & Cross, P. C. (2016). Genomics reveals historic and contemporary transmission dynamics of a bacterial disease among wildlife and livestock. *Nat Commun*, *7*, 11448. https://doi.org/10.1038/ncomms11448

Kang, C. M., Nyayapathy, S., Lee, J. Y., Suh, J. W., & Husson, R. N. (2008). Wag31, a homologue of the cell division protein DivIVA, regulates growth, morphology and polar cell wall synthesis in mycobacteria. *Microbiology (Reading)*, *154*(Pt 3), 725-735. https://doi.org/10.1099/mic.0.2007/014076-0

Kapetanovic, R., Bokil, N. J., Achard, M. E., Ong, C. L., Peters, K. M., Stocks, C. J., Phan, M. D., Monteleone, M., Schroder, K., Irvine, K. M., Saunders, B. M., Walker, M. J., Stacey, K. J., McEwan, A. G., Schembri, M. A., & Sweet, M. J. (2016). *Salmonella* employs multiple mechanisms to subvert the TLR-inducible zinc-mediated antimicrobial response of human macrophages. *Faseb j*, *30*(5), 1901-1912. https://doi.org/10.1096/fj.201500061

Kim, H. W., Chan, Q., Afton, S. E., Caruso, J. A., Lai, B., Weintraub, N. L., & Qin, Z. (2012). Human macrophage ATP7A is localized in the trans-Golgi apparatus, controls intracellular copper levels, and mediates macrophage responses to dermal wounds. *Inflammation*, *35*(1), 167-175. https://doi.org/10.1007/s10753-011-9302-z

Kim, S., Watanabe, K., Shirahata, T., & Watarai, M. (2004). Zinc uptake system (*znuA* locus) of *Brucella abortus* is essential for intracellular survival and virulence in mice. *J Vet Med Sci*, *66*(9), 1059-1063. https://doi.org/10.1292/jvms.66.1059

Kleinman, C. L., Sycz, G., Bonomi, H. R., Rodriguez, R. M., Zorreguieta, A., & Sieira, R. (2017). ChIP-seq analysis of the LuxR-type regulator VjbR reveals novel insights into the *Brucella* virulence gene expression network. *Nucleic Acids Res*, *45*(10), 5757-5769. https://doi.org/10.1093/nar/gkx165

Kohler, S., Foulongne, V., Ouahrani-Bettache, S., Bourg, G., Teyssier, J., Ramuz, M., & Liautard, J. P. (2002). The analysis of the intramacrophagic virulome of *Brucella suis* deciphers the environment encountered by the pathogen inside the macrophage host cell. *Proc Natl Acad Sci U S A*, *99*(24), 15711-15716. https://doi.org/10.1073/pnas.232454299

Krol, E., Stuckenschneider, L., Kästle Silva, J. M., Graumann, P. L., & Becker, A. (2021). Stable inheritance of *Sinorhizobium meliloti* cell growth polarity requires an FtsN-like protein and an amidase. *Nat Commun*, *12*(1), 545. https://doi.org/10.1038/s41467-020-20739-3

Kulis-Horn, R. K., Persicke, M., & Kalinowski, J. (2014). Histidine biosynthesis, its regulation and biotechnological application in *Corynebacterium glutamicum*. *Microb Biotechnol*, *7*(1), 5-25. https://doi.org/10.1111/1751-7915.12055

Kuru, E., Hughes, H. V., Brown, P. J., Hall, E., Tekkam, S., Cava, F., de Pedro, M. A., Brun, Y. V., & VanNieuwenhze, M. S. (2012). In Situ probing of newly synthesized peptidoglycan in live bacteria with fluorescent D-amino acids. *Angew Chem Int Ed Engl*, *51*(50), 12519-12523. https://doi.org/10.1002/anie.201206749

Labischinski, H., Barnickel, G., Bradaczek, H., & Giesbrecht, P. (1979). On the secondary and tertiary structure of murein. Low and medium-angle X-ray evidence against chitin-based conformations of bacterial peptidoglycan. *Eur J Biochem*, *95*(1), 147-155. https://doi.org/10.1111/j.1432-1033.1979.tb12949.x

Latch, J. N., & Margolin, W. (1997a). Generation of buds, swellings, and branches instead of filaments after blocking the cell cycle of *Rhizobium meliloti*. *J Bacteriol*, *179*(7), 2373-2381. https://doi.org/10.1128/jb.179.7.2373-2381.1997

Latch, J. N., & Margolin, W. (1997b). Generation of buds, swellings, and branches instead of filaments after blocking the cell cycle of *Rhizobium meliloti*. *Journal of bacteriology*, *179*(7), 2373-2381. https://doi.org/10.1128/jb.179.7.2373-2381.1997

Lesley, J. A., & Shapiro, L. (2008). SpoT regulates DnaA stability and initiation of DNA replication in carbon-starved Caulobacter crescentus. *J Bacteriol*, *190*(20), 6867-6880. https://doi.org/10.1128/jb.00700-08

Letek, M., Fiuza, M., Ordóñez, E., Villadangos, A. F., Flärdh, K., Mateos, L. M., & Gil, J. A. (2009). DivIVA uses an N-terminal conserved region and two coiled-coil domains to localize and sustain the polar growth in *Corynebacterium glutamicum*. *FEMS Microbiol Lett*, *297*(1), 110-116. https://doi.org/10.1111/j.1574-6968.2009.01679.x

Letunic, I., & Bork, P. (2017). 20 years of the SMART protein domain annotation resource. *Nucleic Acids Research*, *46*(D1), D493-D496. https://doi.org/10.1093/nar/gkx922

Lonergan, Z. R., Nairn, B. L., Wang, J., Hsu, Y. P., Hesse, L. E., Beavers, W. N., Chazin, W. J., Trinidad, J. C., VanNieuwenhze, M. S., Giedroc, D. P., & Skaar, E. P. (2019). An *Acinetobacter baumannii,* Zinc-Regulated Peptidase Maintains Cell Wall Integrity during Immune-Mediated Nutrient Sequestration. *Cell Rep*, *26*(8), 2009-2018.e2006. https://doi.org/10.1016/j.celrep.2019.01.089

Lonergan, Z. R., Palmer, L. D., & Skaar, E. P. (2020). Histidine Utilization Is a Critical Determinant of *Acinetobacter* Pathogenesis. *Infect Immun*, *88*(7). https://doi.org/10.1128/IAI.00118-20

Lubkowitz, M. (2006). The OPT family functions in long-distance peptide and metal transport in plants. *Genet Eng (N Y)*, *27*, 35-55. https://doi.org/10.1007/0-387-25856-6_3

Luizet, J. B., Raymond, J., Lacerda, T. L. S., Barbieux, E., Kambarev, S., Bonici, M., Lembo, F., Willemart, K., Borg, J. P., Celli, J., Gerard, F. C. A., Muraille, E., Gorvel, J. P., & Salcedo, S. P. (2021). The *Brucella* effector BspL targets the ER-associated degradation (ERAD) pathway and delays bacterial egress from infected cells. *Proc Natl Acad Sci U S A*, *118*(32). https://doi.org/10.1073/pnas.2105324118

Lutkenhaus, J. (2007). Assembly dynamics of the bacterial MinCDE system and spatial regulation of the Z ring. *Annu Rev Biochem*, *76*, 539-562. https://doi.org/10.1146/annurev.biochem.75.103004.142652

Ma, Z., Chandrangsu, P., Helmann, T. C., Romsang, A., Gaballa, A., & Helmann, J. D. (2014). Bacillithiol is a major buffer of the labile zinc pool in *Bacillus subtilis*. *Mol Microbiol*, *94*(4), 756-770. https://doi.org/10.1111/mmi.12794

Macomber, L., & Imlay, J. A. (2009). The iron-sulfur clusters of dehydratases are primary intracellular targets of copper toxicity. *Proc Natl Acad Sci U S A*, *106*(20), 8344-8349. https://doi.org/10.1073/pnas.0812808106

Maertens, L., Cherry, P., Tilquin, F., Van Houdt, R., & Matroule, J. Y. (2021). Environmental Conditions Modulate the Transcriptomic Response of Both *Caulobacter crescentus* Morphotypes to Cu Stress. *Microorganisms*, *9*(6). https://doi.org/10.3390/microorganisms9061116

Magnet, S., Dubost, L., Marie, A., Arthur, M., & Gutmann, L. (2008). Identification of the L,D-transpeptidases for peptidoglycan cross-linking in *Escherichia coli*. *J Bacteriol*, *190*(13), 4782-4785. https://doi.org/10.1128/jb.00025-08

Małecki, P. H., Mitkowski, P., Jagielska, E., Trochimiak, K., Mesnage, S., & Sabała, I. (2021). Structural Characterization of EnpA D,L-Endopeptidase from *Enterococcus faecalis* Prophage Provides Insights into Substrate Specificity of M23 Peptidases. *Int J Mol Sci*, *22*(13). https://doi.org/10.3390/ijms22137136

Maret, W. (1994). Oxidative metal release from metallothionein via zinc-thiol/disulfide interchange. *Proc Natl Acad Sci U S A*, *91*(1), 237-241. https://doi.org/10.1073/pnas.91.1.237

Margolin, W. (2009). Sculpting the bacterial cell. *Curr Biol*, *19*(17), R812-822. https://doi.org/10.1016/j.cub.2009.06.033

Martin, J. E., Lisher, J. P., Winkler, M. E., & Giedroc, D. P. (2017). Perturbation of manganese metabolism disrupts cell division in *Streptococcus pneumoniae*. *Mol Microbiol*, *104*(2), 334-348. https://doi.org/10.1111/mmi.13630

Martin, R. G. (1963). The One Operon-One Messenger Theory of Transcription. *Cold Spring Harbor Symposia on Quantitative Biology*, *28*, 357-361.

Martinez-Guitian, M., Vazquez-Ucha, J. C., Alvarez-Fraga, L., Conde-Perez, K., Lasarte-Monterrubio, C., Vallejo, J. A., Bou, G., Poza, M., & Beceiro, A. (2019). Involvement of HisF in the Persistence of *Acinetobacter baumannii* During a Pneumonia Infection. *Front Cell Infect Microbiol*, *9*, 310. https://doi.org/10.3389/fcimb.2019.00310

McDevitt, C. A., Ogunniyi, A. D., Valkov, E., Lawrence, M. C., Kobe, B., McEwan, A. G., & Paton, J. C. (2011). A molecular mechanism for bacterial susceptibility to zinc. *PLoS Pathog*, *7*(11), e1002357. https://doi.org/10.1371/journal.ppat.1002357

McLean, D. L., & Houk, E. J. (1973). Phase contrast and electron microscopy of the mycetocytes and symbiotes of the pea aphid, *Acyrthosiphon pisum*. *Journal of Insect Physiology*, *19*(3), 625-633. https://doi.org/https://doi.org/10.1016/0022-1910(73)90071-1

Meeske, A. J., Riley, E. P., Robins, W. P., Uehara, T., Mekalanos, J. J., Kahne, D., Walker, S., Kruse, A. C., Bernhardt, T. G., & Rudner, D. Z. (2016). SEDS proteins are a widespread family of bacterial cell wall polymerases. *Nature*, *537*(7622), 634-638. https://doi.org/10.1038/nature19331

Meydan, S., Klepacki, D., Karthikeyan, S., Margus, T., Thomas, P., Jones, J. E., Khan, Y., Briggs, J., Dinman, J. D., Vázquez-Laslop, N., & Mankin, A. S. (2017). Programmed Ribosomal Frameshifting Generates a Copper Transporter and a Copper Chaperone from the Same Gene. *Mol Cell*, *65*(2), 207-219. https://doi.org/10.1016/j.molcel.2016.12.008

Mi, W., Li, Y., Yoon, S. H., Ernst, R. K., Walz, T., & Liao, M. (2017). Structural basis of MsbA-mediated lipopolysaccharide transport. *Nature*, *549*(7671), 233-237. https://doi.org/10.1038/nature23649

Miyagishima, S. Y., Kabeya, Y., Sugita, C., Sugita, M., & Fujiwara, T. (2014). DipM is required for peptidoglycan hydrolysis during chloroplast division. *BMC Plant Biol*, *14*, 57. https://doi.org/10.1186/1471-2229-14-57

Moll, A., Schlimpert, S., Briegel, A., Jensen, G. J., & Thanbichler, M. (2010). DipM, a new factor required for peptidoglycan remodelling during cell division in *Caulobacter crescentus*. *Mol Microbiol*, *77*(1), 90-107. https://doi.org/10.1111/j.1365-2958.2010.07224.x

Moran, N. A. (2002). Microbial Minimalism: Genome Reduction in Bacterial Pathogens. *Cell*, *108*(5), 583-586. https://doi.org/https://doi.org/10.1016/S0092-8674(02)00665-7

Moreno, E. (2014). Retrospective and prospective perspectives on zoonotic brucellosis. *Front Microbiol*, *5*, 213. https://doi.org/10.3389/fmicb.2014.00213

Moreno, E., & Moriyon, I. (2002). *Brucella melitensis*: a nasty bug with hidden credentials for virulence. *Proc Natl Acad Sci U S A*, *99*(1), 1-3. https://doi.org/10.1073/pnas.022622699

Moreno, E., & Moriyón, I. (2006). The Genus *Brucella*. In (Vol. 5, pp. 315-456). https://doi.org/10.1007/0-387-30745-1_17

Mueller, E. A., & Levin, P. A. (2020). Bacterial Cell Wall Quality Control during Environmental Stress. *mBio*, *11*(5). https://doi.org/10.1128/mBio.02456-20

Muñoz-Gómez, S. A., Hess, S., Burger, G., Lang, B. F., Susko, E., Slamovits, C. H., & Roger, A. J. (2019). An updated phylogeny of the Alphaproteobacteria reveals that the parasitic Rickettsiales and Holosporales have independent origins. *Elife*, *8*. https://doi.org/10.7554/eLife.42535

Murata, D., Yamada, T., Tokuyama, T., Arai, K., Quiros, P. M., Lopez-Otin, C., Iijima, M., & Sesaki, H. (2020). Mitochondrial Safeguard: a stress response that offsets extreme fusion and protects respiratory function via flickering-induced Oma1 activation. *EMBO J*, *39*(24), e105074. https://doi.org/10.15252/embj.2020105074

Murphy, J. T., Bruinsma, J. J., Schneider, D. L., Collier, S., Guthrie, J., Chinwalla, A., Robertson, J. D., Mardis, E. R., & Kornfeld, K. (2011). Histidine protects against zinc and nickel toxicity in *Caenorhabditis elegans*. *PLoS Genet*, *7*(3), e1002013. https://doi.org/10.1371/journal.pgen.1002013

Murphy, S. G., Alvarez, L., Adams, M. C., Liu, S., Chappie, J. S., Cava, F., & Dorr, T. (2019). Endopeptidase Regulation as a Novel Function of the Zur-Dependent Zinc Starvation Response. *mBio*, *10*(1). https://doi.org/10.1128/mBio.02620-18

Murray, M. L., & Hartman, P. E. (1972). Overproduction of *hisH* and *hisF* gene products leads to inhibition of cell division in *Salmonella*. *Canadian Journal of Microbiology*, *18*(5), 671-681. https://doi.org/10.1139/m72-105

Nairn, B. L., Lonergan, Z. R., Wang, J., Braymer, J. J., Zhang, Y., Calcutt, M. W., Lisher, J. P., Gilston, B. A., Chazin, W. J., de Crecy-Lagard, V., Giedroc, D. P., & Skaar, E. P. (2016). The Response of *Acinetobacter baumannii* to Zinc Starvation. *Cell Host Microbe*, *19*(6), 826-836. https://doi.org/10.1016/j.chom.2016.05.007

Narita, S., Masui, C., Suzuki, T., Dohmae, N., & Akiyama, Y. (2013). Protease homolog BepA (YfgC) promotes assembly and degradation of beta-barrel membrane proteins in *Escherichia coli*. *Proc Natl Acad Sci U S A*, *110*(38), E3612-3621. https://doi.org/10.1073/pnas.1312012110

Naroeni, A., & Porte, F. (2002). Role of cholesterol and the ganglioside GM(1) in entry and short-term survival of *Brucella suis* in murine macrophages. *Infect Immun*, *70*(3), 1640-1644. https://doi.org/10.1128/iai.70.3.1640-1644.2002

Nelson, D. L., & Cox, M. M. (2017). *Lehninger principles of biochemistry* (7 ed.). W.H. Freeman.

Niu, H., Xiong, Q., Yamamoto, A., Hayashi-Nishino, M., & Rikihisa, Y. (2012). Autophagosomes induced by a bacterial Beclin 1 binding protein facilitate obligatory intracellular infection. *Proc Natl Acad Sci U S A*, *109*(51), 20800-20807. https://doi.org/10.1073/pnas.1218674109

Olive, A. J., & Sassetti, C. M. (2016). Metabolic crosstalk between host and pathogen: sensing, adapting and competing. *Nat Rev Microbiol*, *14*(4), 221-234. https://doi.org/10.1038/nrmicro.2016.12

Ong, C. L., Walker, M. J., & McEwan, A. G. (2015). Zinc disrupts central carbon metabolism and capsule biosynthesis in *Streptococcus pyogenes*. *Sci Rep*, *5*, 10799. https://doi.org/10.1038/srep10799

Osman, D., & Cavet, J. S. (2011). Metal sensing in *Salmonella*: implications for pathogenesis. *Adv Microb Physiol*, *58*, 175-232. https://doi.org/10.1016/b978-0-12-381043-4.00005-2

Osman, D., Patterson, C. J., Bailey, K., Fisher, K., Robinson, N. J., Rigby, S. E., & Cavet, J. S. (2013). The copper supply pathway to a *Salmonella* Cu,Zn-superoxide dismutase (SodCII) involves P(1B)-type ATPase copper efflux and periplasmic CueP. *Mol Microbiol*, *87*(3), 466-477. https://doi.org/10.1111/mmi.12107

Osman, D., Waldron, K. J., Denton, H., Taylor, C. M., Grant, A. J., Mastroeni, P., Robinson, N. J., & Cavet, J. S. (2010). Copper homeostasis in *Salmonella* is atypical and copper-CueP is a major periplasmic metal complex. *J Biol Chem*, *285*(33), 25259-25268. https://doi.org/10.1074/jbc.M110.145953

Outten, F. W., Huffman, D. L., Hale, J. A., & O'Halloran, T. V. (2001). The independent cue and cus systems confer copper tolerance during aerobic and anaerobic growth in *Escherichia coli*. *J Biol Chem*, *276*(33), 30670-30677. https://doi.org/10.1074/jbc.M104122200

Outten, F. W., Outten, C. E., Hale, J., & O'Halloran, T. V. (2000). Transcriptional activation of an *Escherichia coli* copper efflux regulon by the chromosomal MerR homologue, cueR. *J Biol Chem*, *275*(40), 31024-31029. https://doi.org/10.1074/jbc.M006508200

Palmer, L. D., & Skaar, E. P. (2016). Transition Metals and Virulence in Bacteria. *Annu Rev Genet*, *50*, 67-91. https://doi.org/10.1146/annurev-genet-120215-035146

Pappas, G., Papadimitriou, P., Akritidis, N., Christou, L., & Tsianos, E. V. (2006). The new global map of human brucellosis. *The Lancet Infectious Diseases*, *6*(2), 91-99. https://doi.org/10.1016/s1473-3099(06)70382-6

Pappas, G., Papadimitriou, P., Akritidis, N., Christou, L., & Tsianos, E. V. (2006). The new global map of human brucellosis. *Lancet Infect Dis*, *6*(2), 91-99. https://doi.org/10.1016/s1473-3099(06)70382-6

Peters, K., Kannan, S., Rao, V. A., Biboy, J., Vollmer, D., Erickson, S. W., Lewis, R. J., Young, K. D., & Vollmer, W. (2016). The Redundancy of Peptidoglycan Carboxypeptidases Ensures Robust Cell Shape Maintenance in *Escherichia coli*. *mBio*, *7*(3). https://doi.org/10.1128/mBio.00819-16

Peters, K., Pazos, M., Edoo, Z., Hugonnet, J. E., Martorana, A. M., Polissi, A., VanNieuwenhze, M. S., Arthur, M., & Vollmer, W. (2018). Copper inhibits peptidoglycan LD-transpeptidases suppressing beta-lactam resistance due to bypass of penicillin-binding proteins. *Proc Natl Acad Sci U S A*, *115*(42), 10786-10791. https://doi.org/10.1073/pnas.1809285115

Plommet, M. (1991). Minimal requirements for growth of *Brucella suis* and other *Brucella* species. *Zentralblatt für Bakteriologie*, *275*(4), 436-450. https://doi.org/10.1016/s0934-8840(11)80165-9

Pontel, L. B., & Soncini, F. C. (2009). Alternative periplasmic copper-resistance mechanisms in Gram negative bacteria. *Mol Microbiol*, *73*(2), 212-225. https://doi.org/10.1111/j.1365-2958.2009.06763.x

Porte, F., Naroeni, A., Ouahrani-Bettache, S., & Liautard, J. P. (2003). Role of the *Brucella suis* lipopolysaccharide O antigen in phagosomal genesis and in inhibition of phagosome-lysosome fusion in murine macrophages. *Infect Immun*, *71*(3), 1481-1490. https://doi.org/10.1128/iai.71.3.1481-1490.2003

Potter, A. J., Trappetti, C., & Paton, J. C. (2012). *Streptococcus pneumoniae* uses glutathione to defend against oxidative stress and metal ion toxicity. *J Bacteriol*, *194*(22), 6248-6254. https://doi.org/10.1128/jb.01393-12

Prashar, A., Bhatia, S., Gigliozzi, D., Martin, T., Duncan, C., Guyard, C., & Terebiznik, M. R. (2013). Filamentous morphology of bacteria delays the timing of phagosome morphogenesis in macrophages. *J Cell Biol*, *203*(6), 1081-1097. https://doi.org/10.1083/jcb.201304095

Price, C. T., Al-Quadan, T., Santic, M., Rosenshine, I., & Abu Kwaik, Y. (2011). Host proteasomal degradation generates amino acids essential for intracellular bacterial growth. *Science*, *334*(6062), 1553-1557. https://doi.org/10.1126/science.1212868

Price, C. T., Richards, A. M., Von Dwingelo, J. E., Samara, H. A., & Abu Kwaik, Y. (2014). Amoeba host-*Legionella* synchronization of amino acid auxotrophy and its role in bacterial adaptation and pathogenic evolution. *Environ Microbiol*, *16*(2), 350-358. https://doi.org/10.1111/1462-2920.12290

Radman, M. (1975). SOS repair hypothesis: phenomenology of an inducible DNA repair which is accompanied by mutagenesis. *Basic Life Sci*, *5a*, 355-367. https://doi.org/10.1007/978-1-4684-2895-7_48

Raulinaitis, V., Tossavainen, H., Aitio, O., Juuti, J. T., Hiramatsu, K., Kontinen, V., & Permi, P. (2017). Identification and structural characterization of LytU, a unique peptidoglycan endopeptidase from the lysostaphin family. *Sci Rep*, *7*(1), 6020. https://doi.org/10.1038/s41598-017-06135-w

Rensing, C., Fan, B., Sharma, R., Mitra, B., & Rosen, B. P. (2000). CopA: An *Escherichia coli* Cu(I)-translocating P-type ATPase. *Proc Natl Acad Sci U S A*, *97*(2), 652-656. https://doi.org/10.1073/pnas.97.2.652

Rocaboy, M., Herman, R., Sauvage, E., Remaut, H., Moonens, K., Terrak, M., Charlier, P., & Kerff, F. (2013). The crystal structure of the cell division amidase AmiC reveals the fold of the AMIN domain, a new peptidoglycan binding domain. *Mol Microbiol*, *90*(2), 267-277. https://doi.org/10.1111/mmi.12361

Rohs, P. D. A., Buss, J., Sim, S. I., Squyres, G. R., Srisuknimit, V., Smith, M., Cho, H., Sjodt, M., Kruse, A. C., Garner, E. C., Walker, S., Kahne, D. E., & Bernhardt, T. G. (2018). A central role for PBP2 in the activation of peptidoglycan polymerization by the bacterial cell elongation machinery. *PLoS Genet*, *14*(10), e1007726. https://doi.org/10.1371/journal.pgen.1007726

Roop, R. M., 2nd, & Caswell, C. C. (Eds.). (2017). *Metals and the biology and virulence of Brucella*. Springer. https://doi.org/https://doi.org/10.1007/978-3-319-53622-4.

Roop, R. M., 2nd, Gaines, J. M., Anderson, E. S., Caswell, C. C., & Martin, D. W. (2009). Survival of the fittest: how *Brucella* strains adapt to their intracellular niche in the host. *Med Microbiol Immunol*, *198*(4), 221-238. https://doi.org/10.1007/s00430-009-0123-8

Ruiz-Ranwez, V., Posadas, D. M., Van der Henst, C., Estein, S. M., Arocena, G. M., Abdian, P. L., Martín, F. A., Sieira, R., De Bolle, X., & Zorreguieta, A. (2013). BtaE, an adhesin that belongs to the trimeric autotransporter family, is required for full virulence and defines a specific adhesive pole of *Brucella suis*. *Infect Immun*, *81*(3), 996-1007. https://doi.org/10.1128/iai.01241-12

Sandström, J., & Pettersson, J. (1994). Amino acid composition of phloem sap and the relation to intraspecific variation in pea aphid (*Acyrthosiphon pisum*) performance. *Journal of Insect Physiology*, *40*(11), 947-955. https://doi.org/https://doi.org/10.1016/0022-1910(94)90133-3

Sasaki, T., & Ishikawa, H. (1995). Production of essential amino acids from glutamate by mycetocyte symbionts of the pea aphid, *Acyrthosiphon pisum*. *Journal of Insect Physiology*, *41*(1), 41-46. https://doi.org/https://doi.org/10.1016/0022-1910(94)00080-Z

Sauvage, E., Kerff, F., Terrak, M., Ayala, J. A., & Charlier, P. (2008). The penicillin-binding proteins: structure and role in peptidoglycan biosynthesis. *FEMS Microbiol Rev*, *32*(2), 234-258. https://doi.org/10.1111/j.1574-6976.2008.00105.x

Scheurwater, E., Reid, C. W., & Clarke, A. J. (2008). Lytic transglycosylases: bacterial space-making autolysins. *Int J Biochem Cell Biol*, *40*(4), 586-591. https://doi.org/10.1016/j.biocel.2007.03.018

Schmidt, K. L., Peterson, N. D., Kustusch, R. J., Wissel, M. C., Graham, B., Phillips, G. J., & Weiss, D. S. (2004). A predicted ABC transporter, FtsEX, is needed for cell division in *Escherichia coli*. *J Bacteriol*, *186*(3), 785-793. https://doi.org/10.1128/jb.186.3.785-793.2004

Schneider, C. A., Rasband, W. S., & Eliceiri, K. W. (2012). NIH Image to ImageJ: 25 years of image analysis. *Nat Methods*, *9*(7), 671-675. https://doi.org/10.1038/nmeth.2089

Sharma, A. K., Kumar, S., K, H., Dhakan, D. B., & Sharma, V. K. (2016). Prediction of peptidoglycan hydrolases- a new class of antibacterial proteins. *BMC Genomics*, *17*, 411. https://doi.org/10.1186/s12864-016-2753-8

Sheehan, L. M., Budnick, J. A., Blanchard, C., Dunman, P. M., & Caswell, C. C. (2015). A LysR-family transcriptional regulator required for virulence in *Brucella abortus* is highly conserved among the α-proteobacteria. *Mol Microbiol*, *98*(2), 318-328. https://doi.org/10.1111/mmi.13123

Sheehan, L. M., Budnick, J. A., Roop, R. M., 2nd, & Caswell, C. C. (2015). Coordinated zinc homeostasis is essential for the wild-type virulence of *Brucella abortus*. *J Bacteriol*, *197*(9), 1582-1591. https://doi.org/10.1128/JB.02543-14

Sieira, R., Arocena, G. M., Bukata, L., Comerci, D. J., & Ugalde, R. A. (2010). Metabolic control of virulence genes in *Brucella abortus*: HutC coordinates virB expression and the histidine utilization pathway by direct binding to both promoters. *J Bacteriol*, *192*(1), 217-224. https://doi.org/10.1128/jb.01124-09

Singh, S. K., Parveen, S., SaiSree, L., & Reddy, M. (2015). Regulated proteolysis of a cross-link-specific peptidoglycan hydrolase contributes to bacterial morphogenesis. *Proc Natl Acad Sci U S A*, *112*(35), 10956-10961. https://doi.org/10.1073/pnas.1507760112

Singh, S. K., SaiSree, L., Amrutha, R. N., & Reddy, M. (2012). Three redundant murein endopeptidases catalyse an essential cleavage step in peptidoglycan synthesis of *Escherichia coli* K12. *Mol Microbiol*, *86*(5), 1036-1051. https://doi.org/10.1111/mmi.12058

Starr, T., Child, R., Wehrly, T. D., Hansen, B., Hwang, S., López-Otin, C., Virgin, H. W., & Celli, J. (2012). Selective subversion of autophagy complexes facilitates completion of the *Brucella* intracellular cycle. *Cell Host Microbe*, *11*(1), 33-45. https://doi.org/10.1016/j.chom.2011.12.002

Starr, T., Ng, T. W., Wehrly, T. D., Knodler, L. A., & Celli, J. (2008). *Brucella* intracellular replication requires trafficking through the late endosomal/lysosomal compartment. *Traffic*, *9*(5), 678-694. https://doi.org/10.1111/j.1600-0854.2008.00718.x

Steele, S., Brunton, J., Ziehr, B., Taft-Benz, S., Moorman, N., & Kawula, T. (2013). *Francisella tularensis* harvests nutrients derived via ATG5-independent autophagy to support intracellular growth. *PLoS Pathog*, *9*(8), e1003562. https://doi.org/10.1371/journal.ppat.1003562

Stepansky, A., & Leustek, T. (2006). Histidine biosynthesis in plants. *Amino Acids*, *30*(2), 127-142. https://doi.org/10.1007/s00726-005-0247-0

Sternon, J. F., Godessart, P., Goncalves de Freitas, R., Van der Henst, M., Poncin, K., Francis, N., Willemart, K., Christen, M., Christen, B., Letesson, J. J., & De Bolle, X. (2018). Transposon Sequencing of *Brucella abortus* Uncovers Essential Genes for Growth In Vitro and Inside Macrophages. *Infect Immun*, *86*(8). https://doi.org/10.1128/IAI.00312-18

Sundberg, R. J., & Martin, R. B. (1974). Interactions of histidine and other imidazole derivatives with transition metal ions in chemical and biological systems. *Chemical Reviews*, *74*, 471-517.

Swanson, M. S., & Hammer, B. K. (2000). *Legionella pneumophila* pathogenesis: a fateful journey from amoebae to macrophages. *Annu Rev Microbiol*, *54*, 567-613. https://doi.org/10.1146/annurev.micro.54.1.567

Taguchi, A., Welsh, M. A., Marmont, L. S., Lee, W., Sjodt, M., Kruse, A. C., Kahne, D., Bernhardt, T. G., & Walker, S. (2019). FtsW is a peptidoglycan polymerase that is functional only in complex with its cognate penicillin-binding protein. *Nat Microbiol*, *4*(4), 587-594. https://doi.org/10.1038/s41564-018-0345-x

Tetaz, T. J., & Luke, R. K. (1983). Plasmid-controlled resistance to copper in *Escherichia coli*. *J Bacteriol*, *154*(3), 1263-1268. https://doi.org/10.1128/jb.154.3.1263-1268.1983

Teyssier, C., Marchandin, H., & Jumas-Bilak, E. (2004). The genome of alpha-proteobacteria : complexity, reduction, diversity and fluidity. *Can J Microbiol*, *50*(6), 383-396. https://doi.org/10.1139/w04-033 (Le génome des alpha-protéobactéries: complexité, réduction, diversité et fluidité.)

Traxler, M. F., Summers, S. M., Nguyen, H. T., Zacharia, V. M., Hightower, G. A., Smith, J. T., & Conway, T. (2008). The global, ppGpp-mediated stringent response to amino acid starvation in *Escherichia coli*. *Mol Microbiol*, *68*(5), 1128-1148. https://doi.org/10.1111/j.1365-2958.2008.06229.x

Tsang, M.-J., Yakhnina, A. A., & Bernhardt, T. G. (2017). NlpD links cell wall remodeling and outer membrane invagination during cytokinesis in *Escherichia coli*. *PLOS Genetics*, *13*(7), e1006888. https://doi.org/10.1371/journal.pgen.1006888

Typas, A., Banzhaf, M., Gross, C. A., & Vollmer, W. (2011). From the regulation of peptidoglycan synthesis to bacterial growth and morphology. *Nat Rev Microbiol*, *10*(2), 123-136. https://doi.org/10.1038/nrmicro2677

Uehara, T., Dinh, T., & Bernhardt, T. G. (2009). LytM-domain factors are required for daughter cell separation and rapid ampicillin-induced lysis in *Escherichia coli*. *J Bacteriol*, *191*(16), 5094-5107. https://doi.org/10.1128/JB.00505-09

Uehara, T., Parzych, K. R., Dinh, T., & Bernhardt, T. G. (2010). Daughter cell separation is controlled by cytokinetic ring-activated cell wall hydrolysis. *EMBO J*, *29*(8), 1412-1422. https://doi.org/10.1038/emboj.2010.36

van den Ent, F., Izoré, T., Bharat, T. A., Johnson, C. M., & Löwe, J. (2014). Bacterial actin MreB forms antiparallel double filaments. *Elife*, *3*, e02634. https://doi.org/10.7554/eLife.02634

Van der Henst, M., Carlier, E., & De Bolle, X. (2020). Intracellular Growth and Cell Cycle Progression are Dependent on (p)ppGpp Synthetase/Hydrolase in *Brucella abortus*. *Pathogens*, *9*(7). https://doi.org/10.3390/pathogens9070571

van Heijenoort, J. (2011). Peptidoglycan hydrolases of *Escherichia coli*. *Microbiol Mol Biol Rev*, *75*(4), 636-663. https://doi.org/10.1128/mmbr.00022-11

Vassen, V., Valotteau, C., Feuillie, C., Formosa-Dague, C., Dufrene, Y. F., & De Bolle, X. (2019). Localized incorporation of outer membrane components in the pathogen *Brucella abortus*. *EMBO J*, *38*(5). https://doi.org/10.15252/embj.2018100323

Vermassen, A., Leroy, S., Talon, R., Provot, C., Popowska, M., & Desvaux, M. (2019). Cell Wall Hydrolases in Bacteria: Insight on the Diversity of Cell Wall Amidases, Glycosidases and Peptidases Toward Peptidoglycan. *Front Microbiol*, *10*, 331. https://doi.org/10.3389/fmicb.2019.00331

Vollmer, W., Joris, B., Charlier, P., & Foster, S. (2008). Bacterial peptidoglycan (murein) hydrolases. *FEMS Microbiol Rev*, *32*(2), 259-286. https://doi.org/10.1111/j.1574-6976.2007.00099.x

Ward, S. K., Abomoelak, B., Hoye, E. A., Steinberg, H., & Talaat, A. M. (2010). CtpV: a putative copper exporter required for full virulence of *Mycobacterium tuberculosis*. *Mol Microbiol*, *77*(5), 1096-1110. https://doi.org/10.1111/j.1365-2958.2010.07273.x

Wattam, A. R., Inzana, T. J., Williams, K. P., Mane, S. P., Shukla, M., Almeida, N. F., Dickerman, A. W., Mason, S., Moriyón, I., O'Callaghan, D., Whatmore, A. M., Sobral, B. W., Tiller, R. V., Hoffmaster, A. R., Frace, M. A., De Castro, C., Molinaro, A., Boyle, S. M., De, B. K., & Setubal, J. C. (2012). Comparative genomics of early-diverging *Brucella* strains reveals a novel lipopolysaccharide biosynthesis pathway. *mBio*, *3*(5), e00246-00211. https://doi.org/10.1128/mBio.00388-12

Weiss, D. S., Chen, J. C., Ghigo, J. M., Boyd, D., & Beckwith, J. (1999). Localization of FtsI (PBP3) to the septal ring requires its membrane anchor, the Z ring, FtsA, FtsQ, and FtsL. *J Bacteriol*, *181*(2), 508-520. https://doi.org/10.1128/jb.181.2.508-520.1999

Whatmore, A. M., & Foster, J. T. (2021). Emerging diversity and ongoing expansion of the genus *Brucella*. *Infect Genet Evol*, *92*, 104865. https://doi.org/10.1016/j.meegid.2021.104865

White, C., Lee, J., Kambe, T., Fritsche, K., & Petris, M. J. (2009). A role for the ATP7A copper-transporting ATPase in macrophage bactericidal activity. *J Biol Chem*, *284*(49), 33949-33956. https://doi.org/10.1074/jbc.M109.070201

White, C. L., & Gober, J. W. (2012). MreB: pilot or passenger of cell wall synthesis? *Trends Microbiol*, *20*(2), 74-79. https://doi.org/10.1016/j.tim.2011.11.004

Wieland, H., Ullrich, S., Lang, F., & Neumeister, B. (2005). Intracellular multiplication of *Legionella pneumophila* depends on host cell amino acid transporter SLC1A5. *Mol Microbiol*, *55*(5), 1528-1537. https://doi.org/10.1111/j.1365-2958.2005.04490.x

Winkler, M. E., & Ramos-Montañez, S. (2009). Biosynthesis of Histidine. *EcoSal Plus*, *3*(2). https://doi.org/10.1128/ecosalplus.3.6.1.9

Wirtz, L., Eder, M., Brand, A. K., & Jung, H. (2021). HutT functions as the major L-histidine transporter in *Pseudomonas putida* KT2440. *FEBS Lett*, *595*(16), 2113-2126. https://doi.org/10.1002/1873-3468.14159

Wolschendorf, F., Ackart, D., Shrestha, T. B., Hascall-Dove, L., Nolan, S., Lamichhane, G., Wang, Y., Bossmann, S. H., Basaraba, R. J., & Niederweis, M. (2011). Copper resistance is essential for virulence of *Mycobacterium tuberculosis*. *Proc Natl Acad Sci U S A*, *108*(4), 1621-1626. https://doi.org/10.1073/pnas.1009261108

Wu, T., Wang, S., Wang, Z., Peng, X., Lu, Y., & Wu, Q. (2015). A multicopper oxidase contributes to the copper tolerance of *Brucella melitensis* 16M. *FEMS Microbiol Lett*, *362*(12), fnv078. https://doi.org/10.1093/femsle/fnv078

Yakhnina, A. A., & Bernhardt, T. G. (2020). The Tol-Pal system is required for peptidoglycan-cleaving enzymes to complete bacterial cell division. *Proc Natl Acad Sci U S A*, *117*(12), 6777-6783. https://doi.org/10.1073/pnas.1919267117

Yang, X., Becker, T., Walters, N., & Pascual, D. W. (2006). Deletion of *znuA* virulence factor attenuates *Brucella abortus* and confers protection against wild-type challenge. *Infect Immun*, *74*(7), 3874-3879. https://doi.org/10.1128/iai.01957-05

Young, V. R. (1994). Adult amino acid requirements: the case for a major revision in current recommendations. *J Nutr*, *124*(8 Suppl), 1517s-1523s. https://doi.org/10.1093/jn/124.suppl_8.1517S

Yu, X. J., Walker, D. H., Liu, Y., & Zhang, L. (2009). Amino acid biosynthesis deficiency in bacteria associated with human and animal hosts. *Infect Genet Evol*, *9*(4), 514-517. https://doi.org/10.1016/j.meegid.2009.02.002

Zhang, X. X., Chang, H., Tran, S. L., Gauntlett, J. C., Cook, G. M., & Rainey, P. B. (2012). Variation in transport explains polymorphism of histidine and urocanate utilization in a natural *Pseudomonas* population. *Environ Microbiol*, *14*(8), 1941-1951. https://doi.org/10.1111/j.1462-2920.2011.02692.x

Zhang, Y. J., & Rubin, E. J. (2013). Feast or famine: the host-pathogen battle over amino acids. *Cell Microbiol*, *15*(7), 1079-1087. https://doi.org/10.1111/cmi.12140

Zhao, H., Patel, V., Helmann, J. D., & Dörr, T. (2017). Don't let sleeping dogmas lie: new views of peptidoglycan synthesis and its regulation. *Mol Microbiol*, *106*(6), 847-860. https://doi.org/10.1111/mmi.13853

Zielinska, A., Billini, M., Moll, A., Kremer, K., Briegel, A., Izquierdo Martinez, A., Jensen, G. J., & Thanbichler, M. (2017). LytM factors affect the recruitment of autolysins to the cell division site in *Caulobacter crescentus*. *Mol Microbiol*, *106*(3), 419-438. https://doi.org/10.1111/mmi.13775